An experimental analysis of solid state pulsed laser melting of aluminium

by

AP Hoult

Thesis submitted in fulfilment for the award of

Doctor of Philosophy
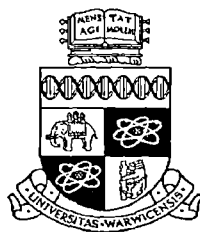
Department of Engineering

University of Warwick

February 1999

Abstract

Novel aspects of solid state laser spot melting of aluminium using a pulsed solid state laser were investigated. After a thorough characterisation of the performance of the solid state laser, an initial series of ranging trials were performed to identify parameters which produced cosmetically satisfactory consistent melt spots on the surface of a commercially available aluminium alloy. These melt spots demonstrated a number of features of interest, including symmetrical concentric ring structures on the surface of the spots. A review of published literature on the use of laser beams as an intense radiation source for pulsed laser surface melting was carried out which confirmed that these phenomena have not been researched or reported in any depth. Experimental work identified the conditions under which they could be reliably reproduced, and these conditions are very close to laser parameters used commercially for pulsed laser welding. Further investigations to understand their origin involved using modified aluminium surfaces and temporally shaped laser pulses. Experimental details are included which will allow reliable reproduction of this effect in the future. Specific thresholds were identified for these phenomena and this has led to an improved understanding of solid state laser spot melting on aluminium. It appears that these rings are part of a continuum of irradiance which leads to melt expulsion due to reactive vapour pressure.
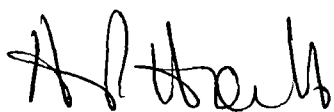
To my family and to Dr Graham Burrows

\

Acknowledgments

I would like to thank Dr. Ian Pashby for his helpful supervision of this thesis and for his support during the period of its completion. I would also like to thank Brian Bryden, Viola Kading and Graham Canham for their assistance at crucial times. I would also like to thank Richard Wong for his assistance counting some of the spots, preparing some of the metallographic specimens and taking some of the photographs. Similarly, I thank Chia Huang Lu for some of the photographs and Ming Yin Shan for his measurements of the anodised layer thickness.

Declaration

I declare that the following piece of work is my own unless otherwise referenced and has not been submitted for any other award.

A P Hoult, February 1999

CONTENTS

3

6

1. Introduction

1.1 Historical perspective

L.A.S.E.R. - Light Amplification by the Stimulated Emission of Radiation is one of the first, and certainly one of the best known scientific acronyms. The laser is a relatively new device for transforming and directing light and although it is basically a scientific device, it has become one of the most widely known inventions of the 20th century. Lasers still retain their attractive "high tech" image even though they have now been in widespread use in certain industries for some years. This image has often led to a widespread misunderstanding of the nature of laser light. It must be noted that laser light has the very important property of being able to be very well focused, and it is ultimately this property that makes the laser a useful tool for both engineers and scientists alike. Electron beams, for example, have been available at high powers for many years, and are also able to be focused to very small diameters, but they have several limitations. Perhaps the most important of these is that they are heavily absorbed in air and hence are usually used *in vacuo*.

Einstein first postulated the fundamental interaction behind the generation of a laser beam in 1917 [1]. He proposed that light of a particular frequency could, under the correct circumstances, stimulate atomic electrons to generate more light of the same frequency. It took until 1958 for Schawlow and Townes to lay out the principles of the optical maser or laser [2]. They proposed that the principles of microwave amplification by stimulated emission used to produce a maser could also be extended to the amplification of light. Building on these principles, the first successful laser was built by Maiman at the Hughes Aircraft Laboratories in the summer of 1960 [3]. Patel

built the first CO_2 laser in 1964 working at the Bell Laboratories [4], rapidly followed by the introduction of the invention of the NdYag solid state laser in the same laboratories.

Since then, the importance of this invention has grown to the point at which lasers are being used in a very wide range of industries and an even wider range of applications. Laser technology in its wider sense, is now used extensively in the fields of communications, information storage, measurement, medicine and entertainment, with new uses emerging all the time. Of particular relevance to this project is the emergence in the last 15 years of high power laser based materials processing.

1.2 Introduction to industrial laser processing

Laser beams are in many respects an ideal tool for engineers - they can deliver pure intense energy in a very carefully controlled manner. A great deal of work has therefore been done on developing lasers for a wide range of applications ever since the first Ruby laser appeared in 1960 [3]. The inherently more stable solid state NdYag lasers allowed more quantitative basic scientific data gathering work to be performed. Soon after, industrial applications of many different types of lasers started to develop. With the advent of the high power CO_2 (carbon dioxide) lasers, capable of average power outputs of several hundreds of watts in the 1970's, industrial applications increased dramatically, especially with regard to laser materials processing. Rapidly, these lasers overtook solid state lasers as the more widely used type. As a result, over the last decade, these lasers have been the prime concern in academia and in industry and the majority of research has been based around this type of laser at the longer far infra red wavelength of 10.6 μm.

The enormous potential for the application of lasers to manufacturing and material processing developed rapidly after their commercial introduction and over the last 20 years, the materials processing applications, laser cutting, drilling, welding, surface heat treatment, cladding and scribing have gradually made their way into a dominant position in the laser industry.

APPLICATIONS	CO_2	Solid state	Excimer	Others
Material Processing	451.0	202.4	107.2	43.7
Medical	39.0	120.5	87.3	56.7
R&D	0.66	100.3	12.8	35.3
Telecommunication	0	4.0	0	0
Optical storage	0	1.3	0	7.9
Barcode scanners	0	0	0	2.1
Inspection &	0	5.8	0	11.6
Entertainment	0	1.68	0	10.3

Table 1.1 1997 Worldwide commercial laser sales by application in $ x 10^6 [adapted from 5].

The Industrial Laser Handbook splits the worldwide materials processing laser applications as follows [6].

World Applications Segmentation
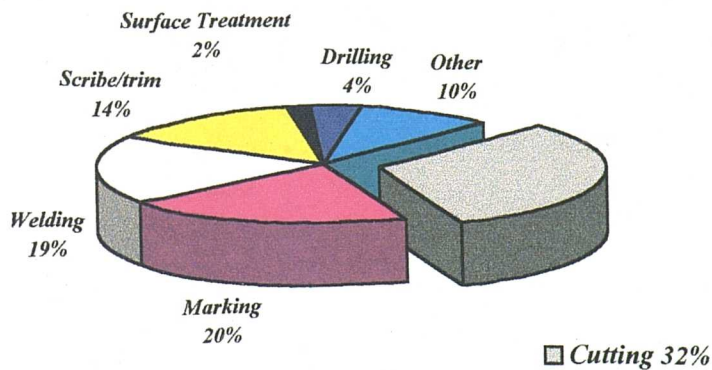
Figure 1.1 Laser Applications [6]

High power industrial laser applications, high power in this sense being defined as greater than 100 watts average power, cover a very wide spread of technologies and industries. However, far more high average power lasers and laser systems are sold for laser cutting, welding, drilling & surface treatment than for any other application area, as shown above. The differences between the laser types are explained in section 3.3.

The majority of these applications are based in the automotive, aerospace, microelectronics and light engineering industries. More recently still, three areas of laser usage have been attracting a great deal of academic and industrial interest.

- the use of lasers in the manufacture of tailored welded blanks

- lasers in Rapid Prototyping - in this technique lasers are used in a variety of ways to create a physical model or a "prototype"

- surface preparation

All of these areas are opening up new fields for industrial lasers, the final area, surface preparation, being the most relevant to this current work.

1.3 Introduction to laser spot melting

As a result of pioneering development work within the last 7-8 years in the field of solid state lasers, there have been important developments which have moved the average power capability of these lasers into the kilowatt output power range [7]. The benefits associated with using these lasers in association with fibre optic beam delivery have been widely heralded [8]. Concurrently, the use of direct diode and diode pumped solid state lasers has also increased, although in this case the developments of interest here are those which are aimed at increasing average power output to the kilowatt level [9]. At this power level, these lasers become of interest for the type of process under discussion here. Less widely reported is the future probable consequent reduction in price per watt of laser power. Both of these developments have generated a great deal of interest in this group of lasers and in the processes for which they are suited. Projecting this trend into the near future will bring a number of processes currently being researched within the realms of industrial exploitation. Amongst these are surface treatment applications, which require relatively low laser intensity, but to be commercially viable, require high coverage speeds and hence high average powers. This project reflects that increasing interest by studying a laser processing phenomena associated with surface melting of aluminium.

1.4 Justification for the project

The motivation for this work emerged from a number of years experience with industrial lasers, in particular, solid state lasers.

The detailed work in this thesis emerged from an interest by the author in laser welding and melting processes for aluminium alloys. One technique for producing a laser textured surface involves the production of a regular array of relatively shallow laser 'melt spots' on the surface of an aluminium alloy surface. During this work it was noted that the regularity, and hence repeatability of the surface produced was disrupted by an apparently random occurrence of weld spots which displayed a curious series of concentric rings on the surface of the melt spots. Investigation of this phenomenon became a major priority.

There are three main justifications for pursuing this project.

- Firstly, the features noted in the preliminary study represent a loss of consistency in the welding process, and although very difficult to measure in terms of surface roughness, they are visible to the naked eye and hence detract from the cosmetic quality and repeatability of the weld.

- Secondly, a review of the scientific literature in this area showed that the areas of interest in this study, spot melting (or welding) of aluminium and the effects of temporal pulse shaping on this process, do not appear to have been studied experimentally to any degree. Although a number of authors have suggested that temporal pulse shaping may be a useful tool in solid state laser processing [10], very little evidence as to how it could or should function has emerged - it is hoped therefore that this work provides some insight.

- Finally, there are a number of industrial welding and surface treatment applications where the ability to control the laser melting process reliably and repeatably may be of real industrial interest.

1.5 Methodology

Figure 1.2 introduces the approach taken to the experimental programme. As shown, the initial work involved characterising the performance of the laser. This involved addressing one of the main limitations associated with solid state lasers, the limited life of the flashlamps that provide optical pumping to the lasing medium. Through a series of ranging trials, the laser spot melting itself was then developed to identify the most appropriate parameters. A large number of melt spots were then produced reliably and repeatably to enable study of the spot melting process itself.

At this stage, inconsistencies were noted in the process. To study in more depth their source, further trials were performed using a range of laser parameters up to the limit of the capabilities of the laser.

Two further techniques were then employed to improve understanding of the process. The first of these was to modify the surface of the aluminium alloy in two different ways, the second was to temporally shape the laser pulse, "pulse shaping".

Flow chart of experimental work

```
                    Flow chart of experimental work

                                          ┌─────────────────────────┐
                                          │  output parameter range │
                                          └─────────────────────────┘
    ┌──────────────────────┐              ┌─────────────────────────┐
    │ Laser characterisation│─────────────│   beam diameter range   │
    └──────────────────────┘              └─────────────────────────┘
              │                           ┌─────────────────────────┐
              │                           │      energy losses       │
              ▼                           └─────────────────────────┘
    ┌──────────────────────┐              ┌─────────────────────────┐
    │   Melting trials      │─────────────│      ranging trials      │
    └──────────────────────┘              └─────────────────────────┘
              │                           ┌─────────────────────────────┐
              │                           │ feedrate & spot overlap trials│
              ▼                           └─────────────────────────────┘
    ┌──────────────────────┐              ┌─────────────┐
    │  Analysis of surfaces │─────────────│ statistical │
    └──────────────────────┘              └─────────────┘
              │                           ┌──────────────┐
              │                           │ metallographic│
              ▼                           └──────────────┘
    ┌──────────────────────┐              ┌─────────────┐
    │   Stage 2 trials      │─────────────│ peak power  │
    └──────────────────────┘              └─────────────┘
              │                           ┌──────────────────┐
              │                           │ pulse shaping trials│
              ▼                           └──────────────────┘
    ┌──────────────────────┐              ┌─────────────┐
    │ Analysis of mechanism │─────────────│ increase oxide│
    └──────────────────────┘              └─────────────┘
                                          ┌─────────────┐
                                          │ decrease oxide│
                                          └─────────────┘
```
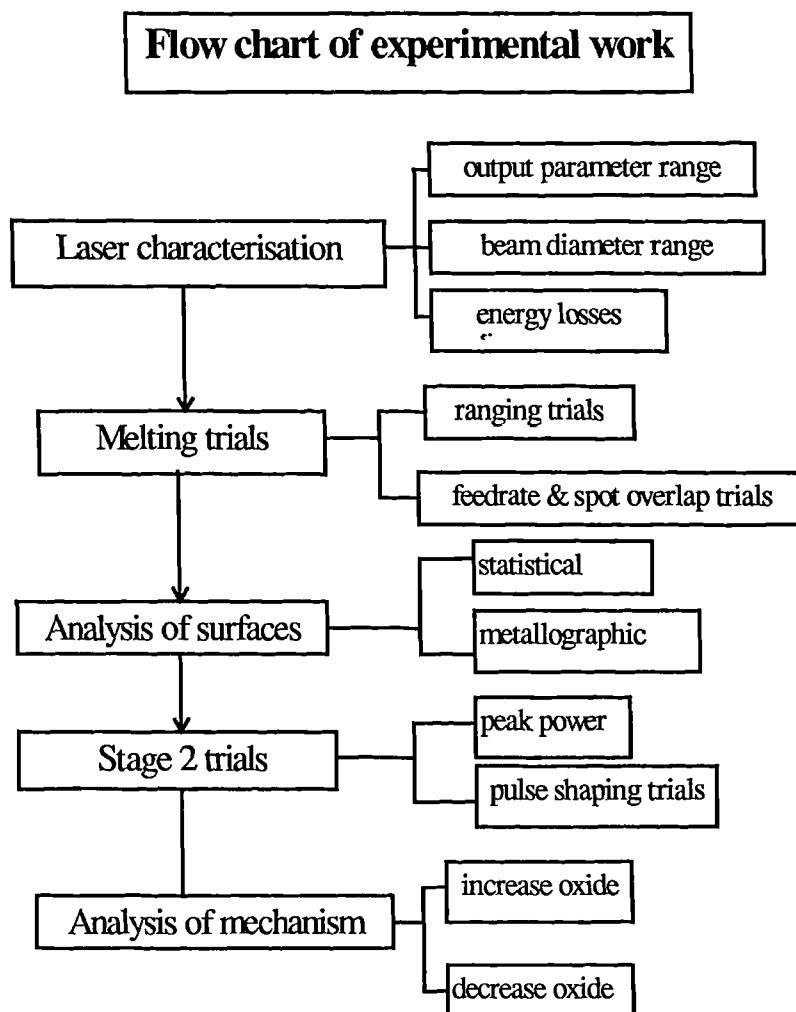
Figure 1.2 Experimental methodology

1.6 Units, symbols & definitions

1.6.1 Units, symbols and definitions

SI units with approved prefixes are used throughout, the only exception being the occasional use of the Celsius scale of temperature (formerly known as Centigrade) instead of Kelvin as it is still widely used in practice. Quantity symbols are generally printed in italics to distinguish them from unit symbols and mathematical constants. The following table identifies the Roman and Greek letters which denote the majority of the physical quantities used in the text in line as far as possible with current usage. All quantities are defined on their first appearance in the text. A few very widely accepted quantities and their symbols are not included in this table.

Quantity	Symbol	Units
energy / pulse energy	E	J
frequency / pulse repetition rate	v	Hz
pulse duration	τ	ms
wavelength	λ	m
wave period	Γ	s
wave amplitude	A_o	m
time	t	s
irradiance	I	$MWcm^{-2}$
peak intensity	I_p	$MWcm^{-2}$
beam waist	w	m
beam radius	r	m
half angle far field divergence	ϕ	mrad
absolute temperature	T	K
power	P	W
peak pulse power	P_p	kW
focal length	f	m
thermal conductivity	C	m^2s^{-1}
thermal diffusivity	K	$Wm^{-1}K^{-1}$
electrical conductivity	σ	Sm^{-1}
optical skin depth	D	m
density	δ	kgm^{-3}
specific heat capacity	H_c	JK^{-1}
heat transfer rate	q	W
complex refractive index	$\tilde{n}$	-
extinction coefficient	k	-
reflectivity	R	-
absorptivity	A	-
transmissivity	$\mathcal{I}$	-
reflectance	R_{ance}	-
absorptance	A_{ance}	-
surface tension	σ	Nm^{-1}

Table 1.2 Major units and symbols

14

1.6.2 Terminology

The terms transmissivity and transmittance, reflectivity and reflectance, absorptivity and absorptance occur widely in the text. In the published literature, these terms are sometimes misused, hence for clarity in this text, the following convention is used: Transmissivity, reflectivity and absorptivity are intrinsic properties of a material, and are derived from basic laws. Transmittance, reflectance and absorptance are quantities measured for real surfaces.

1.7 Objectives

The initial objective of the programme was to develop a consistent low power pulsed laser surface melting process for aluminium alloys.

It became clear that the main barrier to this objective was the occurrence of certain processing variable thresholds and irregularities on the surface of the laser melt spots and hence it was necessary to understand and control these.

2. Laser light

This chapter aims to give a brief overview of the aspects of the theory of light and its propagation which are relevant to laser light. The specific characteristics of laser light which are important to the understanding of this work are discussed.

2.1 The electromagnetic spectrum

An electromagnetic wave can be characterised by its frequency or by its wavelength. The electromagnetic spectrum is the collection of electromagnetic waves of all frequencies. Various regions of this spectrum are referred to by particular names, because of the differences in the way they are produced or detected. Fig. 2.1. shows part of the electromagnetic spectrum, along with approximate boundaries of some of the various regions.

The narrow range of electromagnetic waves from approximately 380 to 780 nm is capable of producing a visual sensation in the human eye, and is properly referred to as "light". This visible region of the spectrum is bounded by the invisible ultraviolet and infrared regions, as shown. The three regions taken together comprise the optical spectrum—the region of special interest in the area of optics. It should be noted that the divisions between the regions are arbitrary. It is important to recognise that the particular type of laser being used in this work has a wavelength of 1.06 μm radiation and is therefore in the near infra red section of the spectrum given below. This has very important implications as shall be demonstrated.

λ in m	Frequency in Hz	
10^{-14}	3×10^{22}	
10^{-12}	3×10^{20}	Gamma rays
10^{-10}	3×10^{18}	X-rays
10^{-8}	3×10^{16}	(Far) Ultraviolet (Near)
10^{-6}	3×10^{14}	Visible light (Near)
10^{-4}	3×10^{12}	Infrared (Far)
10^{-2}	3×10^{10}	Microwaves
1	3×10^{8}	
10^{2}	3×10^{6}	Radio waves
10^{4}	3×10^{4}	
10^{6}	3×10^{2}	
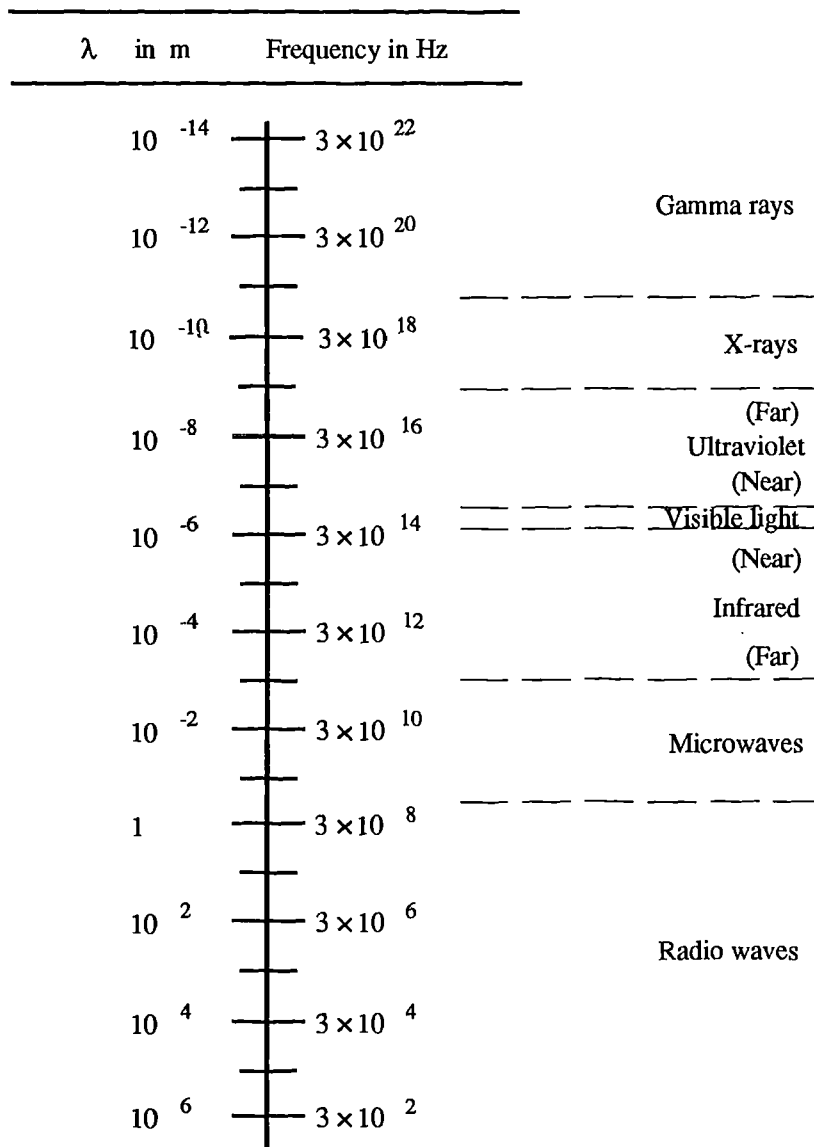
Figure 2.1 The electromagnetic spectrum

2.2 Wave nature of light

Light can be described as coupled oscillating electric and magnetic fields, propagating through space. These oscillations are sinusoidal in nature, as depicted in Figure 2.2. In terms of its basic nature, light is electromagnetic radiation, and in specific cases, these terms can be used interchangeably. The period, Γ, of an oscillation is the time taken to complete its cycle, as shown in fig.2.2. A continuous stream or wavetrain of oscillations constitutes a *wave* and if the oscillations are of identical period the wave is periodic. As such light is said to be made up of electromagnetic waves.

The amplitude, A_0, of a periodic wave is the maximum displacement value. The frequency, v, of a periodic wave, of period Γ, is given by

$$v = \frac{1}{\Gamma}$$
<div style="text-align: right">**Equation 2.1**</div>

where v is the rate of oscillation of the wave in Hz.
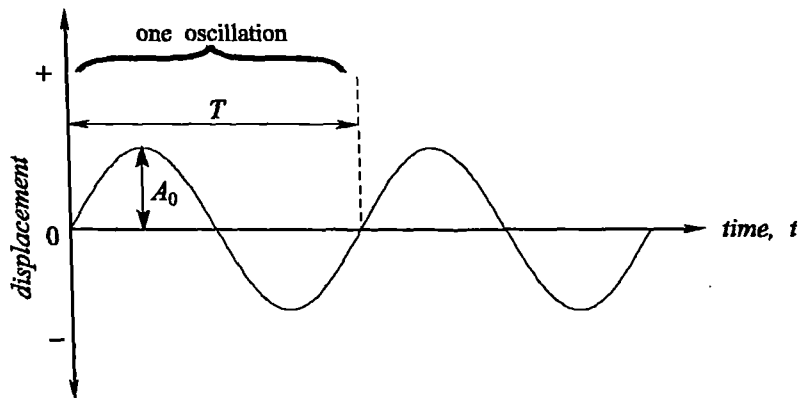
Figure 2.2 The sinusoidal waveform

2.2.1 Fundamental properties of light

Light can only be produced by accelerating charged particles (e.g. an electron changing energy level in an atom) and it has the following fundamental properties

- The electric and magnetic fields, and the direction of propagation, are mutually perpendicular - and their directions relative to each other are fixed

- the electric and magnetic fields are in phase, and their magnitudes are closely related (with one being determined by the other)

- the electric and magnetic field oscillations carry energy in the direction of propagation

- the propagation speed, c, is approximately 3×10^8 ms^{-1} in free space and as long as there are no obstacles, light propagates at this speed c along the original direction of propagation.

The first two properties are illustrated in fig.2.3, showing the electric and magnetic field intensities along the direction of propagation.

For two oscillations to be in phase at some point in time means that they each have completed the same fraction of their respective cycles, at that point in time. Note that here, a cycle is arbitrarily defined to start at zero displacement, with positive displacements immediately following.
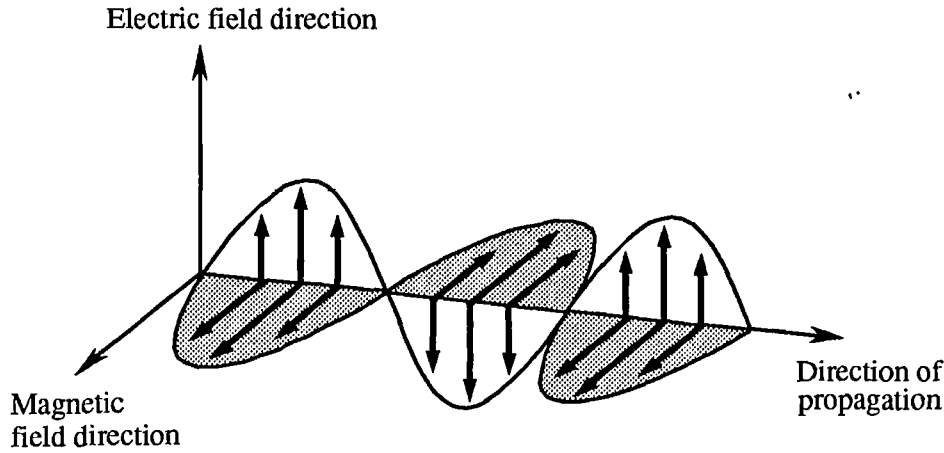
Figure 2.3 Electric and magnetic field intensities associated with an electromagnetic wave

The wavelength, λ, of an electromagnetic wave is given by;

$$\lambda = c\Gamma = \frac{c}{v}$$

Equation 2.2

and represents the distance (in the direction of propagation), between successive points in phase.

2.2.2 Particle nature of light

When light is emitted or absorbed by matter, it exhibits a particle (or corpuscular) nature and hence to understand the nature of the interaction of a laser beam with a surface, this aspect of the nature of light must be pursued.

Atoms or molecules can generally exist in more than one state. These possible states are quantised, each state has a certain energy level and changing from one state to another means a change in energy level by a discrete amount. Atoms or molecules therefore emit or absorb light only in discrete energy packets, or quanta, known as photons. In the particle (or corpuscle) theory, electromagnetic radiation is said to consist of streams of photons. The photon has associated with it the wave properties of

the radiation; frequency, wavelength, propagation speed, polarisation and phase. The energy, E, of a photon is proportional to the frequency of the radiation, v, namely,

$$E = hv$$ **Equation 2.3**

The constant of proportionality, Planck's constant, h, has the value of approximately

$$6 \cdot 63 \times 10^{-34} \, \text{Js}$$

Photons behave like particles because they have a momentum, p, given by,

$$p = \frac{E}{c} = \frac{hv}{c}$$ **Equation 2.4**

This means that although light impinging on a surface can exert a radiation pressure, photons have zero rest-mass, which distinguishes them from particles like electrons and neutrons. For this reason, no significant momentum can be imparted to a target via the impingement of laser radiation in its own right.

2.2.2.1 Wave-particle duality

Wave theory, although intuitively associated with light beams, fails to explain the emission and absorption of light, but succeeds in explaining the interaction of light with light. However, the complementary particle theory explains light emission and absorption, but not light/light interaction (e.g. interference). This is known as the wave-particle duality of light, and hence a basic understanding of both aspects is necessary to proceed.

2.3 The special nature of laser light

The usefulness of lasers in Materials Processing comes from the unique properties of laser light - properties which are very different in some ways from conventional radiation sources. Any conventional light source is a generator of photons, the difference is that generally photons are randomly emitted in all directions. Even when they are directed by a reflector, they form a rapidly diverging beam of light in a wide range of wavelengths over the visible spectrum. In contrast, the photons from a laser have very similar wavelengths, and hence a laser beam can be emitted in a well

collimated (parallel) beam which diverges by a limited amount. This summarises the important basic properties of laser beams which now need to be examined in more detail.

A beam of light may be loosely defined as electromagnetic radiation consisting of a bundle of electromagnetic waves that is, as a whole, propagating along a single-line path which is the axis of the beam.

The frequency (or wavelength), and amplitude of electromagnetic waves have already been discussed. To describe light consisting of possibly more than one electromagnetic wave, other descriptors are also used. Coherence and monochromaticity are the most important of these in the context of this work and are now elaborated on.

As shall be shown, in laser terms, the beam used in this work has, as a result of the inherent limitations of solid state lasers, relatively high divergence and low brightness.

2.3.1 Coherence

A highly coherent beam may be defined as one that has good spatial and temporal coherence across any arbitrary plane perpendicular to the direction of propagation, therefore coherence describes the phase relationship between the electric field components of all the electromagnetic waves which constitute the beam.

If the phase at a point in space changes uniformly with time, then the light is said to show perfect temporal coherence at that point (fig.2.4c). This requires that the light be monochromatic, and thus temporal coherence is a measure of monochromaticity.

If instead, at a single moment in time, the phase of a set of points in space is the same, then these points exhibits perfect spatial coherence (see fig. 2.4b). Spatial coherence is a measure of the correlation of phases at points in space. Perfect coherence is not physically possible for a beam of light, due to unavoidable effects such as diffraction

Perfect coherence occurs for a set of points that have perfect spatial and temporal coherence, fig. 2.4a. Points that exhibit very little spatial or temporal coherence are said to be incoherent (see fig.2.4d).
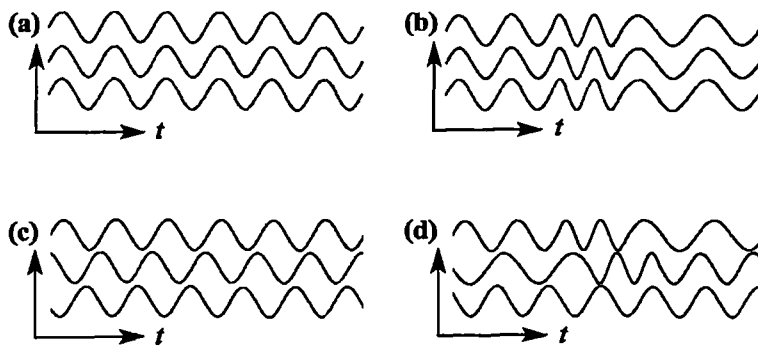
Figure 2.4 An illustration of coherence

Each figure shows the electric field history at three different points in space over a short period of time, i.e. the three distinct waveforms.

(a) shows perfect coherence. All the waves are in phase at all times, and have a constant frequency.

(b) shows perfect spatial coherence, with only partial temporal coherence. This is because all the waves change their phases by an identical amount through time.

(c) shows perfect temporal coherence, with no spatial coherence. All the waves have the same constant frequency, but are out of phase with each other.

(d) shows almost complete incoherence.

Laser radiation exhibits both spatial and temporal coherence. Spatial coherence can best be illustrated by examining the phase relationship between two points in space at identical times. If the electromagnetic waves at the two points are zero phase difference at time t = 0 and this is retained after some time interval, t, then perfect spatial coherence exists between the wavefront at the two points. When the electromagnetic field at the same point in space has the same phase at times t and t + τ, then one has perfect temporal coherence at that point. Temporal and spatial coherence are independent variables, one is possible without the other. Also, complete coherence is not possible, there are always degrees of spatial and temporal coherence. NdYag solid state lasers have relatively low temporal coherence (as distinguished from temporal energy distribution).

2.3.2 Monochromaticity

Monochromatic light consists only of electromagnetic waves of a single frequency. The monochromaticity of light is the degree of adherence to being monochromatic. In other words, the fewer the number of frequencies, or the narrower the frequency range, the higher the monochromaticity. Monochromaticity hence determines the spread of wavelengths or linewidth of radiation from a laser source. Due to the high monochromaticity of laser light, the light (and the laser that produced it) is often characterised by the wavelength which best describes its spectral composition.

Laser linewidth is a function of both the intrinsic width of the laser transition and the existence of a range of longitudinal cavity modes. These modes arise because the wavelength λ_n of standing electromagnetic waves in the laser cavity is quantified by;

$$\lambda_n = 2L\!\big/\!n \qquad\qquad \textbf{Equation 2.5}$$

where L is the cavity length and n is the no. of modes

Because of the relationship between cavity length and the resonant frequencies of the electromagnetic modes, the NdYag laser will always exhibit multi frequency operation.

2.3.3 Beam mode

To assist in the understanding of spatial coherence, the spatial profile of a laser beam must be explained. The spatial profile of a laser beam is determined by the geometry of the laser cavity. The shape of the cavity in a direction transverse to the optical axis provides boundary conditions on the wave equation that determines the permitted configurations of the electromagnetic field in the cavity. If this cross section is symmetrical, as in cylindrical or rectangular resonators, the spatial profile of the permitted Transverse Electromagnetic Modes (TEM's) is particularly simple. The method of identifying these modes is taken from waveguide theory, particular modes are labelled TEM_{mn} where m & n are the number of nodes on two orthogonal directions. Both cylindrical and rectangular geometry's have the TEM_{00} mode as the transverse modes of highest symmetry. TEM_{00} beams have the best focusing

characteristics of all, their focusing behaviour is diffraction limited. The TEM mode of the beam has a significant effect on the degree of spatial coherence present, with the uniphase mode possessing the most. In fact, true TEM_{00}, true Gaussian laser light is extremely coherent.

Intensity

TEM_{00}

$TEM_{01}*$

TEM_{10}

r (radial distance from optical axis)

optical axis
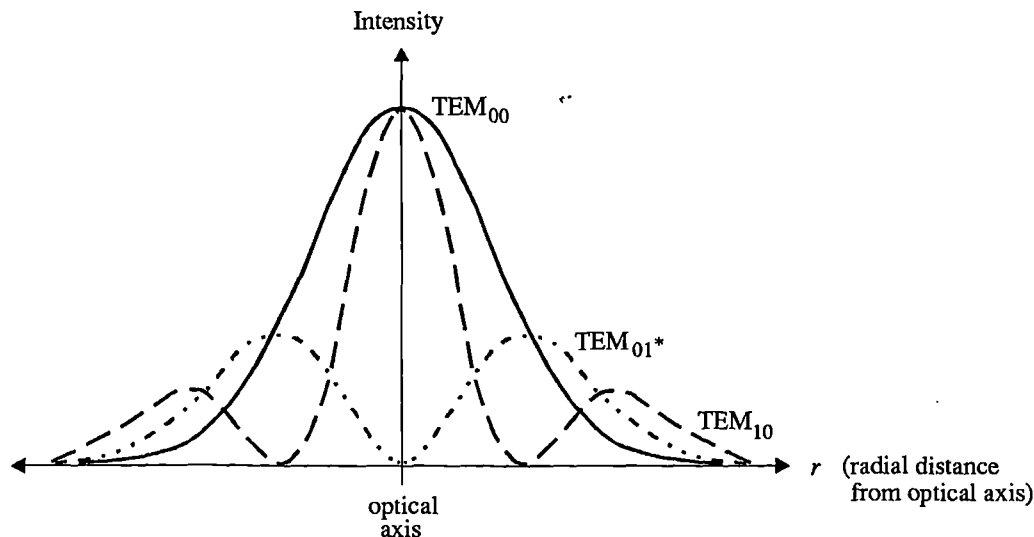
Figure 2.5 Intensity distributions of some transverse electromagnetic modes

Either side of a node, the phase and the direction of polarisation changes. This means that only the TEM_{00} mode has constant phase and polarisation direction across each of its transverse sections. For this reason the TEM_{00} mode is known as the uniphase mode. In most laser applications, it is this mode which is generally of most use, and so is regarded as the highest quality mode. However, high power solid state lasers such as those used in this work are classified as highly multimode and hence only approximately obey these rules. However, as the behaviour of these multimode beams is highly complex, the majority of optical design work is based on approximations to these gaussian mode relationships.

It is these special attributes of laser light that cannot be found in light produced by any other means. These various qualities of laser light are exploited in a whole range of fields such as medicine, holography, and, of course, materials processing.

2.4 The Gaussian beam

The TEM_{00} or fundamental mode has a very simple Gaussian intensity distribution—the maximum intensity is along the optical axis, which falls away exponentially, moving radially outwards from this axis. This mode is generally desirable for many laser applications, due to its uniform phase front, high peak intensity, and very low divergence. These two properties mean that Gaussian beams can be focused down to very small radii in theory, approaching the wavelength of the light, a beam such as this is known as diffraction limited. The location of the minimum diameter of a focused beam is called the focal spot. with consequent extremely high peak intensities on the target material. This makes them very useful for laser machining applications, particularly in laser cutting of materials.

An ideal beam refers to a beam that suffers no diffraction or absorption effects, and thus propagates according to geometric optics theory, with no power loss. Ideal Gaussian beams are much easier to handle mathematically than higher order mode or multimode beams. A good insight into the field distributions for all higher order beams can be gained from approximations to Gaussian beam field equations.

2.4.1 Transverse intensity profile

Fig. 2.6 shows a Gaussian intensity profile with rectangular co-ordinates (x,y).
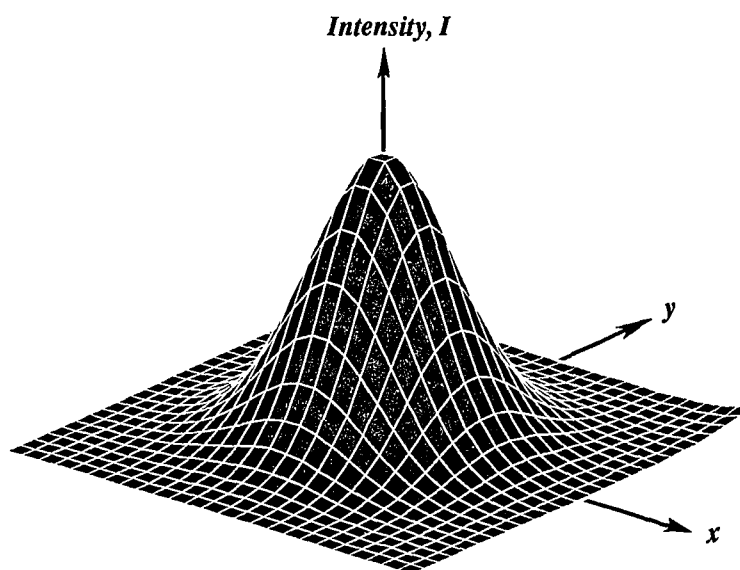
Figure 2.6 Three dimensional Gaussian intensity distribution

The exact equation in polar co-ordinates (R, θ) for the Gaussian beam transverse intensity profile is often given by the expression;

$$I(R) = I_0 \exp\left(\frac{-2R^2}{r^2}\right)$$

Equation 2.6

where $I(0) = I_0$ is the peak intensity (on the optical axis), and r is defined as the beam radius. This definition of beam radius is known as the $1/e^2$ radius, because it is the value of R where the intensity has fallen to the value I_0/e^2 (or equivalently where the beam field amplitude has fallen to $1/e$ of its on-axis value). The transverse intensity profile of the beam is therefore described by the intensity profile across a plane perpendicular to the axis of the beam. The beam will generally have intensity profiles that will vary along this beam axis.

2.4.2 Divergence of ideal Gaussian beams

The waist, w, of an ideal Gaussian beam varies along the optical axis, z, according to the equation:

$$w(z) = w_0\left[1 + \left(\frac{\lambda z}{\pi w_0^2}\right)^2\right]^{\frac{1}{2}}$$

Equation 2.7

where $w(0) = w_0$ is the beam waist, the transverse section of the beam with the smallest radius, and λ is the wavelength of the light. This equation gives the locus of the beam radius, as shown in fig. 2.7.
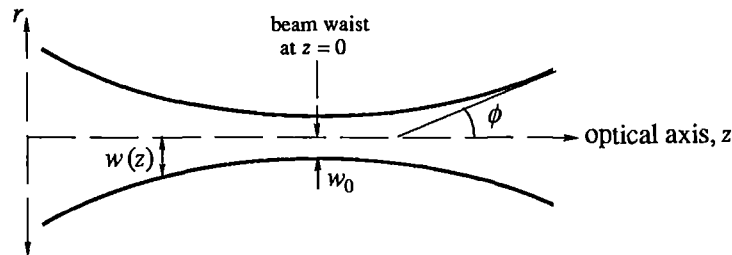
Figure 2.7 Spatial locus of Gaussian beam radius

The beam can be seen to diverge, though the Gaussian intensity distribution is maintained at all distances of z. The locus has asymptotes, which are approached in the far-field, which refers to regions associated with large magnitudes of z (i.e. large distances away from the beam waist). Equation 2.7 reduces in the far-field to

$$w(z) \approx \frac{\lambda z}{\pi w_0} \qquad \text{for } z \gg \frac{\pi w_0^2}{\lambda}$$

Equation 2.8

i.e. these are the far-field approximations to the equations of the asymptotes.

The angle, ϕ, between the optical axis and any one of the asymptotes (as illustrated in Figure 2.7) is known as the half-angle far-field divergence. This is given by

$$\phi = \frac{\lambda}{\pi w_0}$$

Equation 2.9

The measure of beam divergence usually quoted is that of either the half-angle far-field divergence or the full-angle far-field divergence (i.e. 2ϕ), the former being more widely used in industry, and hence is used in the current work.

Equation 2.9 shows that the divergence is directly proportional to the wavelength of the radiation, and inversely proportional to the beam waist radius. This means that, relatively speaking, longer wavelength beams with small waists are inherently highly divergent. As a consequence, there must be a trade off between minimising the divergence or minimising the waist radius. This definition of divergence is only valid for Gaussian beams, and the beam used in this work, in common with most high power solid state lasers, is multimode. In practice, this reduces the accuracy of calculations of focused spot sizes and also puts a lower limit on focused spot sizes.

2.4.3 Beam power

At some transverse section of a laser beam, the total power, P, and transverse intensity profile, $I(x, y)$, of a laser beam are closely related. If the beam suffers no propagation power losses (due to absorption or scattering effects) then P is independent of displacement, z, along the beam axis. In this case, P is the integral of $I(x, y)$ over its transverse-sectional area, A, for any z, and the power of a Gaussian beam can be found by integration of equation 2.6 according to the equation:

$$P = \int_A I(x, y)\, dA$$ **Equation 2.10**

For a transverse intensity profile, with peak intensity, I_0 , and $1/e^2$ beam radius, r, the power P is given by,

$$P = I_0 \left(\frac{\pi r^2}{2} \right)$$ **Equation 2.11**

This equation shows, that as the beam spreads (or w increases) the peak intensity must necessarily drop, because P is a constant for an ideal beam. It is therefore clear that for a given power, to attain high intensities in the beam, r and w should be as small as possible. Lenses can be used to reduce the beam radius and hence to produce just such increases in intensity. It can also be shown that the power contained within the $1/e^2$ radius is always $P \times \left[1 - (1/e^2) \right] \approx 0 \cdot 865 P$, i.e. ~ 86·5% of the total power. This leads to an alternative definition of beam radius, which is particularly useful for higher mode beams, for which the $1/e^2$ radius has little meaning. In this definition, the beam radius is simply the radius that contains ~ 86·5% of the total power.

2.4.4 Gaussian beam focusing

A good approximation for w_f, where w_f is the beam waist at focus and w_0 is the beam waist before entering the focus lens can be made,

$$w_f \approx \frac{f \lambda}{\pi w_0} = f \phi$$ **Equation 2.12**

where ϕ is the half angle far field divergence of the unfocused beam and f is the focal length of the lens. In practice these approximations are often used, and can be found in most texts on laser optics. Equation 2.12 therefore gives a good indication of how the focal spot radius depends on the lens focal length, the wavelength of the light, and the unfocused beam radius. For a given wavelength, the focal length should be as small as possible, and the unfocused beam radius should be as large as possible, in order to minimise the focal spot radius. Also, the shorter the wavelength of the light, the smaller the minimum possible focal spot sizes. In another words, the smallest spot

sizes (and highest intensities) are achieved with low divergence, short wavelength beams, focused by lenses of short focal length. In practice however, short working distances and a small depth of focus are serious disadvantages associated with using short focal length lenses, and as usual a compromise is reached. In this study, the compromise reached was a lens of 80 mm focal length and a beam diameter of 18 mm. The choice of this beam diameter was determined from previous work [11] which showed a performance maximum, probably associated with the design of the beam expanding telescope.

2.4.5 Depth of focus

It is always desirable to know how critical it is to have the beam exactly focused at some reference position, in terms of the beam intensity and radius, at that position. This is particularly true in this work and in the case of most practical laser processing where the actual focus position is usually determined in a fairly arbitrary manner from the measurement of the effective spot diameter of the target spot on the workpiece. The depth of focus, Δ, is a measure of the distance, over which the focused beam intensity profile remains 'fairly similar' to the intensity profile at the focal spot. It can be defined as the distance over which the focused beam radius changes by some percentage, p_w, from the focal spot. Using this definition, manipulation of equation 2.7 yields

$$\Delta = \pm \frac{\pi w_f^2}{\lambda} \sqrt{\left(\frac{100 + p_w}{100}\right)^2 - 1} \qquad \text{Equation 2.13}$$

for a Gaussian beam.

The value of p_w chosen, depends on the accuracy of focus that the application requires. For $p_w = 5\%$ (equivalent to a 10% decrease in peak intensity, I_0), for instance, equation 2.14 simplifies to

$$\Delta \approx \pm \frac{w_f^2}{\lambda} \qquad \text{Equation 2.14}$$

2.5 Non gaussian beams

There are some lasers which operate in a wholly TEM_{00} mode, and may produce beams that can be modelled accurately by the Gaussian beam equations given above. However, few lasers do operate in just this mode, and in particular, high power solid state lasers most certainly do not operate in this mode. These beams have, everywhere in space, a greater diameter and divergence than the 'equivalent' TEM_{00} mode. As a result most laser beams cannot be competently described by the Gaussian beam equations. Beams that deviate from the ideal Gaussian form can be modelled by introducing a quality factor, the M^2 factor. Some authors prefer to use a value Q to express this same measure of beam quality

In order to define this quality factor, it is preferable to use the alternative definition of beam radius, defined in section 2.4.3, that radius that contains ~86·5% of the total power. This definition is consistent with the $1/e^2$ radius for Gaussian beams, as discussed above. Hence, it is reasonable to keep the same notation scheme for beam radii under this alternative definition. For any beam suffering no scattering effects, the product of the beam waist radius and the far-field divergence is a constant. This constant is related to the beam quality, or closeness to the Gaussian form. The larger this constant, the lower the quality of the beam. For a Gaussian beam this constant is simply the wavelength divided by π, i.e. rearranging equation 2.9, we have

$$\text{Gaussian beam constant} = \phi w_0 = \frac{\lambda}{\pi} \qquad \textbf{Equation 2.15}$$

The M^2 factor is widely used in industry because of the ease with which it can be measured, simply from taking two measurements of beam diameter at known locations.

2.5.1 Directionality and divergence

Lasers are generally designed so as to produce a highly directional beam of light. This means that the beam propagates in a very precise, predictable direction and all laser beams generally therefore have very good pointing stability.

Laser beams also propagate with a minimum of angular spread, or divergence. There are two distinct causes of beam divergence —

1.   the light rays leaving the laser cavity will be non-parallel if the cavity has a non-planar mirror. This can be explained by the law of reflection, which can describe the ray directions after reflection at a curved mirror

2.   there are inevitably diffraction effects caused by the laser optics (mirrors and lenses, etc.) and the propagation media.

Divergence cannot be completely eliminated, because diffraction cannot be avoided. The further impracticality of finding correctly shaped, aberration-free optical components, worsens the situation still more. Beam divergence is generally smaller for lower order beams, with TEM_{00} having the least divergence. The practical effect of this is that high powered laser beams can be focused down to small spots, generating a high intensity on the workpiece. This topic is discussed in more detail in the next chapter.

3. The Laser

The basic function of a laser is to convert energy into a high energy density beam of light photons.

3.1 Laser beam generation

The core of every laser, known as the laser resonator, is where this generation of photons occurs by stimulated emission and amplification. In our case, stimulation occurs when electrons are excited by an external pumping source such as a flashlamp. It is the atomic process of stimulated emission (cf. section 1.1) that was predicted by Einstein in 1917 [1]. It is also this phenomenon that permits lasing and the production of a laser beam to occur. This requires the following three key processes, and although these are not truly separate processes in that they are occurring simultaneously, they are treated separately here. As only solid state lasers were employed in the experimental work in this project, this type of laser is used to demonstrate the principles involved, although much of the theory is generally applicable to all other laser types.

3.1.1 Absorption

This initial stage in the process of generating photons requires a source of electrons that have several available transitional energy levels. In our particular case of the solid state laser, this is ensured by the presence of Neodymium (Nd) ions, to a concentration of approximately 3%, within an Yttrium Aluminium Garnet (YAG) glass. An energy level diagram for the Neodymium ion is given below. The complexity of the spectra of the rare earth ions in these solids is due to the fact that possible $4f^n$ electronic configurations give rise to many different electronic states. In the Nd^{3+} ions these $4f$ electrons also have sharp transitions and this transition energy is not highly sensitive to the nature of the host crystal. The laser line at 1064 nm is the transition in Nd^{3+} between 4F3/2 and 4I11/2 states. Other laser transitions are;

4F3/2   4I9/2, λ = 946 nm

4F3/2   4I13/2, λ = 1319 nm

4F3/2   4I15/2, λ = 1833 nm

The emission of Krypton and Xenon lamps, (these types of lamp are typically used as high power photographic flashlamps) produce energy bands which overlap those of the Nd^{3+} ions and when the Nd:Yag crystal is "optically pumped" using these types of lamps, absorption occurs, and numbers of electrons are raised to an excited state.
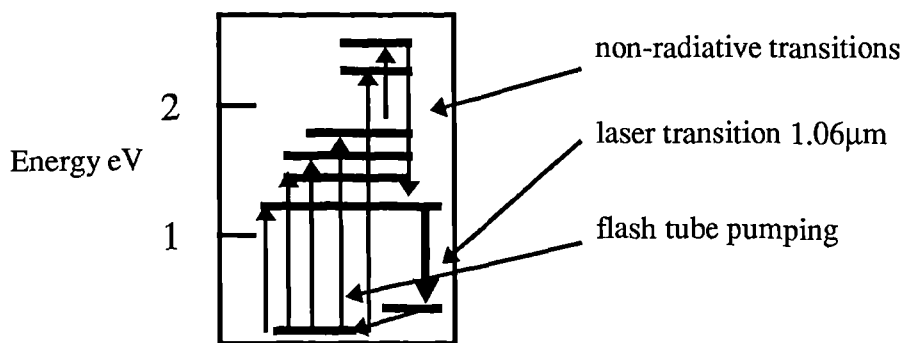
Figure 3.1 Energy levels for Neodymium ions

3.1.2 Spontaneous and stimulated emission

Having produced these metastable electrons, they may then revert to their former state by the spontaneous emission of an photon, which in the case of the solid state laser will have a wavelength of 1.06 μm and its direction is dictated by chance. One of these photons will, again by chance, be travelling down the optical axis of the cavity and will start oscillating between the two mirrors which make up the cavity. During this time, it will inevitably strike a molecule which is already excited, causing this to also release its energy and thus emit another photon of identical energy (and hence wavelength). These two photons, now travelling in the same direction in phase create an avalanche effect and hence the amplification necessary. The excited state becomes depleted but according to the Bolzmann distribution, this state is replenished, giving a good conversion of electrical energy into the upper state.

$$n_i = C e^{-E/kT}$$ Equation 3.1 Bolzmann distribution

where n = number of molecules in energy state i,

C = constant

E = energy of state, J

k = Bolzmann constant, 1.38×10^{-23} JK^{-1}

T = absolute temperature, K

3.1.3 Population inversion

Another condition is necessary, the excited state should be slow to undergo spontaneous emission and the lower energy state should be faster. This allows a "population inversion" of the excited species to occur, making a medium which produces more stimulated emission than absorption, more excited species than unexcited species exist. This condition is known as population inversion.

Quantum efficiency is around 40% but the operating efficiency is low because only a proportion of the radiation from the broad band illumination is able to excite the neodymium ions in the crystal - it lacks the natural coupling that occurs between the carbon dioxide (CO_2) & nitrogen (N_2) in the CO_2 gas laser. It must be noted that the laser line at 1.06 μm is relatively narrow hence most of the laser power emerges at this wavelength. This average power capability is second only to CO_2 laser operation, although at a much lower overall efficiency, (typically ~ 4%). Because the energy levels for the CO_2 laser transitions are lower, emission occurs at a longer wavelength, 10.6 μm, in the far infra red.

3.2 Principal components of a laser

There are three principal components that are required to practically create the above conditions and to make a functional laser:

1. an external energy source or pump

2. an amplifying medium

3. an optical cavity or resonator.

These basic elements are illustrated in fig.3.2.

3.2.1 The pump

The pump is an external energy source that produces the population inversion in the laser medium. Pumps can be optical, electrical, chemical, or thermal in nature, so long as they provide energy that can be coupled into the laser medium to excite the atoms to create the required inversion.

3.2.2 The amplifying medium

The amplifying medium or laser medium is an important part of the laser device, with many lasers actually being named after the type of medium they use. The laser medium, which may be a gas, liquid, or solid, determines the wavelength of the laser radiation. The most important requirement of this medium is its ability to support a population inversion between two energy levels of the laser atoms.
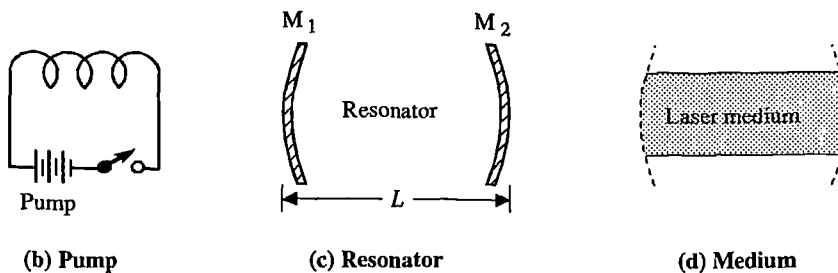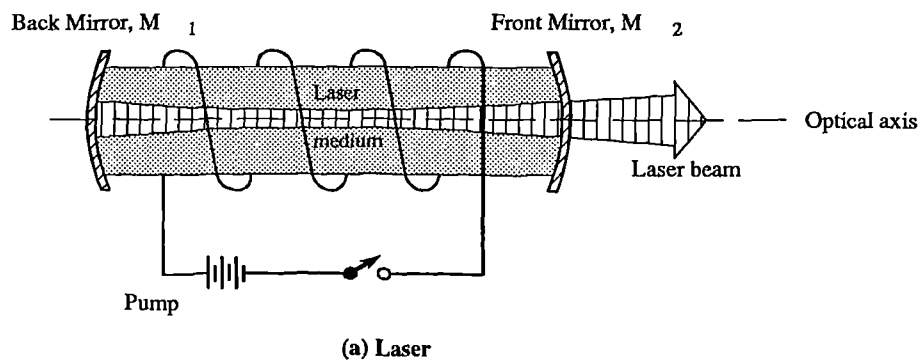
Figure 3.2 Basic elements of a laser

(a) Integral laser device with output laser beam. (b) External energy source, or pump. The pump creates a population inversion in the laser medium. It can be an optical, electrical, chemical, or thermal energy source—the battery and helix picture are only symbolic. (c) Empty optical cavity, or resonator, bounded by two mirrors, M_1 and M_2 with length L separating them. (d) Active cavity, or laser medium.

3.2.3 The resonator

Given a suitable pump and a laser medium that can be inverted, the third basic element is a resonator—an optical "feedback device" that directs photons back and forth through the laser medium. The resonator, in its most basic form, consists of a pair of carefully aligned plane or curved mirrors centred along the optical axis of the laser system. One of the mirrors is chosen with a reflectivity as close to 100% as possible (in the appropriate frequency range). The other is selected with a reflectivity somewhat less (around 90%), in order to allow part of the internally reflecting beam to escape and become the useful laser output beam. This partially reflecting mirror is termed the front mirror, with the other being termed the back mirror. The mirrors can be either circular or rectangular, giving rise to circular symmetry or rectangular symmetry of cavity respectively.

The resonator must also be correctly designed in order to produce a beam of the correct wavelength for the lasing medium. The length of the resonator should be such that the laser beam traverses an integral number of the desired half wavelengths. Any variations in this distance, due to thermal expansion or mechanical vibrations, may cause the laser to vary its output wavelength. Thermal expansion of the resonator components is usually controlled by water cooling.

3.3 Main laser types

Since the invention of the first lasers, many different types of laser have been invented and developed, using many different lasing materials, emitting radiation over a wide range of wavelengths. These range from the ultraviolet to microwaves at the opposite end of the spectrum. These lasers are usually split into a number of fundamentally different types on the basis of the physical state and the nature of their lasing medium, their principle wavelength, as well as the usual modes of oscillation. Because copper vapour and excimer lasers do not fit easily into the categories overleaf, they are not included in table 3.1. Other main types are summarised below;.

Ion	Matrix	Principal Wavelength	Usual Modes of Oscillation
Cadmium	Helium	441.6 nm	continuous wave (cw)
Argon	-	514.5 nm	cw, pulsed, mode locked
Neon	Helium	632.8 nm	cw
Chromium	Aluminium oxide (Ruby)	694.3 nm	pulsed, Q switched
Gallium arsenide	-	905 nm	pulsed, cw
Neodymium	YAG	1.064 μm	cw, repetitively
Carbon dioxide	Nitrogen	10.6 μm	cw, Q switched, repetitively pulsed

Table 3.1 Summary of some of the main types of laser

Q (Quality) switching refers to a technique for rapid shuttering of the laser pulse to obtain very high peak powers.

Apart from CO_2 gas & Nd:Yag solid state lasers, the current power output limitations on all the above lasers restricts them to what are generally classed as scientific, as opposed to industrial applications. Currently, solid state and CO_2 gas lasers are the only laser types capable of producing the high average powers necessary for the type of industrial laser processes of interest here. Other applications, generally classed as scientific applications, are also not included.

As the basic differences between the two types have been identified, more detail on their important features, along with the relative materials processing advantages and disadvantages are discussed. Again, the emphasis is on the solid state laser, as for reasons which will become apparent, this is the most appropriate laser type for the application under study. This is despite the fact that the majority of the scientific literature explains the nature of laser light by using CO_2 gas lasers as examples but it must be noted that most of the basic principles involved are relevant to all laser types.

In most material processing applications the laser must be reasonably powerful to obtain industrially relevant cycle times and to process materials of a thickness suitable for application in a wide range of engineering industries [12]. This limits the possible choice of laser to that of either the carbon dioxide or the Nd:YAG. Generally, the highest power lasers are required for the highest throughputs.

3.3.1 High power industrial lasers

There are many materials which can be made to show the stimulated emission phenomena, but only a few with a significant power capability. The natural coupling which occurs between the nitrogen and CO_2 gases in the CO_2 laser creates very high conversion efficiencies from electrical to laser power (~ 12%) and hence very high powers are possible by increasing the volume of lasant by various techniques. This fact alone accounts for the very widespread use of CO_2 lasers. In the case of solid state lasers, the broad band optical illumination only couples inefficiently into the YAG crystal, hence considerable energy has to be pumped into the rod. Not only does this give a serious cooling problem, but also because of thermal stresses, the power output from a single rod or crystal is limited to approximately 400 watts. Recently, higher power, multi rod continuous wave systems are becoming available which have addressed some of the these limitations. There are currently no other laser mediums that approach these two systems in terms of power output, and it is ultimately, operation at high average power which makes lasers suitable for high speed industrial laser processing that is of concern here.

As shown in section 1.2, the largest group in terms of both numbers and value of lasers sold is the carbon dioxide gas laser. This laser produces a beam of 10.6 μm wavelength and is widely available at average powers up to several kilowatts - hence its current dominant position in the laser marketplace. Secondly, the solid state laser, which produces a beam of 1.06 μm, is currently available at average powers up to 4000 watts [13], although versions up to 400 w are more commonly available from a number of suppliers. Another of the important advantages of Nd:Yag is that they can be operated in the pulsed, continuous wave (cw) or Q switched mode.

These two broad groupings, as well as being based on the nature of the lasing medium, are also based on the different output wavelengths of the laser, which as

shown in chapter 4, has some important effects on the interactions of the beam with the target material.

Of the large amount of research output on industrial lasers and industrial laser processing, almost all lean heavily towards processing with higher power carbon dioxide lasers. The same bias is reflected in the academic fields of theoretical analysis. Much less information, in terms of both practical processing information and theory is available on the less widely used solid state lasers. However, having for completeness introduced the two main types of industrial laser, the solid state laser is discussed from hereon in more detail. This is because as shown later, this laser is the only appropriate type for this study. The relevant areas of laser theory and practice will therefore be covered with emphasis on the solid state laser, but with reference to CO_2 lasers where necessary.

3.3.2 Solid state lasers

The first successful commercial laser was a solid state ruby laser, and it was not until some time later when the CO_2 gas laser and other solid state hosts were developed, overcoming the strength limitations of Ruby, that this type of solid state laser was superseded by other types. The Ruby laser is therefore worthy of a brief mention as the classic example of a solid state laser.

3.3.2.1 Nd:Yag

Nowadays, by far the most widely used solid state laser is the Nd:Yag, which works in a similar manner to the ruby laser. The particular case of the solid state laser was used earlier to describe basic laser principles, but some further relevant points need to be made. Since the Nd:Yag is a four level system, the pumping requirements are modest and for pulsed operation can be met with a fairly simple flashlamp and reflecting cavity. The optical pulse from the flashlamp lasts in the order of 0.5 - 20 ms, and it usually takes ~ 0.5 ms for population inversion to be achieved.

The relatively high thermal conductivity of the YAG (Yttrium Aluminium Garnet) host material aid dissipation of heat in the laser cavity. Many of the attractive characteristics of this type of solid state laser, such as high output power and high pulse repetition rates, originate from the useful combination of properties available from this host material, making it still the material of choice for high power solid state lasers.

High pulse energies, from 200mJ up to 100 J are widely available and peak powers can be very high indeed, up to 20 kW is readily achievable. Pulse repetition rates up to 300 Hz are typical and average powers of approximately 400 watts from a single rod system is usual. Indeed, the factor which determines the maximum average power output from a single rod is the maximum diameter of rod available. This is itself largely determined by the magnitude of the maximum thermal stress which may be induced in the rod without fracture. However, these thermal stresses also generate non uniform heating of the rod, with consequent refractive index differences and beam distortion or 'thermal lensing' [14].

3.3.2.2 Resonator design
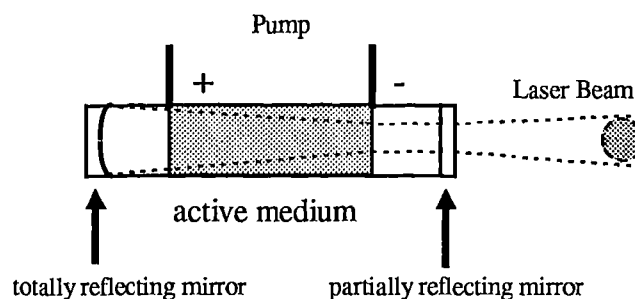
Figure 3.3 Stable cavity, standard resonator

The basic design problem of conventional solid state lasers is to get as much of the optical pumping into the laser medium and to cool it in such a way that the medium does not distort or break. To assist in this, cooling water is flowed over the outside of the optical cavity and the laser rod is encased in a transparent tube. This is to avoid excessive absorption of flashlamp energy by turbulent water which creates optical distortion and imaging problems.

The overall layout of a typical solid state laser is shown in Figure 3.3. The cavity design is fairly standard with plane mirrors at each end of the resonator cavity. The YAG crystal is suspended in the two piece laser reflector which is in this case constructed from alumina ceramic, and is contained within a stainless steel pumping chamber. This chamber also contains the two linear flashlamps with the YAG rod lying along the focal lines of the elliptical reflector. The rear mirror is 100% reflective and the front, 60%. This is the core of the laser, and is referred to either as the laser oscillator, resonator or laser cavity.

It is here that oscillation starts from noise or spontaneous emission, some of which travels perpendicular to the mirrors and hence is fed repeatedly back and forward and is amplified. These repeated passes through the resonator gives rise to a directional, spectrally narrow output beam, some of which is allowed to pass through the partially reflective front mirror.

3.3.2.3 Fibre optic beam delivery

The other major advantage of the solid state laser, again purely due to its short wavelength, is the relative ease with which the beam may be passed along fibre optic cables. The recent availability of reliable fibre optically delivered solid state laser power has led to increasing competition in some areas between the two types of laser. It appears currently that this competition is most apparent in the automobile industry, where the total system cost and manufacturing flexibility benefits of using a laser / fibre optic cable / robot installation are significant.

3.4 Laser machining systems

The implementation of any laser machining process, machining in this sense covering laser cutting, welding, drilling and surface treatment, requires the integration of a number of optical, electrical, and mechanical components into a machining system. This system usually includes four major subsystems for beam generation, beam delivery, and workpiece positioning, and the remaining auxiliary devices. Beam generation is accomplished within the laser device, as discussed in detail earlier, although on / off devices, i.e. shutters, are required.

3.4.1 Beam delivery

In most cases the beam delivery system consists primarily of optical components which focus the laser beam onto the workpiece surface. The major components are mirrors and focusing lenses and in certain cases, beam polarisers and beam splitters. For all but the very highest power solid state lasers, transmissive optics are used and water cooling is generally unnecessary. A brief discussion is given below of the most relevant components for laser processing equipment, mirrors and focusing lenses

3.4.1.1 Focusing optics

During system design, transmissive or reflective optics may be chosen (i.e. lenses or mirrors) to focus the beam. In solid state systems, transmissive optics are used exclusively for focusing and reflective optics are used for beam steering. Both lenses and mirrors for YAG systems are generally anti-reflection (AR) coated so that when suitably coated, virtually all the incident light will be transmitted, reducing reflection losses from 2.5% to typically 0.5%

3.4.1.2 Mirrors

Although conventional coated mirrors are used for most solid state laser applications, metallic mirrors are generally used in very high power beam delivery systems for CO_2 lasers. Since metals generally have high reflectivity, the energy loss from the laser beam to the mirror is minimal. Metallic mirrors can also withstand high energy densities without thermal damage, because of the high thermal conductivity of most metals.

3.4.1.3 Lenses

Conventional high quality optical glass lenses for 1.06 μm light are relatively inexpensive and widely available. A silicate grade known as BK 7 is most widely used for standard components.

3.4.2 Workpiece positioning

The workpiece is necessarily attached to a table of some sort. Whether it is the table that moves, or the laser, or the optics, the movement must be smooth and be capable of high speeds and accelerations. High acceleration is required so that the machine does not 'linger' in the corners of the path profile reducing the cut quality in these areas.

To take advantage of the inherent accuracy of the laser, the machine accuracy should be of the order of 50-100 μm for precision machining work [15], although this depends to a certain extent on the type of application area and the length of the axes concerned .

3.4.3 Auxiliary components

Auxiliary components include equipment not used to direct the laser beam or position the workpiece. The components are used in support of the laser machining process, and include protective windows, gas jet nozzles, and safety equipment, etc. Computer numerical controllers (CNC's), and beam measurement equipment are included under this definition.

3.4.3.1 Laser head

A laser head is used to enclose the focusing laser beam, the focusing optics, a protective window (if used), and to direct an assist gas jet or a cover gas jet, depending on the application, towards the processing area, via a gas nozzle. This nozzle will itself reduce the amount of back-spatter reaching the lens.

3.4.3.2 Protective windows

Protective windows are used to protect the beam delivery optics from back-spatter and dust, etc. In the case of solid state laser systems, a standard optical quality glass slide can be used with no detriment to the beam apart from some reflective losses.

3.4.3.3 Coaxial gas

In most laser processing applications, there is a need to provide a co-axial gas with the beam. This simplifies processing and makes welds more consistent more uniform. There are many reasons for this;

- it provides an inert atmosphere for the melting and solidification processes to take place

- in the case of CO_2 lasers it helps prevent molten material and vapour from contaminating the focusing lens but in the case of solid state lasers, a cover glass is normally provided for this purpose

Various gases are used, such as nitrogen (N_2), helium (He), argon (Ar), oxygen (O_2), and compressed air. Each has its uses, though cost is a major factor in the choice of gas to be used.

3.4.3.4 Gas jet nozzle

The design of the nozzle can play an important role in the gas jet effectiveness [16], although this is more relevant in the case of the higher gas flow rates required for cutting and drilling processes. Nozzle-exit shape and size, for example, can have a substantial influence on the gas jet behaviour.

3.4.3.5 CNC

The CNC controlling a system must be capable of carrying out a stored program correctly, and of moving the relevant component—be it laser, workpiece, or optics—smoothly in the desired way. CNC's are available specifically tailored to laser-processing—controlling assist-gas selection and pressure, laser power settings, pulse settings, focus adjustment, etc. Off-line programming is common, with data being downloaded via direct link or floppy disc [17].

3.4.3.6 Beam measurement equipment

Beam measurement equipment is used to gain knowledge of the total power or in the case of more complex equipment, even the intensity profile (and hence radius), of the beam reaching the workpiece. In a laser system with several optical components in the optical train, the laser power may be reduced by 20% or more, between the laser resonator and the workpiece. As in the current study, most lasers come fitted with an integral power measurement device which samples a fraction of the beam present in the cavity. This can only give a good indication of the power leaving the laser device.

Power measurement devices may be, for instance, calorimetric, or pyroelectric based. The two problems faced with such equipment are, the lack of absolute accuracy, and the limited powers and intensities that they can handle. In addition, even though a typical device may itself produce self-consistent results, two different devices will often give different readings for the same sampled beam.

An example of a measurement device is in the use of pyroelectric detectors to obtain intensity profiles. These detectors respond only to variations in power, and not to power itself, thus it is necessary to move the device through the beam or to use a chopper wheel. The devices are fragile, expensive and susceptible to thermal overload, they are limited to lower irradiances of around $1 Wmm^{-2}$. There are other systems

available that can be used to measure greater intensities, but they require a great deal of expertise in their setting up and in the interpretation of the results they produce.

3.4.4 Pulsed solid state laser beam parameters

It is in this section that the very different approach required for processing with pulsed solid state lasers as opposed to continuous wave (cw) gas lasers emerges and requires explanation.

3.4.4.1 Temporal mode

All laser types operate in one of the two temporal modes, continuous wave (cw) mode or a pulsed beam mode. In continuous wave mode the laser beam is emitted without interruption, Figure 3.4a. In the pulsed beam mode, the laser beam is
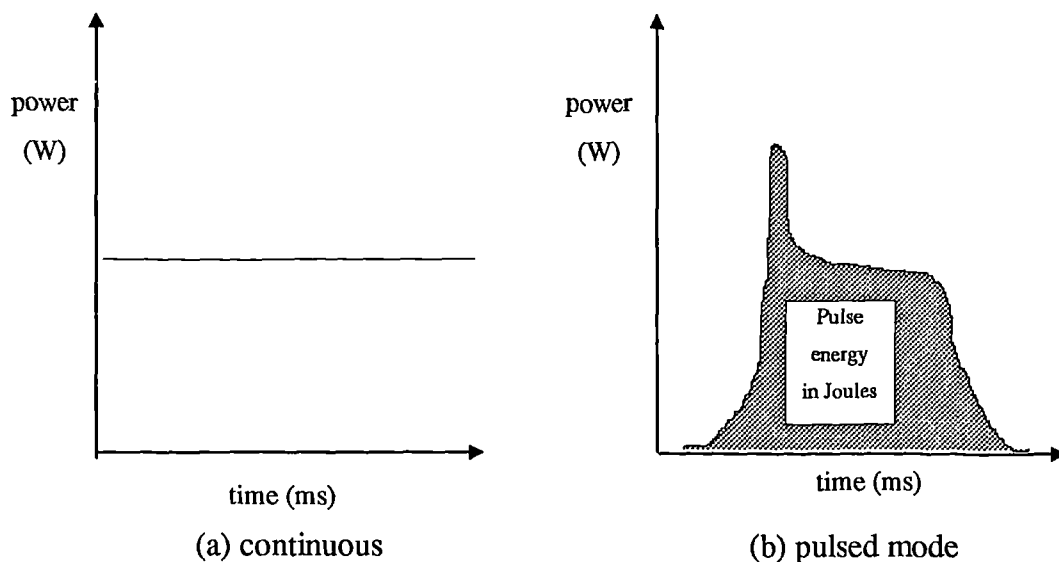
Figure 3.4 Schematic of laser beam temporal modes

emitted periodically, typically at relatively low duty cycles. An example of the temporal intensity behaviour of a pulsed beam is shown in Figure 3.4b.

High power solid state lasers are most commonly used in the pulsed mode. There are three important points to note here concerning processing with pulsed lasers;

- Firstly, there are a number of additional variables which need to be controlled as compared to processing with a continuous beam. These are the

pulse energy, pulse repetition rate (frequency) and pulse duration - their interrelationships are given in section 6.2.

- Secondly, depending on the type of solid state laser resonator used, the relationships between these variables can be either fixed within narrow limits, 'tuned' resonators, or independent of each other.

- Thirdly, most types of solid state laser allow direct control of pulse repetition rate and pulse duration, but the total pulse energy is controlled indirectly through the electrical input to the laser flashlamps.

There is also a further complication, due to the phenomenon of thermal lensing (cf. section 3.3.2.1), an increase in the input power to the flashlamps has the effect of increasing the divergence of the laser beam, with consequent changes in intensity at the workpiece. As shown later, it is sometimes necessary to compensate for this effect optically.

Many studies have highlighted the important practical laser variables with respect to CO_2 laser processing [18]. There are far fewer references which examine the effects of laser parameters specifically on processing with pulsed YAG lasers [19]. However, there appears to be a consensus that the parameters which are presented with their basic interrelationships below are the most important for pulsed laser processing [19].

3.4.4.2 Power

In the case of pulsed lasers, the average output power, P_0, is simply the product of the pulse energy, E in joules and the pulse repetition rate, v, in cycles sec^{-1} (Hz).

$$P_0 = v \times E \qquad \qquad \textbf{Equation 3.2}$$

For this type of laser, pulse duty cycles are typically fairly low, in the order of 5%, the beam is usually off for rather longer periods than it is on.

The overall effect of increasing the power is, as would be expected, to allow processing at faster speeds, although the relationship between beam power and maximum processing speed for a particular application is not always linear.

3.4.4.3 Peak pulse power

The most important difference between continuous and pulsed operation is described practically by the peak, or instantaneous power, Pp, of a laser pulse. Adapting the general equation 2.11 for our particular case of higher peak power pulsed solid state lasers, average power output, P is substituted by an averaged instantaneous peak power of the laser pulse, P_p, in kW. ·-

$$P_p = E/\tau \qquad\qquad \textbf{Equation 3.3}$$

where E is pulse energy and τ is pulse duration in milliseconds.

Although this approximation in calculating peak power inherent in equation 3.3 and figure 3.4 is recognised, because of its widespread acceptance in the field of solid state lasers, the approximation is used in this work. This peak pulse power figure may be up to a factor of 20 higher than the average power of a continuous laser beam, depending of course on the pulse energy capability and the duration of the laser pulse. Many high power solid state lasers are capable of 10 kW peak pulse power and above.

3.4.4.4 Pulse irradiance (intensity)

The concept of intensity was introduced in the previous chapter. Many sources have recognised the importance of this term [20,21] but the terminology is sometimes unclear and confusing. The terms intensity, power density, peak power density and irradiance have all been used in the context of pulsed solid state lasers. A more correct definition is now necessary because in practice, the nature of solid state laser power supplies means that many solid state lasers exhibit a very uneven temporal pulse distribution. This is very commonly not easily measured nor accurately known. In addition, the design of solid state laser resonators and the large number of modes generated therein lead to highly multi mode non gaussian spatially distributed beams. Any intensity figure is necessarily an average and is more correctly described as **pulse irradiance** delivered in the direction of the light propagation. It is arrived at by referring back to equation 2.11, and simply dividing this approximate peak pulse power figure, P_p, in kW, by the focused spot area. This term will be used hereafter in this work, will be denoted I, and is expressed in $MWcm^{-2}$ and is defined as :

$$I = \frac{P_p}{\pi \times \left(\frac{w_f}{2}\right)^2}$$ **Equation 3.4**

where I is pulse irradiance in MWcm^{-2}.

For highly multi mode beams, an approximation for the focused spot diameter is widely used;

$$w_f = \phi \times f$$ **Equation 3.5**

where w_f = focused spot diameter in mm, ϕ = half angle beam divergence in mrad, f = focal length of lens in mm

More precise calculations of spot size are difficult because of the significant deviations from gaussian behaviour demonstrated by multi mode solid state laser beams and precise measurement of high power focused laser spot diameters is again very difficult practically. A practical solution to this is presented in section 6.5.1.1.

It is now possible to improve our understanding of laser processing, pulse irradiance in our specific case and fluence (in Jcm^{-2}) in the case of excimer lasers, is most important to gain an understanding of laser processing phenomena. In practice, lasers are used for a wide range of processing tasks, and the irradiance required is matched to the process by the choice of optics train and the required process speed is generally matched to the average power of the laser. It is the intensity capability of a laser beam, its focusability, that makes a laser extremely useful in materials processing. Irradiances present in a typical focused laser beam are many orders greater than any light produced by a non-lasing source, and for melting and vaporisation are in the order of 0.1 - 10 MWcm^{-2}.

It should be noted that in the case of the resonator design used in this work (in common with most high power solid state lasers) increased laser output power is accompanied by an increased spread in the beam transverse intensity profile.

It is widely accepted that this term pulse irradiance decides the initial reaction of the material to the beam, and generally determines whether or not the beam will be absorbed or reflected by the material (c.f. chapter 4), the average power of the beam then controls the speed of the process in question

It is widely accepted that this term pulse irradiance decides the initial reaction of the material to the beam, and generally determines whether or not the beam will be absorbed or reflected by the material (c.f. chapter 4), the average power of the beam then controls the speed of the process in question

3.4.4.5 Effect of wavelength

For a given mode structure and transmission optics, an increase in wavelength produces an increased divergence. This increased divergence implies decreased focusability (i.e. increased focal spot sizes) as discussed in section 2.4.4. One might therefore expect that shorter wavelength beams are able to perform high intensity laser processing more effectively. In practise, however, this effect is swamped by the multimode, high divergence nature of most high power solid state industrial lasers. It turns out in actual fact that both types of industrial lasers usually employ optics which give focused spot sizes of between 200 - 500 μm depending on the application.

However, the combination of high peak power and short wavelength makes solid state lasers particularly suitable for certain applications such as drilling, cutting and welding of high reflectivity materials.

3.4.4.6 Pulse shaping

Solid state laser output characteristics are influenced very strongly by the pumping discharge waveform to the flashlamps. Most up to date pulsed solid state lasers use switch mode power supplies, and it can be assumed that if a rectangular current pulse is fed into the flashlamps, then the temporal profile of the laser pulse, known as the 'pulse shape', follows approximately the shape of the lamp input pulse when it emerges from the laser as shown in figure 3.5. It is therefore relatively straightforward to produce a temporally shaped laser pulse. Although there has been interest in the possibilities of this technique, there has been very little concrete evidence to date in the scientific literature of the benefits associated with it. As discussed in chapters 5 & 8. This also appears to be the case when industrial materials processing problems are being discussed, although there is some suggestion that it might be possible to reduce cracking in some hardenable steels by producing a slow power ramp down at the end of a welding pulse.

Sector numbers.
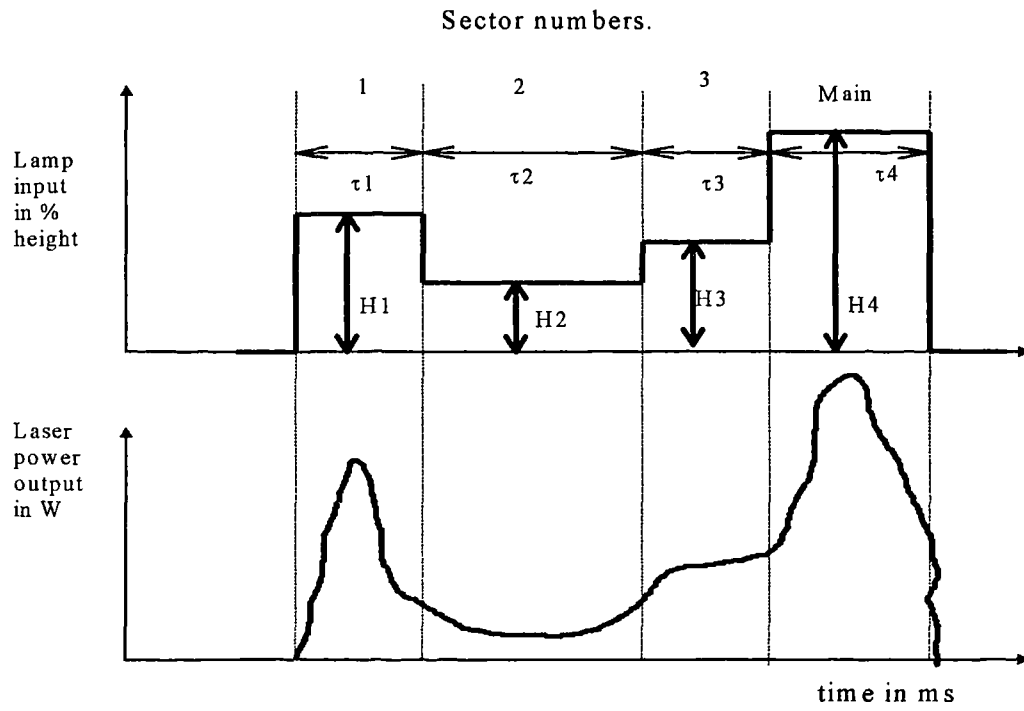
Figure 3.5 Complex temporally shaped pulse [22]

where τ1-τ4 are the durations of the individual sectors of the pulse and H1-H4 are a measure of the input power to the flashlamps for each pulse sector.

4. Laser / material interactions

There has been much discussion in the technical literature about the physical mechanisms that occur when a laser beam is focused onto a metallic surface [23]. It is necessary firstly to identify the basic principles involved in the generalised case when a light beam strikes a surface, hence, covered in this section, are absorption, transmission and reflection processes. Secondly, after absorption of the beam, the resultant thermal energy is then distributed throughout the body according to the mechanisms of heat transfer. Both of these processes are dependent of course on the relevant properties of the target material involved, in this case, aluminium, and these are therefore considered in section 4.4. Again, most of the published work is concerned with the interaction of longer wavelengths, but here mainly information relating to 1.06 μm radiation is considered.

Although the thermophysical properties of aluminium are unusual and different from many metals in some respects, aluminium is nevertheless used in a wide range of scientific and engineering applications. Because of this, its properties have been widely studied. Relevant aspects of metals, and aluminium, and in particular aluminium surfaces, are now examined in more detail also in this chapter.

4.1 The optical properties of metals

The important optical properties commonly used to characterise a material are discussed in this section.
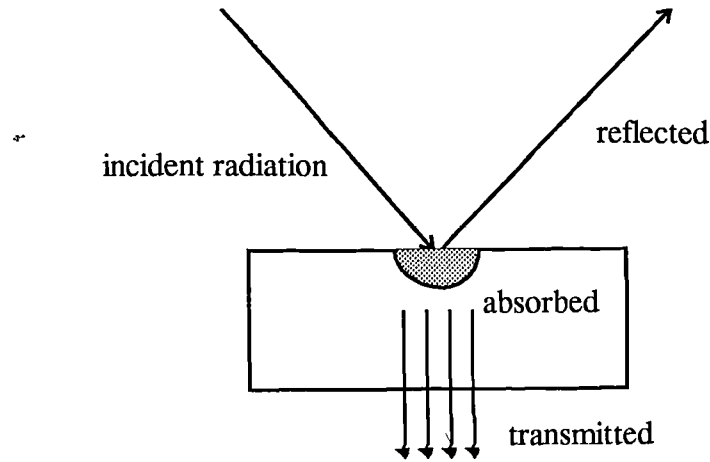
Figure 4.1 Interaction of radiation with a surface

4.1.1 Reflectivity, transmissivity, and absorptivity

The proportion of the incident light energy that is reflected by a surface is known as its reflectivity, R. The proportion of the incident light energy that is transmitted through a body is known as its transmissivity, $\mathcal{T}$. Similarly, the proportion of the incident light energy absorbed by a body is known as its absorptivity, A. The term emissivity is used in some publications, denoted ε. Note that the reflectivity is a property of the surface of the body, whereas the transmissivity and absorptivity are properties of the whole body. The principle of conservation of energy forces the relation,

$$R + A + \mathcal{T} = 1 \qquad \text{Equation 4.1}$$

For a given incident light, reflectivity is essentially dependent only on the surface conditions. These surface properties include the nature of the surface, surface constituent materials, the surface atomic structure, the surface roughness, surface morphology, the level of oxidation, temperature, wavelength, irradiance of incident radiation and angle of incidence. It is therefore difficult to isolate the relative importance of the different parameters in determining the ultimate surface reflectance. The transmissivity and absorptivity are also dependent on these surface properties, only

energy that is not reflected can be absorbed or transmitted. The light energy that is not reflected will be partly absorbed and partly transmitted in almost all practical cases, the relative proportions being determined by the size and shape, as well as the morphology and atomic structure, of the body. However, it has been recognised that the reflectivity falls dramatically with increase in incident power density, time of exposure, surface characteristics as well as temperature [24,25].

The actual measured quantities for real surfaces are called reflectance, absorptance and transmittance. The surface and bulk properties themselves, are likely to be dependent on temperature, and even in certain cases, on pressure.

The optical properties of the medium that contains the incident light, will also affect the proportions R, $\Im$, and A. In most situations this can be neglected, since this medium is often air, which can usually be assumed to have the optical properties of a vacuum. By definition, for an opaque material, $\Im = 0$, so that

$$R + A = 1 \hspace{3cm} \textbf{Equation 4.2}$$

Opacity, and hence R, $\Im$, and A vary depending on the range of radiation frequency; there will always be frequencies that if present will be transmitted through a body. It also depends as well on the polarisation and the angle of incidence of the light. Finally, the irradiance of the incident light may also affect these proportions. As we already know, very intense light, and in particular, laser light, alters the optical characteristics of the surface or body.

The electronic structure of metals means that light in the optical spectrum is unable to penetrate metals to any great depth (only a few atomic diameters). Metals are thus opaque to any such light, so equation 4.2 is valid. This means that having determined the reflectivity, the absorptivity is then also known (i.e. it is simply the complement).

Metals reflect most of the incident infra red energy according to the Drude Free Electron theory and for incident power densities below 10^5 Wcm^{-2}, 90 - 98% of the incident laser power is reflected from most polished metal surfaces. In this case the Hagen Rubens relationship for the reflectance, R_{ance} of a metal surface for light of wavelength 10 μm or greater is approximately:

$$R_{ance} \approx 1\text{-}2\sqrt{(v/\sigma_0)} \qquad \textbf{Equation 4.3}$$

where σ_0 is the electrical conductivity of the metal, and v is the frequency of the light wave.

However, the Nd:YAG laser produces light at a wavelength of 1.06μm, so this equation may not hold. For wavelengths < 10 μm, the absorption is a far more complex relationship. In this case tables of values found through experimentation are used to obtain values for reflectance and absorptance. A good review of this information, and a review of the relevant sources is given by Smith in a chapter of the Handbook of Optical Properties of Solids.

4.1.1.1 Ideal smooth surfaces

The smooth-surface reflectivity, R_s , for a perfectly clean smooth-surfaced sample can be found using the complex Fresnel equations. For insulators, R_s depends solely on the refractive index. With metals, the conventional refractive index, defined as the ratio of the angle of incidence to the angle of refraction, has no meaning. The reflectivity is therefore determined by a complex refractive index, $\tilde{n}$, which is made up of the refractive index, n, and an extinction coefficient, k, according to

$$\tilde{n} = n - i\,k \qquad \textbf{Equation 4.4}$$

where $i \equiv \sqrt{-1}$.

The extinction coefficient represents the ability of the metal to prevent light that is not reflected from being transmitted. Energy absorbed on the surface is, in fact, absorbed in a finite thickness of material, known as the absorption depth, or optical skin depth. The optical skin depth, D, is defined as the distance into the metal from the surface at which the radiation intensity has dropped by a factor of $1/e^2$ from the incident value, for normal incidence radiation. This is often expressed as

$$D = \frac{\lambda}{2\pi k} \qquad \textbf{Equation 4.5}$$

It is the complex refractive index and the extinction coefficient which are usually regarded as the optical constants of a metal. They are, however, both functions of the material temperature and the wavelength of the light. There have been many attempts to model effects such as interband and intraband electron transitions, and phonon (a quantum of lattice vibration) participation, over variations in the incident

light wavelength, and body temperature. This enables predictions to be made for the smooth-surfaced reflectivity, such as given in references [26,27].

The Fresnel equations, not reproduced here, have also shown that reflectivity tends to increase as the angle of incidence is increased over the range $0° \leq \theta \leq 90°$. The maximum reflectivity of 100%, is approached as θ approaches $90°$, and for s-polarised incident light, the reflectivity is minimum at normal incidence, i.e. $\theta = 0°$. These are important in the case of polarised light, for p-polarised incident light, the reflectivity can be shown to possess a minimum at a non-zero angle of incidence, θ_p , known as the Brewster angle. Circularly or randomly polarised light may therefore also have a minimum reflectivity at a non-normal incidence, although this will depend on the values of material optical constants.

4.1.1.2 'Real' surfaces

Two types of reflection phenomena may be observed when radiation strikes a surface. If the angle of incidence is equal to the angle of reflection, the reflection is called specular. On the other hand, when an incident beam is distributed uniformly in all directions after reflection, the reflection is called diffuse. In practice, most engineering surfaces are classed as rough, and hence exhibit diffuse behaviour. Similarly, a polished surface is more specular than a rough surface.

The absorptance of a smooth-surfaced metal is the complement of its smooth-surface reflectance (as given by equation 4.2). The absorptance of a metal sample that does not have a perfectly smooth surface is greater than that of the same metal with just such a surface. The extra absorptance is made up of components due to surface impurities (including oxides), surface morphology, and surface roughness.

It is interesting to note that a wide range of sources agree that all metals at room temperature are highly reflective to infra red laser light, but in practical laser processing situations, this is not necessarily as serious a problem as might be expected for reasons to be examined later. It is a widely held view that the difficulties in laser processing certain materials are not solely a problem of high reflectivity, but are largely due to a combination of high reflectivity and high thermal diffusivity. Common examples that possess these characteristics are the non ferrous metals, aluminium, gold, copper, brass, etc.

4.2 Heat transfer

When a laser beam impinges on a surface, the energy absorbed is very rapidly converted into heat. A summary of the principles involved in the subsequent relevant processes is now presented

Heat flow cannot be measured directly, but it is related to the measurable quantity, temperature. When the temperature distribution $T(r,t)$ in terms of temperature and time within a body is determined, then heat flow is calculated from the laws relating heat flow to the temperature gradient. Heat transfer supports the first and second principles of thermodynamics (which deal with systems in equilibrium), by identifying energy transfer rates. The three modes of heat transfer are conduction, convection, and radiation.

4.2.1 Conduction

Conduction is the mode of heat transfer in which the energy exchange takes place in solids or fluids at rest. The science of heat conduction is principally concerned with the determination of the temperature distribution within solids.

4.2.1.1 Fourier conduction

The basic law that gives the relationship between the conductive heat flow and the temperature gradient, is generally known as the Fourier law. For a homogeneous, isotropic solid the Fourier law can be given in the form

$$q(r,t) = -C\,\nabla T(r,t) \qquad \textbf{Equation 4.6}$$

where the temperature gradient is a vector normal to the isothermal surface, the heat flux vector $q(r,t)$ represents the heat flow per unit time, per unit area of the isothermal surface in the direction of the decreasing temperature, and C is the thermal conductivity of the material which is a positive, scalar quantity. Since the heat flux vector $q(r,t)$ points in the direction of the decreasing temperature, the minus sign is included in equation 4.6 to make the heat flow a positive quantity.

4.2.1.2 Thermal conductivity

It is clear from equation 4.6 that the heat flow rate for a given temperature gradient is directly proportional to the property C, the thermal conductivity of the material, measured in $Wm^{-1}K^{-1}$. In the analysis of heat conduction, the thermal conductivity of a material, the property which controls the rate of heat flow in the medium is an important property. Often, the highest values of thermal conductivity are given by pure metals, with the lowest being given by gases and vapours. With metals, the value generally decreases with increasing temperature. This temperature dependence of thermal conductivity in metals can be usually be represented over a wide range of temperature by a quadratic expression in T although for many situations a linear expression will actually suffice.
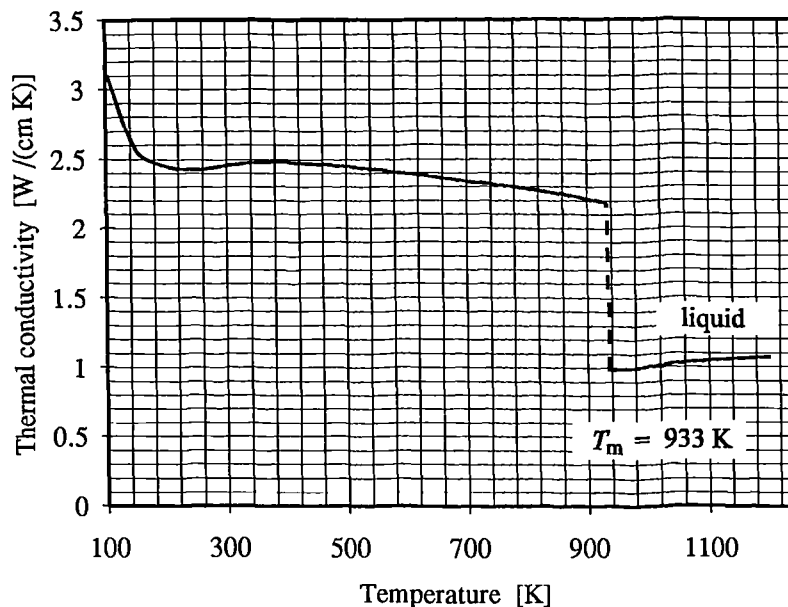
Figure 4.2 Temperature dependence of thermal conductivity for aluminium [46]

This graph shows the experimentally determined temperature variation of thermal conductivity for pure aluminium [46]. It shows that, the thermal conductivity has an approximately linear temperature dependence over the temperature range 300-933 K. There is then, a substantial sudden drop in value upon melting, followed by a further linear relationship in the liquid state, up to the 1200 K extreme shown.

4.2.1.3 Thermal diffusivity

The thermal diffusivity, K, of a material is defined by

$$K = C / \rho H_c \qquad\qquad \textbf{Equation 4.7}$$

where H_c and ρ are the specific heat capacity and density of the material respectively. The thermal diffusivity represents the rate at which thermal energy diffuses through the material when a temperature gradient exists, or more simply the rate at which a material accepts heat.

Thermal diffusivity also has a temperature dependence resulting from the temperature dependence of each of its three constituents C, H_c and ρ.
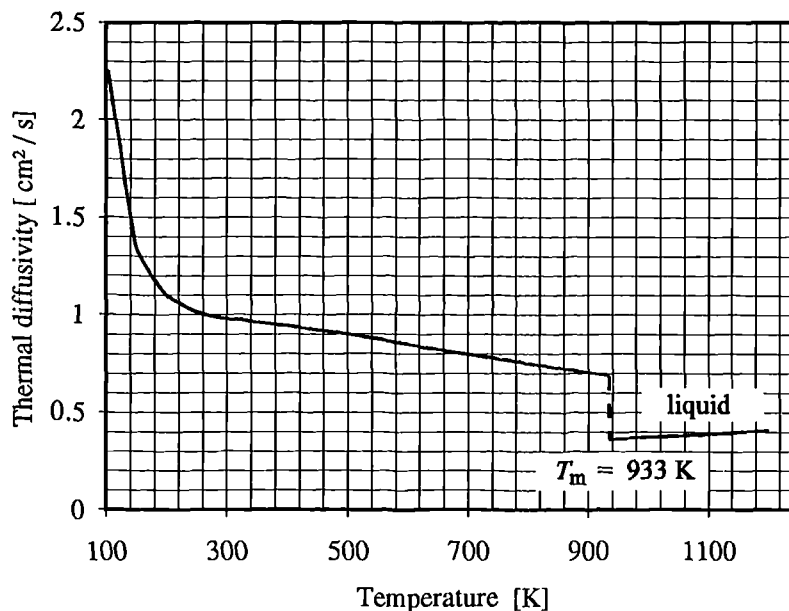
Figure 4.3 Temperature dependence of thermal diffusivity for aluminium [46]

4.2.2 Convection

It is well known that a hot plate of metal will cool faster when placed in front of a fan than when exposed in still air. The heat is said to be convected away, and the process is called convection heat transfer. The overall effect of convection, can be simply described by Newton's law of cooling,

$$q = h a (T_S - T_\infty) \qquad\qquad \textbf{Equation 4.8}$$

where h is the heat transfer coefficient. The heat-transfer rate, q, is related to the temperature difference between the wall and the fluid and the surface area a.

Convection heat transfer has a dependence on viscosity of the fluid in addition to its dependence on the thermal properties of the fluid (i.e. thermal conductivity, specific heat, and density). Viscosity influences the velocity profile and, correspondingly, the energy transfer rate in the region near the wall.

4.2.3 Radiation

In contrast to the mechanisms of conduction and convection, where energy transfer through a material medium is involved, heat may also be transferred through regions where a perfect vacuum exists. The mechanism in this case is electromagnetic radiation, and is mentioned merely for the sake of completeness.

4.3 Aluminium surfaces

Because of the key importance of aluminium to this work, the properties of aluminium and in particular, the relevant properties of its unusual surface, are now examined in some detail.

4.3.1 Natural structure

A layer of aluminium oxide (Al_2O_3) forms rapidly on an aluminium surface in the atmosphere. This layer is both adherent and relatively impervious, so that once formed, it protects the underlying metal from further oxidation. Figure 4.4 shows this structure schematically. Under normal atmospheric conditions the natural oxide layer remains rather thin (less than 100Å, and typically around 40Å) and if damaged mechanically, immediately re-forms. Aluminium owes its high resistance to corrosion to these oxide films on the surface. The thickness of the surface layer depends strongly on the sample structure and history. The natural film provides excellent protection to pure aluminium but is less protective on many strong alloys which have high alloy content. During prolonged exposure the film thickens and roughens, the aluminium loses its characteristic appearance and assumes a dull grey finish.
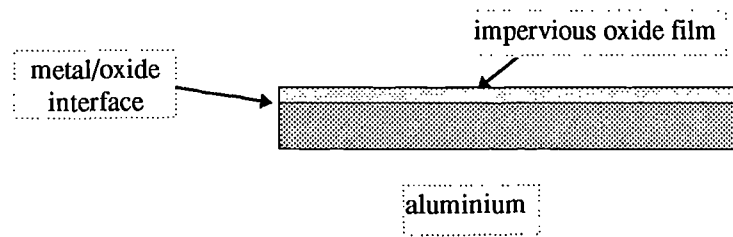
Figure 4.4 'Natural' structure of aluminium surface

4.3.2 Anodising of aluminium

Anodising aluminium is simply a method of building up a much thicker oxide coating than may be obtained by exposure to air. A range of different acids are used under different conditions to produce coatings with a range of properties.

In anodising, the workpiece is the anode, and oxide layers are built up on the surface of the base metal. Since the newest oxide layer always forms next to the base metal, in order for the process to continue, the previously formed oxide layers must be porous enough to allow the oxygen ions to pass through. In almost all cases the transparency of the coating decreases as the film thickness increases.

During anodising the solvent action of the electrolyte on the outer surface of this film constantly degrades it into a porous film which overlies the barrier film. The barrier portion of the film remains approximately the same thickness during the whole time of processing - if at constant voltage - while the porous film increases in thickness up to a maximum under any given set of conditions. The progressive reduction in the rate of film formation at constant voltage arises from the structure of the porous portion of the film, which consists of a compact non-conducting layer pierced by sub-microscopic pores.

As the film thickens, the length of the pores increases and consequently the resistance of the column of electrolyte contained within each pore increases in proportion. As a result, the current density at the metal surface decreases, and less film is formed in unit time.

4.3.3 Structure of anodised coatings

The structural features of porous anodic oxide coatings applied to aluminium have been shown to consist of closely packed hexagonal-shaped cells of oxide, some hundreds of thousand to the square mm, each containing a single pore [34]. The bottom of the pore is separated from the metal by a thin barrier layer of oxide. The structure of a typical cell of an anodic coating showing the basic unit is shown in figure 4.5.
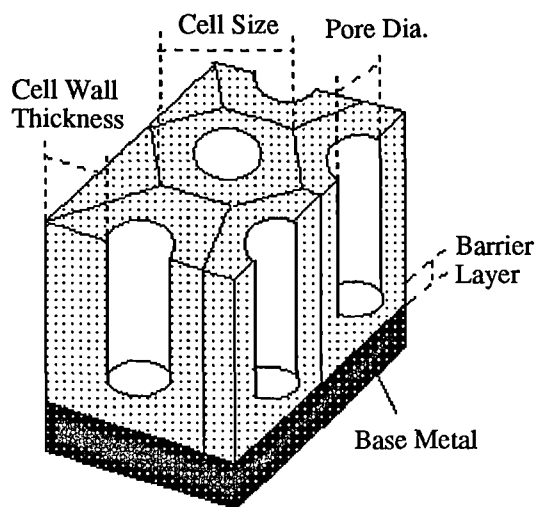
Figure 4.5 Structure of anodic coating

4.3.4 Thermophysical properties of anodic films

It is this porous film which accounts for the major characteristic of anodised finishes. The film is sub-microscopically porous, and in consequence possesses an enormous real surface area as compared with its apparent surface area. This surface is highly active and as seen later, the film absorbs light.

The general characteristics of anodic films are tabulated as follows:

Composition	Unsealed	Al_2O_3
	Sealed	$Al_2O_3.H_2O$
Specific Gravity	Unsealed	2.5
	Sealed	2.7
Refractive Index	Unsealed	1.59
	Sealed	1.62
Resistivity	At 20°C	10^9 ohm-cm
	At 250°C	10^{13} ohm-cm
Boiling Point		3250°C
Melting Point		2050°C
Coefficient of Expansion		approx. 2.4×10^{-6}
Heat Emissivity	As a % of black body	80%
Hardness		From 150 to 600 VPN

Table 4.1 General properties of anodic coatings [from 25]

In essence, there are three different properties that describe the thermal properties of anodic coatings. These properties are heat resistance, thermal conductivity and heat emissivity. Due to the importance of the first two of these properties to laser processing, those characteristics are briefly discussed.

4.3.4.1 Heat resistance

Aluminium oxide is a refractory material having a melting point of 2050°C. Under severe heating the aluminium substrate will melt long before the film is directly affected. The film does not blister or peel under heating, but at temperatures above 100°C may become crazed [34].

4.3.4.2 Thermal conductivity

The thermal conductivity of anodic films is about 10% of aluminium. Bulk conductivity values ranging from 0.61 to 1.0 $Wm^{-1}K^{-1}$, depending on the process used to produce the anodised layer, were reported by [35].

4.3.5 Optical properties of anodic films

Fundamentally, there are several optical properties of an anodic film. These include reflectivity, image clarity and refractive index. However, in high power laser material processing, the property of reflectivity mainly concerns us here.

4.3.5.1 Reflectivity of aluminium surfaces

The amount of laser energy that is actually absorbed by the surface of the target depends on the optical and chemical properties of the surface and the factors affecting these are now examined.

Reflectivity values of around 99% have been reported from experimentally based sources for $10 \cdot 6 \, \mu m$ light normally incident on very pure vacuum deposited or evaporated films at room temperature. Touloukian's book gives probably the most comprehensive compilation of such experimental data. A detailed study of the wavelength and temperature dependence of the absolute reflectivity of metallic aluminium, from $\lambda = 4000 \text{Å}$ to $10 \, \mu m$, has also been made by Decker and Hodgkin [36].

Ujihara [27] calculated theoretical values for refractive index, extinction coefficient, skin depth, and reflectivity, at $10 \cdot 6 \, \mu m$, for aluminium at various temperatures. This was done on the basis of Drude theory and the theory of electron-phonon collisions, and using available electronic property data for aluminium. In his book, Prokhorov [37] has performed similar Drude theory calculations using a typical set of theoretically calculated optical constants, such as $\{ n \approx 34, k \approx 108 \}$ for an ideal smooth surface. These constants equate to a reflectivity of $\sim 99\%$, showing good corroboration with the experimental results.

4.3.6 Engineering aluminium surfaces

The previous section covered information relevant for specialised high quality surface finishes on aluminium such as mirrors, but far less data is available when data is needed for engineering finishes. These are usually unpolished or roughened samples, with variable and inconsistent oxide coverage. Temperature, the presence of impurities and, in particular, the roughness of the sample can drastically increase the absorptivity. Arata [29] has performed perhaps the most relevant work on laser interaction with engineering aluminium surfaces, and despite the fact that $10.6 \mu m$ laser light was used,

this is covered in the following sections in some detail. It was shown that the absorptance of aluminium can be improved by sulphuric acid anodising especially at the 10.6μm wavelength. The absorptivity of aluminium is virtually 100% if the anodised layer formed is approximately 5μm.

4.3.6.1 Effect of temperature

Generally for metals, as the temperature of the body increases, the absorptivity also increases. Most of the available data on the temperature dependence of absorptivity in metals—either obtained experimentally or calculated theoretically—may generally be described by a rather simple function of the type

$$A(T) = a_0 + bT$$

Equation 4.9

where T is the temperature in degrees Kelvin, and a_0 and b are constants (independent of T). In other words a linear relationship, is generally a good approximation for the temperature behaviour. In addition, according to Libenson [38], a_0 can usually be neglected. This linear form is valid for a metal while in its solid state. As described in [36], any further increase in temperature, will generally give rise to a step change in absorptivity as the metal melts. For temperatures greater than the melting temperature T_m, the liquid metal temperature/absorptivity relationship may again be modelled by an expression in the form of equation 4.9 but with different values of a_0 and b to those used in the solid state. This assumed relationship is illustrated in Figure 4.6
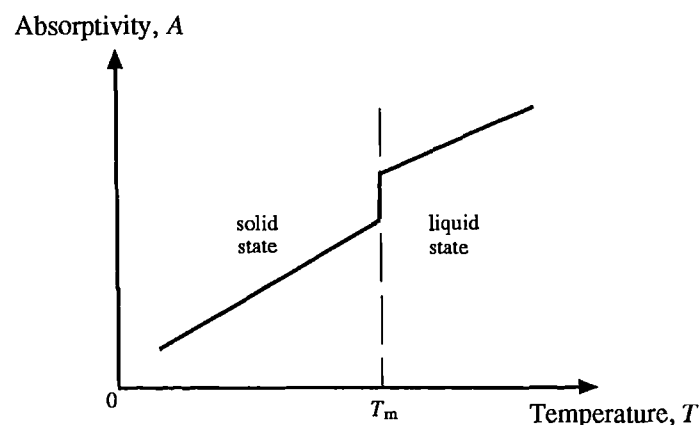
Figure 4.6. Theoretical temperature v absorptivity relationship for metals

For applications involving the melting or evaporation of the target, such as laser cutting and welding, the tabulated reflectivity may lead to a substantial

underestimate of the amount of laser energy that is absorbed and converted to heat. Figure 4.7 shows experimentally determined reflectivity as a function of temperature specifically for 1.06μm radiation - as the temperature of the structure rises there will be an increase in the phonon population causing more phonon-electron energy exchanges. Thus the electrons are more likely to interact with the structure rather than oscillate and re-radiate, reducing reflectivity with a rise in temperature. This is particularly true in the case of aluminium where reflectivity may fall dramatically.

Reflectivity, %
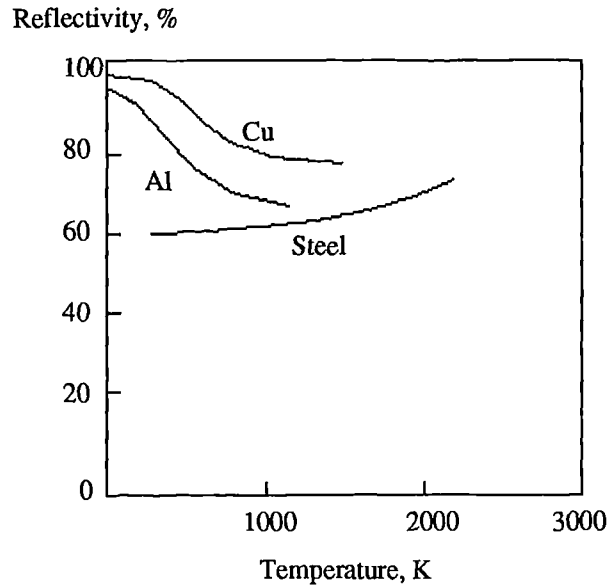
Temperature, K

Figure 4.7 Reflectivity v temperature at 1.06 μm [Steen]

It should be noted that the experimental determination of reflectivity / absorptivity data is not straightforward, hence the paucity of relevant data.

Ready proved that for the case of CO_2 radiation, if the temperature rises sufficiently, evaporation occurs and the well known dynamically stable void called a keyhole can be created [39] at very high irradiance, 10^8-10^9 Wcm^{-2}. This keyhole then acts as a black body as far as radiant absorption is concerned.

4.3.6.2 Effect of wavelength

Tabulated values of reflectance serve as a guide to the ability of different materials to absorb laser light. Values for several materials are shown in Figure 4.8. Most metals absorb shorter wavelengths more readily and this is usually ascribed to more efficient absorption of the higher energy photons by the bound electrons in the metal surface. In practice, due to the non linear effects on absorptivity described in this chapter, the practical effect of this is less significant than might initially appear to be

the case. Also, there is an additional practical problem in that there are almost no high average power lasers in use which emit light at visible wavelengths.
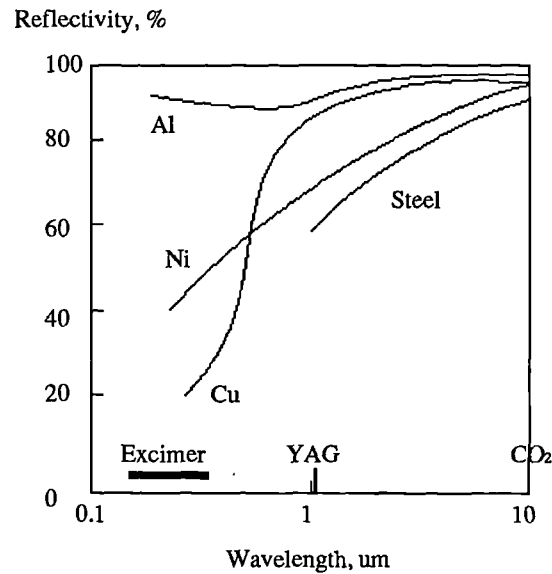
Figure 4.8 Reflectivity v wavelength for various metals [from Steen]

Evidence is presented above for a number of metals, in particular, the reflectivity of aluminium is shown to increase as the incident radiation wavelength decreases from the infrared to the ultraviolet spectral range. Generally, for radiation with a wavelength $\lambda \approx 10 \cdot 6 \mu m$, the absorptivity of metals is very low, of the order of a few per cent, or sometimes even of a few fractions of a per cent. Aluminium is particularly reflective at $10 \cdot 6 \mu m$, with its exact behaviour depending on the purity and morphology of the sample, as well as the surface condition.

Hettche [40] gives a very good description of the coupling of 1.06 μm radiation to aluminium surfaces which is discussed in more detail in chapter 8. He points out that "effects are considerably stronger than those expected on the basis of the simple free electron model". They show thermal coupling coefficients of 0.35 for aluminium targets at an intensity of 2 $MWcm^{-2}$ with a sharp trend towards higher figures for lower irradiance. Smith also gave a good overview of optical property theory and its experimental validation, focused on aluminium.

Most metals therefore absorb more readily at shorter wavelengths and consequently, it is sometimes suggested that less laser power is required for processing applications with visible lasers than with infrared lasers [41]. For similar reasons, this difference in reflectivity between the NdYAG and CO_2 wavelengths has also been

considered by some authors to cause major differences in processing performance between these two types of lasers. Although this may be true in the case of certain materials (of which aluminium is one) at low average powers and at low irradiance, the situation again is more complex at higher powers and irradiance due to the aforementioned threshold effects. Recent work by Dausinger [42] suggests that the lower the aspect ratio of a particular weld configuration the greater the advantage of using shorter wavelength beams might be.

4.3.6.3 Thickness of anodised layer

Arata [29] studied the effect of an anodic coating on absorptance of 10.6 μm radiation by an aluminium surface. A 15% sulphuric acid anodising solution at 0.012 amps per square metre anode current & 20 °C was used. He showed (fig. 4.9) that for 10.6 μm radiation the anodised film produced by this technique can easily grow up to sufficient thickness to provide 100% absorptance at room temperature. This is thought to be due to its porous structure and large effective surface area.
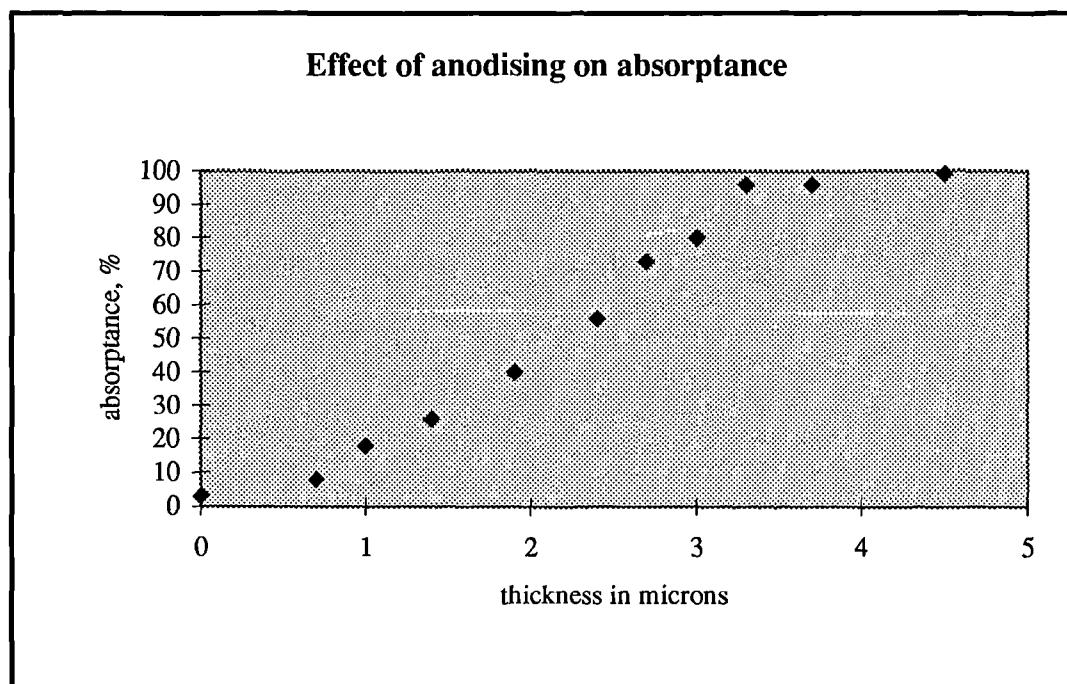
Figure 4.9 showing effect of sulphuric acid anodising on absorptance [29]

100% absorptance is associated with oxide depths in excess of about 4μm and so commercially anodised grades with oxide depths of ~20μm have a surface which is fully absorptive despite the fact that pure Al_2O_3 is transparent to 1.06 micron radiation. Although this data has been collected at the longer wavelength, similar behaviour

might be expected at shorter infra red wavelengths, especially as most oxidised aluminium surfaces have absorbed at least some moisture during their life as suggested by [33]. This anomaly is therefore explained by the fact that water has pronounced absorption bands in and around the infra red and the presence of hydrated oxides in an anodised surface might also be expected to increase absorption.

Additional confirmation of enhanced absorption was provided by the author in recent work where laser cutting speeds were significantly increased due simply to the presence of an enhanced oxide layer on the surface of an aluminium alloy [43].

4.3.6.4 Surface roughness and morphology

The roughness of the sample surface is an important factor in determining effective optical properties [24]. Surface roughness causes both diffuse reflection and increased absorption. Prokhorov [37] suggests that if the roughness is less than about one quarter of the incident radiation wavelength, the surface will be perceived (by the radiation) to be smooth. He also suggests that if this is not the case, the surface will not appear flat but will instead appear to have undulations, grooves, and cracks, and diffuse reflection will occur. Absorption increases also occur where the radiation incidence is non normal, and also in grooves and cracks which favour waveguided propagation of radiation and multiple reflections and absorptions in undulations.

Arata [29] also experimentally investigated the relation between the surface roughness and absorptance for a number of metals by preparing targets using sand papers with various grit sizes. Results for aluminium and lead are shown in Figure 4.10.
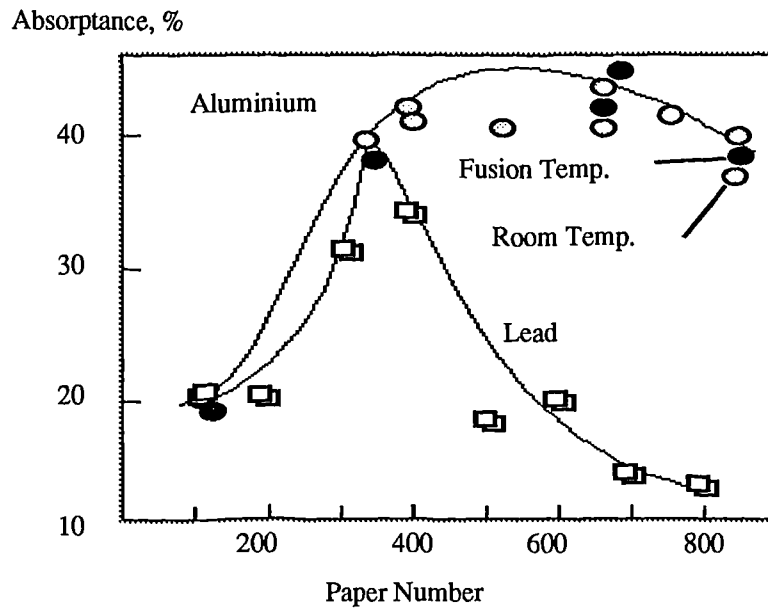
Absorptance, %

Figure 4.10 Absorptance v surface roughness

For roughened aluminium, values of absorptance were almost a factor of 20 larger than those measured for polished specimens. Conclusions were that the increase in absorptance was caused more by the absorptance of fine residual sand particles rather than roughening.

The surface morphology, particularly grain size and orientation, also has a substantial influence on optical properties. The problem is that both surface roughness and morphology are difficult to quantify exactly. Prokhorov [37] also gave an approach for estimating the increase in absorptance due to random surface roughness.

4.3.6.5 Surface impurities

Quantities of alien substances are often present on the surface of metals, and in the case of oxide layers, these cover the material completely or may simply be scattered over the surface. If the impurities are invisible to the particular wavelength of light, then the absorptance of the metal sample will hardly be affected. This is not usually the case, with metal absorptance often being substantially increased by impurities, depending on the absorptivity of the impurities, even if surfaces have been conventionally degreased.

4.3.6.6 Purity and type of alloy

Other main factors contributing to variations in reflectance properties of aluminium are the purity and composition of the substrate and also finishing practices which contribute to the topography of the surface such as etching, buffing and polishing as well as anodising.

An increase in the purity of the aluminium increases the clarity of the anodic film, with a consequent reduction in absorptance of the film. A useful review of these effects is given in [44,45]. Of the elements most commonly found as alloying constituents in aluminium some are oxidised and retained in the oxide film, others are not affected at all and become entrapped in the aluminium oxide in the elemental or intermetallic state, others dissolve chemically or electrochemically and leave voids in the film. The concentration and distribution of alloying elements therefore and the metallurgical practices used in processing the alloy also have a pronounced effect on the reflecting characteristics of the anodised surface. Although not directly relevant to this work, because it is not measured at specific wavelengths, data is available in [36] on the specularity (S.R.F.) values of anodised aluminium alloys arranged in order of purity.

4.4 Beam / plume interactions

A number of authors have worked in this area, the most relevant being Lewis and Dixon [28], Arata [29], Matsunawa [30] and von Allmen [31]. The latter presents perhaps the best overview of evaporation and plasma effects in his book. He identifies the range of irradiance covered in this work, 0.5 - 1 MWcm^{-2} as that in which the vapour plume is changing from a transparent vapour to one which is becoming supersaturated. At the top end of this irradiance range these condensing droplets are of sub micron size and lead to absorption and scattering. Alongside this effect is an effect due to changes in refractive index caused by the vapour plume. Although some of these conclusions are discussed in more detail later, it is widely accepted that at longer wavelengths and higher irradiance the vapour becomes partially ionised and more absorbing. However, especially in the infra red this absorbing plasma re-radiates blackbody energy which tends to be absorbed more efficiently by the solid target. What seems to be less clear, particularly at lower irradiance, is how much of the laser pulse

does the plume/plasma absorb and at what stage of the pulse does this start to absorb and reradiate the pulse energy.

On hitting a target with a high irradiance laser beam, vapour generation occurs and there have been several estimates of the speed of the ejected vapour. This work published by Matsunawa [30] on the beam plume interactions in pulsed YAG laser processing concludes that at relatively low irradiance the plume consists of a subsonic metallic vapour jet of atoms and clusters of target material. It is also stated that the smaller the ejected particles, the more the incoming beam is absorbed, and at high irradiance the ejected material (ejecta) consists of larger vapour particles which absorb less of the beam. Later work on high speed photographic studies of YAG laser plumes showed that plume velocities are very high and are not therefore able to be controlled by air jets as is usual with CO_2 lasers. It is as shall be shown however at the lower end this low irradiance regime where the current work is performed.

Reference must be made to an effect commonly noted to the interaction of 10.6 μm radiation with metallic surfaces, and its dependence on laser irradiance which has also been studied extensively, for example in [20]. The available experimental results show that for irradiance in the range 10 - 10^2 MWcm^{-2}, there is a substantial stepwise increase in the reflectivity of aluminium. Some authors claim this increase is not attributable to the increase in temperature or melting alone produced at the irradiation spot by such irradiance, and other explanations are proposed in [32,33]. In this region the classical Drude formalism has been shown not to be applicable, hence the effect is often referred to as 'anomalous' absorption.

4.5 Mathematical approaches to laser processing

The solid state laser is widely used industrially for a number of micro welding applications, of particular interest is the manufacture of thermally sensitive products that require intricate welding operations- a current application is the laser welding of microwave packages, where the bulk temperature rise of the component must be kept to a minimum to avoid damage to adjacent microelectronic components. In this case, a mathematical model of the process could be important to minimise heat input and also to control the Heat Affected Zones (HAZ) and metallurgical properties of the joint.

Most of the many attempts to model laser processing have been aimed at understanding high power continuous wave (cw) fusion cutting and welding processes and their associated heat flows with a continuous laser beam. The review has also shown that very little has been done on the modelling of pulsed laser welding. Even fewer authors have attempted to investigate the flow of heat in smaller finite metal samples, this being more appropriate for the lower power pulsed solid state laser heating / melting process under study in this thesis. Relevant information is now presented.

In modelling the particular case of low duty cycle pulsed solid state laser melting, the process must be split up into two parts. The initial mechanism, the transfer of energy from the beam to the target, has been the subject of much research and some of the non linear threshold effects have already been discussed briefly in section 4.2. Theoretical analysis however requires knowledge of the behaviour of the reflectivity of the material, and its relationship with temperature, which presents a very complex series of dynamic problems, and although progress has been made in some areas [47,48], each individual situation presents different process conditions. Currently therefore there are no satisfactory assumptions as to the percentage of energy absorbed which can be made. As the heat conduction equation for any subsequent laser heating problem must include a heat source term representing the energy absorbed by the laser beam, a serious problem arises.

Secondly, the heat transport mechanisms within the target may also be analysed. The most appropriate analytical model found for heat flow during pulsed welding was thought to be that by Vishnu & Easterling [49].

4.5.1 Heat conduction models

In most cases apart from the low duty cycle conditions under study here, the laser beam is scanning the workpiece, and the problem becomes a moving heat source problem. In the case of such a moving heat source, an analysis can be limited to the case of temperature (and time) independent thermal and optical properties of the material, with a continuous, constant strength and constant velocity, moving heat source. For the application to laser processing of metals analytical methods have been

used, but all but the most complex models are subject to the following significant limiting assumptions and approximations as follows;

4.5.1.1 Model assumptions

1. *The workpiece is infinite in width and length.* In practice this is certainly not true. Processing often begins at the edge of a workpiece which is of relatively small dimensions. The problem may be tackled by adding extra boundary conditions to the differential equations, to model the finiteness of the workpiece. Ölçer [50] has presented relevant theory on heat conduction in finite regions. This theory, however, generally results in very complicated solutions. Other models use approaches based on the semi-infinite body approximation, proposed by Prokhorov. He suggests that a semi - infinite solid approximation can be applied if the thickness of the metal sample, h, is much greater than the heat penetration. These models are therefore considered to be valid when the heat diffusion to the bottom surface of the workpiece can be neglected. This is the case in the current work and in many practical situations, thus simplifying the problem somewhat. Other typical applications of this type of model are in laser heat treatment applications with and without change of phase but not valid for cutting.

2. *There is no temperature gradient across the depth of the workpiece.* This assumption, generally becomes a large source of error when the depth is relatively large. In cutting, the bottom surface of the workpiece must be reaching at least melting temperature and the majority of the models available for laser cutting, tend to reduce the problem to a two-dimensional one. This is done by assuming the heat source is uniform in the z direction, i.e. in the direction of the workpiece thickness. In this event a workpiece with initially no internal temperature gradients, will continue to have no temperature gradient in the z direction, throughout the heating.

3. *The thermophysical properties of the workpiece are independent of temperature.* In practice, the thermal conductivity, specific heat capacity, and density all vary with temperature. The overall effect is very significant in metals beyond the melting temperature. Modelling these temperature dependencies introduces difficult to handle non linearities. A laser cutting model that attempted to do this could not be found in the available literature.

4. *Latent heats of melting and vaporisation may be ignored.* At temperatures greater than the melting temperature this assumption can lead to significant errors [51]. Latent heats can be incorporated into a temperature dependent specific heat term, by including an appropriate step function region at a phase change temperature, as done by Henry et al [52]

5. *Heat dissipates solely by conduction in the plate* (i.e. radiation and convection are ignored). Again, radiation effects become significant in metals at high temperatures—due to the radiative emission being proportional to the fourth power of the absolute temperature. Convection may become significant in the presence of fast moving gases, such as a cutting assist gas.

6. *The power absorbed is independent of workpiece temperature.* As shown in section 4.1.1.2, the absorptivity of metals increases with temperature, which if included in the model, again results in difficult to solve equations.

7. *The heat source geometry is either a line or a cylinder, and the heat is uniformly distributed.* The laser beam intensity profile is usually modelled better by a Gaussian shape, as discussed in Chapter 2. Also the beam absorption is suggested to be at a sloped erosion front. The net result is a 3-dimensional non-uniform heat source, that is far different from the line or cylinder. The detailed effect of this assumption should be investigated.

8. *The quasi-stationary condition has been reached.* Though this condition may be approximately achieved in practice, it should be noted that the time taken to reach it will not be insignificant in metals. Quasi-stationary models do not give any indication of transient behaviour. Hence, for instance, they cannot be used to predict the variation in maximum process speed as the workpiece 'heats up'.

9. *Material removal may be ignored.* A portion of the molten material will be expelled from the workpiece, at the erosion or melting front, throughout the process. This will also carry with it some energy that the heat source had previously contributed—giving another source of error to the model.

All these assumptions generally result in significant errors hence modelling was not considered appropriate for the experimental approach used here.

Numerical approaches have fewer of these limitations. Finite element and finite difference models which solve the basic Fourier equations for all internal points and

have special equations for boundaries have been used with some success but are again beyond the scope of this current work.

4.5.2 Semi quantitative methods

These are a range of techniques which use lumped heat capacity semi - quantitative calculations. These are used given in a number of sources, for example in Steen [53] and are used for approximate calculations. Some of these approximations are used to assemble the phenomenological model in chapter 8.

4.5.3 Future goals

Further developments of laser processing are aimed at extending process limits in terms of speed, maximum thickness, and quality. These and other processing developments can be more successful if the physical mechanisms of laser processing, and the resulting technical limits, are understood. Improved theoretical models are therefore required to predict the influence of the beam properties on processing performance and quality, and is therefore of importance to this work.

5. Laser surface modification & melting

5.1 Introduction

The above title best describes the wide range of laser processes reviewed in this chapter. It refers to a range of processes in which the heat produced by the interaction of a laser beam and the surface of a material is used to bring about an improvement in the properties of a surface. Because of the specialised nature of the work covered in this report, the range of treatments which are included in this review of relevant surface modification processes is wide - novel processes such as laser surface cleaning and indirect laser surface texturing are included. Sub-divisions appear, based on whether a change of state on a macro scale does or does not occur, and a further division occurs depending on whether the effects are due to the beam alone (autogeneous) or due to the combined effects of the beam and material added during the melting process (non autogeneous). A wide range of properties of the target material may be altered including material strength, wear resistance and corrosion resistance being the most important.

This section is limited to those laser applications which currently or in the future will employ high power industrial lasers.

An initial stage in evaluating these techniques is usually to examine the microstructures produced using conventional metallographic means such as metallographic analysis, electron microscopy and spectrographic analysis. Although metallurgical microstructural analysis is important as an analytical tool to examine the results of the laser processing, successful research also relies on correct optimisation of the laser process parameters.

The generic advantage of all these processes is that the heating can be done in a localised, controllable manner, both in space and time. By matching the wavelength

and specific beam power to the optical and thermal properties of the target material, the amount of heating can be chosen accurately to suit the needs of the process.

Although there have been a great number of academic studies concerned with these laser treatments, the take up in industry of high power laser surface treatment processes has been relatively low. The one significant exception, and a very early one in terms of industrial laser development, has been a large installation in the US where laser hardened stripes are produced on steering columns by the Saginaw steering division of General Motors [54]. The purpose of this chapter is to put the subject of this work in its correct context amongst similar laser treatment processes. It must be noted that these surface treatment processes are all at various stages of research or industrial exploitation.

5.2   Principles of laser treatment

As a starting point, it is useful to consider these surface modification techniques from the viewpoint of von Allmen [55] . He considers the primary product of absorbed laser light not as heat but as excess energy imparted to particles - the excitation energy of bound electrons, the kinetic energy of free electrons and perhaps excess phonons. The partition of the absorbed energy among degrees of freedom of the material is not initially thermal. The degradation of the ordered and localised primary excitation energy into uniform energy involves three steps. Firstly, spatial and temporal randomisation of the motion of excited particles occurs by the collision of the particles in question. The times involved are very short, shorter than the shortest laser pulses. The next step involves several energy transfer mechanisms, each with their own time constants and these processes are usually approximated to an overall energy relaxation time, which is typically of the order of 10^{-13}s for metals. Once this conversion to heat has taken place, the final stage is heat flow, and although the heat is highly localised on a macroscopic scale, the mathematical treatment of heat conduction considered in the previous chapter becomes relevant.
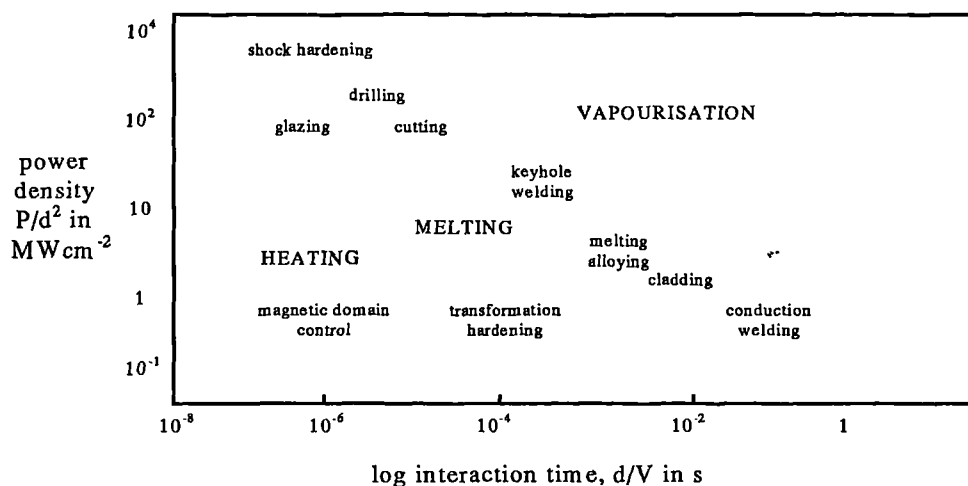
Figure 5.1 Operating regimes for laser materials processing [adapted from 56]

Figure 5.1 identifies semi quantitatively typical beam irradiance and beam interaction times for laser surface treatment processes, these having been identified earlier as controlling factors. Ion also gives a very thorough review of the area in [57]. Beam irradiance is well below those required for cutting processes, but increases as melting is required. It is clear that although heat conduction plays a large part in these lower irradiance processes other beam / material interaction mechanisms such as those considered in the previous chapter may also play a part if a change of phase takes place. Although there has not to date been many applications of solid state lasers in this area, their capabilities as described in section 3.3 & 3.4 ensures that they will be serious candidates in the future. This will certainly be the case if costs per watt decrease and if surface treatment processes are combined with other cutting or welding tasks in a multi functional station, as proposed by [58].

5.3 Treatments without change of state

5.3.1 Laser transformation hardening

The most straightforward laser surface treatment, it is usually applied to hardenable steels and occasionally, hardenable cast irons. Coverage is obtained by rastering a laser beam over the surface. In metallurgical terms, the laser is used to raise

the temperature of a localised area above the austenitizing temperature, but below the melting point of the steel. Laser process parameters are chosen such that the power density is in the region of 0.1 to 1 MWcm^{-2}. The surface coverage rate is reduced to the point at which incipient surface melting is occurring. The depth of hardening depends upon thermal conduction of heat into the workpiece and hence the thermal properties of the material are important. In this case, surface heating is required and volume heating is to be avoided, therefore a large absorption coefficient and a short interaction time is required and hence sharply delineated areas can be heated to a high temperature. Rapid cooling of the heated material occurs due to self quenching by the bulk of the cold material. Heating and cooling rates are of the order of 10^6 Ks^{-1}. A worthwhile fundamental study of the metallurgical aspects is presented in [59]. The structures produced are often metastable and have particular properties of interest. Advantages are that the beam is chemically pure, is free of inertia and can be manipulated easily to inaccessible areas of a workpiece. In the case of high power CO_2 gas lasers, this can be performed by manipulation of mirrors or lenses, and it is this flexibility which is one of the main advantages of performing this application by laser as opposed to conventional techniques. A useful review of the more practical aspects is given in [60].

Various types of focusing optics such as beam integrators and segmented mirrors have been employed to optimise the spatial distribution of the beam for this application [61], depending on the particular application or range of applications. In the case of solid state lasers, beam delivery to the workpiece might be by manipulation of a lightweight fibre optic cable output housing. This has the advantage of being, compact, lightweight and relatively inexpensive because of the straightforward nature of the conventional optics employed.

A number of attempts have been made to model this process with varying degrees of success, even though the lack of a change of state makes this the simplest of laser processes to analyse mathematically - the only effect of the beam is to raise the temperature of the material, which then reacts according to the laws of conduction. Perhaps one of the more notable attempt at a realistic practical model is that of Mazumder [62].

A wide range of industrial components have been proposed as prospective candidates for this technique and these include gears, crankshafts, cylinder liners and

camshafts [63]. As an example of a recent application, work in Germany has led to industrialisation of a process for hardening the leading edges of turbine blades. A 6kW CO_2 gas laser is used to increase the erosion resistance of a hardenable steel. Hardness values of 580 - 750 Hv, and a case depth of 0.1 - 0.9 mm are quoted depending on the carbon content of the steel used [64]. Another very recent project is that by Tamada et al of Toyota, who have used a 3kW laser to locally harden and strengthen steel auto panels for increased crash resistance [65].

5.3.2 Shock hardening

A small number of groups have been working on this process since its initial invention at Battelle Institute in 1972. Early work carried out by Fairand & Clauer established the principle of producing deformation in metal surfaces by inducing a shock wave [66], which they have named Laser Shock Processing (LSP). Work carried on to establish many of the process parameters [67,68]. There are two regimes of treatment, the first is direct ablation. In this technique, experiments conducted in vacuo [69] found a relationship between the induced impulse momentum and the energy density. The second less widely used technique generates a plasma which is confined by various means. In these experimental studies, glass slides have been used and an airtight seal is made between this and the target. The laser beam in this case has an irradiance two orders of magnitude greater than in the previous approach. This process appears to rely on absorption and re - radiation of energy by the plasma and hence utilisation of the energy is much greater, resulting in a much greater impulse value, again approximately a factor of 100 times greater.

Most workers have used solid state glass, ruby or NdYag lasers with very short, high peak pulse power, high irradiance pulses of 10^3 MWcm^{-2} on the surface of the material. Pulse duration therefore needs to be $\sim 10^{-7}$ s. At these irradiances there is a very rapid vaporisation of material of a small volume of material, and an associated plasma creation. The rapid expansion of this plasma produces a recoil at the surface, which is in effect, a shock wave, which in certain alloys causes an overall increase in hardness of the surface. This increase has been ascribed to increase in dislocation density at which a shock wave is produced which work hardens certain materials. Dramatic increases in fatigue strength of steel and aluminium alloys have been

demonstrated on a number of prototype parts and very recently a production facility has been established. This facility now processes a range of high added value aerospace components [70].

5.3.3 Magnetic domain refinement

This is another interesting allied laser technique which has yet to find widespread industrial application. Work in both Japan and Germany [71] showed that it is possible to refine the magnetic domain size in transformer steel, (3% silicon iron) by a very rapid laser scanning technique. Reductions in the magnetic core loss have been reported. It has been suggested that the mechanism is similar to that of the previous section, shock hardening, where laser induced thermal stresses produces dislocations within the material. In this application, it has the effect of producing new magnetic domain boundaries in the scanned areas. Consequently under the influence of applied AC fields, energy loss during back and forth movement of the domain walls is minimised. By adjusting the spacing of the laser scan lines, this loss can be minimised. One of the major advantages of this process is that the inorganic insulating coating on the steel remains unaffected.

5.3.4 Surface preparation

This area of processing is between laser ablation processes and laser melting processes in terms of average power and depth of treatment. Here the treatments considered range from, in the case of laser cleaning of microelectronic components, a monolayer of contaminant to 200 μm in depth. The whole field of laser cleaning or surface preparation is now a very rapidly growing area of laser technology and commercial laser cleaning equipment and processing is now being offered by a number of commercial organisations. Applications are developing rapidly in a wide range of technology areas. It is also currently a subject of interest academically because of the possible functional benefits associated with using lasers to modify the microtopography of surfaces in a controlled manner. Also, environmental benefits might accrue from the development of solvent free processes for cleaning or etching surfaces.

Early development of this process was undertaken by Asmus [72], who removed oxides and scales from a range of metallic and non metallic antique artefacts using solid state lasers. Although this work was the first published in this area, it is not concerned with engineering surfaces and hence is not referenced. However, a very good review of the technology is given by Reitz [73]. Now, several different types of laser and laser wavelengths are being used so the topic is approached by considering each of the main laser types and their applications in turn.

5.3.4.1 Excimer lasers

The effect of excimer lasers on a wide range of materials has been studied. Srinavasan [74], Dyer [75], Tavakoli [76], Arnold [77], Tonshoff [78] & Thomas [79] have all examined the use of ultra violet radiation to produce a range of etching and ablation effects. Of particular interest is work by Peyre [80] on etching of semiconductors materials. Lu [81], & Zapka [82] all perform lower irradiance work aimed specifically at laser cleaning. Doyle [83] performed excimer treatment to enhance adhesive bond strength on high density polyethylene (HDPE). In this work, results showed improved adhesive bond strength due to the laser pre-treatment.

Thomas et al [79] studied a number of polymer and ceramic substrates after exposure to short wavelength uv radiation. The interest here is in the ablative photodecomposition mechanism using direct chemical bond scission in the top layer of the material. This is thought to be responsible for the very precise removal of material, but at relatively low rates. This work is a extension of ablative machining using Excimer lasers, now a well established technique. The three Excimer wavelengths of 193, 248 & 308 nm have been used at a range of fluences, from 0.064 to 1.4 Jcm^{-2}, depending on the threshold irradiance for the target material. This has produced a range of very interesting structures on the surfaces of Poly Vinyl Chloride (PVC), where unusual cone like structures were produced at a fluence of 0.11 Jcm^{-2}. These cones are thought to because by small particulate type impurities, either intrinsic or added, which are embedded in the polymer and are acting as masks for material underneath. Further interesting structures are found when Polyethylene Terepthalate (PET), polyvinylidene fluoride, (PVDF) and Polyether Etherketone (PEEK) are ablated near to their threshold. Generally, small crystallites, on the scale of a few microns, are thought to have different uv absorption properties and etch at a slower

rate than the surrounding area. At higher fluences, these particles are ablated with the bulk material and the final surface is smooth. They also showed that some surfaces can show dramatic changes in contact angle after excimer laser treatment. It has been suggested that a possible application area for this work is the improvement of adhesion. In the same work, similar phenomena are reported for ceramic materials in that cone type structures can again be produced on the surface of a number of different high performance engineering ceramics such as silicon carbide (SiC), zirconia (ZrO_2) and alumina (Al_2O_3).

Arnold [77] studied the modification of metallic surfaces with excimer lasers. He performed a study to determine ablation rates and surface topography using a range of different laser parameters for micromachining of a range of metals.

These examples demonstrate two important points. Firstly, the shorter wavelength beam is demonstrating a selective removal ability, i.e. subtle changes in material properties are producing different material removal rates. Secondly, although excimer lasers have very interesting capabilities, this type of process is always going to be very slow. Combining this with the rather poor prognosis for the development of high power Excimer lasers leads to the conclusion that this type of process will always be limited to high cost, low volume removal processes.

Attempts have been made in the US to patent a laser cleaning process [84]. UV radiation from an Excimer laser is used for surface cleaning of a range of metallic and non metallic materials. Again the short wavelength of the UV radiation it is claimed, removes contaminants by ablation with no heat input to the target surface It is claimed that particles up to $80\mu m$ in size can be removed, also organic and inorganic films, native oxides and metallic ions. Cost and environmental advantages are claimed.

5.3.4.2 CO_2 lasers

To date, the work in this area has been largely experimental. Duley [85] has achieved some improvements from the use of CO_2 lasers in lowering the fuel permeability of HDPE surfaces. Dyer [86] has also studied the decomposition processes involved during CO_2 laser ablative etching of polyethylene terephthalate at low fluences. Very recent work using high power CO_2 lasers for surface preparation of metallic substrates has been reported by Critchlow [87]. A low irradiance defocused CO_2 laser beam was used to remove organic contaminants from aluminium surfaces.

Although this is not a novel idea in itself, advanced surface analysis techniques were used to examine the surfaces produced. An increase in shear strength of 22% was reported for a bonded aluminium substrate, although this increase might also be possible with a range of other chemical treatments. An increase in the thickness of the magnesium rich oxide layer, a very slight decrease in macro roughness and removal of residual organic contamination was also was also reported in the same work

5.3.4.3 Solid state lasers

Purpose built solid state laser cleaning equipment is now available commercially [88], and prospects for increasing the numbers of applications appears good, although currently average power and hence coverage rates are limited. It appears that cleaning of metallic surfaces can be achieved by a high irradiance, short duration pulse or a lower irradiance millisecond pulse duration technique. There appears to be some confusion as to the nature of the actual material removal mechanism.

Work at Warwick using solid state lasers has also demonstrated the feasibility of removing surface coatings, in this particular case, zinc coatings on steel, prior to adhesive bonding [89].

5.3.5 Paint stripping

Recently, CO_2 laser based equipment has become available both in the US and in Europe [90,91,92] aimed at this application. Although some scientific study has been performed on these techniques, it appears that they have largely come about from process development by laser and system manufacturers. Claims have been made that $100\mu m$ thick coatings can be removed at $1m^2hr^{-1}$ and that there is no damage to underlying layers. Information has emerged from a large US Navy funded programme, Automated Laser Paint Stripping (ALPS). Two systems have been built, designed to selectively remove paint from aircraft. These sophisticated systems, using real time vision feedback control, have been shown to be capable of removing topcoats, paints, textured coatings, sealants and primers from both metallic and composite substrates. Dramatic cost and environmental benefits are claimed.

A pulsed TEA (Transverse Excitation at Atmospheric Pressure) CO_2 laser operating at 1000 Hz, $6\mu s$ with a 5.2 J pulse, currently still under development, is

aimed at removing paint at a target rate of 1.5 m^2min^{-1}. This is a high irradiance process, performed using a rastering technique, and is therefore slow. The removal process appears to rely on rapid absorption of the laser beam in the surface layer, producing a combination of exfoliation, decomposition and shock effects [91]. Pulsed TEA lasers with rectangular cross section pulses are used to allow surfaces to be uniformly treated. In Europe, Urenco [90] also use a pulsed TEA laser, with a 2μs pulse duration, and have recently announced a high power 2 kilowatt system.

5.3.5.1 Solid state laser paint stripping

Two NdYAG laser/fibre optic cable based paint stripping systems are being developed, the first in the US, the second in Japan. Work performed by HDE Systems has demonstrated the feasibility of using an 1800W continuous wave high power solid state laser coupled to fibre optic beam delivery for stripping of aircraft components [93]. In Japan, the possibility of using a similar laser to strip paint from power transmission towers is being investigated [94].

5.4 Treatments with change of state, autogeneous

With reference to Figure 5.1, at irradiances approximately two orders of magnitude below those required for cutting, a range of processes such as melting, cladding and other heat treatment processes are possible. It is also clear from Figure 5.1 that although heat conduction plays a large part in these processes other mechanisms such as beam/material interactions are also important. It is in this area of processing that the pulsed solid state laser can perform novel processing tasks.

5.4.1 Laser surface melting

Many authors have investigated possible benefits of using laser surface melting to improve particular properties of a surface. Advantages are that a good surface finish of ~ 25μm Ra can be obtained with minimal thermal distortion as compared to other high energy sources such as plasma.

Practical applications of this process have not developed simply because the process of laser alloying covered in the next section is only marginally more difficult

but can produce much greater improvements in material properties. Also, surface finishing is often required after processing, increasing costs.

Although many different materials have been examined, the majority of work has been carried out on the following two systems:

- Cast irons; in this case hardening effects occur largely due to martensite formation.

- Stainless steels; improved corrosion resistance has been noted by a number of authors due to a refinement of the grain structure in the surface layer. This has been referred to as a surface homogenisation process and the finer structure is thought to be less susceptible to intergranular corrosion.

5.4.2 Laser glazing

A number of authors such as Matsunawa [95] have examined these rapid solidification phenomena, although a useful review by Breinan and Kear is referred to here [96]. If a high power laser beam is passed at high speed over a surface, cooling rates at the surface can be very high, of the order of 10^6 $^{\circ}Cs^{-1}$. This LAYERGLAZE ™ process utilises irradiances of 1 $MWcm^{-2}$ with 10^{-4} s interaction times, during which localised surface melting occurs with negligible heat transfer into the base material. The sharp temperature gradient produces, for materials exhibiting a deep eutectic, a very hard amorphous metal skin from supercooling to the glass transition temperature. This has the effect of solidifying the material as a glass without a crystal structure and hence most of these deep eutectic materials are very brittle. Corrosion and wear resistance is improved, but the recrystallisation temperature of these materials is low. Hence in a tribological situation, the localised temperatures achieved during asperity contact reduce the wear performance of components. However, to quote Steen "the research importance of this new material is obvious, the engineering importance is less so" [53].

5.4.2.1 Laser glazing of aluminium

Relevant work on surface treatment of aluminium alloys [97] used a laser glazing technique to investigate laser strengthening mechanisms on eutectic cast aluminium silicon alloys. Because of the problems associated with using 10.6 μm radiation and high diffusivity alloys, most of the work has been aimed at refining the

grain structure of eutectic or near eutectic alloys. Significant reductions in friction and wear have been reported. A wider range of possible solute elements was also examined, but as with other glazing techniques, it is debatable whether the property improvements justify the high cost of the process.

5.4.3 Laser assisted deposition processes

Due to the very highly controlled nature of this process, only very low pulse energy and hence low average powers are currently used to deposit very thin coatings and very small quantities of material. As this chapter is concerned mainly with high average power lasers, these two processes do not easily fit in to this thesis. However, as these are currently active topics for laser research and the differences are to an extent only a question of scale, these processes have been briefly considered on the basis of information from Steen.

5.4.3.1 Laser chemical vapour deposition

This process consists of laser heating a controlled area of the target material and introducing a thermally sensitive vapour into the heated zone. The typical rates of deposition are slow, in the order of microns per minute as the reaction must proceed at the rate of the chemical reaction (according to the Arrhenius equation) and it is necessary to avoid mass transport. Excimer lasers have been used, in which case the vapour is broken down directly by photolysis.

5.4.3.2 Laser physical vapour deposition

In this case, the surface of a specific material is ablated in a controlled atmosphere by a laser pulse. The high pressure plume generated results in a deposit on a target substrate. This process has been used to deposit a wide range of thin coatings on a wide range of substrate materials.

5.5 Treatments with change of state, non autogeneous

5.5.1 Laser surface alloying

This is essentially an extension of the process in section 5.3.1 but with the injection of an alloy ingredient in some form into the molten melt pool. A wide variety of surface alloys are possible. Advantages are similar to laser surface melting and surface profiles can be smooth, ~ 10 μm Ra, if the process is correctly controlled. If process speeds are kept low, for a fixed average power, then mixing can be very thorough and consistent composition throughout the melt pool can be obtained. High solidification rates may also permit some metastable alloys to be produced. The following systems have been investigated with varying degrees of success.

5.5.1.1 Gas alloying of titanium and its alloys

This is the most successful of the laser alloying processes, having been developed by Mordike [98] it is now being exploited commercially in Germany. Titanium, although very costly, is used in a variety of high technology applications but its major shortcoming is its poor tribological properties. Fortunately, titanium is very readily laser alloyed using a nitrogen shroud gas. This process is very attractive, in both a commercial and an aesthetic sense. This is due to the formation of a gold coloured layer of very hard nitrides. The hardness of the surface can range from 500 - 1500 Hv depending on the concentration of the TiN phases, which are formed as dendrites and adhere very strongly to the substrate. A similar process has been evaluated by Wehr [99], the main difference being the simultaneous injection of ceramic powder.

5.5.2 Laser cladding

Laser cladding is a treatment application in which wear and corrosion resistant layers are incorporated into the laser melt pool to enhance the performance of the component. During the process thermal gradients in the molten pool produce a vigorous stirring process in the melt pool, ensuring a homogeneous deposit. On cooling, the clad layer is intimately bonded with the substrate and the dilution of the substrate is far below that produced by conventional cladding processes such as plasma

arc. The materials used are usually based on conventional wear resistant or corrosion resistant alloys such as Stellite. Continuous surfaces are produced by overlapping clad layers. Pre-placed, or more usually, blown powder deposition is used. To limit dilution, careful control of processing parameters is required so that an even distribution of alloying elements and hard surfacing metals is melted on to the base material. In certain instances carbide particles are injected into the molten pool to provide a wear resistant layer. A useful review is given in [100].

5.5.2.1 Laser cladding of aluminium

Work by Volz [101] has shown that if very high laser power is available, 10 kW were used in this work, then it is possible to overcome the disadvantageous thermal properties of aluminium. He demonstrated the feasibility of a powder feed cladding process on AlMgSi alloys. Nickel base powders were used in a one step process to produce good quality but relatively thin clad layers with 500 - 700 Hv. This work suggests a process whereby a tribological surfaces may be produced directly onto aluminium surfaces.

5.6 Related processes

There are a number of related processes which are important because of their practical relevance but which do not fit clearly in to the structure of the report, for reasons which will become clear.

5.6.1 Laser surface texturing

It is important for the sake of clarity here to define what is meant by direct and indirect texturing. Direct texturing is defined as using the laser to directly etch a functional component and indirect texturing refers to laser texturing of a tool surface which is then used to produce a texture or pattern on a secondary surface. This is however an arbitrary practical distinction as lasers can be used for both tasks.

5.6.1.1 Direct laser texturing

The work covered in this thesis is essentially a direct laser texturing technique, and is of course covered in detail in the later chapters.

5.6.1.2 Laser milling

A technique developed in Germany, known as 'Lasercaving' [102] has been used for laser milling of cavities or textures in steel moulds, graphite electrodes, glasses and ceramics. In this instance, a 750 W pulsed CO_2 laser has been incorporated into a five axis milling machine with limited commercial success to date [103].

5.6.1.3 Indirect laser texturing

For a number of years, pulsed CO_2 lasers have been used for texturing, or more correctly, patterning, of elastomeric and chromium oxide coated rollers used in the printing industry. Equipment is now also commercially available, based on the Lasercaving process in the previous section, to accurately scan naturally textured materials such as leather, and to reproduce this texture by engraving the pattern on to a matching pair of embossing cylinders [104].

Also, originally developed in Belgium, and now being used by Nissan in Japan, is a similar technique. This process has been developed using a Q switched NdYag laser to produce a pattern of pits on the surface of steel mill texturing rolls. Sheets passed through the mill are indirectly surfaced to aid paint adhesion and paint flow on the surface [105].

5.6.2 Laser dulling

Scott [106] has performed a feasibility study to produce a highly random surface on steel to be used either directly or indirectly as an alternative to shot blasting. The work was aimed at producing a controllable surface for coinage stamping dies. A NdYag laser was used and some interesting results were produced on specular and diffuse reflection values after laser treatment.

5.6.3 Laser annealing

Interest in this process was stimulated by a desire to remove damage from ion implanted semiconductors and research has spread to a wide range of similar processes. A great deal of theoretical analysis in this area is reviewed in [107], although no large scale industrialisation of these processes has occurred. This work led however, to a lot of interest in material damage thresholds under laser radiation.

5.6.4 Laser shaping technology

This is not normally classified as a laser surface modification process, as it is not the primary objective of the process. The objective here is to induce a change of shape in a sheet material using the highly controlled directional heat input of a laser beam. It is included because of the very similar principles involved. The technology of shaping metals and their alloys by means of a laser beam (LST), without the use of shaping tools and external forces, is currently being studied by a number of research groups. A group at the Institute of Fundamental Technological Research of the Polish Academy of Sciences [108] have demonstrated the mechanism of this technology. The laser is used to induce thermal gradients and thermal stresses in the material by traversing a laser beam along a chosen line on the metal surface. Rapid cooling, which can be natural or artificial, evokes permanent plastic strains and shape change. The technique is being promoted as suitable for industrial use and examples of prototypes produced by this technique have been shown. It is suggested that significant savings in tooling costs might accrue from this technique. There are a number of questions still to be answered as to the range of shapes possible by this technique, and the effect of the process on mechanical properties of the formed components. It is unclear at this stage of development of the process as to whether a limited amount of melting might not be too detrimental to the process.

5.7 Laser surface melting

A great deal of academic interest has centred on laser - material interactions, much of this work emerged from the work mentioned in section 5.6.3 . Of particular relevance to the current work are the thresholds for laser melting. Von Allmen [55] provides perhaps the most comprehensive overview of this work. A good review by Patel & Brewster [109] also summarises the effect of irradiance with respect to solid state laser processing. They point out that power density (in our case pulse irradiance) is the most important variable in determining the reaction of a surface to a laser beam.

5.7.1 Irradiance dependency

As already discussed briefly in 3.4.4.4, in the case of solid state lasers (as opposed to Excimer lasers, where the term fluence is employed), the term intensity is widely used as a semi quantitative measure of power per unit area. Sometimes, marginally more specifically, peak intensity or peak power per unit area is used. However, this term is still only at best semi quantitative for two reasons. Firstly, many laser users and even manufacturers assess collimated beam dimensions using relatively inaccurate techniques, such as exposed photographic paper ("burn paper"). A second technique based on the use of Kapton film for measuring focused spot sizes is also known to be unreliable if a range of pulse energies and peak pulse powers are used [111]. More accurate measurement is difficult unless costly and complex beam analysis equipment is available [110]. Combined with approximate calculation of focused spot sizes, inaccuracy is inevitable. It was also noted that many researchers in this field use similarly inaccurate techniques for assessing irradiance and this uncertainty concerning irradiance (intensity) values appears regularly in the published literature. Secondly, the term intensity does not take into account spatial energy distribution across the beam nor does it take into account temporal variations within the pulse energy. The term 'irradiance' or more correctly 'pulse irradiance' allows for the averaged nature of both the temporal and spatial distribution within the laser pulses, and is therefore a more correct definition of the average energy flux per unit area at the workpiece and is used in this work. It is measured and referred to in units of $MWcm^{2}$. Pulse irradiance largely determines the initial reaction of the target to the laser beam. Taking the difficulties described above associated with interpreting irradiance results into consideration, published work on the effect of pulse irradiance is now considered.

Von Allmen suggests that material vaporisation can take place over a very wide range of irradiance, from $0.001-10^{9}$ $MWcm^{-2}$, the upper end of this range being the highest achieved to date. The specific effect depends on wavelength, and many distinct regions are found over this enormous range. At the lower end of this irradiance range, melting occurs and as irradiance increases, an increasing degree of vaporisation takes place. At the lower end of this range, of interest here, some authors are in close agreement with von Allmen, who states that below an irradiance of ~ 1 $MWcm^{-2}$, depending on the wavelength of the radiation, ejected vapours are tenuous and

transparent [31]. With increasing irradiance, the vapour tends to become supersaturated as it evolves from the surface. Condensing droplets of sub micrometer size lead to absorption and scattering. In addition, von Allmen [31] states that the vapour cloud becomes a medium with a different refractive index from its surroundings and distorts the incoming beam. At higher irradiance, approximately 10 MWcm^{-2} for 1.06 μm radiation, which von Allmen predicts as a vaporisation threshold, vapour becomes partially ionised and absorbs a substantial fraction of the beam. However, what then appears to happen is that the black body radiation emitted by the vapour plasma is absorbed more efficiently by the solid, particularly in the case of 1.06 μm beams, improving energy transfer into the target. Typical values for laser melting, are shown to be in the order of 0.01 - 1 MWcm^{-2} for 1.06 μm radiation.

Less convincingly, Lewis and Dixon [28] produce evidence of enhanced coupling from plasma generation, and they demonstrate an enhanced coupling effect. They suggest that absorption of the beam by a plasma can occur at lower irradiance, 0.1 - 0.2 MWcm^{-2}, and the concept of Laser Supported Combustion waves (LSC) for this irradiance range is introduced. Again, using 1.06 μm solid state laser radiation, and using similar pulse duration and pulse energy to the current work, high speed photography and sound intensity measurements were used to support their findings. In a later paper by the same authors, Lewis & Dixon [114], it is suggested that a number of short lived plasmas form rapidly within each long laser pulse (3-8 ms), it is proposed that this phenomenon contributes to heat input during welding by creating the step reduction in reflectivity. The values quoted for threshold irradiance however, are in agreement with values from von Allmen for similar effects.

Most of the above agrees with work by Matsunawa [30], whose work is perhaps the most relevant. He has studied solid state laser welding plumes extensively and has clarified, by various optical diagnoses, that evaporation of target material takes place throughout most of the duration of the laser pulse. He suggests that the emission of light, which is the result of photon absorption by evaporated atoms, happens only for a short time at the beginning of the pulse, but the scattering of the incoming beam associated with this was apparently shown to continue for a while after the end of light emission. Matsunawa also shows that what is referred to as a plume blocking effect, as opposed to a plasma effect, is accompanied by a tall narrow highly energetic plume

which is responsible for absorbing up to 40% of the pulse energy. He suggests that this type of plume will be very difficult to control by normal aerodynamic means because of the very high speeds involved, and that pulse shaping may well be a technique for controlling the laser plume. The existence of another threshold is also suggested for 1.06 μm radiation above which the plume is no longer composed of finely divided absorbing droplets, but consists of larger, less absorbent molten particles, which can cause less beam blocking. below the plume threshold. One confusing aspect of Matsunawa's otherwise very useful work, is the uncertainty surrounding the irradiance under which the target irradiation occurs. It appears that an estimate of effective spot area on the target surface is used as a basis for irradiance calculation as in the current work, but figures quoted are factor of 10 less than expected at 0.03 MWcm^{-2}. This puts some doubt over the interpretation of these results.

Prokhorov [115] also produces evidence for a coupling threshold associated with material removal for aluminium at an intensity (irradiance) of 2 - 3 MWcm^{-2} using a Nd:glass pulsed laser.

Dausinger [42] also shows a threshold effect, from non keyhole to a keyhole type weld at 2 MWcm^{-2} in recent work based on continuous wave high power solid state laser welding of aluminium alloys.

To conclude, a number of workers have looked at these threshold effects and have suggested that they occur over a wide irradiance range of 0.1-10 MWcm^{-2}, but both estimated and calculated values of irradiance for these threshold effects vary widely for each situation.

5.7.2 Laser induced molten metal flow

Many authors have tackled the problem of analysing laser induced molten metal flow. Most of this work has been aimed at modelling the high irradiance cutting or keyhole welding process, produced by continuous laser beams. This subject is still an active research area, with many questions still to be answered [112]. Most authors have incorporated aspects of heat flow theory and the dynamics of keyhole production in their analytical work on high irradiance laser processing [116-119]. Of these authors, theoretical analysis by Postacioglu [116] on high frequency instabilities in fluid flow which occur during high irradiance laser welding processes is of some relevance

to the current work. However, in the case of the current thesis, a single low duty cycle laser pulse simply produces a symmetrical melted spot. Although this a far less complex problem, molten metal flow is common to both situations.

5.7.3 Laser induced surface phenomena

A range of different surface effects have been noted on laser melted and resolidified surfaces. These have been referred to by a number of different names and these are now reviewed. A summary of the most relevant current published work is now presented. Rykalin [120], Von Allmen [31], Prokhorov [37] and others [121] have identified periodic structures on the surface of laser irradiated materials. These are referred to by a number of names, von Allmen refers to "surface corrugations", "Laser Induced Periodic Surface Structures" (LIPSS), and "periodic ring structures" [113]. Prokhorov [37] refers to "Resonant Periodic Structures" (RPS) & "Non Resonant Periodic Structures" (NRPS). Golubev, who refers to 'surface corrugations' [112] Rykalin [120] refers to 'concentric ring structures', Bagratashvili [123] refers to 'periodic structures of relief'. In work by Kreutz [119], the phenomenon of annular ring generation is included as additional information acquired during a study of InSb & Si single crystal wafers which concentrates mainly on the unrelated LIPRS phenomenon (incipient surface damage on high reflectivity optical surfaces). It has so far been impossible to obtain full details of his work referred to in [119], where Kreutz refers to modelling calculations on the generation of annular rings.

There appears to have been some debate, arising from early Russian work aimed at annealing of semi conductor materials, as to how these various phenomena, which are classed by some authors simply as forms of surface damage, are created [107]. The first type manifests itself in the form of linear or circular corrugations, a form of surface periodicity [123]. This is thought by several authors to be due to an interference effect involving the primary laser beam and scattered optical waves. Von Allmen [31] recognised that controlling the onset of these 'surface corrugations', which occur at much lower power densities than expected from theory, is necessary to control heat input to the surface. However, it is clear that there is a wide range in the scale of melting between these phenomena introduced above. Most are quite different from those under consideration in this work, although in some cases they can produce

interesting effects, in the case of [122], features identified as LRPS are used for a novel design of strain gauge, highlighting the small scale, optical effects which are possible. Because of the significant amount of melting occurring in the current work, the effect of interest here comes quite clearly under the second type of LIPSS effect, identified and named by von Allmen [31], LCW, laser induced capillary waves, (LCW). He clearly identifies the production of these rings as associated with a significant amount of melting having taken place, and therefore as a feature of the laser spot melting process. He identifies the ring phenomenon and has related it to surface acoustic or frozen in capillary waves. He proposes two possible formation mechanisms. They may be either natural frequencies of oscillation of the weld pool itself or they may be forcing frequencies imposed on the weld pool by dynamic instabilities in the molten pool. He also admits that the phenomenon has not been studied to any extent.

It should be noted that to avoid confusion which could occur due to the plethora of laser related acronyms, LCW waves refers to the Laser induced Capillary Wave phenomenon, which is completely different from LSC, laser supported combustion waves, a mechanism of beam / material interaction identified by Lewis and Dixon mentioned in section 8.2.2.

Rykalin [120] suggests that for the case of steel, these annular, axially symmetric perturbations, are due to the emerging vapour exerting a reactive pressure on the molten pool which in turn generates capillary waves, but he makes no mention of the particular case of aluminium. He examines the forces involved in molten metal flow and suggests that other factors such as convective flows caused by surface tension driven flow also play a part. He suggests that a surface tension gradient extends radially from the centre of the beam. This produces increased surface tension towards the circumference of the spot due to the spatial distribution of the energy in the pulse, causing capillary flow and wave motion with a certain period. A pressure head develops inducing a counterflow in a steady state molten flow situation. In short time scales, only ripples are produced. He suggests these are frozen in within the solidification time of the pulse. He also analyses the solidification rate of a small volume of molten metal with time. He quotes an unobtainable obscure Russian reference which associates this effect with reactive pressure of the ejected vapour and that this effect is enhanced by increasing irradiance.

Golubev, who refers to 'surface corrugations' [112] has performed experiments in order to understand the mechanism of keyhole formation, by measuring the speed at which they are formed when using pulsed Nd:Yag laser radiation. He states that over the range 10^4-10^5 Wcm^{-2} , the vapour pressure of the ejected vapour can be ignored due to the limited amount of vaporisation and that melt flow is controlled simply by capillary and thermocapillary forces. At slightly higher irradiances, 3 MWcm^{-2}, he ascribes the concentric rings to the effect of reactive vapour pressure, and produces important evidence to show that in the case of steel, the effect is linked indirectly via the speed of melting of the keyhole, to incident laser irradiance. He also proposes that the irradiance range of 0.5-1 MWcm^{-2} is the range over which keyhole welds are formed, this being the range studied as part of his analysis into keyhole motion. He also identifies a pulsed regime of "metallic plate breakdown" , which is taken to mean the onset of a material removal process. He associates this with the vibrational pattern of melt motion in the keyhole. Although the target in this case is steel, the concentric, annular or symmetrical ring or perturbation phenomenon was identified. It is suggested that they may well be responsible for improving absorption in the keyhole processes. In his experimental work, some very relevant trials were performed using a pulsed solid state laser similar to the one used in this work and a similar set of laser parameters. The pulses used in his work produced single shot keyholes, and he measured, using thin sheets of material and fully penetrating pulses, the velocity of the base of a keyhole during its formation.
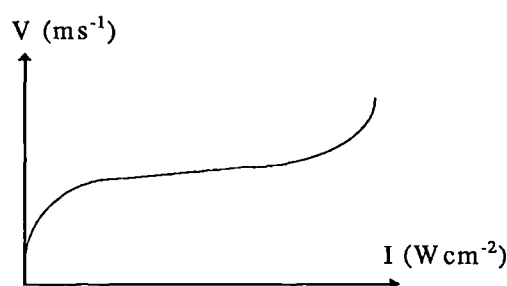
Figure 5.2 Relationship of melt pool cavity motion and irradiance [from 112]

Figure 5.2 shows their plot of melt velocity (keyhole velocity) v irradiance. Again, values of irradiance are unclear, and are not quoted with any degree of certainty. To restate his interpretation of these very relevant results, he suggests that this graph also shows several mechanisms of material removal. At low irradiance, with

limited evaporation, he identifies the mechanism of material removal as being thermocapillary with no vapour pressure effect on melt motion. In the high irradiance regime, the molten material is squeezed out due to the vapour pressure of the melt. At higher irradiance and hence even higher temperatures still boiling and vaporisation dominate, creating a vapour pressure above the material surface and a consequent reactive vapour pressure on the molten material. The end result of this is the generation of a single shot keyhole type hole in steel, on the sides of which annular rings are clearly visible as shown later in this work. His view is that capillary waves are frozen on the side of the keyhole with a pulse period of the order of 30 μm. He relates these to excitation of capillary waves on the melt surface within the keyhole. Furthermore, he proposes that the presence of these rings within the keyhole during the formation of the keyhole is contributing to the very high absorption. This experimental evidence clearly identifies the conditions under which these waves are formed, as well as identifying the changing mechanisms involved in the production of melt spots. Although Golubev's work [112] refers to steel alone, these features have been clearly identified to exist for aluminium in work by Kreutz [110], It therefore seems reasonable to expect that all metals will have similar regimes where annular rings are generated.

Laser generated frozen in surface waves, referred to as annular rings, were therefore identified as a key feature of the melt spots produced, but again, there is no firm data as to threshold conditions for their initiation. However, throughout the course of an extensive literature survey, the deliberate production of this phenomenon on engineering aluminium surfaces has not been recognised and no information has been found on any practical technique to deliberately optimise or avoid this effect on metallic surfaces.

5.7.4 Effects of convection

A number of authors have pointed out the substantial contribution of surface tension driven flow, or Marangoni convection, to the behaviour of molten metal pools, and Gratzke [118] gives a good overview of this subject. He points out that forced convection currents occur in many types of molten pools, and once a significant volume of material has become molten, convection currents play an important role

[125]. Other authors have also highlighted the influence of convection on the geometry of the weld pool in all laser applications which involve melting of significant volumes of metal [62], as is the case in most laser welding and some laser heat treatment applications. Melt pool shape, undercut and ripples and their associated weld defects are all attributed to convection effects, and the effect under study here can be viewed here in the same light - as weld defects. Convection is also primarily responsible for mixing and therefore affects the composition and ultimately, the solidification microstructure of the melt pool, as demonstrated by [62]. They identified solute redistribution during laser surface alloying which could only be due to the presence of convection currents. Furthermore, surface tension driven flow has been identified as responsible for this convection within the melt pool. Most of the authors who discuss this phenomenon identify the presence of surface tension driven flow during high power continuous laser welding processes, and there are far fewer references to the particular case of a single laser melted spot, one of the few being some very comprehensive work by Russo [48].

In contrast, Nonhof's book suggests that significant Marangoni effects would make laser welding a poorly repeatable process, which he claims it clearly is not. He therefore dismisses such effects as negligible.

5.7.5 Fluid mechanics considerations

For further insight into the formation of these waves, basic hydrodynamic equations from Landau & Lifshitz [126] are reproduced. Any liquid surface is in a state of tension, which acts as a restoring force, enabling the surface to support waves in a manner analogous to other waves. From first principles it is possible to derive a_k, the capillary constant for the substance concerned and this determines the shape of the fluid surface.

$$a_k = \left(\frac{2\sigma}{\delta g} \right)^{1/2}$$
Equation 5.1

where in this case σ is the surface tension, δ is density in kgm^{-3} and g is the gravitational constant.

Considering the propagation of these annular, axially symmetric waves on the surface of the molten pool, it is clear the problem is not a steady state problem for the following reasons:

1. the solidification process changes the diameter of the pool.

2. the boundary conditions are non-linear for the arbitrary amplitude of the wave

3. rapid solidification effects such as super cooling will also produce non-linear effects on the motion of the waves, and an accurate analytical solution therefore becomes complicated very rapidly.

Assuming shallow melt pools, in the case of the small wavelength limit, it is shown from first principles [126] using Laplace's formula that the capillary wave is defined by:

$$v^2 = \frac{\sigma \kappa^3}{\delta}$$
Equation 5.2

where v=frequency, σ=surface tension, κ is the wave vector and ρ is density, which can be used to find the profile of the capillary wave. Hence, an increase in density will decrease the frequency of the wave whereas an increase in surface tension will increase the frequency.

There are two further basic fluid mechanics relationships which can be of use in understanding wave phenomena. The attenuation or damping coefficient, γ can give an estimate of the time to fix or level the wave [126].

$$\gamma = \frac{2\upsilon_a^{4/3}\eta}{\delta^{1/3}K^{2/3}}$$

Equation 5.3

where υ_a= angular oscillation frequency in rads^{-1}, η= dynamic viscosity in Nsm^{-2}, δ = density in kgm^{-3} & K = thermal diffusivity in m^{2}s^{-1},

Because of incomplete data on many of the above properties, this equation is included merely as a guide to the possible influences on damping of LCW effects. It is also interesting to note that similar wavelengths to those found in this work, 20 - 50 μm, are reported for steel [112].

It is also shown in [126] that an adsorbed oxygen layer on the surface of the molten aluminium can be expected to have an effect on the damping of thermocapillary waves.

5.7.5.1 Capillary waves

These are described simply as short wavelength waves where surface tension forces resist the increase in free surface area that accompanies deviations from the horizontal. In this general case, usually applied to low viscosity fluids and small amplitude waves, surface tension forces are larger than the gravitational forces.

5.7.6 Effect of surface layers

A brief discussion follows on the possible effects of the presence of surface layers on laser melting of engineering aluminium surfaces.

The direct effect of the damping of capillary waves due to the presence of surface layers is covered in [126]. A paper by Kreutz [119], which leads on closely from the work by Rykalin, and very similar to work by Patel & Brewster [109] identifies the phenomenon of frozen in annular features, but he also suggests that oxide thickness has a significant effect on the generation of these rings.

The work by Patel & Brewster claims to have measured a significant reduction in reflectance when oxygen is used as an assist gas in the laser melting process as opposed to the use of argon. This is said to be due to the formation of an oxide layer, and it is also suggested that a plume formed in an oxidising atmosphere is more absorptive and exists for longer than under an argon atmosphere.

Previous work by the author [43] and by Powell [136], has demonstrated the effect of anodised layers on laser cutting. Laser cutting speeds were increased in the case of CO_2 laser cutting in Powell's work by up to 30%, and it was suggested that this was due to enhanced beam absorption in the anodised layer. The author [43] also identified similar increases in cut speed using both main types of lasers to cut anodised aluminium. The effect on laser cut speed of a range of anodised layer thickness was studied. It was shown that laser cutting speed was increased by a factor of 2.5 when the thickness of the natural oxide layer was increased to 3 μm by sulphuric acid anodising. It was also noted however, that this effect only occurred up to a coating thickness of 5 μm. In the case of the shorter wavelength solid state laser the speed increase was not as large but was still significant. It was proposed that this was largely due to improved absorption of the laser beam by impurities and hydration products in the anodised layer and the anodised layer/metal interface rather than in the oxide layer itself. Otherwise, very little information on the practical effect of a known oxide thickness was found.

The oxide layer itself should, in its pure Al_2O_3 form. a non metallic insulator, transmit the infra red beam well, as shown by Prokhorov [37]. He suggests the effect of a 'thin' naturally occurring oxide layer should be negligible when 1.06 μm radiation is used for two reasons. Firstly, the naturally occurring layer is very small compared to the wavelength of the radiation. Secondly the ionic structure of pure Al_2O_3 should theoretically be fully transmissive. Figure 4.6, from work by Arata [29], shows only a small decrease in the very high reflectivity of an aluminium surface however, due to the use of a shorter wavelength beam Most of this work [29] is performed using longer wavelength 10.6 μm beams, as discussed in section 4.3.5, and shows that surface condition, and in particular, oxide layer thickness, increases absorption of the laser beam into the surface of the material dramatically as expected. A great deal of experimental evidence is produced for this.

Kreutz [124] and Patel & Brewster [109] also suggest that the oxide thickness dominates the coupling of the beam to the material where commercially finished alloys are used as opposed to highly polished mirror finishes which have been used for accumulation of most available specular reflectivity data, such as that in Touloukian's book [46]. Further evidence for the presence of a thin absorbing hydroxide crust is also given by [137].

The slight conflict identified above would appear to be due to the quality differences between thin high quality optical surface layers and the non uniform oxidised surfaces containing hydration products found on standard aluminium engineering materials.

6. Experimental details

6.1 Experimental methodology

The structure of the experimental work is shown below. Several separate series of experiments have been performed.
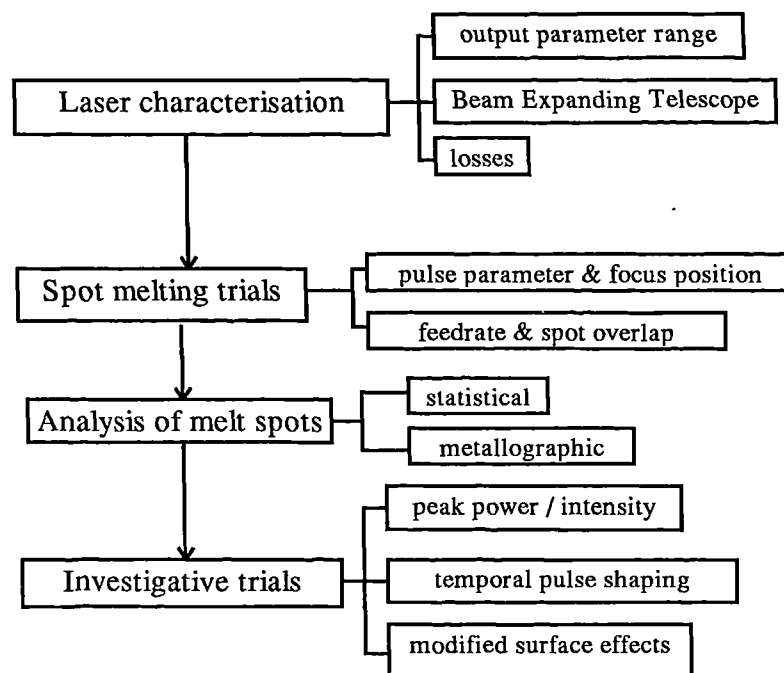
Figure 6.1 Flow diagram of experimental approach

The first of these, the laser characterisation, requires a description of the basic layout of the laser, and an understanding of the interaction of the laser operating variables as described below to justify the experimental methodology.

6.2 General description of laser
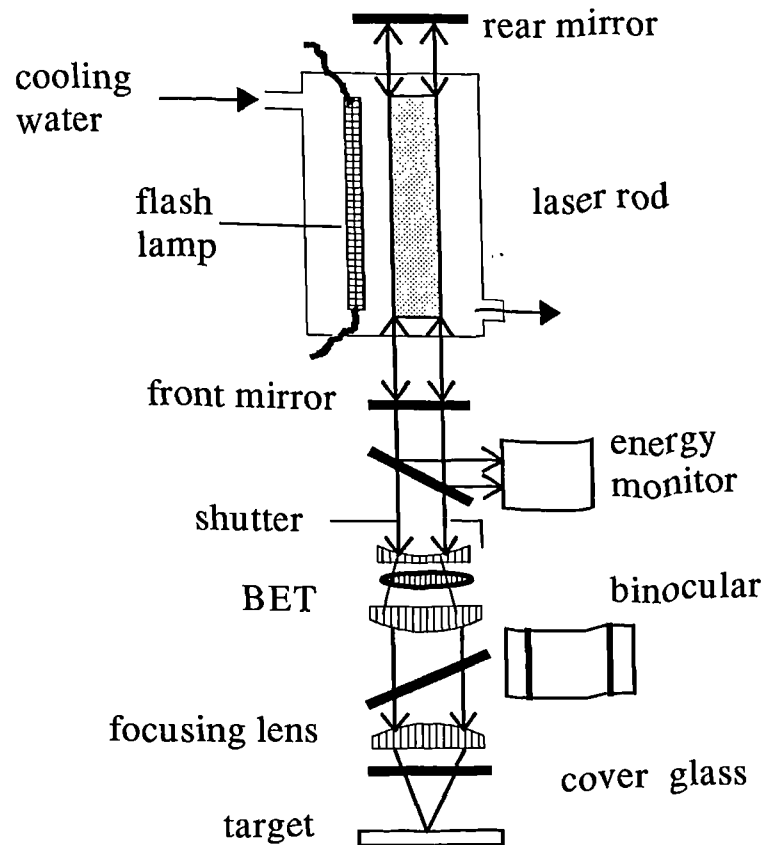
Figure 6.2 Diagram of the essential components of the laser

A JK 701 400 watt solid state laser, designed and manufactured by Lumonics, Rugby was used throughout this experimental work. Details on the laser are given in appendix 2. It is a conventional high average power solid state laser which differs only in detail from many other such lasers on the market. The resonator configuration employed in these trials, was again a relatively straightforward design, with no intra cavity optics, although an external beam expanding telescope was used to modify the diameter of the beam after leaving the resonator. It is demonstrated later that although this design does not produce the smallest focused spots and hence the highest irradiance, in this case this is not essential for the research programme - in laser processing terms only a low irradiance spot is required.
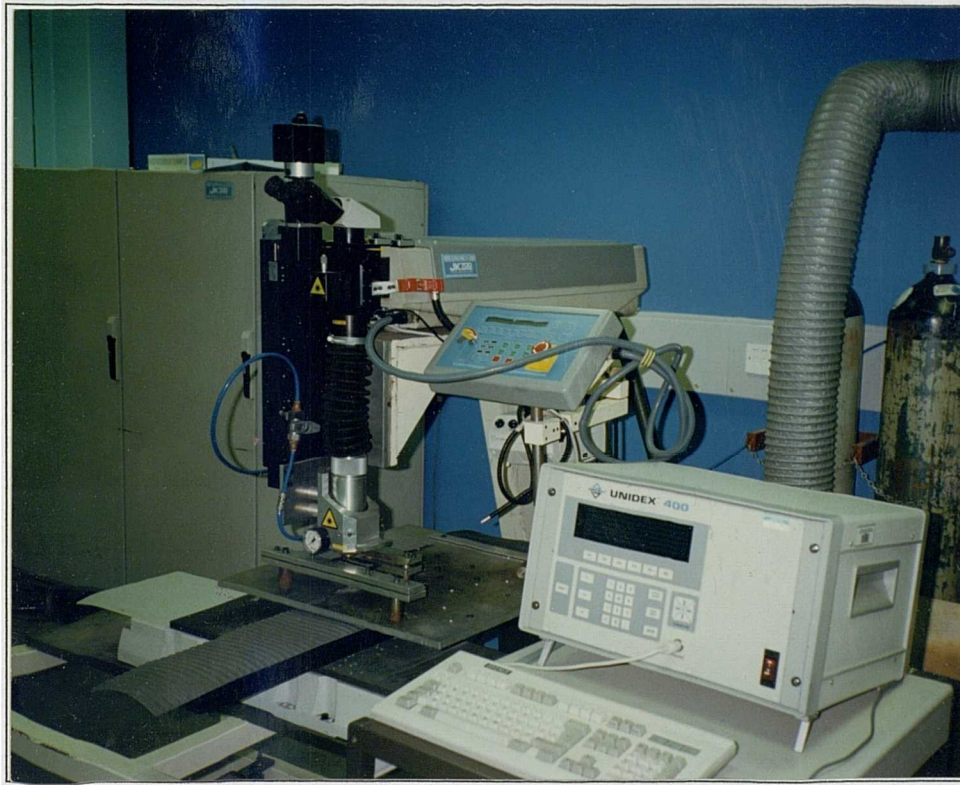
Figure 6.3 Experimental set up

The three primary laser variables as described in section 3.4.4 are;

Pulse repetition rate, expressed in Hertz, denoted v

Pulse duration, expressed in milliseconds, denoted τ

Pulse energy, expressed in joules, denoted E

It must be noted that on this laser, in common with most solid state lasers, the laser pulse repetition rate and the laser pulse duration, often referred to as the pulse length or pulse width, are controlled directly whereas the pulse energy is controlled indirectly through the input power to the laser flashlamps. This quantity is identified as "lamp height". This is an arbitrary figure, which is a percentage of the total allowed lamp current (as defined by the capacity of the laser power supply) at a given combination of laser parameters. This is related to the pulse energy output of the laser by the following approximation [21];

$$\text{Average power, } P = c \text{ x lamp height}^2 \text{ x } \tau \text{ x } v \qquad \textbf{Equation 6.1}$$

where c is a constant, other parameters as above

The simple design of resonator has the advantage that each of these three variables can be adjusted independently over a wide range.

6.2.1 Laser optics

In any laser processing application, the correct laser optics must be identified to produce the correct irradiance for the process. This is usually achieved by selecting first and foremost, the correct focusing lens. A standard Lumonics supplied optical glass singlet focus lens (sometimes referred to as the machining lens) with the widely used focal length of 80 mm was employed. This lens gives a good compromise between available irradiance and depth of focus and is widely used for this type of relatively low irradiance laser application involving mainly melting.

A standard optical set up was used for reasons of interchangeability. Standard factory supplied proprietary optical components were used throughout. To allow reproduction of this experimental work, the part numbers of the key optical components are given in appendix 2.

6.3 Laser characterisation trials

Some limited information was available from the equipment supplier on the range of laser parameters, but extensive experimental work was also necessary to permit the design of an experiment based on this full range.

The trials also establish a benchmark to check the set up and monitor performance before each processing session

6.3.1 Divergence v lamp power

Information on the relationship between beam divergence and lamp input power was supplied by the lasermanufacturer.

6.3.2 Output parameter range

Certain parameter limits are recommended or are built into the laser software control. These are;

1. Pulse duration; Minimum 0.5 ms, maximum 20 ms
2. Pulse repetition rate: Minimum 0.2 Hz, maximum 400 Hz
3. Pulse energy: Maximum recommended is 40 Joules

4. Minimum pulse energy is dependent on the minimum lamp input power at which a stable pulse is emitted. This is usually ~0.5 kW per lamp.

5. Maximum input power to flashlamps: 6 kW per lamp

It is also recommended by the manufacturer of the laser to maintain the maximum peak pulse power of the laser pulses below 5 kW, although as shown later, it is possible to produce higher peak pulse power pulses over a limited area of the operating envelope. As this area was of particular interest the laser was used to produce pulses of up to 6.5 kW peak pulse power.

Additionally, to avoid excess power input to the flashlamps and hence into the laser rod, software limits put a boundary on the operating envelope of the laser. These limits are considered to be proprietary information and are therefore not freely available. Depending on the range of operation of the laser, it is any one of the above conditions which decided the upper practical limit of laser parameters during the characterisation process.

Having taken all the above into account, it became clear that to understand the effect of these laser variables on the process under study and to allow a structured series of experiments, each laser requires an extensive characterisation exercise to identify the full range of performance relevant for this application.

Previous work [11] has shown that, of the primary laser processing variables, pulse duration, pulse energy and pulse repetition rate, it is the peak pulse power, or more correctly, the peak irradiance, (equation 3.4) which is the most significant variable in establishing initial conditions for a particular laser process. It is on this basis therefore that the characterisation was performed.

The significance of pulse repetition rate is easier to identify than the relative effects of τ and E on laser processing - pulse repetition rate clearly controls only the speed of the process.

To commence the characterisation exercise, the complete parameter range of the laser was identified and was split into relevant increments of repetition rate. The available range of pulse duration and pulse energy at these increments of pulse repetition rate was identified over the range of peak pulse powers.

6.3.3 Experimental errors

There are three possible sources of inaccuracy or repeatability errors when establishing the performance of a conventional high power pulsed solid state laser.

6.3.3.1 Lamp ageing

The most significant of these is the phenomena known as "lamp ageing". Due to relatively rapid deterioration in the condition of the high power flashlamps used to "pump" the laser rod, the power output of the laser can decrease in a non linear manner. Fortunately, if the laser parameters chosen are well within the operating envelope of the laser and are not close to any of the software limits imposed by the controller, it is possible to compensate for the reduced efficiency of lamp operation by increasing the input power to the flashlamps. It must be noted however that tabulated values of lamp height are very dependent on the condition of the flashlamps.

6.3.3.2 Alignment

If, as in the characterisation trials, the beam diameter and hence cone angle are altered significantly, the nozzle assembly must be carefully designed and aligned so that at maximum beam diameters the beam is not 'clipping' any components in its path. This can lead to very misleading results, and in the worst case, damage to optical components. Practically, clipping was avoided by checking beam alignment using a photographic burn paper technique before each experimental session and after each change of laser parameters to eliminate such losses.

6.3.3.3 Optical reflection losses

The internal energy monitor within the laser identifies the power output of the laser resonator and therefore does not measure the losses associated with all the other optical components in the optical train as shown in fig. 6.2. During laser processing, all optical surfaces reflect a certain fixed percentage of the beam which is identified by optics suppliers as 2.5 % per uncoated optical surface. These losses are reduced to ~ 0.5 % by using an anti reflection coating specifically tailored to the laser wavelength. These losses, as shown in the following section, can still build up to be a significant proportion of the power of the beam, especially if there is any deterioration or contamination of the optical coatings through everyday wear and tear. As the laser is used for a wide range of other processing tasks, these sources of error need to be quantified and controlled prior to commencing the test programme.

An external power measuring device, a Coherent Fieldmaster, was used to allow comparison between the internally monitored laser power and the power as measured at the target. The Coherent Fieldmaster is a calibrated calorimeter type device. Energy loss measurements were undertaken initially across the spectrum of laser parameters to establish an acceptable figure for losses as a percentage of the beam power, a form of 'condition monitoring' of the laser. These internal and external losses were then monitored before each session throughout the experimental work and any significant increase outside the +/- 0.5% repeatability of the power meter was investigated and rectified.

6.3.3.4 Focus position

The focal plane was located on the surface of the target material for each series of trials. This was achieved by using the binocular viewer on the laser output housing. Although this technique is subjective to a small degree, this subjectivity was reduced by ensuring the measurements were performed by one operator using a consistent procedure.

6.3.4 Beam Expanding Telescope (BET) operation

It is a fundamental property of solid state lasers that the laser beam emerging from the laser rod is of the same diameter as the laser rod itself, but one of the important features of this type of solid state laser is the Beam Expanding Telescope (BET). In optics terms this is a Gallilean telescope whose primary function is to compensate for "thermal lensing", the increase in divergence associated with an increase in pumping power (input power to the flashlamps) mentioned in chapter 3. In practice, the BET has two functions. The first is to allow recollimation of the beam to a parallel beam of the required diameter after alteration of the level of optical pumping through the flashlamps has produced an increase in beam divergence through thermal lensing. Secondly, it has been suggested that the BET may be used to adjust the diameter of the beam to that required for the particular application. The optics principle used here is that an increase in the beam diameter produces a smaller focused spot size, hence increasing irradiance at the workpiece. As shown in chapter 3, it is the lamp input power which controls the divergence of the beam, hence if peak irradiance at a given vertical plane in the beam after the focus lens is to be maintained constant over a range of laser parameters, then either lamp input power must be maintained

constant or the Beam Expanding Telescope must be used to compensate by increasing or decreasing the diameter and recollimating the beam as it enters the focusing lens. Equally, if it is required to increase the pulse irradiance (intensity) for a particular laser application, then this may be achieved by using the BET in the same way to achieve a non linear increase.

In this case, the BET is designed to increase the beam diameter from its nominal 9.525 mm diameter (3/8 in, the diameter of the laser rod as purchased in imperial units) by a factor of 3. In practice however, neither of these techniques are as useful as might be expected due to the following uncertainties:

1. In this type of laser, the lenses are purchased with a wide tolerance on the focal length, making accurate calibration very difficult.

2. The adjustment of the lens position is in this case is performed by a rather imprecise rod linkage making it poorly repeatable.

3. The widely used technique which was employed in this work for measuring the actual diameter of the beam is of limited accuracy. This is despite the precaution of using a constant set of laser parameters on every occasion.

4. Previous work [11] has shown that in the case of this design of telescope, there is an optimum operating condition at a beam diameter of 18 mm.

A graphical representation of the functioning of the BET and the approximate settings as supplied by the laser manufacturer is included in appendix 3. In addition, a preliminary calibration for a single set of laser parameters is included. However, for the reasons given above, a fixed beam diameter of 18 mm has been used from this point onwards.

As a result of the laser characterisation trials, a range of laser parameters over the full range of peak pulse power capability were identified, but all were at a fixed average power, and hence an approximately fixed pumping power. Hence beam divergence remained unchanged and adjustment of the BET was only necessary over a very limited range. In this way one of the major problems associated with investigating solid state laser processing was overcome [111]. Results presented in tables 6.2 - 6.4 show the BET settings which produced a collimated beam of 18 mm diameter for this particular laser and optics train for all the laser parameters used for the pulse parameter trials.

6.4 Spot melting trials

The large number of variables to consider when processing with solid state lasers can be split up into three main groups: process conditions, the nature of the target material and the laser parameters employed. The techniques by which the conditions used were identified is given in order below.

6.4.1 Spot melting conditions

To allow analysis of the effects of modifying laser parameters on the production of melt spots, it was necessary to produce a large number rapidly. This was achieved by a straightforward CNC controlled rastering motion of the target beneath the stationary output housing. As in almost all high power laser processing, a coaxial assist gas is employed. Argon is commonly used as a cover gas in this type of application to provide a degree of protection to the target area from atmospheric contamination. Initial trials showed that melt spots produced without using a cover gas produced badly disrupted surfaces.
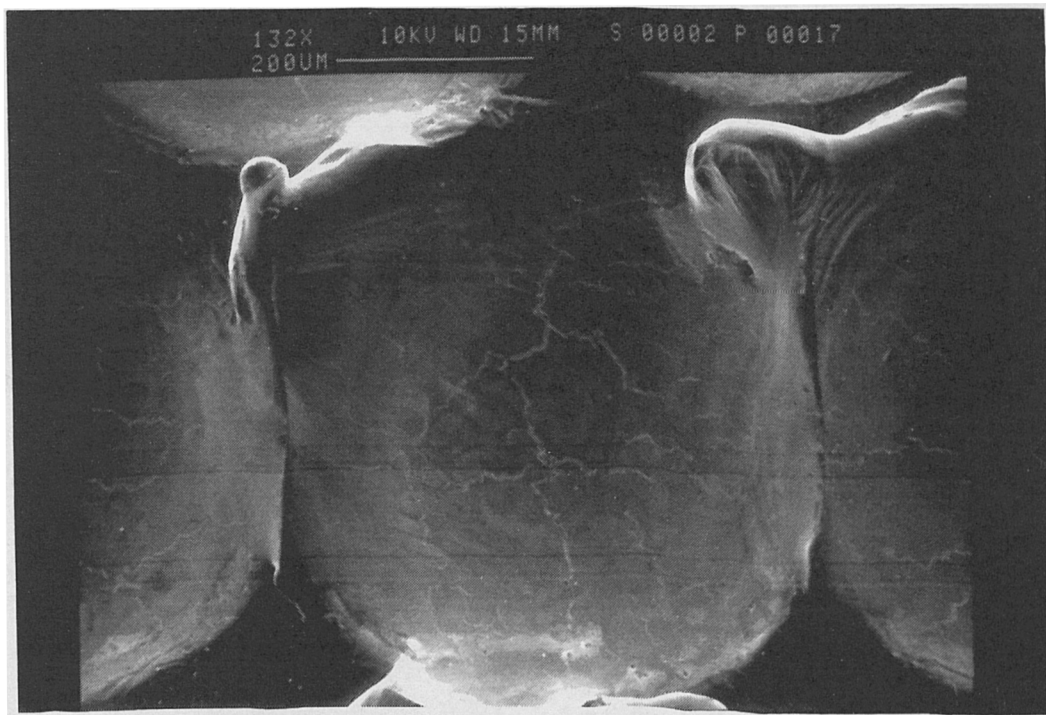
Figure 6.4 showing effect of excessive gas pressure [138]

In this work therefore, a standard laser machining head set up was used throughout with a only a very low flow rate of 0.5 lmin^{-1} of argon delivered co-axially to the workpiece through a large diameter aperture. Higher argon flow rates and gas

delivery speeds were seen to cause undesired disruption of the melt pool (fig.6.4). The exact conditions at the horizontal plane of impact of the laser beam are governed by the geometry of the nozzle and the nozzle to workpiece distance, known as the "nozzle stand off". Although the nozzle to workpiece distance in this case varied with the distance of the target plane from the focal plane, the flow rate of the cover gas was low enough so as not to produce any significant effect on the laser melt spot. The main practical benefit of using such a gas flow was to keep the focusing optics free from fume deposits. To produce large numbers of these melt spots, the process speed, v in mmmin^{-1}, is set by the pulse repetition rate of the laser and to a lesser extent by the melt spot size.

6.4.2 Target material

The properties of aluminium surfaces in general were introduced in 4.3.1. More details are now presented on the particular aluminium alloy used in this work. A single 2m x 1m sheet of material, purchased to a standard specification, with a standard mill surface finish was used for all the trials. The sheet was guillotined into a large number of small samples for all the trials, hence no significant macro scale variations in material and surface properties were expected. All samples were acetone degreased prior to use.

To use the internationally accepted four letter designation of the Aluminium Association (AA), commercial aluminium alloys with magnesium and silicon as their main alloying elements are denoted 6xxx alloys [139]. These alloying elements combine to form magnesium silicide, (Mg_2Si), which in turn forms a simple eutectic system with aluminium. It is precipitation of the Mg_2Si after artificial ageing (denoted by the T6 temper) which allows these alloys to reach their full strength. This group, which also contains alloys such as 6053, 6061, and 6063 are characterised by excellent corrosion resistance and are more workable than other heat-treatable aluminium alloys. Table 6.1 identifies the more common 6000 series alloys, their chemical composition and applications.

AA Designation	Chemical Composition	Typical Application
6009	0.8Si-0.6Mg-0.5Mn-0.35Cu	Automobile body panels
6010	1.0Si-0.8Mg-0.5Mn-0.35Cu	Automobile body panels
6061	1.0Mg-0.6Si-0.3Cu-0.2Cr	Trucks, towers, structural applications
6016	1.0-1.5Si-025-0.6Mg-0.5Fe-0.2Cu- 0.2Mn-0.1Cr-0.2Zn-0.15Ti + others	Automotive exterior panels body panels
6063	0.7Mg-0.4Si	Pipe, railings, truck and trailer flooring,

Table 6.1 6000 series alloys and their applications [139]

The best known characteristic of aluminium is its light weight, the density being about one-third that of steel or copper alloys, (certain aluminium alloys have better strength-to-weight ratio than that of high-strength steels). Aluminium has good malleability and formability, high corrosion resistance, and high electrical and thermal conductivity. Of great relevance to this work are the unusual, interesting, and often very useful surface properties of aluminium. Although there are many applications where these properties are put to good use, ultra-pure of forms of aluminium are widely used for reflectors to take advantage of its high reflectivity.

AA-6016, or to use the manufacturers trademark name Anticorodal -120 ® is a recently developed aluminium magnesium-silicon alloy. Used in the T4 temper condition (solution heat treated & naturally aged to a substantially stable condition), it is designed especially for automotive panel applications, and because of its acceptance by major car manufacturers, it was accepted as the primary material for study in this work. A full material specification is given in appendix 1.

In this work, the material utilised was purchased to a specification which identified the surface finish as a standard mill finish. This is described as a ridged surface in the rolling direction (appendix 1) and a microscopic examination of the surface was performed. Prior to each trial, the target surface was thoroughly degreased.
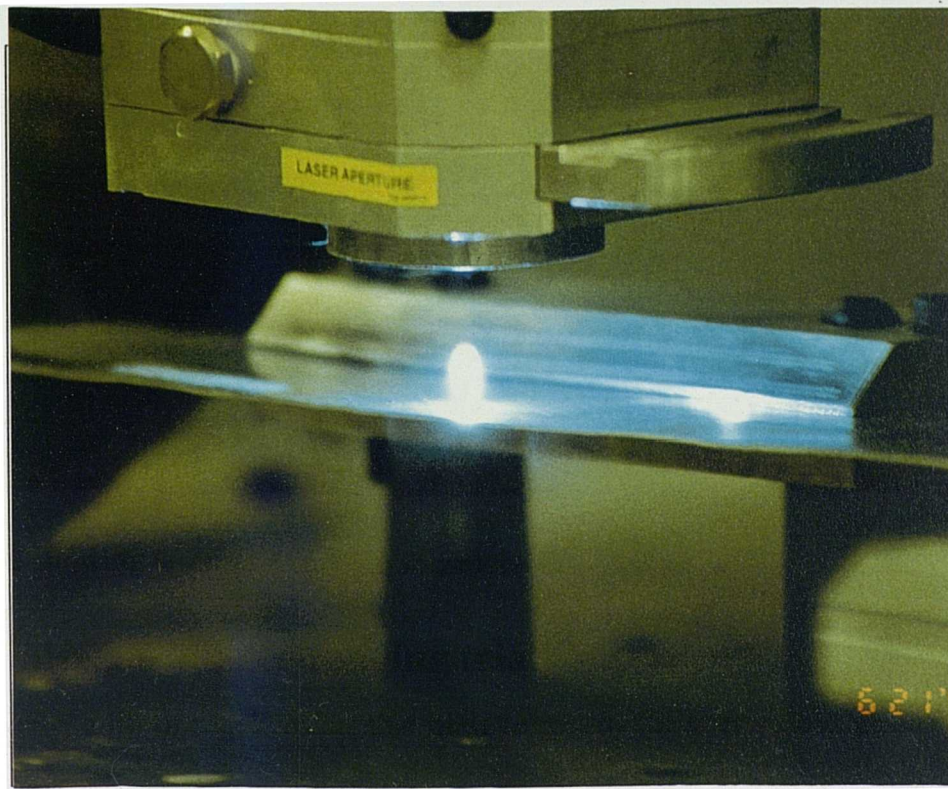
Figure 6.5 showing laser spot melting in process

6.4.3 Pulse parameter ranging trials

Firstly, a list of requirements that must be met by the laser melted spots were identified:

- The spot must be produced at the focal plane of the lens. Although using a defocused beam was satisfactory for the ranging trials, evidence in [113] suggests that a focused beam is preferable.

- The parameters used must be comfortably within the operating envelope of the laser to allow stable laser operation and pulse to pulse repeatability, hence 20 J was the maximum pulse energy.

- The workpiece speed must be well within the capabilities of the workstation to ensure accurate spot position.

- The effective melt spot size must be large enough to allow easy optical and metallographic examination.

- Focused spot size must be small enough to provide significant melting of the aluminium surface. It is necessary to melt a substantial surface layer of the material to allow investigation of the spot melting process.

- The minimum pulse energy was taken to be the minimum pulse energy required to produce a measurable melt spot on the surface of the material.

- The specific heat input to the surface must be low enough to reduce distortion of the workpiece to an acceptable level - any thermally induced distortion altered the position of the target with respect to the focus position. This was necessary to avoid altering the vertical position of the target during processing.

To meet these requirements, an experimental matrix of laser parameters was designed based on the results from the characterisation exercise which identified the relevant operating envelope of the laser.

At a fixed average power of 100 watts, and for each increment of peak pulse power, pulse energy, and over a range of defocus positions, parameter settings which covered the complete operating envelope of the laser were used to produce a large number of spots for assessment. It should be noted that speeds were of the order of $1mmin^{-1}$, hence the time taken to produce large numbers of melt spots was realistic. As can be seen from the following tables, lamp power remains approximately constant,

Pulse duration	Lamp	Av. lamp	Peak	BET	
τ,ms	ht, %	power, kW	power, kW	Focus	Ratio
2	27.6	1.9	1.00	370	635
1	39.8	1.8	2.00	370	635
0.7	48.8	1.8	2.86	370	635
0.5	58.3	1.8	4.00	370	635

Table 6.2 Parameters at 50Hz, 2J

Pulse duration	Lamp	Av. lamp	Peak	BET	
τ, ms	ht, %	power, kW	power, kW	Focus	Ratio
5	49.8	1.75	1.00	370	632
2.5	43.2	1.65	2.00	370	632
1.7	55.1	1.6	2.94	370	632
1.3	63.8	1.6	3.85	370	632
1	77.9	1.65	5.00	370	632

Table 6.3 Range of parameters at 20 Hz, 5J

Pulse duration	Lamp	Av. lamp	Peak	BET	
τ, ms	ht, %	power, kW	power, kW	Focus	Ratio
10	29.5	1.75	1.00	376	635
5	44.2	1.6	2.00	376	635
3.3	57.7	1.55	3.03	376	635
2.5	68.5	1.55	4.00	376	635
2	80.7	1.6	5.00	376	635

Table 6.4 Range of parameters at 10Hz, 10J

It was noted that a conduction limited melt pool could be achieved for a range of combinations of peak pulse power and irradiance.intensity. Even with a high reflectivity target material such as aluminium, a melt spot with a relatively smooth surface could be produced. It was concluded that the production of melt spots was repeatable and reliable at mid range laser parameters which could easily reproduced over long periods of time.

6.4.3.1 20 Hz, 2.5 ms, 5 J

At these parameters, the laser is functioning under optimum conditions. Lamp input power is constant at 1.6 kW per lamp, 3.2 kW in total. Lamp height, in % (equation 6.1) is 42%, and varied only very slightly as lamps aged. As with most solid state lasers, a slight adjustment of this figure to obtain the required parameters before each experimental session is normal. A comprehensive evaluation of melt spots produced at the 20Hz, 2.5 ms, 5 J parameters was performed.

6.4.4 Feed rate and spot overlap trials

A CNC programme was produced to raster the workpiece under the laser machining head. The process speed was calculated from the effective diameter of the chosen melt spot to produce melt spots which were as close as possible. The orthogonal (y co-ordinate) distance in the rastering programme was also altered to obtain the maximum surface coverage. Using preferred laser parameters from the previous section, closely aligned melt spots were produced for assessment. In this way, the parameters of 20 Hz, 2.5ms and 5 Joules were identified as producing the best surface features.

During the course of these trials, some key observations were made on the nature of the melt spots produced.

6.5 Assessment of melt spots

6.5.1 Surface characteristics of melt spots

An investigation into the surface diameter of the melt spots was initiated, the first step being to identify any outstanding features and any variation in their surface area.

For those melt spots produced under the ranging trials, the diameters of a significant number of melt spots were measured using a low power travelling microscope. For a minimum of six melt spots for each parameter setting, spot diameters were measured in both orthogonal axes and results were averaged.

For those melt spots produced under section 6.4.3.1, a more in depth investigation was performed on a large number of melt spots. Image analysis techniques were used to investigate melt pool depths and diameters. At this point, the lack of consistency caused by the occasional presence of symmetrical rings on the surface of the melt spots was noted. An initial evaluation of this phenomenon was performed by analysing the frequency of their occurrence over a large number of melt spots.

For the optimisation trials, a technique using a low power optical microscope and an eyepiece measuring graticule proved by far the simplest and most accurate measurement of spot diameter

6.5.1.1 Determination of pulse irradiance (intensity)

Pulse irradiance (in $MWcm^{-2}$) is recognised as being the controlling variable when determining the initial reaction of a material to a laser beam. Hence, any understanding of the spot melting process must be based on an assessment of peak irradiance at the workpiece. In practice it is very difficult to measure accurately [111]. However, at this stage of the experimental programme, it became clear from initial results that the measurement of surface spot diameters over the limited range of parameters used in the later trials agreed well with spot measurements taken from transverse sections (fig. 6.6).

6.5.2 Metallographic analysis

The specimens produced in the preliminary trials were examined using the Seescan Image Analyser to facilitate the measurement of the actual length, d_3 , and depth, d_4 , of the melt pools. Several transverse metallographic specimens were prepared from the textured samples according to a conventional metallurgical preparation technique. Because of the difficulty of identifying the true diametral cross section of each individual melt spot, it was necessary to develop an appropriate technique shown schematically below for the later trials.

exploded view of part of transverse section AA/, BB/

spot depth, d
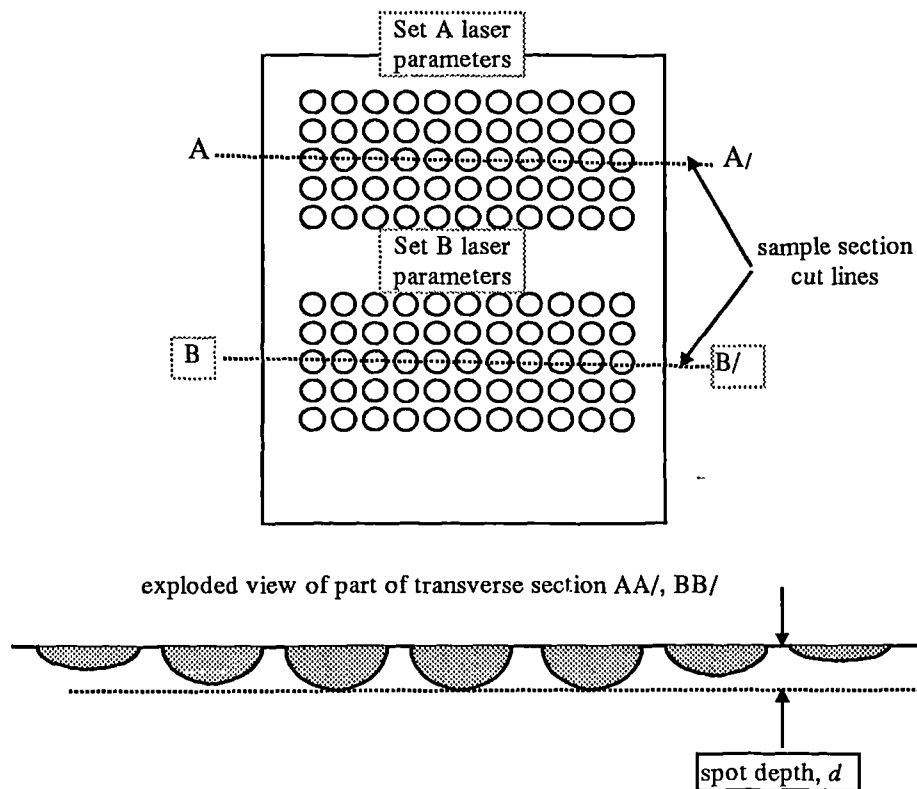
Figure 6.6 schematic of transverse sample preparation

Another feature of this analysis work was the use of a ferric chloride macro etch which reliably identified the melt zone area. The volume of the melt spots was calculated from the depth and diameters using simple geometrical formulae.

6.6 Stage 2 trials

Consideration of the results from the previous sections showed that at certain conditions the surface of particular melt spots consisted of a pattern of concentric rings. This was a very unexpected result from the initial trials, and in order to investigate the spot melting process further, and if control was to be maintained over the process, the reasons for the production of concentric rings needed to be identified and controlled.

A working hypothesis was formulated as follows:

The occurrence of symmetrical concentric waves on the melt pool surface might be due to the freezing in of waves during solidification of the melt pool.

A number of techniques were considered to modify the mechanism of heat input to the target material to permit further investigation of the phenomena now identified on the textured surfaces. Only three were considered practical. The first was to investigate more closely the threshold for generation of these surface features. The second was based on temporal modification of the laser pulse. The third proposal was to use a different approach and to modify the aluminium surface by anodising.

6.6.1 Peak pulse power and pulse irradiance

The literature review had identified references to similar threshold phenomena [37,55,112, 119]. To study this further, a more accurate mechanism for changing irradiance incrementally was required. This is most easily achieved in practice by changing pulse peak pulse power in isolation and in small increments through changing the pulse duration, which is controlled accurately. The comprehensive characterisation exercise permitted this to be readily achieved. It was found that over what had now been identified as the relevant section of the working envelope of the laser, i.e. 20 Hz, 5 J, the laser was capable of 6.25 kW peak pulse power, well above the specified 5 kW maximum. A further range of texturing trials were therefore conducted in which the peak pulse power was varied over this extended range. Identical processing parameters were used throughout, only pulse duration was changed in smaller increments of 0.1 ms. A series of laser surfacing trials using the full range of peak pulse powers at the 20 Hz, 2.5 ms, 5 J parameters were therefore carried out to identify the peak pulse power at which similar phenomena were identified.

Measurements of surface spot diameter were made and these were supported by the measurement of transverse cross sections of the melt spots shown in the previous section.

6.6.2 Pulse shaping trials

Although the previous trials identified specific parameters at which symmetrical waves were generated, a number of questions still remained unanswered. An improved understanding of the mechanism of the beam material interaction and the timescales involved in the generation of these waves had still to be determined.

A possible technique for improving the heating and cooling rates of pulsed laser welding processes has been suggested by a number of sources, [130,131,134].

The laser based technique considered practical for controlling the rate of heat input was temporal modification of the laser pulse - "pulse shaping".

The particular solid state laser used for this programme is equipped with a capability to produce temporally shaped pulses, which it has been suggested might lead to changes in solidification rates during laser melting processes. This ability to temporally modify laser pulses has become a standard facility on all solid state lasers manufactured recently, since its initial inception by Lumonics. Essentially, the technique allows the input pulses to the flashlamps to be split up into a series of segments whose parameters can be individually tailored. Because the laser pulse follows the flashlamp pulse rapidly, (response times are approximately a factor of 10^{-2} less than the minimum laser pulse duration) the temporal distribution of energy within the pulse is modified indirectly. The accuracy with which the temporal profile of the pulses could be monitored was limited by the sampling rate of the oscilloscope used and by the pyroelectric detector (energy monitor) within the laser head. Hence, the oscilloscope trace is only a representation of the true nature of the laser pulse and can only approximate the laser pulses. However, this only becomes a problem when attempting to identify the height of the 'spike' at the start of the laser pulse and it is the average peak pulse power of the pulse which is of interest here.

The relatively short pulse duration of 2.5 ms identified as optimum conditions for spot melting limited the number of possible combinations simply due to the fact that the minimum programmable pulse duration for each sector of the laser pulse is 0.5 ms, hence the total number of sectors in the pulse is initially limited to a maximum of 5.

Furthermore, limitations associated with the rise and fall times of capacitors in the laser power supply does not allow a stable repeatable pulse at low lamp inputs at this minimum pulse duration. Hence, a minimum pulse duration of 0.6 ms was used, further limiting the maximum number of sectors to 4. within these limitations, a "rising" and a "falling" pulse shape were identified. For both rising and falling pulse types, a 2, 3 and 4 sector pulse was devised by adjusting the input power of each sector of the laser pulse, the objective being to achieve an approximately linear slope to the leading and trailing edges of the pulse. The aim was to produce different heat input characteristics of the laser pulse from those of the standard pulse, whilst maintaining the total pulse energy of 5 joules. In addition, it was necessary to maintain the same pulse duration, 2.5 ms. It is most important to note that in each case, the total pulse energy and peak pulse power were maintained as constant as possible, within the accuracy limitations of the internal power meter. The laser parameters developed are presented in chapter 7.

A series of surfacing trials using the same processing parameters were then carried out using these shaped pulses. The surfaces produced were examined as before.

6.7 Further investigations
6.7.1 Modified aluminium surface layers

The third and final technique for modifying the input from the laser pulse to the material was non laser based. All aluminium alloys possess a natural oxide coating, cf. section 4.3. Enhancement of this high melting point low thermal conductivity coating by anodising is a well established industrial technique. Previous work has shown that this oxide layer has a very important effect on laser processing of aluminium, largely due to enhanced absorption of the incident beam by this surface layer.

There were two reasons for pursuing this approach. Firstly, it was felt that the effect of these surface layers would improve understanding of the absorption of the laser beam by the surface layer, which theoretically should not, in its pure form, absorb infra red radiation (section 5.3). Secondly, the damping effect of surface layers on the behaviour of molten metal weld pools is a well known fluid mechanics phenomenon, and the presence of these films might allow further insight into the formation of the melt pools.

To investigate the effect of this layer more thoroughly, a series of aluminium alloy test coupons were prepared from the same sheet of the same aluminium alloy as used for the previous work. These were sulphuric acid anodised under rigorously controlled standard bath conditions of temperature and current density. Coupons were anodised for a range of times to deposit a range of layer depths up to 35 μm. In addition, a batch of identical samples were sodium hydroxide (NaOH) etched to remove as much as possible of the naturally occurring oxide layer to provide a comparison with the above samples. Oxide layer thickness was measured by an appropriate technique. In the case of the thin oxide layers this was performed using an Auger technique and in the case of the enhanced anodised layer, a metallographic technique was used.

Identical laser pulses to those used in the previous section were employed to produce textured surfaces on etched samples and samples with the minimum anodised layer thickness, 3 μm. The effect of these modified surfaces on the laser melting was examined again using optical examination and standard metallographic techniques as before. Spot diameter and depth were again measured.

Enhanced absorption from the presence of surface layers has been noted in the literature but apart from [29], the subject has received little attention, particularly in the case of 1.06 μm radiation.

6.7.2 Pulse shaping and modified surface layers

Temporally shaped pulses were also used to produce melt spots on the modified aluminium surfaces as before. Optical and metallographic investigations were again carried out to determine the contribution of temporal pulse shaping to the surface melting process. A total of eight pulse shapes were used on etched and anodised surfaces.

7. Experimental results

7.1 Laser characterisation

7.1.1 Beam divergence
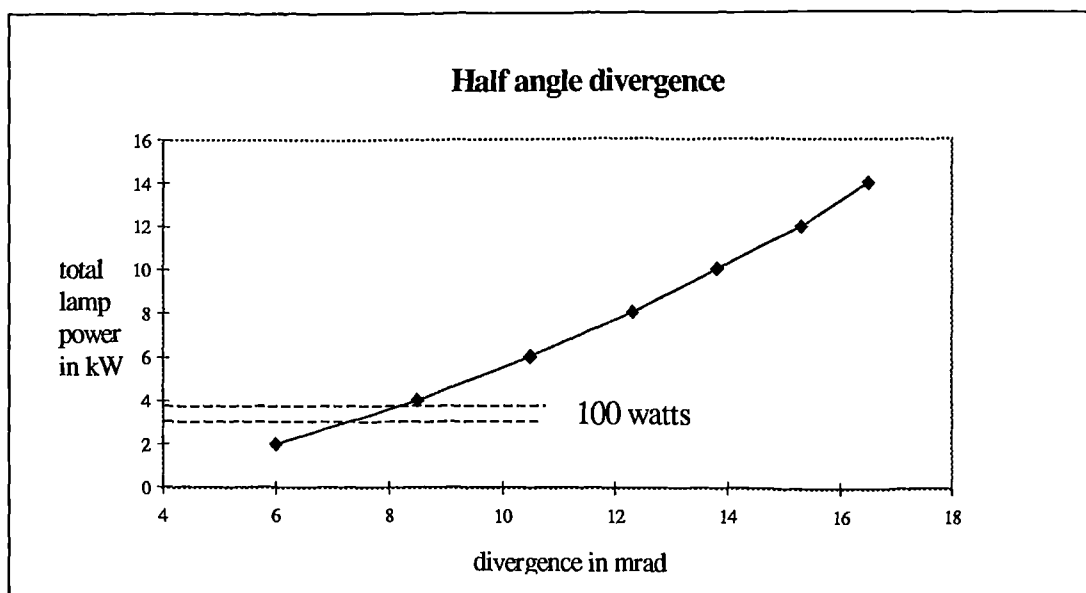
Figure 7.1 Divergence v lamp input power for Lumonics JK 701 laser [140]

Lumonics supplied these figures, taken from a well developed theoretical model of the resonator.

7.1.2 Output parameter range

The resonator was characterised to identify the widest possible range of laser parameters over which the laser functioned in a stable manner. An abbreviated version showing the range of results is given in below, full results are given in appendix 1.

Pulse duration	Pulse rate	Lamp	Av. lamp	Pulse	Int. output
τ, ms	Hz	ht, %	power, kW	energy, J	power, W
0.5	5	40.1	0.1	0.5	2.5
20.0	5	31.0	6.0	20.0	100
0.5	10	32.5	0.1	0.5	5
20.0	10	30.4	3.6	20	200
0.5	20	30.3	0.25	0.5	10
17.0	20	30.7	6.0	17	340
0.5	50	37.7	0.7	0.5	25
6.5	50	30.5 ··	6.0	6.5	325
0.5	75	27.7	1.1	0.5	37.5
4.2	75	30.3	5.6	4	300
0.5	100	27	1.4	0.5	50
3.1	100	30.4	6	3.1	310
0.5	150	28.3	2	0.5	75
2.0	150	30.2	6	2	300
0.5	200	28.9	2.8	0.5	100
1.4	200	30.2	5.9	1.4	280

Table 7.1 Laser characterisation at 1 kW peak pulse power

Table 7.1 shows that at this low peak pulse power, maximum average power is not possible.

Pulse duration	Pulse rate	Lamp	Av. lamp	Pulse	Int. output
τ, ms	Hz	ht, %	power, kW	energy, J	power, W
0.5	5	53.1	0.1	1.0	5
20.0	5	46.3	3.0	40	200
1.5	10	44	0.5	3.0	30
20.0	10	45	6.0	40.0	400
0.5	20	41.0	0.35	1.0	20
9.8	20	45.0	6.00	19.6	392
0.5	50	38.6	1.15	1	50
3.7	50	44.5	6.00	7.5	375
0.5	75	39.0	1.65	1.0	75
2.4	75	43.5	6.00	4.8	360
0.5	100	38.5	2.25	1	100
1.8	100	43.5	6.00	3.6	360
0.5	150	39.8	3.25	1	150
1.1	150	43	5.95	2.2	330
0.5	200	41	4.35	1	200
0.8	200	43.8	6	1.6	320

Table 7.2 Laser characterisation at 2 kW peak pulse power

Pulse duration	Pulse rate	Lamp	Av. lamp	Pulse	Int. output
τ, ms	Hz	ht, %	power, kW	energy, J	power, W
0.5	5	65.4	0.15	0.5	2.5
20.0	5	59.1	2.95	39	195
1.0	10	58.2	0.55	3	30
13.0	10	59.0	5.9	39	390
0.5	20	53.8	0.55	1.5	30
6.6	20	58.5	6.0	20	400
0.5	50	51.5	1.5	1.5	75
2.6	50	56.8	6.0	7.8	390
0.5	75	50.9	2.35	1.5	113
1.6	75	56.4	5.9	4.8	360
0.5	100	52.6	3.0	1.5	150
1.2	100	55.8	6.0	3.6	360
0.5	150	52	4.5	1.5	225
0.7	150	54	5.65	2.1	315
0.5	200	53.2	5.8	1.5	300

Table 7.3 Laser characterisation at 3 kW peak pulse power

Again, it should be noted that maximum average power is available over a limited range of parameters.

Pulse duration	Pulse rate	Lamp	Av. lamp	Pulse	Int. output
τ, ms	Hz	ht, %	power, kW	energy, J	power, W
0.5	5	78.4	0.2	2	10
10.0	5	72.7	3.1	40	200
1.0	10	68.8	0.7	4	40
10.0	10	71.7	6	40	400
0.5	20	60.8	0.75	2	40
5.0	20	69.8	5.95	20	400
0.5	50	58.3	1.8	2	100
1.9	50	69	5.95	7.6	380
0.5	75	59.7	2.95	2	150
1.2	75	67.0	5.9	4.8	360
0.5	100	65.0	3.9	2	200
0.9	100	63.7	5.95	3.55	355
0.5	150	58.9	5.45	2	300

Table 7.4 Laser characterisation at 4 kW peak pulse power

Pulse duration τ, ms	Pulse rate Hz	Lamp ht, %	Av. lamp power, kW	Pulse energy, J	Int. output power, W
0.5	5	76.6	0.2	2.5	12.5
5.0	5	84.3	1.95	25	125
2.0	10	83	1.6	10	100
8.0	10	83.3	6	40	400
0.5	20	71.3	0.9	2.5	50
4.0	20	81.6	6.0	20	400
0.5	50	73.6	2.3	2.5	125
1.5	50	81.5	5.9	7.5	375
0.5	75	76.3	3.5	2.5	188
1.0	75	79.1	6.0	5.0	375
0.5	100	78.6	4.65	2.5	250
0.6	100	78.7	6.0	3.45	345

Table 7.5 Laser characterisation at 5 kW peak pulse power

Table 7.4 & 7.5 show that 400 watts average power, the nominal maximum output of the laser is available over a reasonable spread of parameters at these higher peak pulse powers.

These figures are most important to put the whole thesis in context, one of the main problems with published information on solid state lasers is that very little information is supplied to put the experimental trials into context. These figures show where the selected parameters fit into the operating envelope of the particular laser chosen for this work.

It was observed at this stage that to obtain good repeatable stable laser output, and to allow for the inevitable deterioration in lamp output over the extended period of the experimental programme, it was necessary to use laser parameters well away from the limits of the operating regime of the laser. From this stage therefore laser parameters were chosen which were well within the working envelope of the laser, and the required parameters could always be reproduced.

7.1.3 Power losses

As before, a summary is given here, the full data is given in appendix 1.

Pulse duration	Pulse rate	Av. lamp	Int. output	Ext. output	Loss
τ, ms	Hz	power, kW	power, W	power, W	%
4.0	5	0.7	40	35	12.5
20.0	5	3.0	200	171	14.5
2.5	10	0.8	50	44	12.0
20.0	10	6.0	390	328	15.9
1.0	20	0.7	40	37	7.5
9.8	20	6.0	392	328	16.3
0.5	50	1.15	50	44	12.0
3.7	50	6.0	375	313	16.5
0.5	75	1.65	75	64	14.7
2.4	75	5.95	360	308	14.4
0.5	100	2.25	100	87	13.0
1.8	100	6	360	309	14.2
0.5	150	3.25	150	131	12.7
1.1	150	5.95	330	289	12.4
0.5	200	4.35	200	179	10.5
0.8	200	6	320	279	12.8

Table 7.6. Losses at 2 kW peak pulse power

The standard manufacturer supplied internal power meter is positioned within the laser head, between the two turning mirrors as shown in fig.6.2. To ensure repeatability between experiments, the power was measured using an external power meter before each series of trials and the loss figure compared to those shown above. The total power loss is relatively consistent over the majority of the operating range of the laser, although losses do appear to increase at the extremes of the operating envelope of the laser. These effects have previously been ascribed to lens inaccuracies.

After having decided on the 20 Hz, 2 kW peak pulse power parameter settings a further loss calibration was undertaken and results are given below;

Power loss at 20 Hz, 2 kW peak power
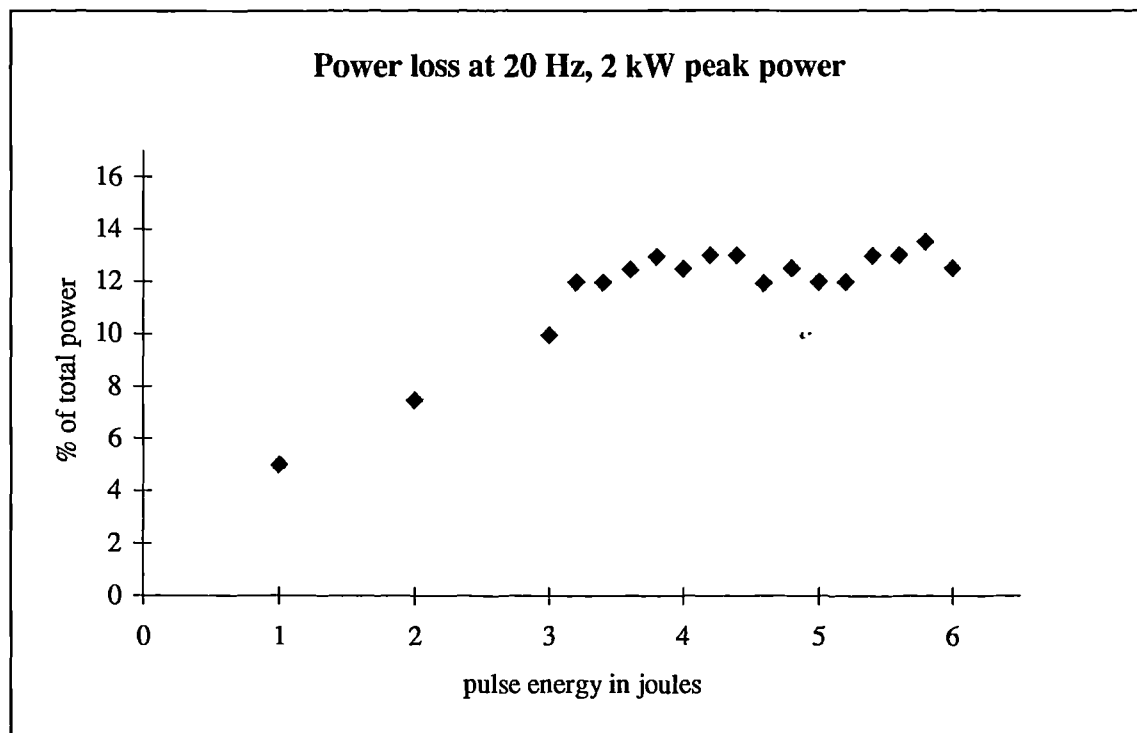
Figure 7.2 showing relationship between power loss and pulse energy

At a fixed peak pulse power of 2 kW losses change with pulse energy over the full operating envelope as shown in Fig.7.2.

On the basis of these results for the particular optical set up used in this work, the losses fall consistently within 12 - 17 % of the total internal power of the laser. It was decided that a figure of 14% should be taken as the maximum permissible loss. Any increase above this figure required investigation. Although this occasionally occurred, the cause was always found to be either a contaminated or incorrectly fitted cover glass, or an incorrectly aligned beam.

7.1.3.1 Experimental errors

During the identification of the above laser parameters, a number of possible sources of experimental error and poor repeatability were identified:

Start up: It has been noted that beam structure can change significantly during warming up. It is most important for this type of processing that an adequate start up time is established and adhered to. In this case, a period of 10 minutes was used to ensure stability. After this period, a loss measurement was taken. If necessary, the rear mirror and / or lamp input power were adjusted to achieve the required parameters.

Lamp deterioration: The progressive deterioration of flashlamps, largely due to sputtering of electrode material, affects the long term repeatability of the laser

output. Although the laser used has a facility to compensate for lamp ageing, parameters were selected which are well within the operating envelope of the laser. It should be noted that lamp deterioration is very dependant on the laser parameters selected, as a general guide, short pulse duration and lower duty cycles lead to long lamp lives.

Condition monitoring: Before each processing session, it was confirmed that the output power at the workpiece was within the 14% figure derived from figure 7.2. If the total loss exceeded this figure, the fault was investigated and rectified.

7.1.4 Beam Expanding Telescope (BET)

As the lamp input power was maintained approximately constant over the ranging trials, thermal lensing effects were minimised. Also, no major optical components were replaced during the course of the trials, (the only exception being lens cover glasses). Therefore only minor adjustments of the BET were occasionally necessary to ensure a fixed beam diameter of 18 mm throughout. Settings are given in tables 6.2-6.4 for the parameters used.

7.2 Spot melting ranging trials

7.2.1 Pulse parameter / focus position trials

Rastering the target under the stationary beam produced different series of melt spots using each of the parameter combinations given in table 6.2 - 6.4. Firstly, at each of these combinations, a range of defocus conditions were used to produce melt spots at different intensities - results plotted graphically in fig. 7.3. Secondly, melt spots were produced at focus, and the operating range of the laser was split up into increments of pulse repetition rate / pulse energy combinations and fig. 7.4 was produced.

A minimum of six melt spots were measured for each parameter combination and defocus position using a x 20 binocular microscope with eyepiece graticule and X Y positioning tables to +/- 10 μm.
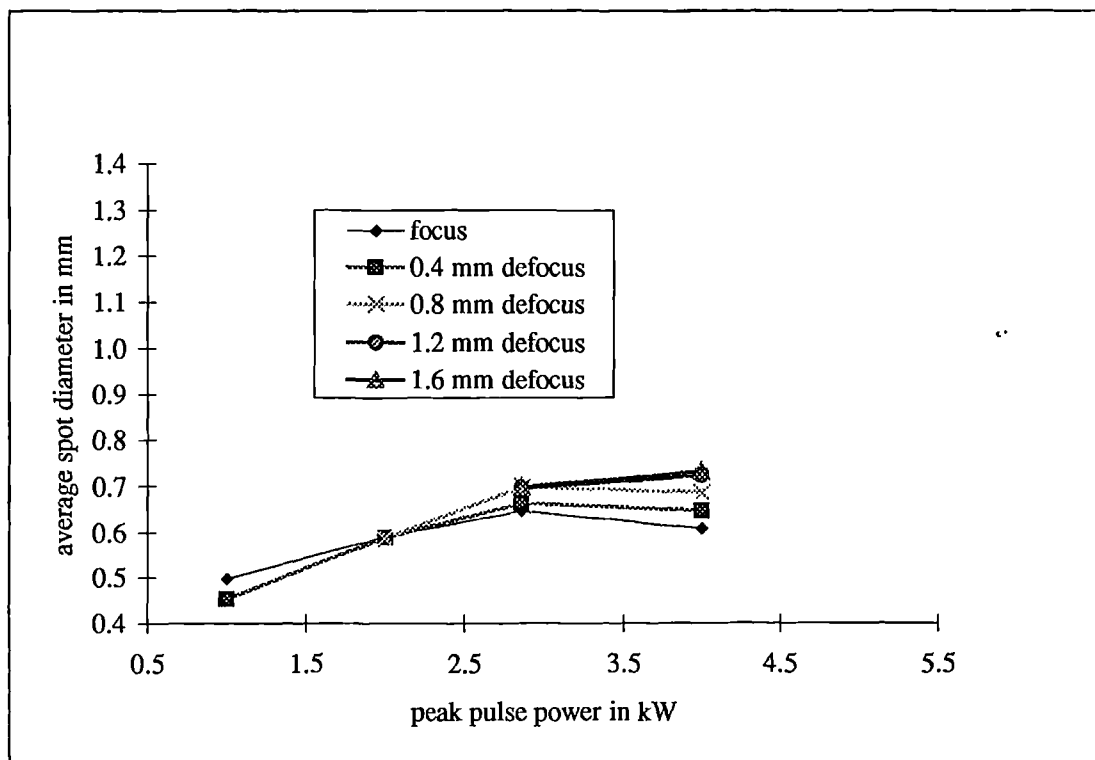
Figure 7.3 showing average spot diameters for full range of laser parameters

Fig. 7.3 identifies the range of melt spot diameters possible with a defocused beam and shows a general increase in spot diameter with peak pulse power and defocus. There is a suggestion towards a maximum spot size near the middle of the peak pulse power range.
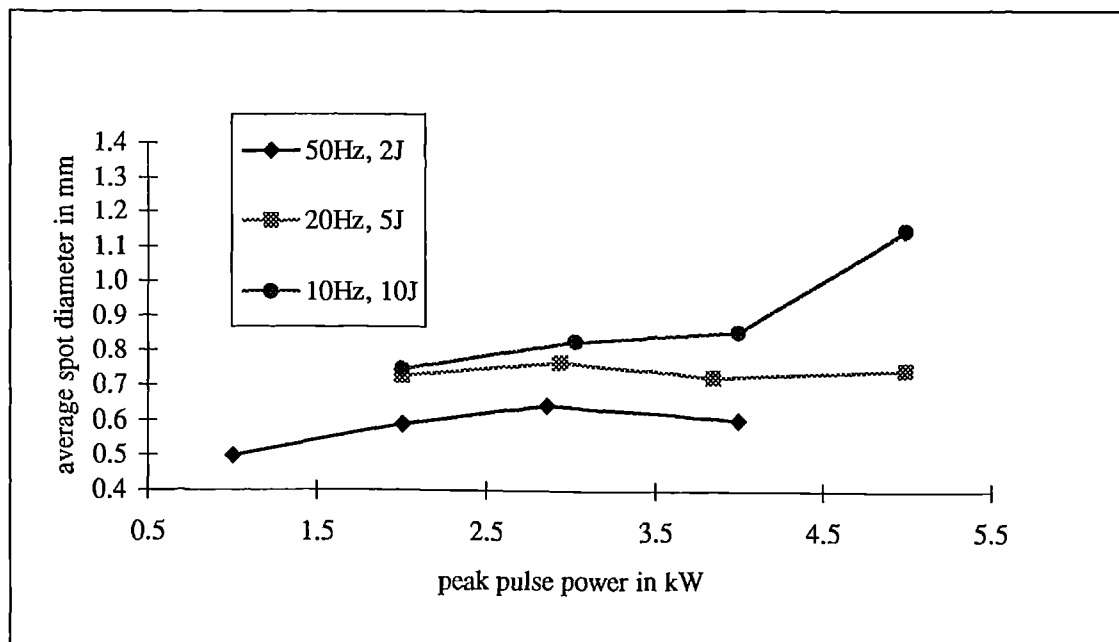
Figure 7.4 showing variation in average spot diameter with pulse energy

Figure 7.4 is a summary using three sets of parameters that span the relevant range of the operating envelope identified in the characterisation exercise. This plot shows the full range of spot sizes achievable using a focused beam, showing an increase in spot size with pulse energy and a suggestion of a threshold effect at higher pulse energy and higher peak pulse powers.

Although these summary plots gave good indications of the range of melt spot sizes, further analysis was required. Graphical plots were produced at each of the three pulse energy settings to identify more closely these trends in melt spot size.
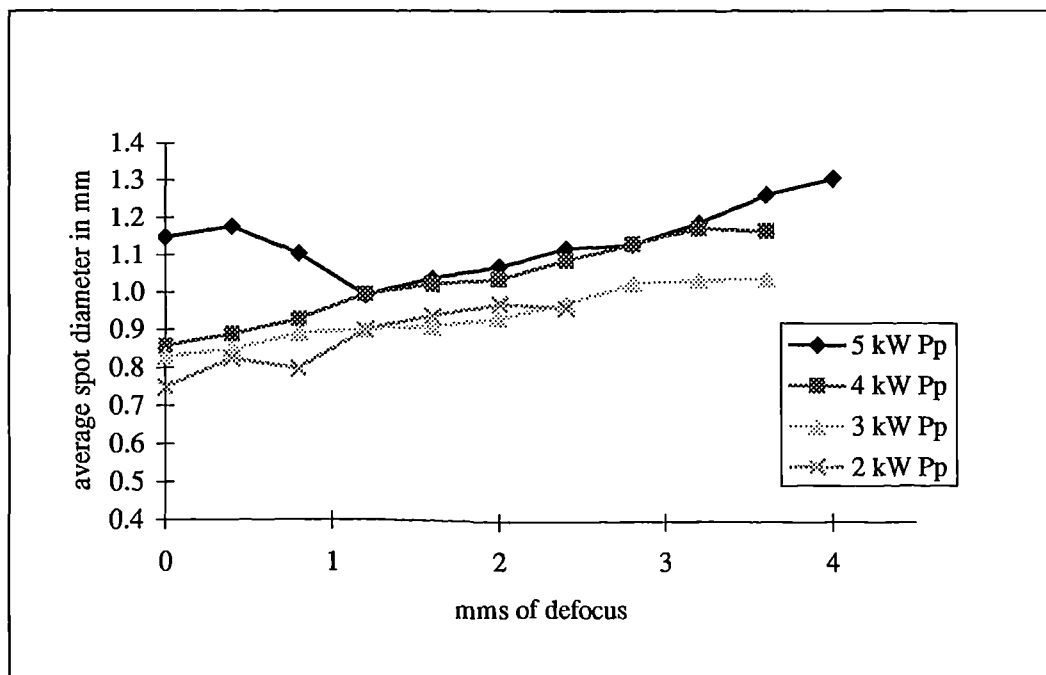
Figure 7.5 showing variation in average spot diameters at 10 Hz, 10 J

Fig.7.4 shows a gradual increase in spot size with defocus, but again with a possible threshold effect at high irradiance and high peak pulse power. There is also generally an increase in spot size with peak pulse power over most of the range of defocus.
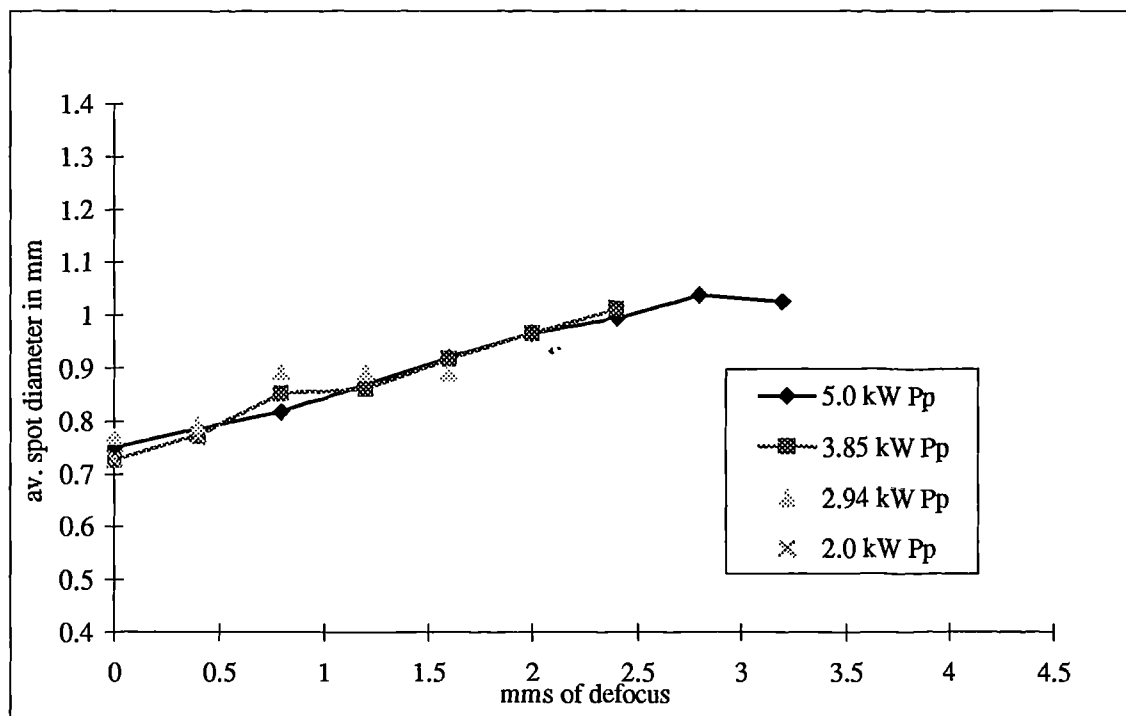
Figure 7.6 showing variation of average spot diameters at 20 Hz, 5 J

In this case of mid range laser pulse energy, there is a predictable approximately linear relationship between spot diameter and defocus distance, but with a possible low irradiance threshold at large defocus distances. On the basis of spot diameter alone, there does not appear to be a large increase in spot size associated with an increase in peak pulse power over this range.
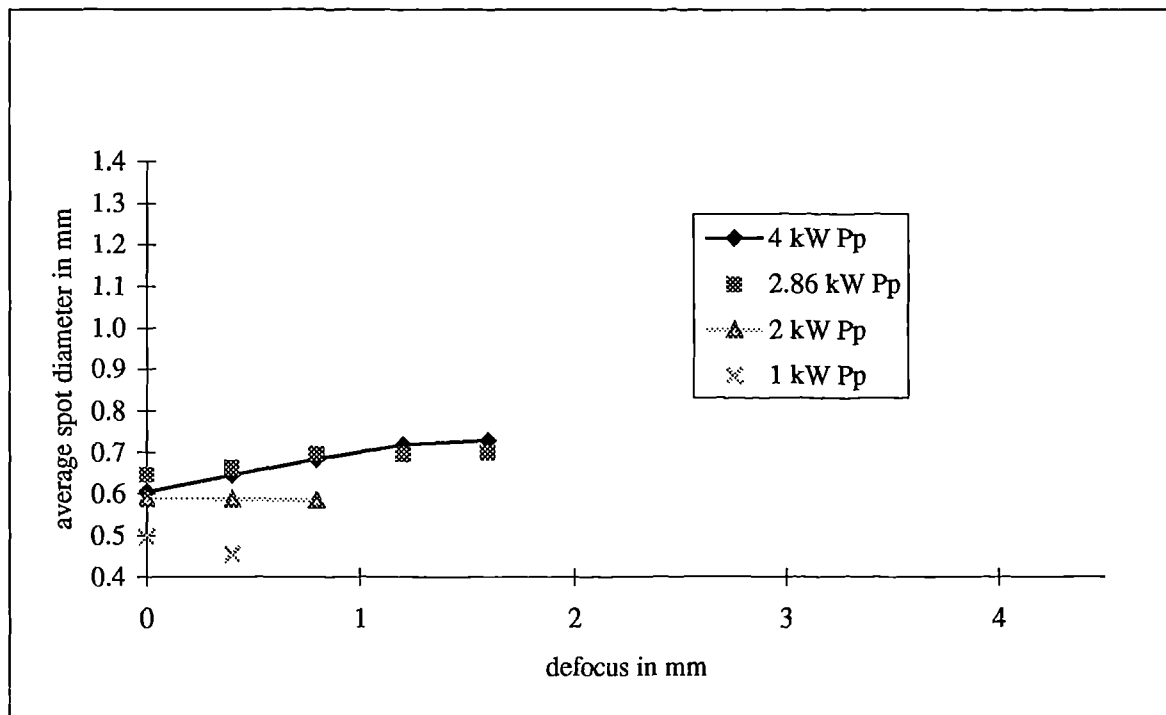
Figure 7.7 showing variation in average spot diameters at 50 Hz, 2J

At this pulse energy level, the range of spot diameters is limited due to a low irradiance threshold below which no significant melting occurs. At low peak pulse powers, coupling of the beam to the workpiece appears very unpredictable, but at high peak pulse power coupling behaviour appears more predictable.

Low magnification optical and SEM examinations identified a number of important features, which are shown in figs. 7.8 - 7.12.

High irradiance / high pulse energy parameter combinations produced disrupted melt spots, as below, fig.7.8 & 7.9. Both of these photographs show holes produced by laser melting and both show evidence of concentric ring structures frozen in to the sides of the hole. It is suggested that both of these photographs show a border between weld formation and hole formation, and hence identify a particular threshold for material removal. At this stage, it was noted that certain parameter combinations produced a very high percentage of spots exhibiting concentric surface rings, fig. 7.10 shows conditions under which all spots exhibited prominent concentric rings. Other parameters produced almost *no melting, fig. 7.11.*

Figure 7.8 10 Hz, 10 J, 2 ms, 0.4 mm defocus, excess energy / irradiance

Figure 7.9 Same conditions as 7.8, showing melt ejection and ring structure
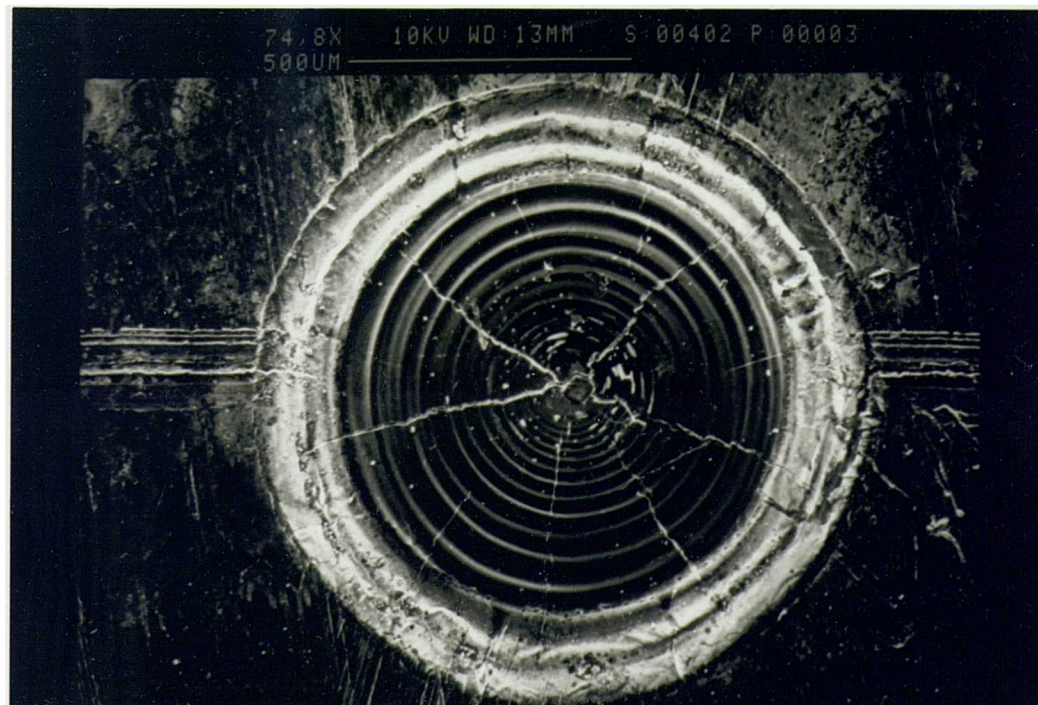
Figure 7.10 Same conditions as 7.8, except 1.2 mm defocus

Fig. 7.10 shows prominent rings at high peak pulse power, and close to the melt ejection threshold.
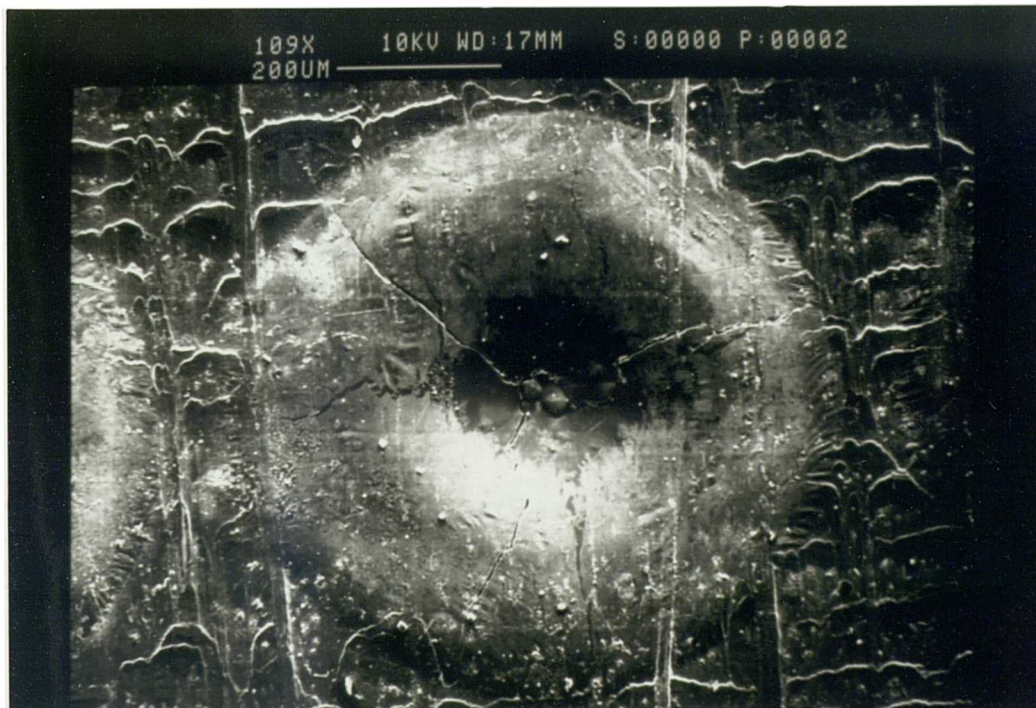
Figure 7.11 20 Hz, 5J, 4 ms, at focus
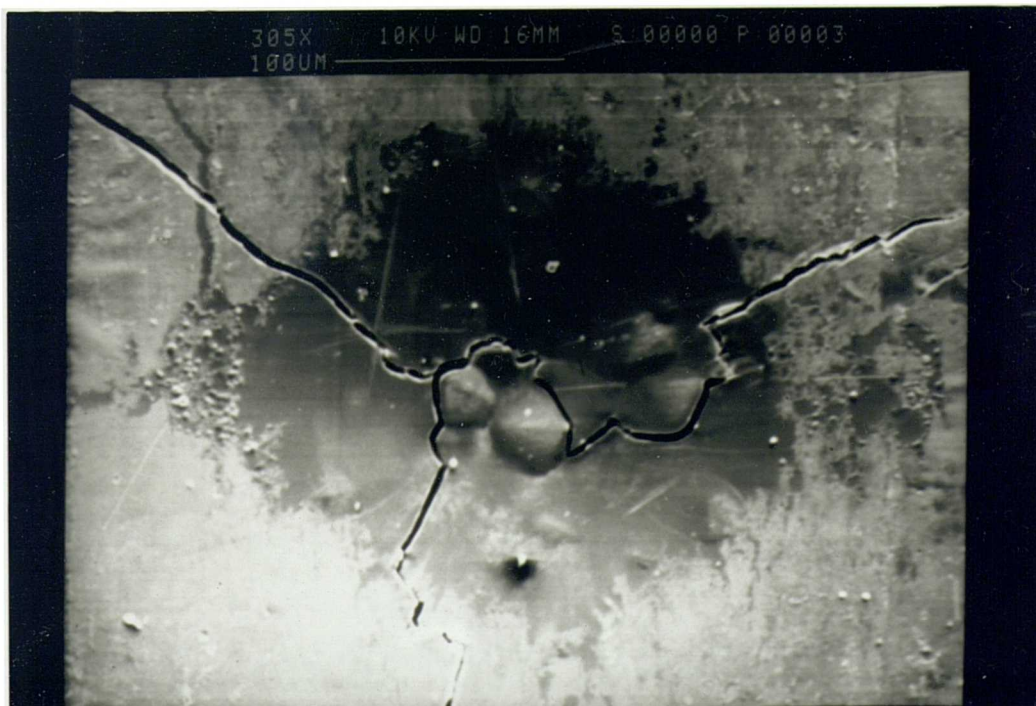
Figure 7.12 High magnification detail of 7.11

Fig. 7.11 shows a lower peak pulse power melt spot, with insufficient energy / irradiance to produce complete melting of the oxide surface, note continuation of features of oxide surface over the melted area. Fig. 7.12 shows limited disruption of the oxide layer in the centre of the melt pool.

The requirements laid out in section 6.4.3 were considered and, for the purposes of this study, certain areas of the operating range were rejected as follows;

Parameters in the upper half of the repetition rate and average power range were rejected because of the problem of maintaining laser parameters comfortably over a long period of time. In this way, significant lamp deterioration was allowed for. Taking these factors, and the results of the ranging trials into consideration, the best surface was produced using a focused spot at laser parameters of 20 Hz, 2.5ms, 5J.

7.2.2 Feedrate and spot overlap trials

Using the preferred 20 Hz, 2.5 ms, 5 J parameters and with straightforward adjustments of process speed and rastering co-ordinates a surface as shown in fig. 7.13 was produced. Coverage speed was 0.84 mmin^{-1}.
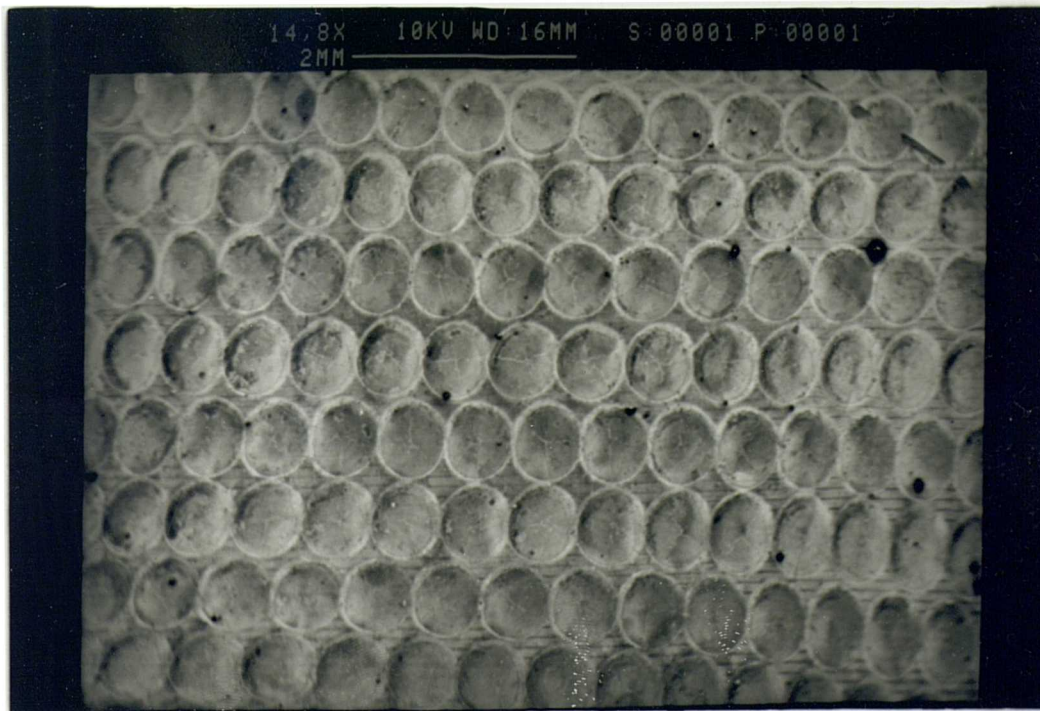
Figure 7.13 Melt spots at 20 Hz, 2.5 ms, 5 J parameters

Figure 7.14 Higher magnification shot of 7.13 showing more detail of melt spots

An important experimental observation was made at this stage. During the spot melting process, once a bright blue plume had been initiated, any change in focal position did not apparently affect the dimensions of the melt spot, the process appeared to become focus independent. However, if the starting focus position was altered, the process changed accordingly. Because of the dynamic nature of this particular experimental phenomenon, it was very difficult to record or quantify in any concrete manner and hence is only acceptable as unconfirmed observations.

7.3 Examination of melt spots

7.3.1 Surface features

A number of 6016 plates were then subjected to laser melting using the optimised parameters. All of the laser melt spots from the ranging trials were examined optically at low magnification, but those produced using the 20Hz, 2.5 ms, 5J parameters were examined in much greater detail due to the occurrence of the concentric rings. To commence an investigation into the mechanism by which the concentric rings were generated, their occurrence was mapped using several areas of

textured surface, details are given in appendix 10. No clear patterns or groupings emerged, and it was not possible to correlate this effect with defects in the surface of the material. A summary is given in table 7.7. It appeared that these spots occurred completely at random at 20Hz, 2.5ms, 5J parameters, despite the fact that these areas were textured under identical conditions.

Designation	No of spots	concentric rings	%
1	1400	44	3.1
2	1680	23	1.4
3	182	5	2.7
4	182	3	1.6
5	182	1	0.5
6	182	0	0
7	182	4	2.2

Table 7.7 Frequency of abnormal spots produced using 20Hz, 2.5sm, 5J

In addition, the optical investigation showed a degree of cracking on the surface of the spots. It was initially suspected that these were the result of hot cracking during resolidification of the melt pool. Close examination of figs. 7.11 & 7.12 suggests that for these low irradiance parameter combinations, a limited area in the centre of the melt pool has been melted whilst the majority of the oxide layer has remained unmelted during laser irradiation.
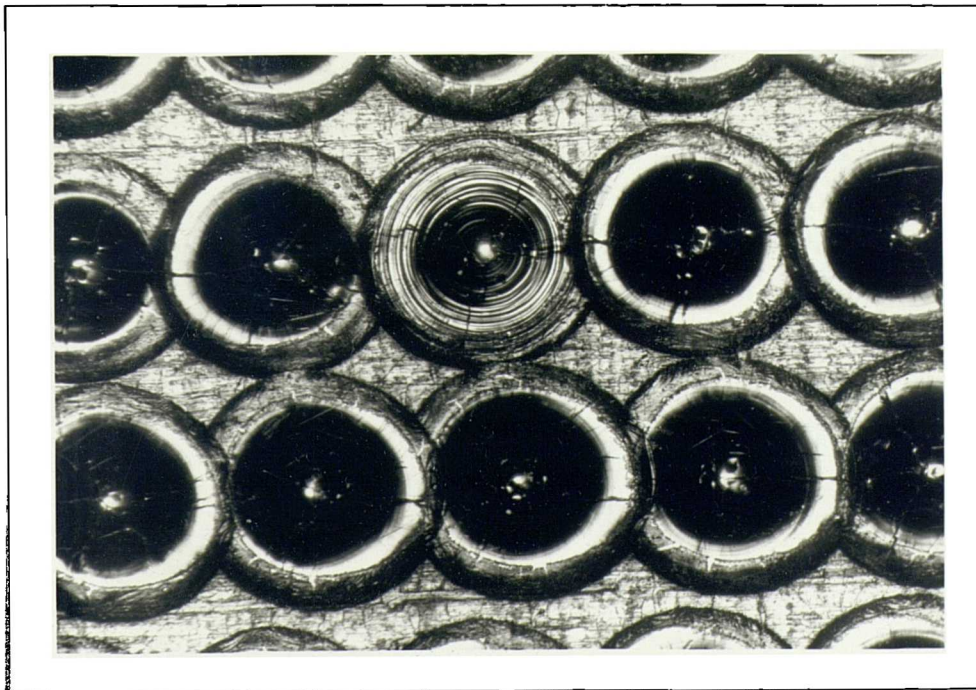
Figure 7.15 20Hz, 2.5ms,5J, occasional occurrence of abnormal melt spots

Fig. 7.13 - 7.14 show a spot melted surface produced using the preferred parameters of 20Hz, 2.5 ms, 5J, they appear to be repeatable. However, when observed under

particular light conditions, inconsistencies are noted. When photographed using an optical microscope and oblique lighting, the feature shown in fig. 7.15 is clearly visible.

7.3.2 Surface dimensions

A total of 20 melt spots produced using the standard laser parameters of 20 Hz, 2.5 ms, 5 J, were selected at random for further investigation and measurement, from two textured plates, 1 & 2. Two orthogonal diameters, d_1 and d_2 were measured for each, and table 7.8 below gives their mean values. Measurements were accurate to +/- 10 μm.

Spot diameter in mm	Plate 1	Plate 2
$\bar{d_1}$	0.69	0.69
$\bar{d_2}$	0.69	0.70
Mean d	0.69	0.695
Overall mean	**0.692**	

Table 7.8 Mean diameters of the melt pools on Plate 1 and Plate 2

Taking a value of 8 mrads for half angle beam divergence at these parameters, (from fig.7.1), and using non gaussian approximations, equations 2.12, 2.13, calculation of the focused spot diameter for the 80 mm focal length lens gives a value of 0.64 mm. This compares well with the average measured values in table 7.8. If pulse irradiance, in MWcm^{-2} is calculated using equation 2.17 for both calculated and measured values, then figures of 0.66 MWcm^{-2} and 0.78 MWcm^{-2} respectively are arrived at.

7.3.3 SEM investigation

Under higher magnification, the concentric ring structure and the hot cracking could be seen more clearly as shown in figure 7.12. Cracks radiating from the centre of the melt pool appeared on almost all the spots.

Figure 7.16 Higher magnification detail of 7.13 & 7.14, showing radial cracking

Figure 7.17 Details of cracking, X 200

Fig. 7.17 shows two interesting features. Firstly, for adjacent melt spots, cracking extends across between the spots.

Figure 7.18 20Hz, 2.5ms, 5J parameters, showing disrupted oxide skin at edge of melt pools

Secondly, fig. 7.17 is an optical photograph, again, the ring features are enhanced.

7.3.4 Metallographic examination

A number of transverse cross sections of melt spots produced at 20Hz, 2.5ms, 5J were prepared for metallographic examination. The limit of the melted zone was clearly delineated by fluoroborate etching. The dimensions of the transverse sections were measured using an image analysis technique

Sample no.	$\bar{d}_3$ mm	$\bar{d}_4$ mm
1	0.73	0.15
2	0.72	0.15
3	0.72	0.15
5	0.74	0.12
Mean	**0.73**	**0.14**

Table 7.9 Mean depth and length of the melt pools [141]
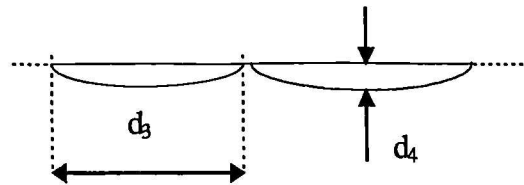
Figure 7.19 Diagrammatic representation of melt pools

It was noted that measurement of transverse sections of the melt spots generally gives higher values than those measured from the surface of the melt spot. Otherwise, the image processing shows that the solid-state laser pulses produced dimensionally consistent melt spots on the 6016 aluminium alloy - depth and diameter of the spots varied by ± 0.01 mm which was considered acceptable. Details of these measurements are given in Appendix 10. Although several melt spots containing concentric rings were included in this analysis, and taking into consideration the accuracy of the measurement technique, no significant differences in the shape and volume were noted between those spots with concentric rings and those without.
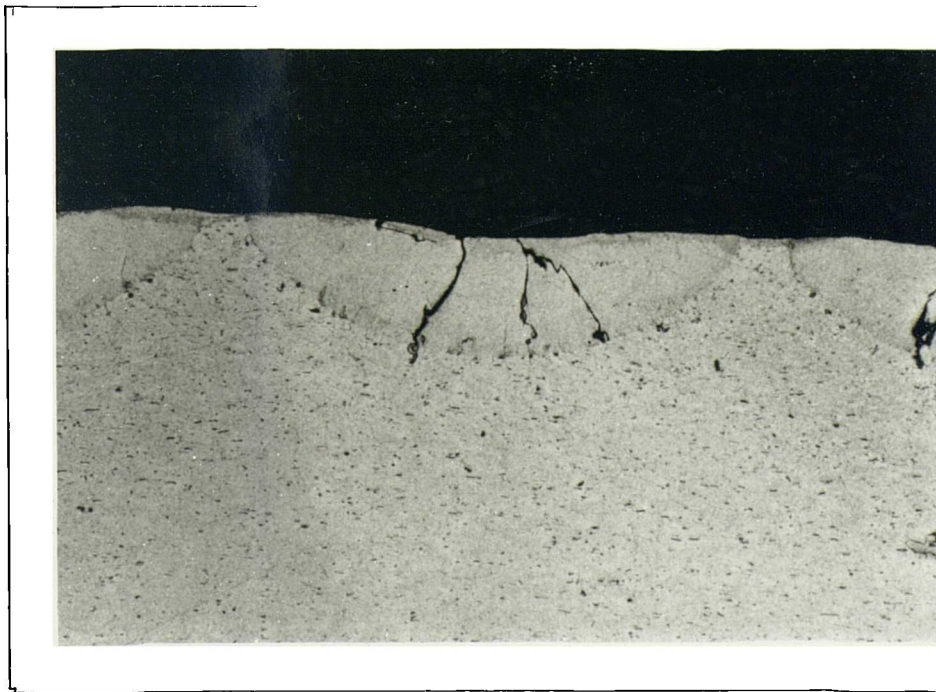
Figure 7.20 Standard pulse parameters, cross section of melt spot, X 100

As shown in 7.20-7.23, it was confirmed that the surface cracks did extend to the boundary of the melt zones, and beyond in some cases, to the adjacent melt spot.

Figure 7.21 Standard parameters, cross section of melt pool showing two surfaces with overlapping melt spots, X 50

Figure 7.22 Detail of fig. 7.20, X 200
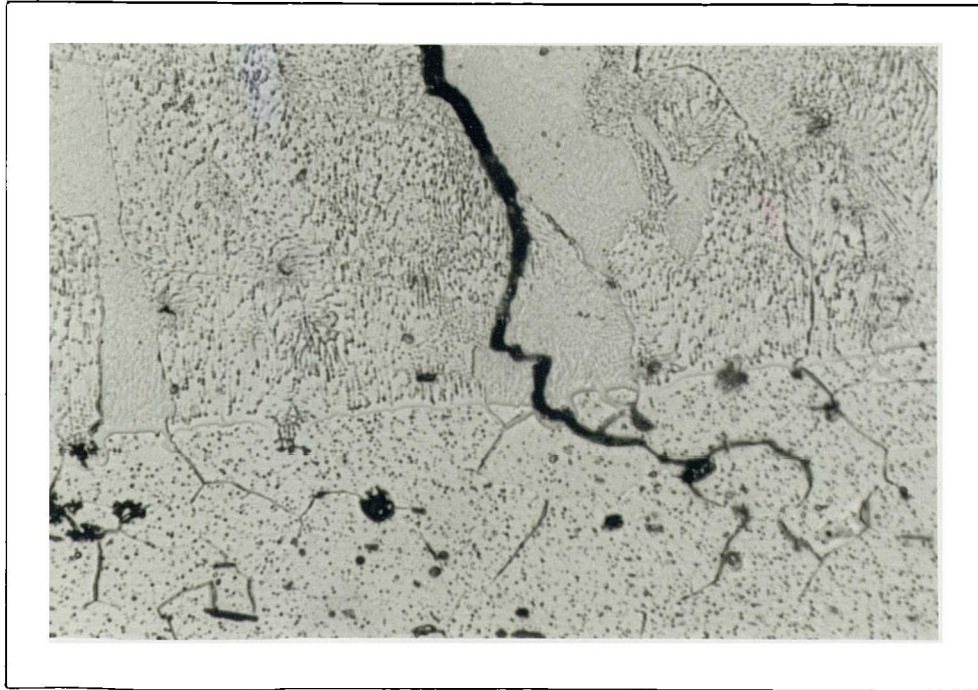
Figure 7.23 Detail of fig. 7.22, x 400

Figs. 7.21 - 7.23 show crack progression along grain boundaries into parent metal from melt zone.
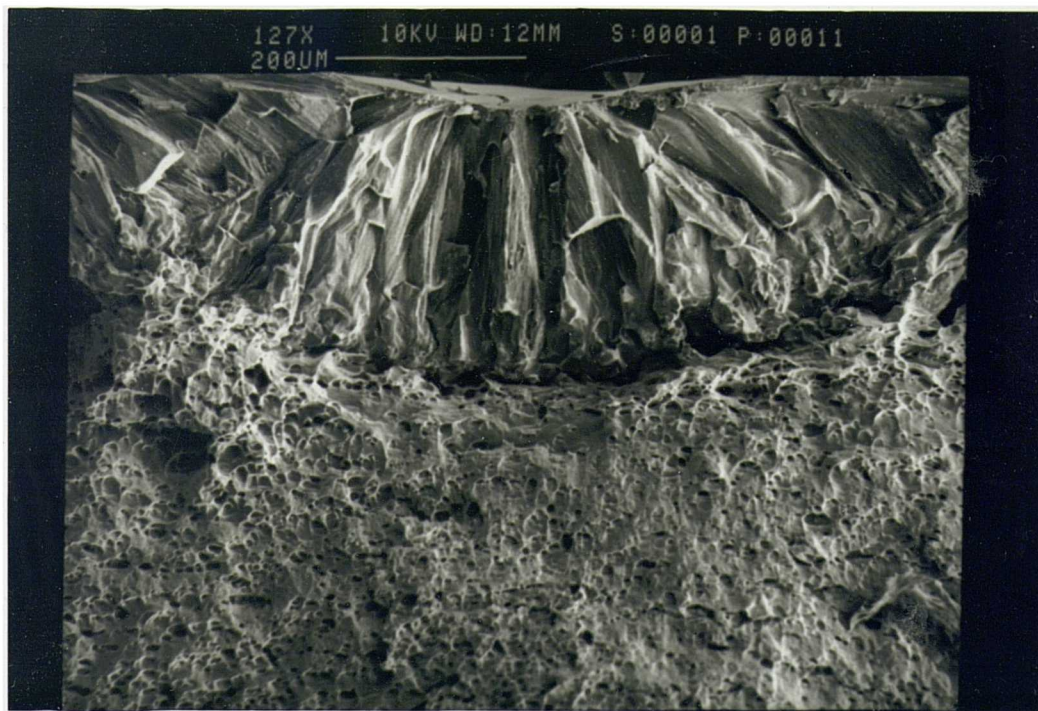
Figure 7.24 Same parameters, fractograph of melt spot, outlining melt zone

Figure 7.24 shows clearly the directional grain growth along the direction of heat flow. These early results clearly show isotherms outlining the relatively shallow melted zone, with directional grain growth produced during resolidification (figs 7.20-7.24). It was noted that a small number of apparently randomly distributed melt spots exhibited an interesting surface phenomenon, a series of closely spaced symmetrical surface corrugations or rings. These results drew attention to the condition of the aluminium surface and an examination of the mill finish material identified the following features of the surface:

Figure 7.25 Variations in oxide layer thickness - "ridged" finish

This ridged finish is visible on areas of the low irradiance melt spots, suggesting no melting of the oxide has occurred in these cases (fig.7.11).

Figure 7.26 Tearing defect in natural oxide layer

Figure 7.27 showing small defect in natural oxide layer, note high magnification

Despite the examination of the mill finish aluminium surface, the explanation for the apparently random occurrence of the concentric rings was not immediately obvious, although the presence of this phenomenon was a serious limitation to the repeatability of the spot melting process. It was also noted at this stage that concentric rings were present on the surface of melt spots when particular combinations of laser parameters from the trials were used. In some cases, they were present on all melt spots.

7.4 Stage 2 trials

The objective of the trials in this section was to identify more closely the particular parameters at which the concentric rings were generated.

7.4.1 Peak pulse power and irradiance

During these trials, several significant experimental ojservations were made. A definite change was noted in the nature of the laser plume, both in its colour and shape as peak pulse power was increased, and these changes occurred at a specific peak pulse power level.
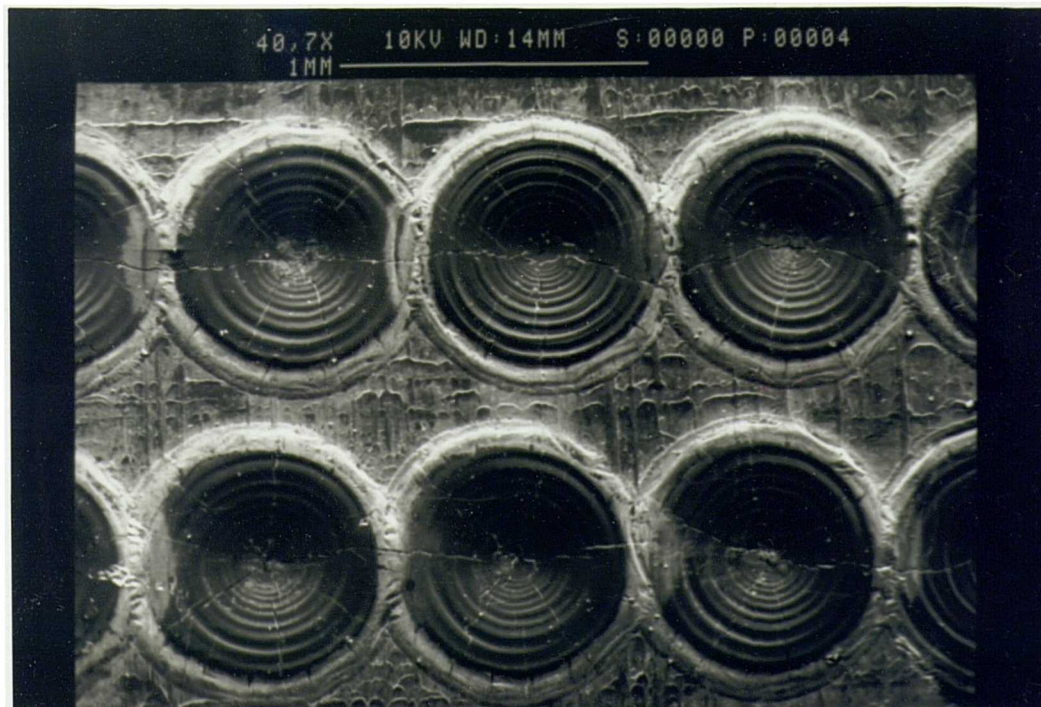
Figure 7.28 100% concentric rings at 5J & 5 kW peak pulse power
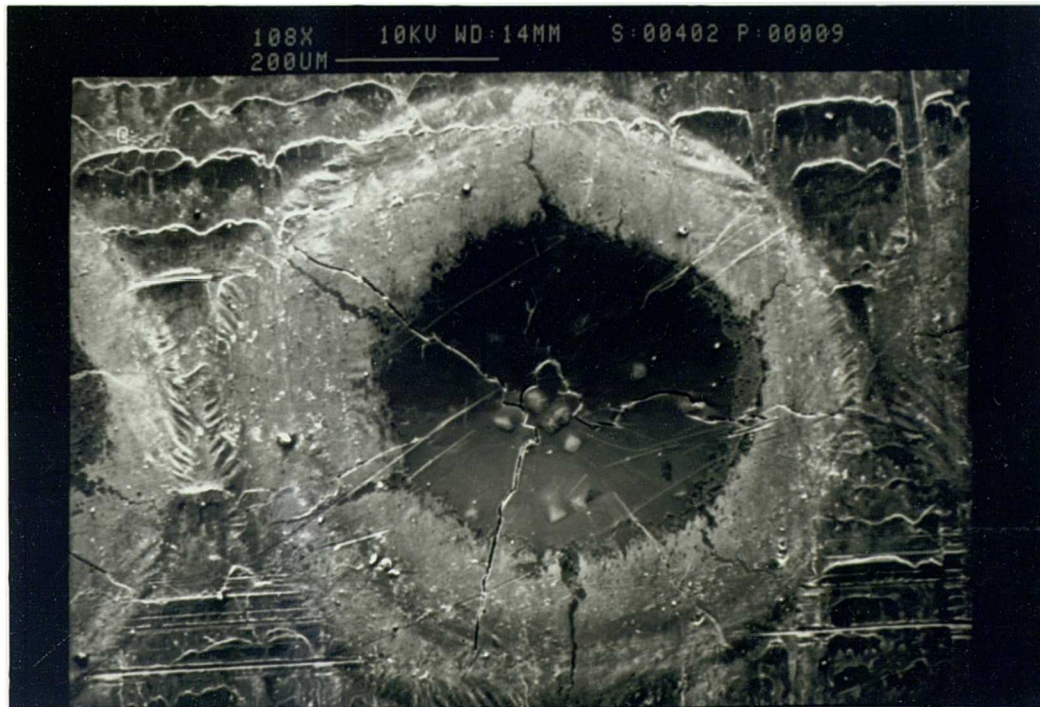
Figure 7.29 20Hz, 2ms, 5J, 2.5kW peak pulse power - no rings
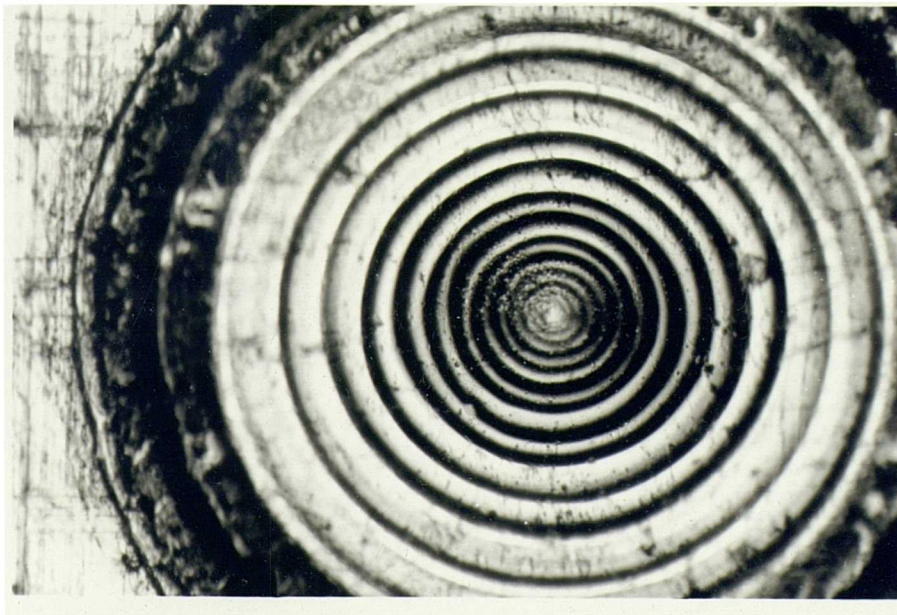
Figure 7.30 Concentric rings at 20Hz, 5J, 0.8ms - 6.25 kW peak pulse power, showing increase in wave period towards periphery

The optical photograph above, (Fig. 7.30) again shows the tendency of the optical technique to artificially enhance the prominence of these rings.
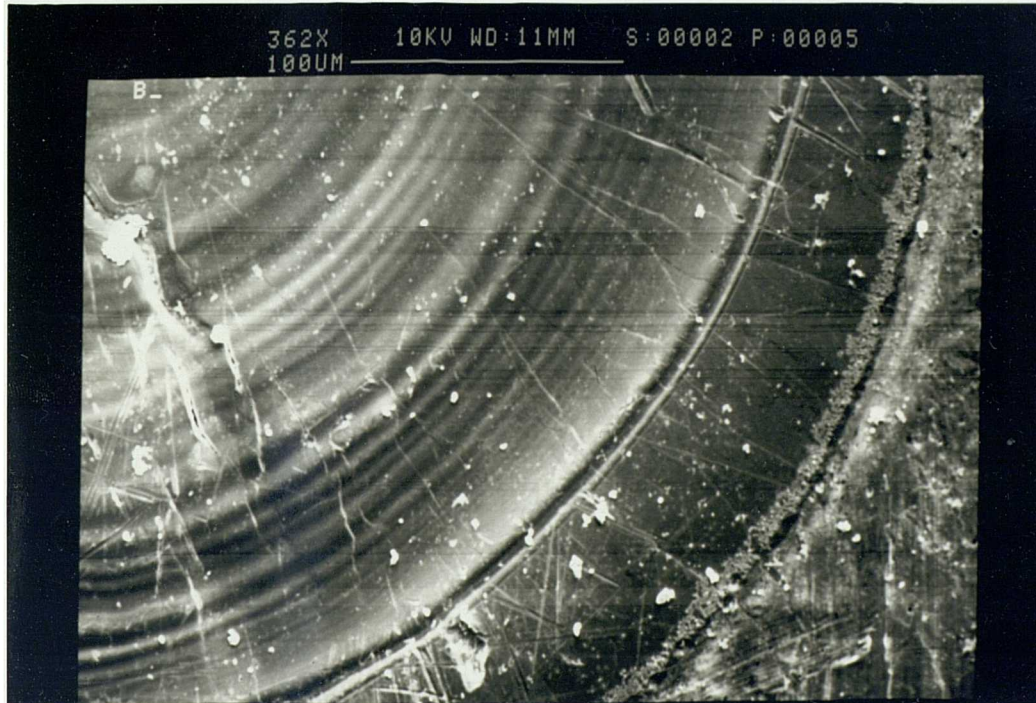
Figure 7.31 showing "rings on rings"

Fig. 7.31 demonstrates the small scale of the rings, and confirms the difficulty found in measuring consistent wave periods or wave heights. High magnification examination invariably identified smaller and smaller scale rings, making measurement of the wave period difficult..
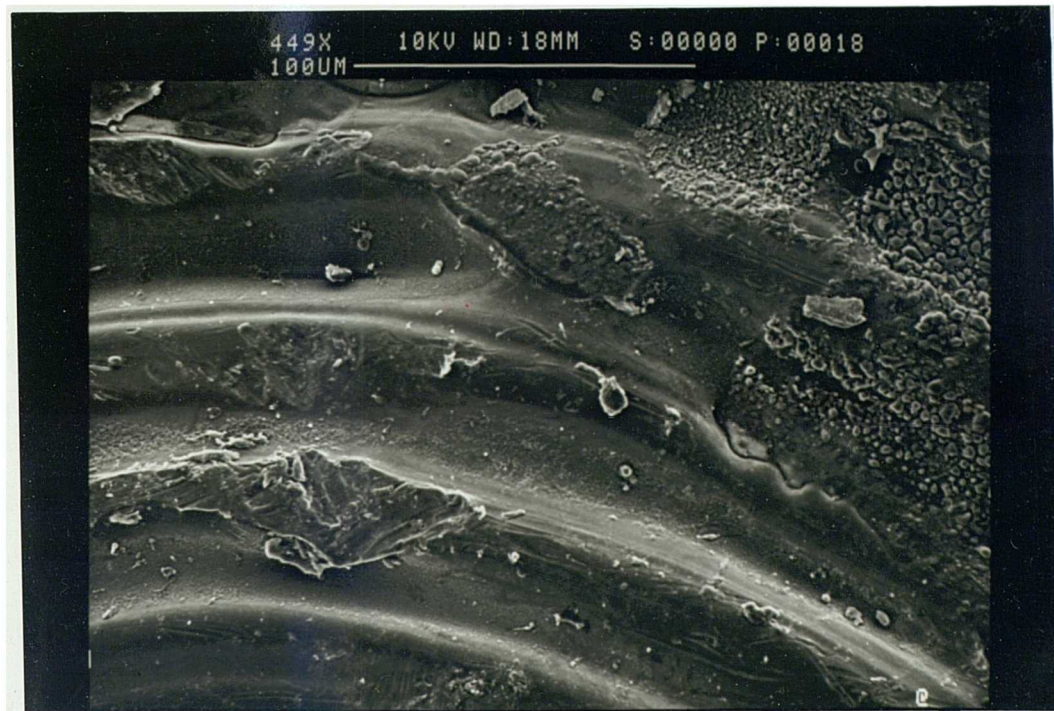
Figure 7.32 Detail of fig. 7.30, close to perimeter of melt spot showing solidification features

7.4.1.1 Increase in melt efficiency

The following results were obtained for the surface dimensions of the melt spots over the critical range of peak pulse power and irradiance identified in the characterisation trials.
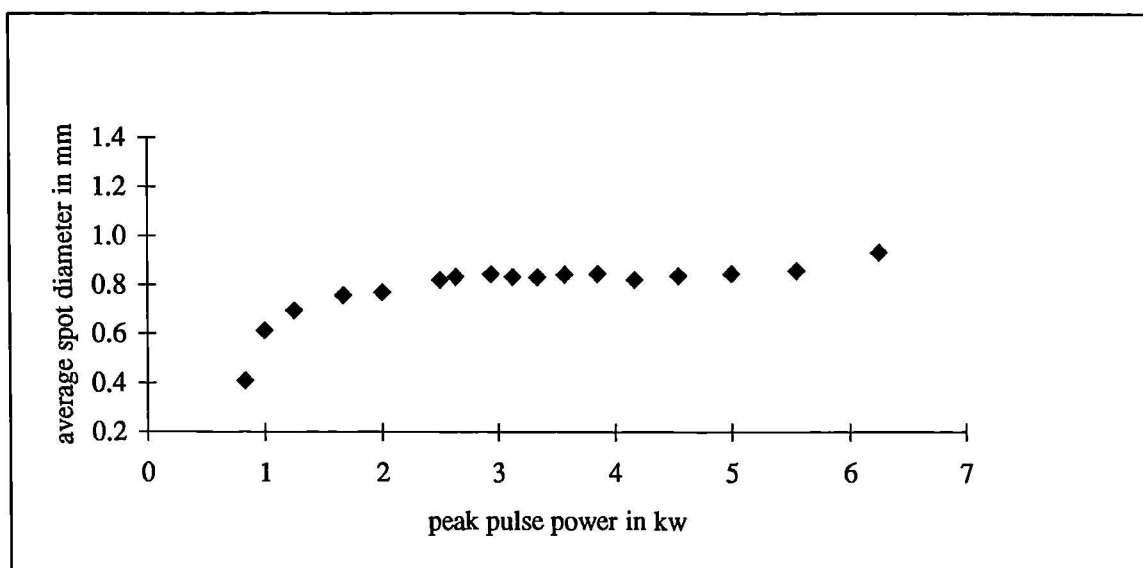
Figure 7.33 showing relationship of laser spot diameter to peak pulse power for standard material

Fig. 7.33 shows that for a particular pulse energy, in this case 5 joules, the melt spot size increases with peak pulse power to reach a plateau at ~ 0.8 mm, at a peak pulse power of 2.7 kW. There appears to be an upturn in the curve close to the peak pulse power upper limit, which in this case is the maximum peak pulse power capability of the laser.
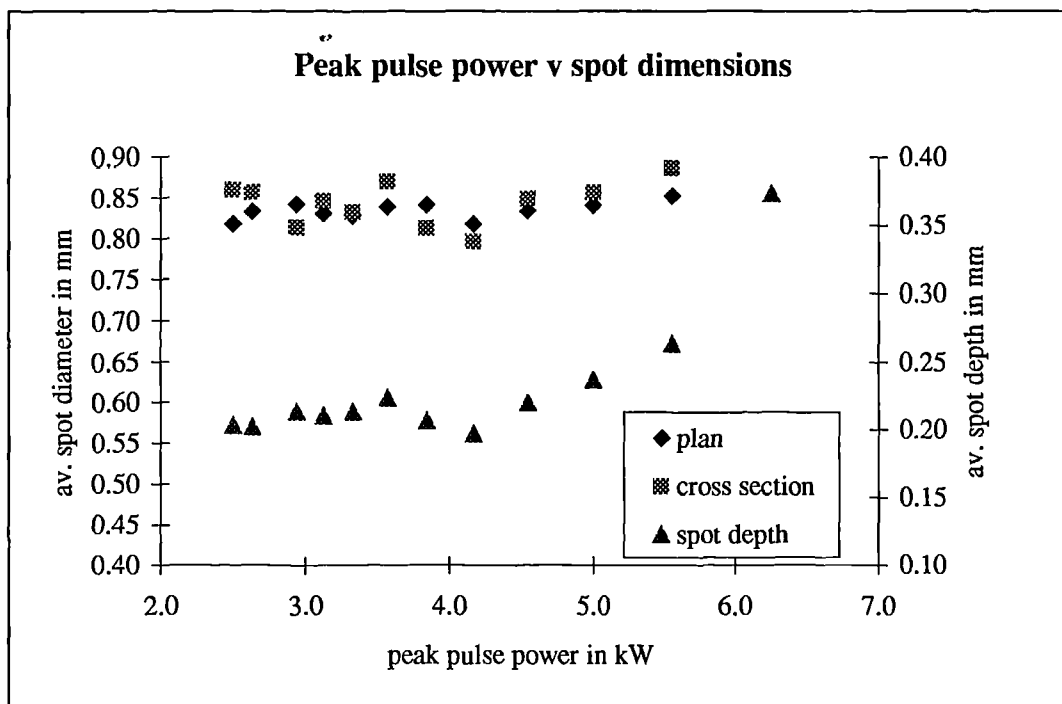
Figure 7.34 showing the effect of peak pulse power on melt spot dimensions

If melt spot depth dimensions are taken into consideration, as in fig. 7.34, two important points are noted. There is not a significant difference between the two techniques for measuring spot diameters, and they both appear to follow a similar trend. Spot depth, however, does appear to increase from a peak pulse power of ~ 4.5 kW.

The next stage in the analysis of these results was to compute the volume of the molten pool via a straightforward geometrical calculation, assuming a symmetrical sector of a sphere shape for the melt pool. Fig. 7.35 again confirms a significant threshold effect associated with an increase in peak pulse power.
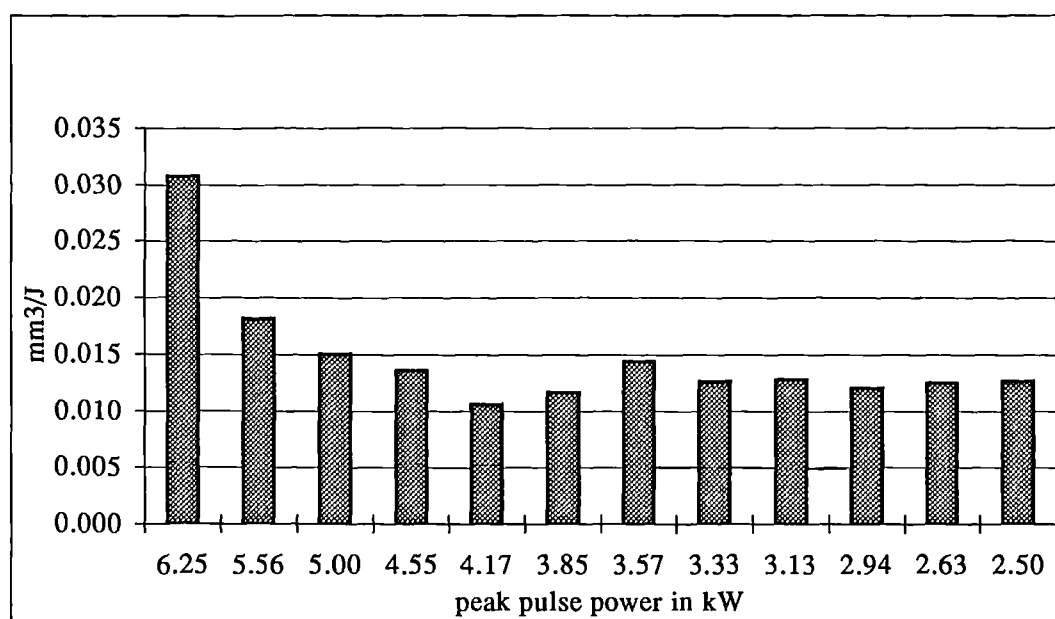
Figure 7.35 showing effect of peak pulse power on melting efficiency

7.4.1.2 Threshold effects

From the ranging trials values of spot diameter were identified below which no significant melting and at which annular rings occurred. From these, values of irradiance were calculated and tabulated for each major combination of laser parameters. It should be noted that these parameters are consistent in that as shown in table 6.2 - 6.4, no other change in the optical characteristics of the pulse is occurring.

Laser parameters 50Hz, 2J

p pulse power in kW	min. irradiance for waves, MW/cm2
1.00	no waves
2.00	no waves
2.86	0.83
4.00	1.09

Laser parameters 20Hz, 5J

p pulse power in kW	min. irradiance for waves, MW/cm2
1.00	no waves
2.00	0.48
2.94	0.60
3.85	0.95
5.00	0.75

Laser parameters 10Hz, 10J

p pulse power in kW	min. irradiance for waves, MW/cm2	min. irradiance for material removal, MW/cm2
1.00	no waves	-
2.00	no waves	-
3.03	0.54	-
4.00	0.51	-
5.00	0.50	0.48

Table 7.10 Approximate pulse irradiance threshold values for generation of waves and material removal on standard 6016 material

7.5 Further investigations

7.5.1 Temporal pulse shaping

The following shapes were developed for the pulse shaping trials.

Shape number (type)	Sector no.	Sector lamp ht., %	Sector duration τ, ms	Measured Pp (scope)	lamp power, kW
1	main	43.6	2.5	3.3,2	1.7
2, (rising)	1	21.0	1.0	2.0	
	main	54.3	1.5	2.8	
3, (falling)	1	53.0	1.5	(4), 2.3	
	main	31.8	1.0	1.0	
4, (rising)	1	21.0	1.0	1.1	1.65
	2	44.7	0.8	2.0	
	main	61.0	0.7	3.1	
5, (falling)	1	53.0	0.5	3.3	
	2	50.0	1.0	2.1	
	main	32.0	1.0	1.0	
6, (rising)	1	20.0	0.8	1.3	1.65
	2	37.0	0.7	2.3	
	3	51.0	0.5	3.2	
	main	63.4	0.5		
7, (falling)	1	21.0	0.7		1.7
	2	69.6	0.6	4.0	
	3	52.5	0.6	2.4	
	main	54.3	0.6	1.1	
8,(symmetrical)	1	19.3	1.3	1.6	1.7
	2	70.0	0.7	3.0	
	main	50.2	0.5	1.6	
9, (prepulse)	1	100.0	0.6	4.0	1.7
	main	45.0	1.9	1.5	

Table 7.11 Details of pulse shapes

Figures 7.36 - 7.44 are diagrammatic representations of the oscilloscope traces of each of the temporal pulse shapes employed. It must be remembered however, that these are only representations of the temporal shapes of the laser pulses and their accuracy is limited by the detector and the oscilloscope used, hence a mathematical analysis would be unrealistic.
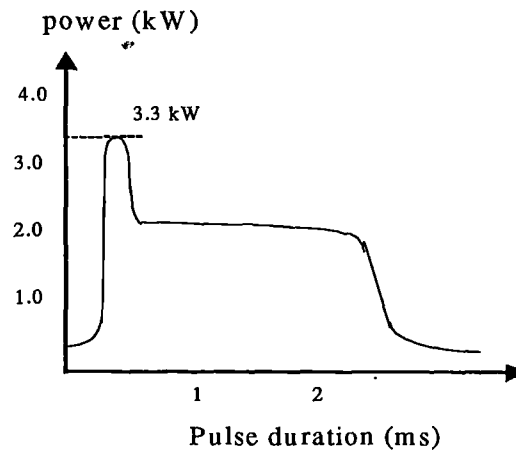
Figure 7.36 Pulse shape 1

Shape 1 is the standard pulse with the standard leading edge "spike". This leading edge spike is a typical feature of solid state laser pulses and in the case of the moderate pulse duration's used in this work comprises between 2 - 5 % of the pulse energy.
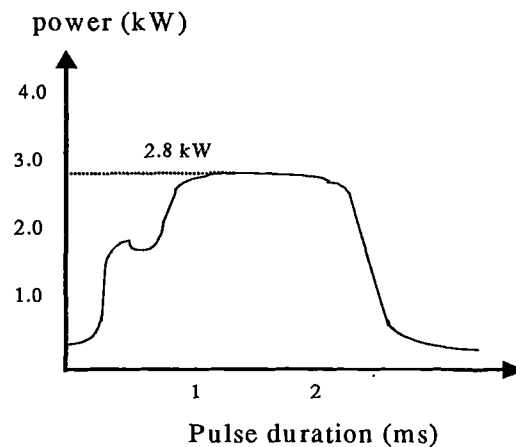
Figure 7.37 Pulse shape 2, 2 sector rising slope
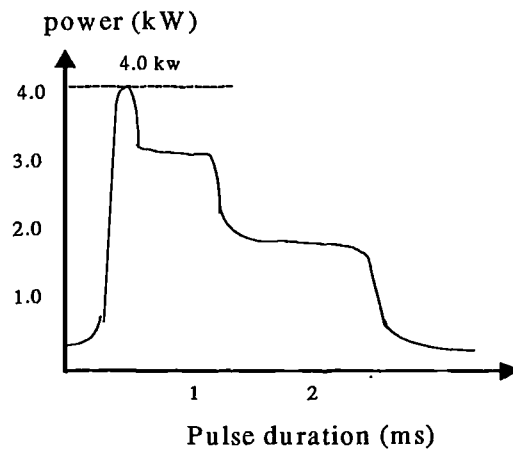
Figure 7.38 Pulse shape 3, 2 sector falling pulse
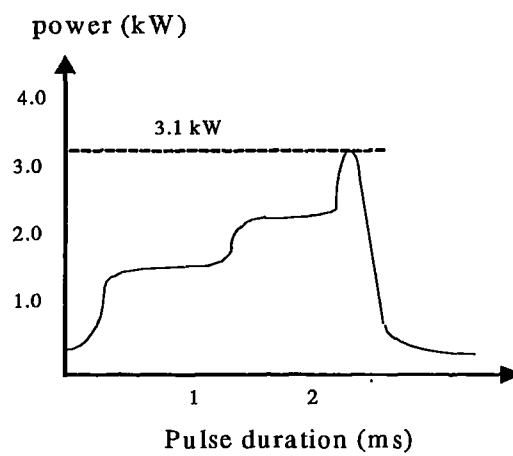
Figure 7.39 Pulse shape 4, 3 sector rising pulse
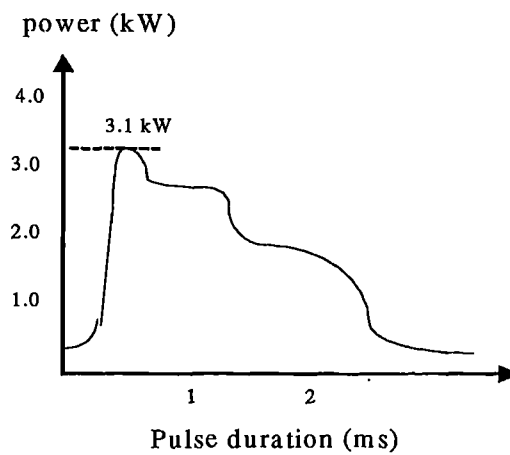
Figure 7.40 Pulse shape 5, 3 sector falling pulse

power (kW)
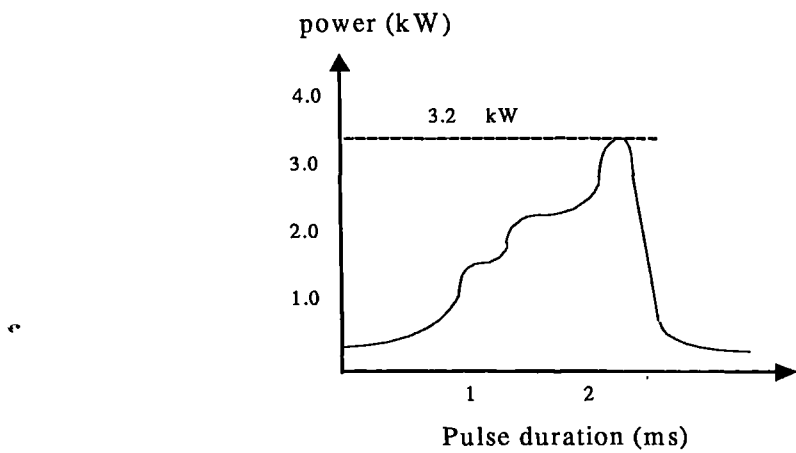
Figure 7.41 Pulse shape 6, 4 sector rising pulse

power (kW)
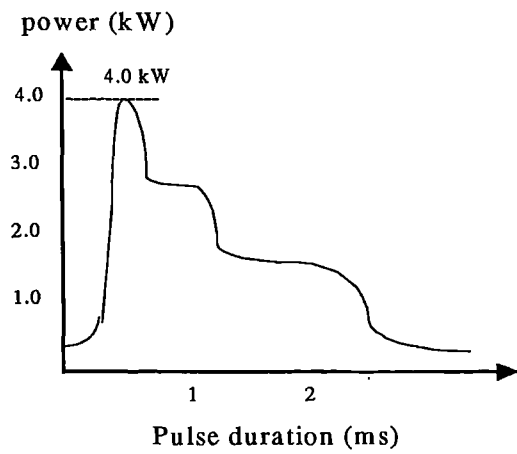
Figure 7.42 Pulse shape 7, 4 sector falling pulse

power (kW)
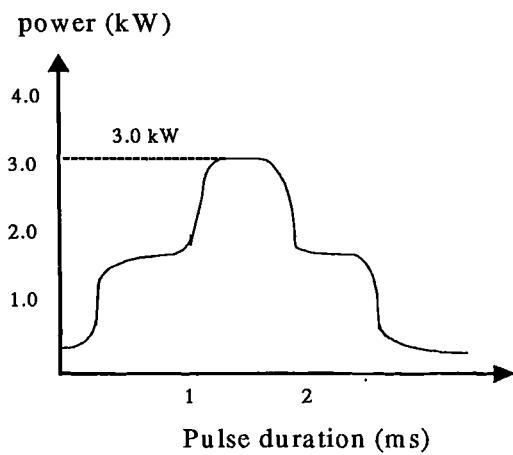
Figure 7.43 Pulse shape 8, symmetrical pulse

power (kW)

Pulse duration (ms)
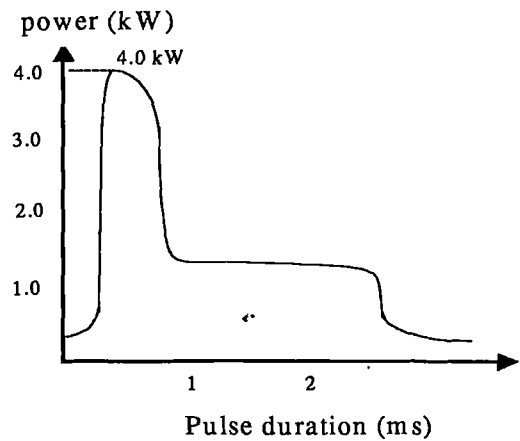
Figure 7.44 Pulse shape 9, trailing edge pulse (only used on peak pulse power trials)

7.5.2 Effect of temporally shaped pulses

Melt spots were produced using the same 20 Hz, 2.5 ms, 5 J pulses as before, the only variation being a range of temporal shapes were used as shown above.

A similar assessment of each of the textured surfaces led to the following observations of the melt spots produced by temporally modified pulses:

- results noted are shown in table 7.12. Pulse shapes 7 & 8 produced melt spots with no discernible symmetrical concentric rings.

Pulse	shape 1	shape 2	shape 3	shape 4	shape 5	shape 6	shape 7
shape	standard	top hat	trailing	rising	trailing	rising	trailing
waves	yes	yes	no	yes	no	yes	no

Table 7.12 Effect of shaped pulses on wave generation on standard material

Examination of these melt spots identified the following notable features:
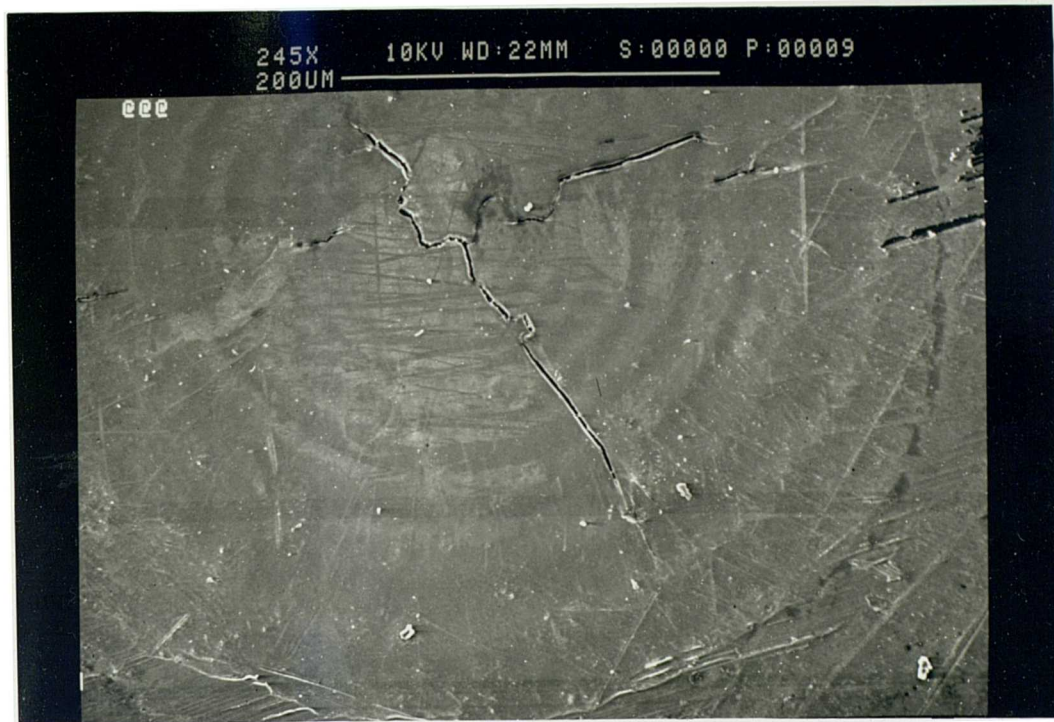
Figure 7.45 Mill finish material, rings generated by pulse shape 4

Although concentric rings were visible, in general they were less prominent than and hence even more difficult to quantify.
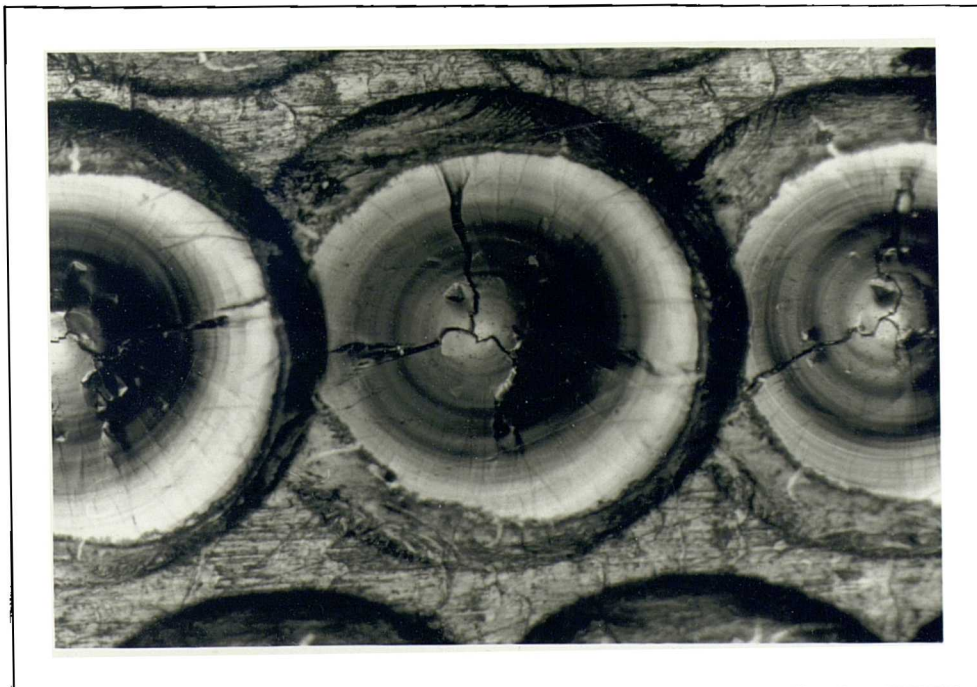
Figure 7.46 Mill finish material, melt spots produced by pulse shape 8

It was also noted that pulse shapes 3, 5 & 7 all produced taller, narrower more energetic plumes.
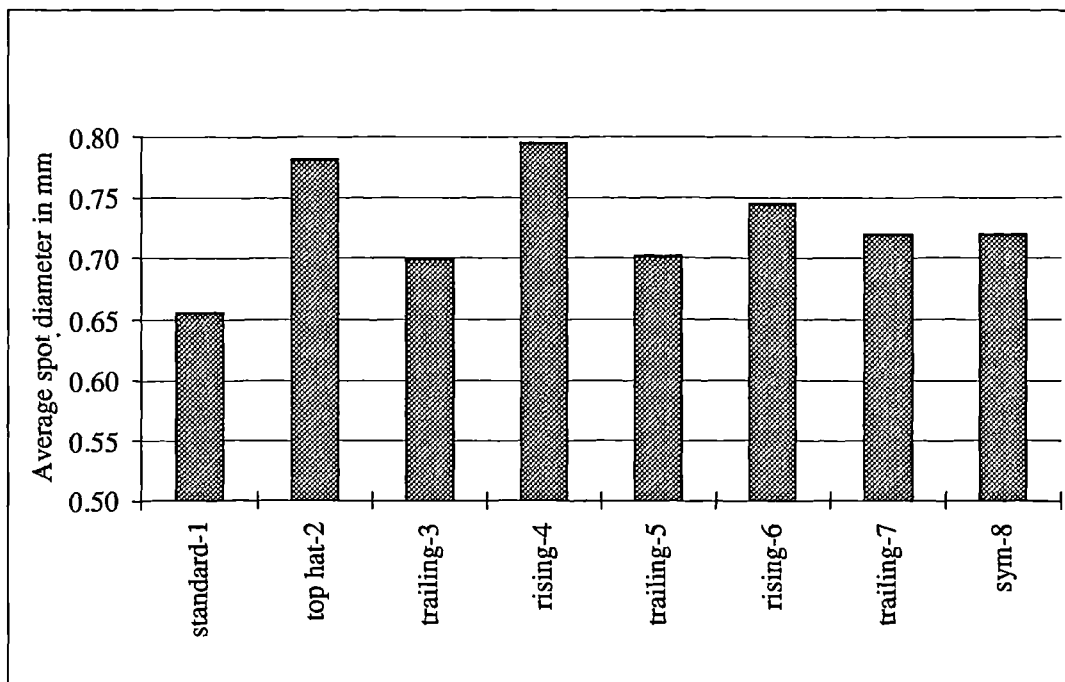
Figure 7.47 Effect of temporal pulse shaping on spot diameter on standard material finish

Pulse shapes 2, 4 & 6 all appear to produce an increased melt volume for the same pulse energy, 5 joules. Interestingly enough, it is the pulse shapes which appeared to produce less efficient melting which generated the more energetic, noisy plumes. Also of interest is the relatively low figure for the standard laser pulse.

7.5.3 Modified surface layers

Two alternative surface finishes were used, firstly, the 6016 material was etched using NaOH to reduce the thickness of the oxide layer. The natural thickness of the mill finish surface oxide was estimated using an Auger technique to be ~ 40 nm, and the oxide thickness on the etched sample was found to be ~ 25 nm. Secondly, an anodised layer was deposited on samples of the same sheet of 6016 aluminium. The thickness of the anodised layer on each of the 6016 aluminium alloy was measured metallographically as when deposited, the anodised layer thickness had only been estimated from immersion time. Results were as follows;

Sample ID	Treatment	Coating thickness in μm
2	NaOH etch	0.025
3	anodise	3
5	anodise	6
7	anodise	12
9	anodise	24
11	anodise	35

Table 7.13 Sulphuric acid anodised layer thickness [142]

Only the thinnest anodised thickness, 3 μm, was used in the trials, thicker anodised layers produced cosmetically unnattractive melt spots.
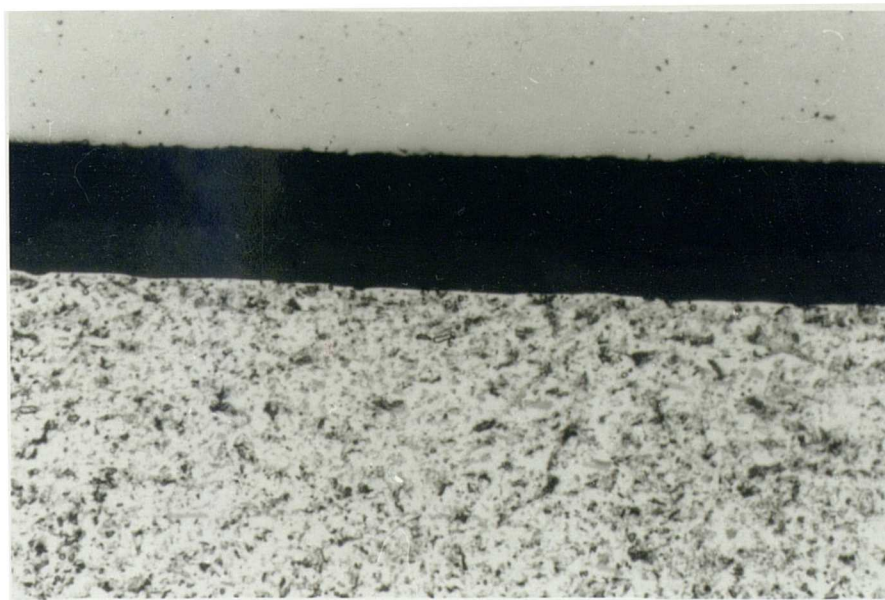
Figure 7.48 Measurement of anodised layer thickness, x 600

Figure 7.49 showing small defects in surface of 3 µm anodised coating

High magnification examination of the sulphuric acid anodised surface showed the existence of small defects, fig. 7.49.

Further spot melting trials were undertaken using the preferred laser parameters on the etched and anodised aluminium sheets. Firstly, the peak pulse power trials were repeated on both additional surface finishes, etched and anodised. Secondly, standard and shaped pulses were also used to produce large numbers of melt spots on etched and anodised surfaces, the only variable being changed was the surface of the aluminium. Details of the melt spots produced on the anodised 6016 surface are shown first:
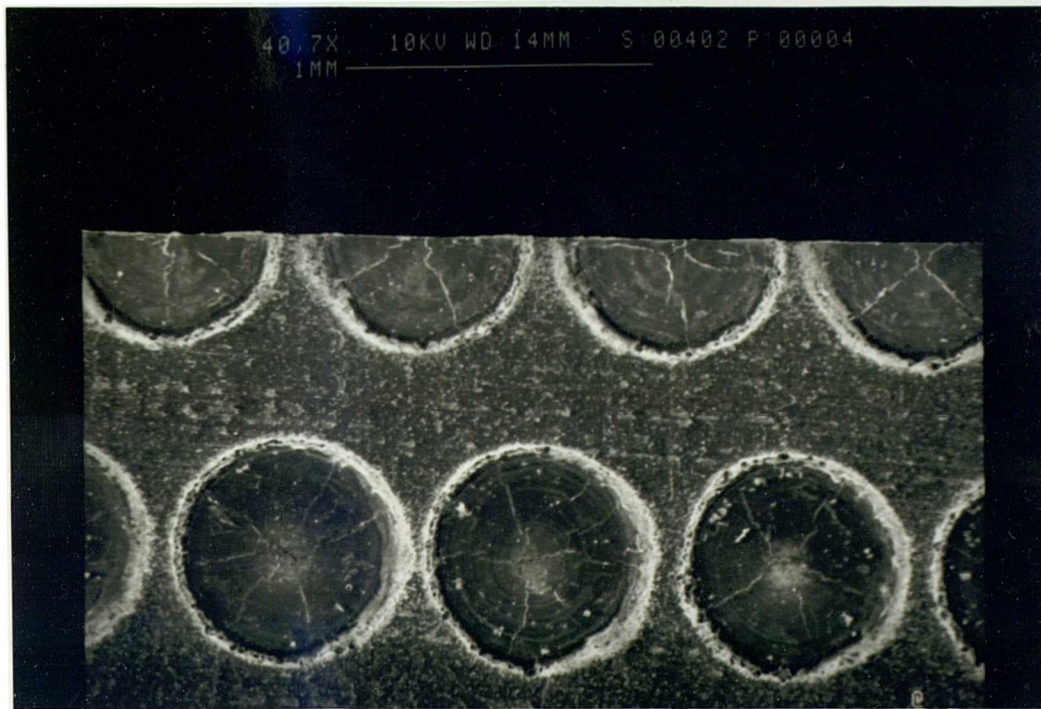
Figure 7.50 showing melt spot using 20Hz, 2.5ms, 5J parameters on 3 μm anodised surface, slight rings
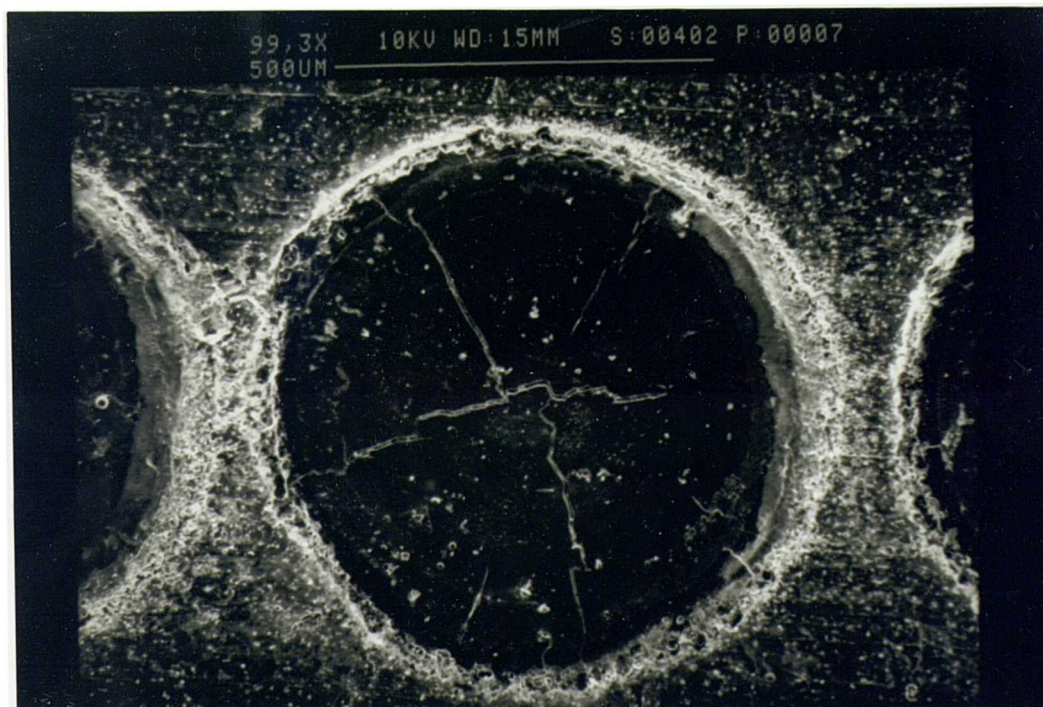
Figure 7.51 Detail of fig. 7.50 showing melt spot on anodised material

Fig. 7.50 also shows a small area of sample used in the laboratory technique used for accurate measurement of melt spot cross sections.
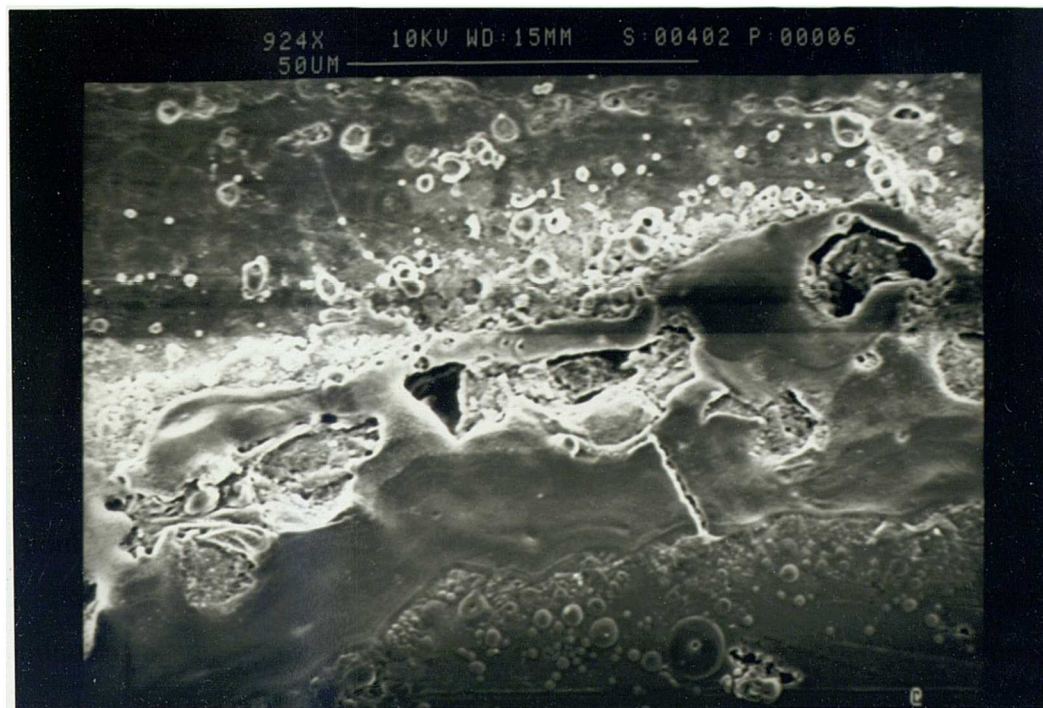
Figure 7.52 Further detail of 7.51 showing disruption of oxide at periphery of melt pool

Figs. 7.50-52 show the effect of the anodised surface on the spot melting of aluminium using the preferred parameters of 20Hz, 2.5 ms, 5 joules. The surface of the spot does not appear to be dramatically different initially from those produced on standard finish material. However, subtle differences become apparent when optical and dimensional examinations were carried out.
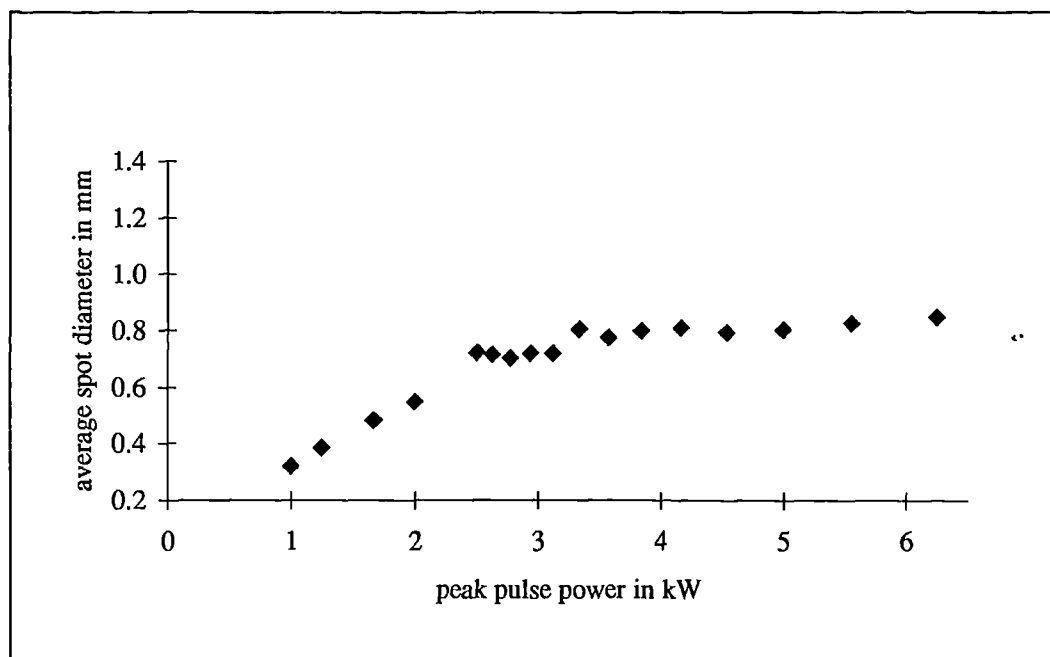
Figure 7.53 showing relationship of spot diameter to peak pulse power for etched material

Fig. 7.53 shows that not only is a higher peak pulse power required, ~1kW, to produce an initial melt spot on the etched material, but a higher peak pulse power, ~3.5 kW, is required to reach the maximum spot size, ~0.8 mm. This should be compared with fig. 7.33, standard finish material, where a maximum spot size of 0.8 mm is achieved at 2.7 kW peak pulse power.
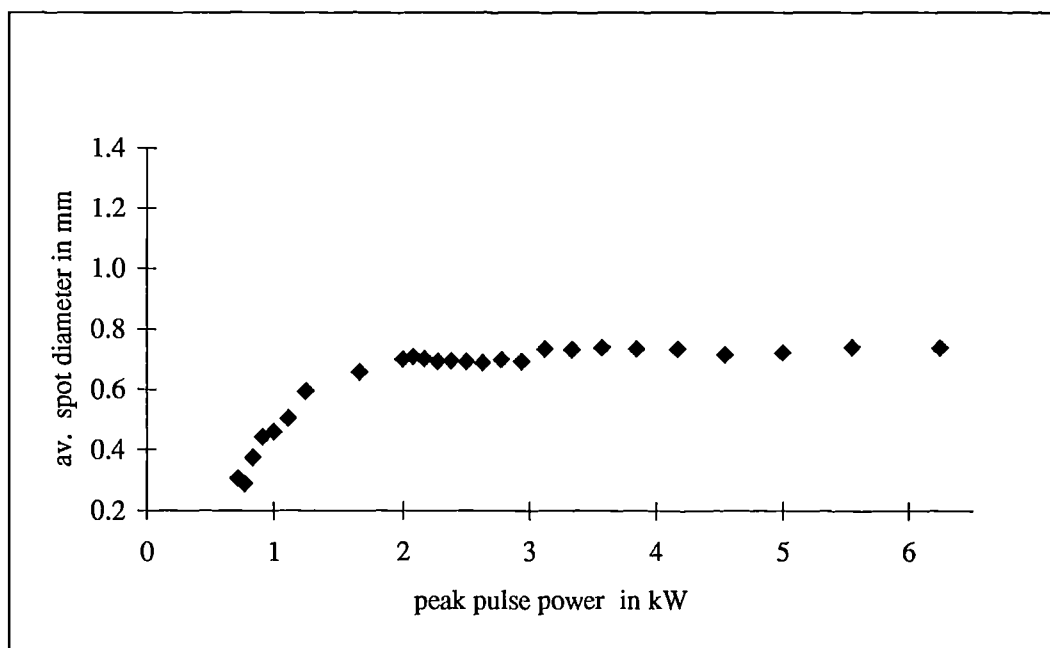
Figure 7.54 showing relationship of spot diameter to peak pulse power for anodised material

Fig.7.54 shows that a maximum spot diameter of ~0.75 mm diameter is achieved at 2 kW peak pulse power. Also, because the spot melting trials were performed on the basis of reducing peak pulse power to the point at which no observable melting occurred, melt spots were possible at a lower peak pulse power than the case of 7.33 & 7.53 - melting was observed at peak pulse powers as low as 0.85 kW, as opposed to 1 kW in the case of etched material and 0.9 kW in the case of the standard material finish.

7.5.4 Pulse shaping & modified surface layers

The range of pulse parameters used previously for the spot melting trials on the mill finish material were also employed on the etched and anodised surfaces. Of interest was the effect these temporal pulse shapes on the generation of the waves and on melting efficiency.

Pulse shape	shape 1 standard	shape 2 top hat	shape 3 trailing	shape 4 rising	shape 5 trailing	shape 6 rising	shape 7 trailing
etched	yes	yes	yes	yes	yes	yes	yes
anodised	yes	yes	none	yes	none	yes	none

Table 7.14 Generation of waves with various pulse shapes, etched & anodised samples

As before, the surfaces of melt spots produced with pulse shapes 3 & 7 did not exhibit annular rings. However, energetic plumes were again noted during the production of these melt spots using pulse shapes 3 & 7 on the anodised surface. However, on the etched surface, with a reduced oxide layer thickness, waves appeared on all of the surfaces using all of the pulse shapes. In this case, no plumes were identified during processing.

7.5.4.1 Increase in melting efficiency

The following graphs show how the dimensions of the melt spots are influenced by the condition of the surface and by the temporal shape of the laser pulse.
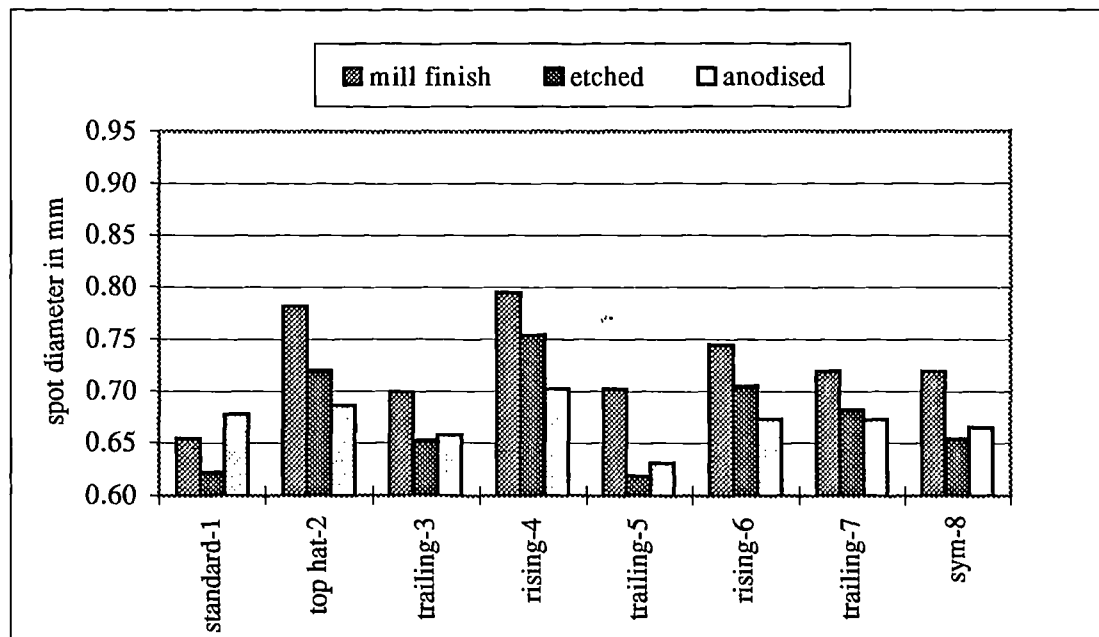
Figure 7.55 Effect of temporally shaped pulses on surface spot diameters for various surface conditions

Fig. 7.55 shows that spot diameters were generally increased by the different pulse shapes on the standard and the etched material samples, the only exceptions being pulse shapes 3 and 5, trailing pulse shapes. In the case of the anodised material, only slight increases were noted, the exception again being shapes 3 & 5.
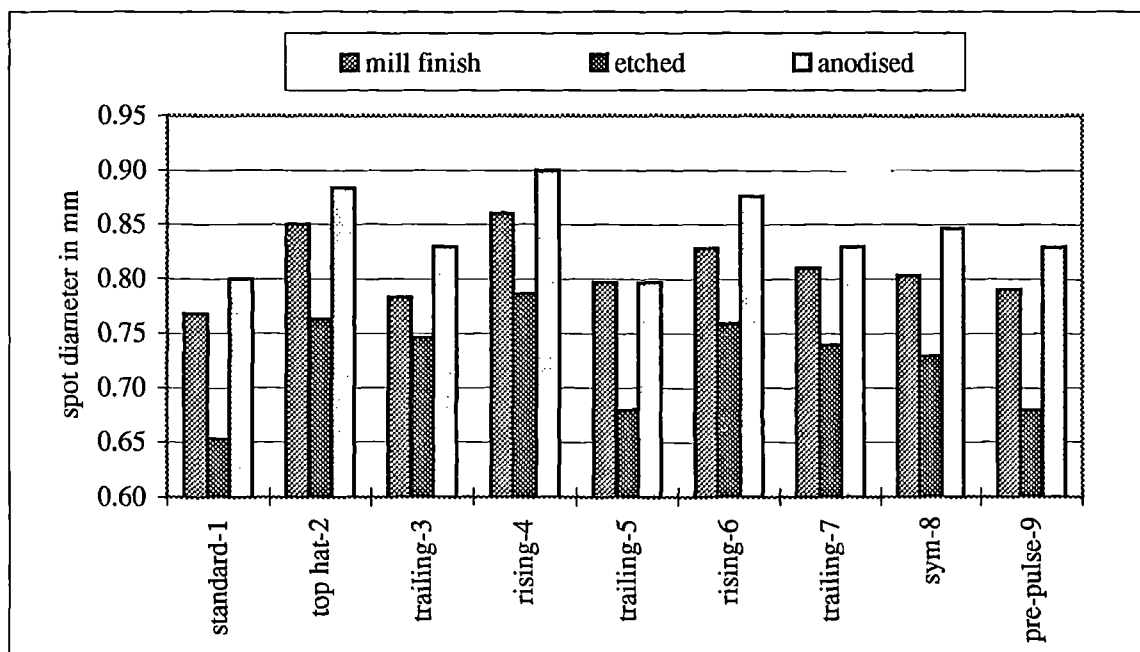
Figure 7.56 Effect of temporally shaped pulses on cross section spot diameters for various surface conditions

Fig. 7.56 shows a common trend with 7.55, in that generally the flat top (or top hat) pulse shape, no. 2, and the rising pulse shapes (with reduced slopes to the leading edge of the pulse) produced a general increase in spot diameter. In effect, these figures are comparing two different techniques to measure the same dimension, fig. 7.55 via a surface measurement, and fig. 7.56, measuring a cross section. The difference between the two, (the cross section measurement is always larger than the surface measurement) may be due to an error introduced by the surface oxide layer masking the true extent of the melt pool.
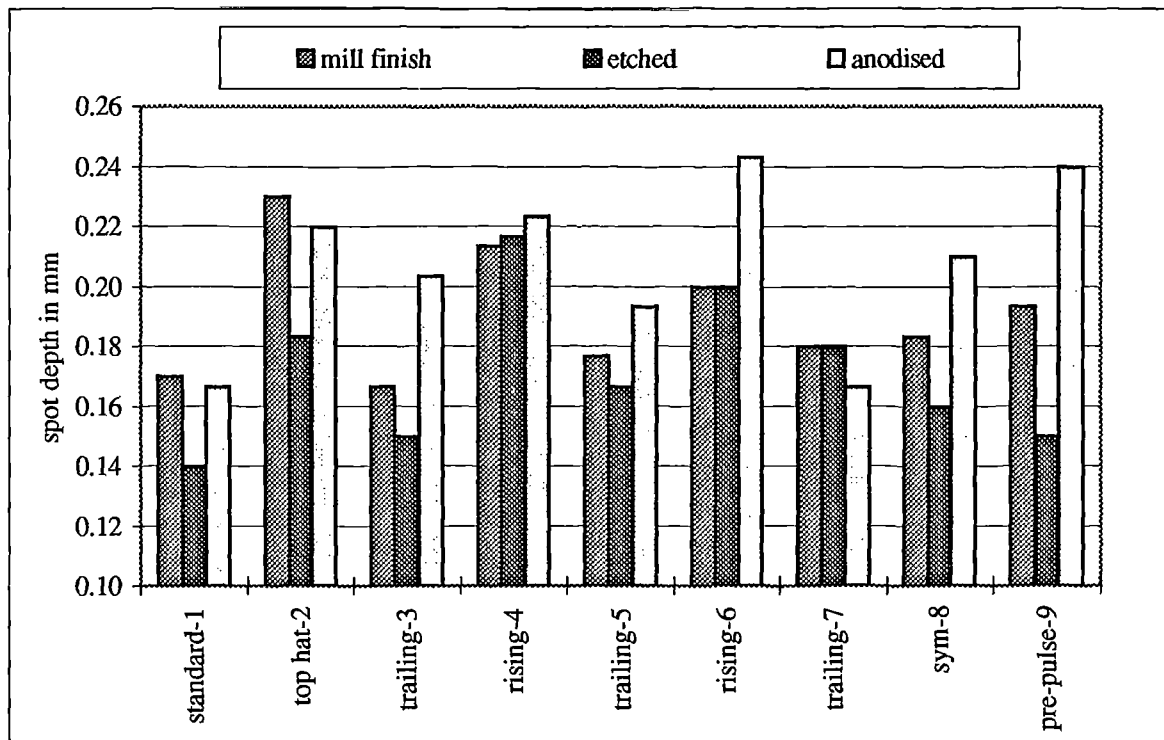
Figure 7.57 showing the effect of temporal pulse shaping on spot depth

Fig. 7.57 again shows a similar trend in that pulse shapes 2,4 & 6 again produce deeper melt spots. In the case of pulse shape 9, with enhanced pre pulse, this shape produced significantly deeper spots on the anodised surface.
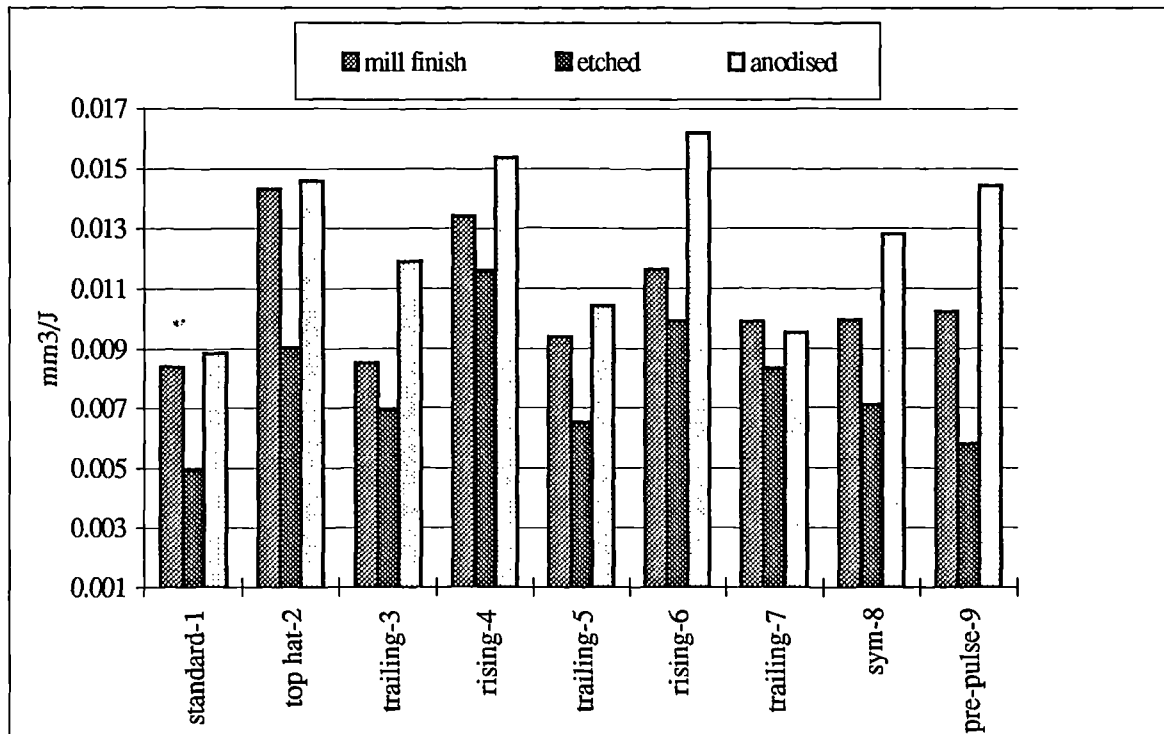
Figure 7.58 showing effect of pulse shaping and material finish on melt efficiency at 5 J

When the results from figs. 7.55 - 7.57 are put into the form of melt efficiency, fig. 7.58 shows a similar general trend again, with rising pulse shapes proving more efficient. Also clear is the efficiency improvement from anodised surfaces, which appears to improve efficiency for all pulse shapes.

8. Discussion

8.1 Introduction

Properties of the laser beam and the target have been modified experimentally in a controlled manner, the results of these modifications on the laser spot melting process have been examined and the results are reported in chapter 7. The review has shown that these experimental process parameters have not been covered in the published technical literature to any depth. However, the results are now discussed in conjunction with the most relevant published work.

The key phenomena noted are:

- thresholds for the onset of melting and vaporisation processes

- freezing in of symmetrical annular waves into the surface of the melt pool

- melt efficiency effects at low irradiance using temporally shaped pulses

- changes in melting efficiency due to modifications of the target surface

8.2 Preliminary observations and assumptions

Figs. 7.20-7.24 clearly show that although most of these spots are shallow in terms of conventional high power laser welding, (in the order of 200 μm), a significant volume of material has melted and resolidified. If conduction limited spot welds are defined as those welds in which the diameter of the spot is equal to or exceeds its depth, these initial spots are conduction limited welds. This however, is not so as irradiance increases, figs.7.8 – 7.10. At lower irradiance conditions, fig. 7.11, and shown in fig. 7.16 & in more detail in fig. 7.18, it appears that the oxide layer across the complete diameter of the spot has also been melted. This suggests that, as a result of each laser pulse, temperatures have been high enough to melt the oxide layer. As the melting point of the oxide is ~ 2045°C, it is safe to assume that some vaporisation of the aluminium alloy, melting range 570 - 660°C, boiling point, 2480°C, has occurred.

Figs. 7.20 - 7.24 confirm however that the volume of evaporated material is small compared to the total volume of the melt pool. At lower pulse irradiance, careful examination of fig. 7.11 & 7.29, suggests that in some areas, melting of the oxide layer does not appear to have taken place over the full diameter of the melt spot.

Optimising pulse repetition rates and process speeds and modification of the CNC program to match the spot welds led to immediately adjacent melt spots and maximum surface coverage for the fixed average power of the laser.

It can be assumed therefore on the basis of these metallographic observations made on the early ranging trials, figs. 7.20-7.24, that the laser melted surface consists of a series of shallow melt spots, which exhibited all the characteristics of resolidified aluminium.

It would appear that grains at the fusion interface act as seeds for epitaxial grain growth into the molten material. These melt spots are therefore similar to shallow laser welds. In aluminium alloys, the very high thermal diffusivity allows rapid removal of heat from the melt zone and hence the noticeable change in grain orientation (fig. 7.24) in the direction of heat extraction clearly identifies the laser melted area.

No assumptions can however yet be made as to the nature of the surface phenomena exhibited by the melt pools. More detailed consideration of the key experimental criteria involved in the production of these melt spots is therefore required. Later in the discussion, figures taken from the literature, which have been arrived at from experimental results and from straightforward semi empirical models, are employed, to identify approximate values for laser melting and solidification times.

8.3 Peak pulse power & pulse irradiance

8.3.1 Measurement of pulse irradiance.

The problems associated with accurate pulse irradiance measurement were mentioned in section 5.7.1. Measurement techniques can be unreliable [110,111] particularly if wide ranges of pulse energy and peak pulse power are employed. Alternative practical techniques that have been used elsewhere in the published literature [30], were evaluated and employed for this current work. The techniques are

based on a physical measurement of effective melt spot diameters produced on the target in the focal plane. Because of the effects of conduction and melt flow, these techniques will always give slightly higher values for spot diameter than those calculated from basic optics formulae and from equation 3.5, hence producing lower figures for focused pulse irradiance at the workpiece. It would appear that many of the values for pulse irradiance quoted elsewhere in the literature are also based on very approximate estimates [28,30]. This may be due to non availability of suitable measuring devices at the time most of the referenced work was performed.

For the early spot melting trials at 20 Hz 2.5 ms, 5J, a number of metallurgical cross sections were prepared and the Seescan Image Analyser was used to produce the results in tables 7.7, 7.8 & 7.9. Spot surface measurement was used to calculate the pulse irradiances identified in table 7.10. Two variations on this spot melt measurement technique were used to produce the data for fig.7.34. This shows that plan and cross section measurements of spot diameter were in good agreement, but in the case of figs. 7.55 & 7.56 differences were noted between the two measurement techniques in the dimensions of the melt spots when surface condition was modified. In this case, it was therefore necessary to use measurements taken from transverse cross sections, prepared as shown in fig. 6.6, of the melt spots. In these cases, depth measurements were included to produce fig. 7.58.

In some respects, measurement of surface spot diameters was a more accurate and hence more appropriate technique, as the equipment used was capable of producing large numbers of melt spots at high speed and large numbers could be measured rapidly for each condition. This involved the measurement of the surface diameter on two orthogonal axes for a minimum of six spots, which were subsequently averaged to find a grand mean.

To generate the preferred laser parameters, 20 Hz, 2.5 ms, 5 J, a total lamp input power of 3.4 kW is required. Fig. 7.1 shows that at this pumping level, a half angle beam divergence of 8.2 mrads is obtained. Using equation 3.5 gives a figure of 0.65 mm for the calculated focused spot diameter. Figures for averaged effective measured spot diameters taken for the same parameters, from a large number of spots are given in table 7.8. The 6% difference between these converts to an 11% difference in irradiance, again considered acceptable in the light of the wide ranges of irradiances quoted.

8.3.2 Pulse energy and pulse duration

All solid state laser power supply and resonator combinations only allow a limited range of pulse energy / pulse duration combinations. The peak pulse power & pulse irradiance trials described in section 6.6.1 are aimed at understanding the effect of the peak (or instantaneous) power of the laser pulse, E/τ, (equation 3.3) on the spot melting process. In other relevant published work, either the effects of pulse energy and pulse irradiance are not treated separately [112], or only a very limited set of laser parameters are used [28,30,109]. This may be partly due to the fact that many solid state lasers power supplies and resonator designs do not allow these variables to be altered independently, or only allow variation over a very narrow range. This is especially true in the case of older capacitor discharge power supplies. During the characterisation exercise and the pulse ranging trials it became clear that for a constant pulse energy (E), it was possible to vary the pulse duration, (τ), over a wide range simply by adjusting the third controllable variable, lamp height. This has the effect of changing total lamp input power according to equation 6.1. In practice, as shown in appendix 5, the actual change in lamp height is minimal, hence the change in divergence, as shown in fig. 7.1, is also limited and the pulse irradiance and the focused laser spot size remains constant. In this way, changing the pulse duration changes peak pulse power and pulse irradiance together in small accurate increments but independent of divergence effects. This feature of these trials alone justified the extent of the characterisation exercise. In this way, the stage 2 trials were conducted in a consistent manner on the basis of incrementally changing pulse irradiance at constant pulse energy.

A constant average power was also used in all of the experimental trials that succeeded the characterisation exercise. At an average power of 100 watts, the laser is very much in the centre of its operating regime, and as seen above operating variables can be changed over a wide range independently.

The decision to focus in closely on the laser parameters at which these annular rings were noted, 5 J, 2.5ms was justified. It was now clear that by changing pulse duration from 0.8 ms to 5 ms, a range of pulse irradiance was possible which spanned, in a consistent manner, the range of irradiance from initiation of melting to material removal. As the welding process is now well under experimental control, it was now

possible to explore the hypothesis that these annular rings were associated with the effect of reactive vapour pressure.

Figures 7.33, 7.35, 7.53 & 7.54 therefore show simply the effect of peak pulse power and pulse irradiance in isolation from any other properties of the beam. In this way, the validity of these straightforward easily understandable plots is ensured.

Previous work by the author [11] has also shown pulse irradiance to be the controlling variable in pulsed laser processing. A number of authors [23,28] & [30] have shown that melting and vaporisation occurs in the first ms of the pulse, but the independent effect of pulse irradiance does not appear to have been studied in this way before.

Another important point shown by these results is that the depth of a laser welded spot using low duty cycle pulsed lasers in the conduction limited regime will always be limited. Although the results do not entirely differentiate the effect of pulse duration from the effect of pulse irradiance, for a fixed pulse energy, spot depth appears to only increase marginally. This is probably due to the limited additional melting and heat conduction occurring during the latter stages of longer laser pulses. It becomes clear that the only way increased penetration will be achieved is by a keyhole welding technique, where a continuous molten vapour filled keyhole is maintained. However, even if high power continuous wave lasers are used, deep penetration welding of aluminium is still problematic because of the physical properties of aluminium discussed earlier.

8.3.3 Peak pulse power / pulse irradiance thresholds

More general trends shown by the results in chapter 7 are now considered along with the most relevant work published work.

Most of the graphical results appear in very general terms to show two thresholds. The first threshold, as confirmed by optical and metallographic examination of the laser spots, is associated directly with a noticeable amount of surface melting. Below this 3 kW instantaneous pulse power threshold, the amount of melting diminishes rapidly (fig.7.11). However, in this regime effective spot size is not a reliable measurement for calculating pulse irradiance as significant melting is not occurring over the full area of the focused laser spot. However, for the purposes of this

exercise it is assumed that once the threshold plateau is reached, melting is occurring across 100% of the $1/e^2$ portion of the pulse.

The general shape of figs. 7.33, 7.35, 7.53 & 7.54 all bear some resemblance to the graph of Golubev [112], reproduced as fig. 5.2, which also shows different mechanisms of material melting and removal, but at very different laser parameters, as in his study, keyhole formation speed is being investigated. At low irradiance, with limited evaporation, he identifies the mechanism of material removal from the keyhole as being thermocapillary, with no vapour pressure effect on melt motion. In the high irradiance regime, the molten material is squeezed out due to the vapour pressure of the melt. At higher irradiances and hence even higher temperatures still boiling and vaporisation dominate, creating a vapour pressure above the material surface and a consequent reactive vapour pressure on the molten material. The end result of this is the generation of a single shot keyhole type hole in steel, on the sides of which concentric rings are clearly visible as in fig. 7.8 & 7.9 of the current work. As shown in section 5.7.3, the view of Golubev [112] is that these are capillary waves frozen on the side of the keyhole with a pulse period of the order of 30 μm. These wave periods are similar to those observed in figs. 7.10, 7.17 & 7.28, even though a target material with very different thermal properties is used. The uncertainty involved in the determination of irradiances in this work however leads to some doubt as to the explanation of the phenomena. There is also some doubt as whether the results are comparable. What is encouraging is the ever present nature of these rings whenever similar melting regimes are carefully investigated. Because of the remarkably predictable and reproducible nature of these effects observed in the current study, the author's view is that the rings are always present and are an inevitable precursor to melt ejection. This also in turn suggests that their formation is more likely to be due largely to the well-documented effects of reactive vapour pressure.

It was also confirmed by measuring the approximate wavelengths of the annular rings from fig. 7.10 & 7.32, and from measurements noted in [112], that in the case of both steel and aluminium, alloys with very different thermal properties, the wavelength appears to range from 20-50 μm in both cases.

Considering reference [114], a similar pulse duration and pulse energy and similar target materials were used to the current work, but irradiances (referred to as

intensities) were calculated differently. They identified enhanced coupling thresholds, but at lower pulse irradiances, 0.15 - 0.22 MWcm^{-2}. They also produced a great deal of experimental evidence, largely based on monitoring plasmas using photomultiplier tubes, for initiation of plasma. They claim that the plasma is responsible for enhancing absorption and improving melt efficiency through re-radiation of broad band energy back to the surface of the target where it is more efficiently absorbed. If the irradiance values presented are to be believed, then the thresholds quoted occur below the values for melting obtained in this work. As discussed later, other authors, notably Nonhof, demonstrate that the existence of plasmas at these low irradiances is most unlikely. The evidence from this work clearly shows that these low irradiance thresholds in figs. 7.33, 7.34, 7.35 and in 7.53 & 7.54 are all clearly associated with surface melting.

8.3.3.1 Plumes

Von Allmen shows in [31] a pressure-temperature diagram, which demonstrates that at high temperatures, both liquid and vapour co-exist and there is no thermodynamic distinction between the two, the density of the two phases merge smoothly. The melting point having been reached, both melting and vaporisation will be taking place concurrently.

Nonhof has also shown [134] that although plasmas are probably generated within the laser welding plumes, in this regime they are not playing an important role. This is in contrast to the very significant role of plasmas when keyhole welding with 10.6 μm radiation.

In the current experimental work, it was noted that plumes changed from tall energetic and bright blue (fig. 6.5), at lower pulse energies and lower pulse irradiances to diffuse spattering plume at the higher irradiances and higher pulse energies associated with increased penetration. This identical experimental phenomenon was noted in [30] by Matsunawa, where laser plumes are discussed. His was supported by changes in thermal and optical measurements of the plume. A plume was generated by laser parameters of 38 J pulses of 3.6 ms duration, and it was stated on the basis of optical and plume analysis measurements, that the plume consisted of a weakly ionised subsonic jet of vaporised particulates. He also states that a plume blocking mechanism was proven for these parameters. In the current study, pulse lengths shorter than the 3.6 ms pulses used by Matsunawa [30] were used so a direct comparison is not

possible. Figs.7.33-35 all suggest however a similar threshold effect associated with changes in the coupling of the beam to the workpiece, but not due to a plume blocking mechanism. In this work, the experimental evidence suggests that this low irradiance threshold effect and increase in melt efficiency is closely associated with melting.

8.3.3.2 Constant melt efficiency

The possible explanations for the regions of constant melt efficiency between the two thresholds discussed above are now considered. These appear to be a typical feature of the graphical results. In the light of evidence from the literature and experimental evidence, only two explanations for the plateau on figures 7.33, 7.35, 7.53 & 7.54 are considered feasible.

Is this associated with a latent heat effect? The latent heat of melting of aluminium, 10.7 kJmol^{-1} is small compared to the combined latent heat of melting and vaporisation, 336.5 kJmol^{-1} [31]. However, if it is assumed that no enhanced coupling is occurring in this regime, (the shape of the melt spots suggests this is not occurring), at a constant pulse energy, no change should be expected. Secondly, a beam blocking mechanism as proposed by Matsunawa [23] and discussed earlier could possibly be taking place. It is however thought highly unlikely that the plume particles, which Matsunawa has shown to be mainly < 20 nm in diameter for this regime of laser welding, will have any effect on a 1.06 µm wavelength beam.

The confusion regarding irradiance estimates partly explains the various enhanced coupling effects and beam blocking effects reported by Matsunawa, Lewis & Dixon and von Allmen discussed earlier.

8.3.4 Material removal threshold

The threshold effects observed in fig. 7.5, table 7.10 and shown in figs. 7.33 - 7.35 all show an upper limit. Figs.7.8 & 7.9 show this to be associated convincingly with melt ejection. Whereas in the results from the ranging trials given in figs. 7.6 & 7.7, no material removal is occurring, in photographs figs. 7.8 & 7.9 clearly show incipient hole drilling. Fig. 7.8 shows molten material partially ejected from the hole. The minimum irradiance for the condition under which this occurs is again calculated at 2kW peak pulse power (using equation 3.5) on the basis of effective spot size, taken

from fig. 7.5, to be 0.48 MWcm^{-2}. In the final series of peak pulse power trials, pulse energy remained constant and pulse duration was changed incrementally, hence the pulse irradiance is also increasing. As the irradiance increases, the surface temperature and the molar energy of the vapour will also probably increase, as explained by von Allmen [31]. Reactive vapour pressure should also increase to the point at which melt ejection occurs, especially in the case of the high pulse energy parameters (fig.7.8), at the threshold pulse irradiances identified above. These reactive forces will impinge on the evaporating melt layer, but lateral pressure gradients are also inevitably present which explains the resultant changes in surface topography.

At some point, which in this work is associated with a particular set of laser parameters and a pulse irradiance of 0.48 MWcm^{-2}, the increasing reactive vapour pressure overcomes the smaller surface tension forces in the liquid layer and melt ejection occurs. This figure coincides with the end of the plateau's in figs. 7.35, 7.53 & 7.54 and also coincides with the production of a single shot laser keyhole with obvious beam trapping capability.

The presence of increasingly prominent rings, which are formed with incremental increases in pulse irradiance approaching the material ejection threshold, appear to be an inevitable precursor to molten metal ejection. The fact that these ring features are increasing in prominence continuously with increasing pulse irradiance suggests that the plateaux are due to increases in reactive vapour pressure and are simply associated with incipient keyholing.

Consideration of the 'conduction limited' melt spots shown in Figs. 7.20-7.24, show that they are very close to that of a sector of a hemisphere, there is no suggestion of the classic nailhead shape associated with most high irradiance keyhole welding processes. Having performed a consistent series of spot melting trials over a range of pulse irradiances, as opposed to other authors who have simply examined a very limited number of data points, there is convincing evidence to go further than other authors have been able to go in confirming the effect of increasing reactive vapour pressure leading to melt ejection.

It is at the upper end of the pulse irradiance range however that care must also be taken in interpretation of the melt efficiency results, as a change in aspect ratio of the melt pool indicates a change to a higher irradiance enhanced coupling regime, (fig. 7.34). Although this limits the accuracy of the melt volume calculation, and any

predictions as to melt efficiency in this high irradiance regime would be inaccurate, a significant change in mechanism is nevertheless confirmed by fig.7.35. This plot does take into account melt volume, and at the high pulse power of 5kW, a threshold exists at 0.75 MWcm^{-2}.

These melt volume calculations assume the melt pool to be a sector of a sphere, a good assumption as shown in figs. 7.20-7.24, and by performing a simple geometrical calculation for the volume of a sphere. This is easily then converted into efficiency in terms of volume melted per joule.

Calculating pulse irradiance directly from peak pulse power and spot dimensions from fig. 7.33 & 7.34 shows a range from a pulse irradiance of 0.57 MWcm^{-2} at which a consistent spot size is achieved, to a point at a pulse irradiance of 0.9 MWcm^{-2}. These irradiances are generally, considering the uncertainties involved the measurements, of the same order of magnitude as values quoted elsewhere [109,112] and are widely accepted as typical values occurring for solid state laser welding.

8.4 Generation of annular rings.

One of the major strands of the current investigation started with the identification of the ring generation problem during the ranging trials outlined in section 6.4. and during the feedrate & coverage trials. Three different sets of parameters were used at a range of defocus conditions. Only later after re-examination of these ranging trials was the identification of thresholds for generation of these waves made. It was found that these thresholds occurred at different pulse irradiance for different peak pulse power conditions for each combination of laser parameters, table 7.10. The next series of trials referred to as feedrate and overlap trials were to identify speeds and overlaps so that the laser melt spots could cover a complete surface.

After the ranging trials, having identified the preferred parameters of 20 Hz, 2.5 ms, 5J a large number of spots were produced. The occasional occurrence of annular rings was identified at this stage and was mapped in table 7.7. It then became apparent during the peak pulse power trials that in all cases these concentric rings occurred occasionally prior to their occurrence on all melt spots. A continuum of irradiance appears to exist which starts with an infrequent occurrence of annular rings and

extends to repeatable generation of rings on 100% of melt spots. It then became clear that the initial laser parameters identified, 5J & 2.5 ms, coincided with the lower irradiance regime where rings occasionally occurred or were occasionally visible.

During the course of the literature survey, only a limited number of references to frozen in annular rings were identified. Von Allmen [31], Rykalin [120], Kreutz [119] & Golubev [112] were the only authors who identified the phenomenon, and Rykalin is the only author who has attempted to investigate further, section 5.7.3. However, all the authors have identified the ring phenomenon as due to the freezing in of waves generated by reactive vapour pressure. The contribution of thermocapillary effects is discussed by Golubev [112] and Rykalin [120] but Golubev places more emphasis on the contribution of thermocapillary effects than other authors. This is based however, on some very approximate figures for pulse irradiance, and some rather dubious experimental techniques for measuring the speed of melting. An objective view of the literature referenced above, making particular note of the work done on the recoil forces exerted by the evolving vapour described by von Allmen [31], where he performed approximate calculations of the magnitude of these forces, has led to the conclusion that the reactive vapour pressure is very largely responsible for the production of these waves. Indeed, he described a technique whereby these forces are measured by the use of a target in the form of a small ballistic pendulum. However, as presented in section 5.7.5.1, for the general case and as shown by Rykalin [120] for the particular case of laser spot melting, surface tension forces are larger than the gravitational forces and surface tension forces must therefore play an important role. To call these features capillary or thermocapillary waves is misleading, capillary waves are generally considered to be due almost completely due to the effect of surface tension forces. Although capillary forces are of importance in the propagation of these waves, the primary mechanism of their formation is the reactive vapour pressure of the vaporising metal.

Experimental evidence for the predictable reproduction of these features at this stage appears convincing. Table 7.10 & figs. 7.28 & 7.29 show during the peak pulse power trials, the rings can be turned on and off as required simply by controlling peak pulse power / pulse irradiance. At the 20Hz, 5J parameters, the minimum peak pulse power is 2.5 kW, related to a pulse irradiance of 0.55 MWcm^{-2}, and 5 kW peak pulse power.

At the upper limits of pulse irradiance, 5kW, ~1MWcm^{-2}, the material removal threshold is approached. If the increments of pulse irradiance are small enough, as in this work, the existence of these rings is now seen as an inevitable precursor to material removal.

Further evidence comes from von Allmen [31]. He considers this process of melt ejection as part of the laser drilling process and the continuum described in the results of this work show that similar but reduced forces are at work even during low average power pulsed laser welding processes. Again, this links the creation of these annular rings with a steady increase in reactive vapour pressure, causing surface waves. These become more and more energetic to the point at which material is ejected and the drilling regime commences.

These results demonstrate in a very clear practical manner, the link between reactive vapour pressure and the start of melt ejection, which is relevant to both laser welding and drilling processes. This link has not been adequately discussed in the technical literature, the majority of which has concentrated on the effects of welding plumes or plasmas.

8.4.1 Investigation of ring phenomenon

Several attempts were made to measure these waves by conventional metallographic and surface profile measuring techniques, but results were not repeatable due to the very small micron scale of many of the concentric rings (fig. 7.28, 7.30 &.7.31). It was also clear from the optical photographs that these features must be of a scale comparable with the wavelength of light to explain the enhanced images of the concentric rings obtained from optical photographs, hence these effects were not measurable by all except the most sensitive techniques. Although these effects were also visible via electron microscopy, (fig.7.28), the effect was not as dramatic as when visible light was used.

As discussed above, the evidence for the reactive vapour pressure mechanism whereby these annular features are generated and frozen into the surface of the molten melt pools has been confirmed by a small number of authors. What is less clear is the role of capillary or thermocapillary action, which as we have seen, is referred to by a number of sources. One important fact should be noted and that is the basic definition

of capillary waves [126]. Capillary waves always have a very short wave period, and they are almost exclusively associated with surface tension forces. This seems to have been overlooked by a number of authors who as we have seen, consider the formation of these waves to be due largely to capillary or thermocapillary action. The author's view is now that the continuous and reproducible nature of these waves shows that they are closely connected with the increasing reactive vapour pressure generated by increasing pulse irradiance. These are then frozen in due to solidification of the melt pool during wave propagation.

To investigate this phenomenon further, a number of approaches were evaluated and rejected. Any variation in laser pulse energy introduces a number of new variables into the process. Equally any optical modification to the pulse such as using a defocused beam will change the irradiance of the pulse drastically (pulse irradiance = peak pulse power/area of focused spot). Two approaches were identified as providing a controllable practical modification to the beam / material interaction process, both techniques were arrived at by consideration of published work in this area.

Matsunawa's work [30] is useful in clarifying a key aspect of this work. He identifies "the rising slope of the laser power wave form" as determining the initiation time for evaporation. Of importance also were measurements of plume speed, which show conclusively that a reduction in pulse energy, with its associated reduced plume initiation speed, produces a reduction in plume velocity. Matsunawa [30] showed that that if a less steep leading edge to the temporal pulse shape was used, decreased reflection may lead to improved absorption, and hence the availability of more energy for vaporisation. The trials devised therefore maintained a constant pulse energy, and the sole property modified was the temporal pulse shape. When modifying the temporal pulse shape in this way, there are three main options. Firstly, 'detuning' the enhanced spike at the start of the standard unshaped pulse. This involves increasing the input to the flashlamps early in the laser pulse to cancel out the spiking which occurs as a feature of the electrical design of the solid state laser power supply. This has the effect of reducing the initial slope of the laser pulse, fig. 7.37, 7.39 & 7.41. A slower delivery of energy to the surface might be expected, with a consequent reduced reactive vapour pressure and reduced generation of melt pool waves. Secondly, enhancing pulse sectors at the start and at the end of the laser pulse, fig 7.43, and

finally, enhancing the sectors towards the end of the pulse, which has the effect of lowering the rate of fall of the laser pulse.

Although this involved a number of significantly different pulse shapes, figs. 7.36-7.44, several factors limited the range of temporal pulse shapes beyond these. Firstly, the limitations of the laser monitoring devices, the internal power meter and the external oscilloscope, gave only approximate readings for the peak pulse power of the laser pulse, hence limiting calculated values of pulse irradiance to approximations. To accurately identify any significant irradiance difference between a temporally shaped pulse and a normal pulse would be difficult in practice due to limitations in resolving accurately the exact temporal nature of the pulse. By maintaining a constant pulse energy, it was clear that significant differences in the initial rise time of the laser pulse, figs. 7.36 - 7.44, were possible.

Secondly, it was essential, in order not to change any other characteristic of the pulse, that constant pulse energy of 5 joules and pulse duration of 2.5 ms was maintained. It was also essential that lamp pump power and hence divergence did not vary significantly. As the minimum pulse sector width was 0.5 ms, this limited the number of pulses to a maximum of 5. In practice, the number was less than this, because in some instances, it was not possible to achieve the desired pulse temporal profile using the minimum pulse duration (table 7.11). Finally, it was not possible to accurately identify the slope of the leading edge of the laser pulse, all that can be claimed is that pulse shapes 1, 3, 5 & 7 all had very much steeper slopes than 2, 4 & 6. Shape 8 had a symmetrical pulse shape but with an intermediate slope. The following pulse shapes were derived.

Pulse shape ID	no. of sectors	type
1	1	standard
2	2	rising
3	2	falling
4	3	rising
5	3	falling
6	4	rising
7	4	falling
8	3	symmetrical
9	2	prepulse

Table 8.1 showing range of pulse shapes.

8.4.1.1 Pulse shaping trials

Increases in melting efficiency shown in fig. 7.57 & 7.58 in these low aspect ratio melt spots suggest that melting efficiency is improved by a particular type of temporal pulse shaping. The pulse shapes which appear to be most successful are those which have a more gradual rise at the start of the pulse and a steeper trailing edge to the pulse; shape numbers 2,4 & 6. One possible explanation for this comes from Matsunawa [30], who suggests that a slowly rising pulse will reduce the initiation time for plume generation, hence delaying the onset of the plume blocking mechanism. The more likely explanation is simply that the more efficient temporal pulse shapes have reduced reflection losses and increased the effective peak pulse power, hence increasing the incident pulse irradiance.

However, the low duty cycle associated with this pulsing regime must be recalled, the on/off ratio is only 1:20. Specific heat input to the target is low and the temperature of the bulk material remains low. The initial reflectivity of the surface must be overcome with each laser pulse. This is very different to the continuous wave welding or cutting regime, where heat is localised at the leading edge of the focused spot. Unfortunately, it would be necessary to measure the pulse energy in the relevant portions of the laser pulse far more accurately than was possible with the current equipment to obtain a definitive answer.

Those melt spots, produced using what are referred to as falling or trailing pulse shapes, i.e. with a sharp initial rise in slope and a gradual trailing off, shape numbers 1, 3, 5 & 7, did not produce the best melt efficiency nor significant annular ring effects. There is a certain irony in this, in that the power supply of the solid state laser has been designed to provide a laser pulse with just such a pre-pulse as shown in fig. 7. 36. Laser designers accept that in certain circumstances, this built in pre-pulse is preferred to enhance coupling!

Another uncertainty involves the actual shape and size of this 'spike', which contains 2% - 5% of the energy of the pulse [22]. Unfortunately, limitations on the time resolution of the monitoring devices did not permit any further detail to be uncovered on this commercially confidential aspect of laser design. Because of the uncertainty concerning the exact pulse energy content of the spike and hence the exact pulse irradiance of these pulses, it is impossible to check whether these melt efficiency effects can be related directly to irradiance. Equally, to calculate a slope from the scope

traces shown in figs. 7.36-7.44 would be at best, inaccurate. Similarly, although peak pulse powers are indicated on figs. 36 – 44, these are also inevitably inaccurate because of the limitations of the time resolution of the oscilloscope used. These results were encouraging enough however to justify pursuing further trials using pulse shapes, further investigation was required.

Returning to consider table 7.12, and those pulse shapes that did not appear to generate annular rings and which produced lesser increases in melting efficiency, shapes 3, 5 & 7. Referring to the laser pulse temporal profiles in figs. 7.36 - 7.44, all of these pulse shapes were as far as possible identical laser pulses, the only difference being a differing distribution of energy temporally within the pulse. The effect of using a laser pulse with a reduced slope to its leading edge can be seen as simply a technique whereby laser energy is introduced into the material less rapidly. In these cases, by temporally shaping a pulse, the slope of the leading edge of the laser pulse is being increased, and more energy is contained in the earlier sectors. This may well be responsible for increased reflection losses at the start of the pulse, hence reducing the rate of heat input during the critical coupling stage at the beginning of the pulse. Conversely, those pulse shapes with reduced leading edge slopes may well lose less by reflection. It is felt that this view is supported by the practical observation that during the spot melting experiments, it was noted that on the falling pulse shapes, energetic blue plumes were visible, combined with a loud detonation accompanying the impact of each pulse. A similar experimental observation was described by Matsunawa. Although there is some doubt over the irradiance figures quoted in Matsunawa's work, in his view the energetic absorbing plumes noted during spot melting are typical of the plume blocking regime - our work, disagrees with this. The conclusions of the current work are more in line with the work of Nonhof. He presents very convincing experimental and theoretical evidence to support a number of unequivocal statements. In order to achieve plasma blocking with NdYag lasers, pulse irradiances must be x100 those required for plasma blocking in the case of CO_2 laser welding, ~ 10^2 MWcm^{-2} - clearly these pulse irradiances are not being approached here. He suggests that calculations have shown that although plasmas probably exist under these typical solid state laser welding parameters, there is no danger at all of any blocking mechanisms.

It is therefore suggested that those temporally shaped pulses with steep leading edge slopes may be producing more rapid but less efficient initiation of evaporation,

causing a reduction in reactive vapour pressure and less tendency to ring generation. This might also explain the reduced increase in melting efficiency. This supports to a degree what now appears to be a relationship between pulse irradiance and higher melting efficiency approaching keyhole irradiances – reduced absorbed energy, less rapid vaporisation, less generation of rings.

8.5 Effect of peak pulse power on alternative surface conditions

Surface	Pp, kW	dia., mm	MWcm-2
mill finish	3.125	0.831	0.576
etched	3.846	0.800	0.766
anodised	2.000	0.701	0.518

Table 8.2 showing peak pulse power and pulse irradiance values for pulse irradiance plateau.

Figures 7.33 & 7.53 & 54 show that no significant increases in melt pool size is occurring over a wide range of pulse irradiance for each of the surface conditions. Table 8.2 attempts to summarise the effects of the pulse irradiance trials on the three different surface conditions, giving the pulse irradiance lower limit for melting for each surface condition. Firstly, for the standard material finish, a maximum spot diameter 0.8 mm diameter is obtained at a pulse irradiance of approximately 3 kW, These results must be considered in the light of the depth and melt volume increases identified in fig. 7.34 & 7.35.

Secondly, for the etched material, with an approximate oxide thickness of 25 nm, the height of the plateau, i.e. the maximum spot size at these parameters ~0.8 mm, is greater, but the initial slope of the graph is lower, and the maximum spot size is reached at a higher pulse irradiance, ~ 3kW. Similarly, the slope for the anodised material is steeper, but reaches a maximum spot diameter of ~0.65 mm at a lower pulse irradiance of 2 kW. Also, the minimum threshold for surface melting at these parameters, in the case of trials on anodised surfaces, the melting threshold was lower, and melting was observed down to a maximum pulse duration of 6 ms, a minimum

pulse irradiance of 0.83 kW. For the standard mill finish, with an oxide thickness of ~ 40 nm, melting was seen down to a pulse irradiance of 0.95 kW. It is clear that accurate irradiance values can not be attributed to these results as melting is only occurring over a limited unknown portion of the spatial distribution of the beam, which cannot reliably be identified. As previously discussed for the pulse irradiance trials, these results are probably due for the standard finish material to overcoming of the latent heat of vaporisation. It is expected that a similar effect is occurring to explain the same shape of curve for the etched and anodised surface finishes.

Despite the evidence given in chapter 4, showing that theoretically, pure alumina should transmit infra red radiation very well, evidence emerged from the literature review of enhanced absorption due to presence of surface layers. So there are perhaps three different mechanisms to consider here;

1. increased absorption in anodised surface layers

2. reduced absorption by etched surface

3. combination of both of these with latent heat of vaporisation effects

These possible mechanisms need to be examined in the light of Patel & Brewster's paper [109]. In this paper, in addition to reviewing the evidence for the existence of plume or plasma absorbing effects, they claim to have shown that for an aluminium target, plumes formed under an oxygen atmosphere are more absorptive and last longer than those formed under an argon atmosphere. They propose this is due to the high absorptivity of a thin non stoichiometric aluminium / magnesium oxide layer formation which is also an important factor affecting laser energy absorption. Their reflectance results from the low irradiance conditions show a significant reduction associated with the presence of an oxygen atmosphere, and hence presumably, an enhanced oxide layer. They also performed plume transmittance measurements to examine the effect of an oxygen assist gas on plume blocking, and it is suggested the results show a more opaque and longer lasting plume due to the presence of the oxide layer, again for 6061 aluminium targets. These results suggest a possible mechanism whereby the modified oxide layers in the current thesis might increase or decrease beam coupling and rate of beam coupling.

The different values for maximum spot diameters shown in figs. 7.33, 7.53 & 7.54 could therefore be accounted for on the basis of a reduced oxide layer and hence reduced beam absorption by the etched surface. The increased pulse irradiance

required to attain the plateau can be similarly explained for the etched material, in that a higher proportion of the beam energy is likely to be reflected, hence a higher pulse irradiance is required. Equally, for the anodised material, increased absorption is leading to a lower pulse irradiance to achieve an equivalent spot size. Also as expected, the increased absorption of the anodised surface leads to increased absorbed power and increased efficiency, this coincides with a deeper melt spot, as confirmed by figs. 7 57 - 7.58.

8.6 Combined effects of surface layers and pulse shaping

To investigate further the pulse shaping results, the surfaces of the same 6016 aluminium alloy were modified as described in 6.7.1. These surfaces were also subjected to identical parameters to those used for the pulse irradiance trials, with the addition of an extra pulse shape no. 9. This was an attempt to further suppress the annular ring effect by enhancing the initial spike at the beginning of the laser pulse.

This final complex series of trials, where all of the temporal pulse shapes were used to produce melt spots on two additional surface conditions, is now discussed. The rather interesting variations in spot dimensions and hence, melting efficiency between the different pulse shapes and the three different surface conditions can be summarised as follows on the basis of an examination of figs.7.56 - 7.58.

- Effective spot diameters are smaller than spot diameters measured from cross sections of spots. As shown in fig. 7. 18, it is difficult to measure the exact spot diameter as it tends to be masked either by a perimeter of damaged oxide (fig.7.52) or by an unmelted oxide coating (fig.7.11). It is thought that this masking effect is responsible for the reduced spot sizes on anodised surfaces (fig. 7.55).

- A straight comparison between the standard pulse, shape no. 1, with the other pulse shapes for the standard material shows that some increases in melt efficiency are obtained in the case of all of the rising pulse shapes, that is those pulses which have a less steep rising slope to the temporal shape of the pulse

- the differences between these rising pulse shapes, shapes 2,4 & 6 do not appear significant.

- in the case of all the pulse shapes except pulse shape 7, the anodised surface causes an increase in melt efficiency.

- in general pulse shapes 1, 3, 5 & 7 produce smaller weld spots and less efficient melting for all three surface conditions.

- for almost all pulse shapes except rising pulse shapes 3 and 7, the reduction in oxide thickness due to the etching process has led to less melting.

- pulse shape nos. 6, 8 & 9 appear to cause a significant increase in melt efficiency when used to produce melt spots on anodised surfaces, figs.7.55 –57.

In addition to those points noted above, some interesting experimental observations were made. Those pulse shapes which produced the more efficient melting were those which produced the least notable plumes, pulse shapes 2, 4 & 6. This tends to suggest that the less energetic plumes can be associated with slower vaporisation and reduced tendency to generate rings.

8.6.1 Effect of oxide layer

As discussed in section 4.3, oxide layer thickness on both the standard mill finish material (40 nm) and the etched material (25 nm) is very much thinner than the wavelength of the incident radiation and hence is less likely to reduce reflectivity and increase absorption, as suggested by Prokhorov [37]. Also, in [31,109] it is stated that the effect of a 'thin' oxide layer should be negligible, as pure Al_2O_3 should ideally be fully transmissive to 1.06 μm radiation, which can easily be readily demonstrated to be the case for low irradiance infra red radiation. However, other work, notably that by Arata , as discussed in section 4.3.5, and Patel & Brewster [109], has shown that surface condition, and in particular, the presence of oxide layers, can increase absorption of the laser beam into the surface of the material dramatically. A great deal of experimental evidence is produced to support this. One may suppose that the additional constituents incorporated into the anodised aluminium surface during commercial sulphuric acid anodising treatments, performed in an aqueous environment, will introduce species capable of absorbing shorter wavelength radiation, although there is no hard experimental evidence for this. However, it should be remembered that at 3 μm, the thickness of the anodised layer is two orders of magnitude thicker than the oxide layer on the mill finish and etched surfaces, and is approximately three times the

wavelength of the laser radiation. Nonhof points out [134] that oxide layers should theoretically have a thickness of $> \lambda/4$ (250nm) to enhance absorption.

But why do these slowly rising pulse shapes produce more efficient melting on both these modified surfaces? The view of the author is that these results support the assertion that reflection losses are reduced by the more efficient temporal pulse shapes and similarly, reflection losses are also increased by the reduced oxide layer on the etched surface and are reduced by the thicker anodised surface layer.

The significant differences between etched and mill finish material shown in fig. 7.58 are more difficult to explain, at 25 nm & 40 nm these oxide layers might both be reasonably expected to be transparent to the laser beam. However, Patel & Brewster [109] suggest that absorption perhaps takes place at a thin non stoichiometric transition layer near the surface of the aluminium, and it may well be that differences between the exact nature of the oxide is producing these results. Assuming that the surfaces under study here fall very much into the category of engineering surfaces, differences in absorption of the 1.06 μm beam into contaminated oxide layers appears to be occurring even with these relatively small differences in oxide thickness. It would appear therefore from these results, that the practical effect of the oxide layer is not closely related to its thickness but more to its composition.

Evidence presented in table 7.14, shows that the three trailing pulse shapes employed that produced melt spots with annular rings on etched samples did not exhibit the same on anodised samples. Although the thermal history at these short timescales is very complex, a possible explanation for this may be that under the specific heating/cooling cycles produced by these pulses, waves are damped by the coating, as supported in section 5.7.5, equation 5.3.

One final point still requires clarification. All of the pulse shapes employed produced annular rings on the etched material. If we accept the hypothesis that reduced oxide layers cause the measured decreases in melt efficiency (due to increased reflection losses), this observation is harder to explain. A considered view of the evidence suggests that the presence of rings on the etched material may be due to two opposing effects. Although the reduced oxide layer increases reflection, this effect may be outweighed by more rapid and efficient absorption of that energy which is absorbed. The possible result may perhaps be an increased reactive vapour pressure and

consequent increase in annular waves and frozen in rings, although this is admittedly rather speculative.

Returning now to early in the experimental programme, it should be remembered that it was the random occurrence of melt spots exhibiting these rings at intermediate irradiances that stimulated further trials. Having established the link between irradiance, annular rings and melt expulsion, a possible explanation for the occasional premature occurrence of these rings may be the existence of localised inconsistencies in the oxide surface, figs. 7. 25 - 7.27. Fig. 7.58 suggests that if a pulse did strike an oxide depleted area, less absorption, more reflection might result.

8.6.2 Effect of pulse shaping on solidification

Since solid state lasers became commercially available with power supplies capable of producing temporally shaped laser pulses there have been suggestions, not least by Matsunawa [130], that 'pulse shaping' might be able to beneficially influence solidification characteristics of pulsed laser welding and plume control [131, 132]. Bransch [10] has shown an increase in weld area using a temporally shaped pulse on stainless steel, and Mohanty [133] attempted a mathematical explanation for this using incomplete experimental data. There has been no other evidence published in the literature however demonstrating improved welding associated with temporally shaping laser pulses, particularly in the case of melting or welding of aluminium. In [133], a model based on the balance of surface tension forces and energy at liquid / vapour and liquid / solid interfaces is used. The effect of temporal pulse shape on the final weld dimensions is predicted on the basis of this model and an increase in the depth of spot welds produced by a low power (100W) solid state laser, is noted at relatively low intensities, 0.45 MWcm^{-2}. In both aluminium and stainless steel an increase in weld volume is noted from using a "ramp up" pulse type as opposed to a "gaussian" type pulse. Although these results are not unexpected - an increase in weld volume with increase in incident irradiance, there is a confirmation of an increase in weld volume when a 'ramp up' pulse is employed. In all of this work there is no suggestion as to how temporal pulse shaping may reduce cracking in solid state laser welds.

In [133] it is suggested that pulse shaping has no significant effect on low irradiance conduction limited welds, our evidence suggests that this is not the case; there is a small increase in melt efficiency in this regime. Whether this would be significant in an industrial situation is less clear.

Both Bransch [10] and Nonhof [134] suggest however that temporal pulse shaping may well have the beneficial effect of reducing solidification cracking in spot welds, although no evidence at all has been presented again. Changing temporal pulse profiles whilst maintaining pulse duration and total pulse energy constant has shown here that there does not appear to be any effect on solidification cracking due to pulse shaping alone. The reason for this may be that solidification times are generally an order of magnitude shorter than the typical range of pulse duration used for spot welding [127]. Temporal pulse shaping in practice can only, as has been shown earlier, change slightly energy distribution within the laser pulse and this seems very unlikely to reduce the very high cooling rates which cause solidification cracking of laser spot welds.

No other relevant work in this area has been identified and the reason for this may be as follows. The pulse energy capability of single rod pulsed solid state lasers is limited by the maximum commercially available size of laser rod to approximately 50 J at a maximum pulse duration of 20 ms. This limits penetration to 1.5 - 2.0 mm in depth. Any further increase in pulse energy does not produce a deeper weld. As peak pulse power and hence irradiance is also increasing, and as has been seen earlier in this work, melt ejection occurs. Although some higher power pulsed multi rod oscillator amplifier systems have been built [12] these have not been widely accepted in industry. At this high pulse energy, >50 J, welding speed is very low because of the repetition rate and duty cycle limitations of 400 watt average power solid state lasers. If higher penetration depth is required, higher average power lasers, usually continuous wave units, or CO_2 lasers [135], operating at 10.6 μm are required or a different non-laser welding technique is employed.

8.7 Phenomenological model of laser spot melting

Now that all of the major features of the laser spot melting technique have been discussed, it is necessary to identify in more detail the various stages of the melting process. For reasons outlined in section 4.5.1.1, simple semi quantitative models only are applicable in this case. Results from published solutions of these simple semi quantitative models are now incorporated into a phenomenological model, Fig. 8.1, of the general case of a laser melted spot produced by a single pulse. Some experimentally measured figures taken from the literature are also incorporated in this model.

It must be remembered that in the early part of this work, standard laser parameters of 2.5 ms were used, giving a constant pulse energy of 5 J. As a low pulse repetition rate of 20 Hz was also used, giving a pulse period of 50 ms, duty cycles were low at 20:1 off:on. In this case, it was noted that due to the high thermal conductivity and diffusivity of aluminium ($\sim$75 x 10^{-6} m^2s^{-1}), heat loss by conduction (and perhaps to a limited extent, convection and radiation) maintained the temperature of the workpiece close to room temperature.

The following sections are intended to organise the work above by putting it in the form of a phenomenological model. The standard laser pulse will be used but reference is also made to the higher irradiance, shorter pulses employed in the later trials. Each section identifies the major steps involved in the process of laser spot melting, and each sub-section is related to the stages shown in figure 8.1.

8.7.1 Relaxation time

The reflectivity and transmissivity, their relationship, of metals and their relationships to temperature were discussed in chapter 4. We now move on to consider what happens to that energy which is absorbed. Von Allmen [31] describes the primary product of absorbed laser light as particle excess energy. This takes the form of excitation of bound electrons, kinetic energy of free electrons and perhaps excess phonons. The partition of the energy among the degrees of freedom of the material is at first not thermal, and the first step involves spatial and temporal randomisation of the motion of the excited particles in question. The timescale is thought to be very

short, shorter than the shortest laser pulses, in the pico second regime. The second step, again very short in metals, is energy equipartition, this involves a large number of elementary collisions and intermediate states, although this step is usually more significant in dielectrics and non-metals. These combined processes are referred to as thermalisation and for metals are usually summarised using the term energy relaxation time, typical orders of magnitude are 10^{-13}s in metals.

8.7.2 Melting and vaporisation

• The next step is heat flow and once the laser energy is converted to heat it tends to remain initially localised on a macroscopic scale within the skin depth of the metal. This skin depth (equation 4.5) of aluminium has been calculated by Nonhof [134] to be of the order of 10 nm, significantly less than the thickness of the oxide layer. Localised melting occurs after absorption of sufficient energy to reach the melting point of the metal and to overcome the latent heat of fusion, L_f.

Surface reflectivity will initially be significant, Nonhof has suggested it could be as high as 50%, we can nevertheless assume that melting begins to occur on a microscopic scale very soon after the relaxation time. The starting point for a mathematical model has to be the laws of heat conduction introduced briefly in section 4.1. All problems in unsteady state heat transfer have to solve Fourier's second law, and solutions of this equation have been found if the boundary and starting conditions are known. Section 4.5.1.1 presented the reasons why these heat conduction models are inaccurate. To summarise, this is due partly to the unknown contribution of reflection and partly due to temperature dependence of material constants and to phase changes. It is also accepted that as well as varying with temperature, all three of these terms also vary with composition, in particular thermal conductivity is generally much lower for alloys than for pure metals. Rykalin [120] assumes that K and H_c can be approximated by complex third degree polynomials but at this stage the mathematical analysis becomes very problematic. To calculate thermal properties, an approximate rule of mixtures might be used if data was available on a range of alloys, but this does not appear to be the case. The thermal conductivity of the Anticorodal 120 is given as 160-190 $Wm^{-1}K^{-1}$ [appendix 1] which compares with values of 220-240 $Wm^{-1}K^{-1}$ for pure Al from Touloukian [46]. Further uncertainty is introduced by doubts over the

consistency of measurement techniques for the thermal properties that are available. Fig. 4.10 shows that thermal diffusivity generally can be expected to decreases with temperature but no precise data is available for this particular alloy. To summarise, diffusivity values taken from the literature vary from 64 to 100 x 10^{-6} m^2s^{-1} for aluminium.

More specifically, a number of authors have attempted solutions to the conduction equations aimed at identifying the time taken to achieve melting. The single laser pulse melt pool is in fact the simplest case, and many authors' start off with this before moving on to attempt analysis of keyhole welding. Those most relevant to the current case are presented in books by Nonhof, by Luxon & Parker, by Steen and by Wilson & Hawkes. They all employ a similar technique which is derived from work presented in Carslaw & Jaeger's book, "Conduction of Heat in Solids". All have performed relevant calculations; some backed up with experimental evidence, which contribute to a phenomenological model of the laser spot melting case. The approach employs a straightforward one-dimensional analytical model based on a continuous point source of heat. In addition to the assumptions pointed out above and in section 4.5.2, constant pulse irradiance at the surface, relating to a completely flat top laser pulse and a constant temperature at the metal surface equal to the vaporisation point is assumed. For the case of aluminium, a widely held view is that Lf can be ignored as it is relatively low compared to the latent heat of vaporisation, L_v. L_f for aluminium is given as 1/3 L_v in [31].

All of the authors mentioned above use a version of the following approximation, derived from a solution of the heat conduction equations. They show the depth of penetration of heat is proportional to the factor:

$$\tau = {z^2}/{4K} \qquad \qquad \textbf{Equation 8.1}$$

where K = thermal diffusivity, 100 x 10^{-6} m^2s^{-1}, τ = time to achieve melt depth, z =heat penetration depth, 0.22mm.

As reported in chapter 6, spot depths were measured for the optimised parameters to be ~ 0.22 mm. An approximation based on equation 8.2 gives very low values for melting times, an order of magnitude shorter than those observed experimentally in [130] & [134]. Although it is well known however that these

approximations give much shorter melting times than observed experimentally, the discrepancy is so great as to question the validity of this simplified approach for the current work. This suggests that because of the extremely complex dynamic events that occur when a high power, high irradiance laser beam impinges on any target material, a complete theoretical understanding is almost impossible, especially when some vaporisation is taking place. For the purposes of our phenomenological model some of the limited experimental measurements and some relevant data from more complex semi empirical models must therefore be used. The best sources are Nonhof [134] and Matsunawa [30,130].

Nonhof used very similar laser parameters but a more sophisticated mathematical model to calculate melt velocities in a similar size of melt pool; he identified melt velocities of 850 ms^{-1}. He also measured time to boiling for aluminium substrates of 1 ms, again, using very similar welding parameters to those in this study.

Similar times to vaporisation were also noted in [114]. Matsunawa [30] also performed experimental measurements on time to vaporisation for solid state laser spot welds. He used similar laser parameters and he suggests evaporation starts at ~1 ms. Although calculated estimates are far shorter than those measured experimentally due to inaccurate model assumptions, these various estimates lead us to conclude that approximate vaporisation times are ~ 50% of the value of pulse duration (2.5 ms) used most widely in this work. These are similar to the shorter values of pulse duration and higher peak pulse power values that produced the concentric rings in this work.

The thermodynamics of the liquid-vapour equilibrium are now considered briefly for the purposes of the phenomenological model. Von Allmen presents the pressure-temperature relationship schematically which shows that [31] at high temperatures, both liquid and vapour co-exist and there is no thermodynamic distinction between the two, the densities merge smoothly. We can therefore assume that the melting point having been reached, both melting and vaporisation will be taking place until the end of the laser pulse. As visible vapour plumes were observed over the complete range of the irradiance studied (even though the appearance of the plume to the naked eye changed), it can also be assumed that both liquid and vapour exist to varying degrees in the plume towards the end of the laser pulse.

At this stage, as von Allmen points out, the primary target of the reactive vapour pressure (vapour recoil pressure) is the evaporating melt layer and the liquid

layer is subjected to measurable recoil forces exerted by the evolving vapour. Because of the finite nature of the cross section of the beam, lateral pressure gradients also exist which result inevitably in lateral displacement of liquid producing waves in the molten metal. If the surface temperature is very much in excess of the boiling temperature, vaporisation ultimately produces excess reactive vapour pressure, which in turn causes melt ejection as seen in figs. 7.8 & 7.9. This additional evidence supports the assumption that this describes accurately the case in this work, where higher peak pulse powers and higher irradiances generate more prominent annular waves and ultimately, melt expulsion.

8.7.3 Laser on time

Having arrived at an estimate for time to melting and vaporisation, it can be assumed that this process continues until the end of the laser pulse. Nonhof has suggested that ideally for a conduction weld it is wise to reach the boiling point only at the very end of the laser pulse so that energy is not used to vaporise metal unnecessarily. It appears from published data that this is certainly the case for the shorter laser pulses used in this work.

For the shorter pulses used, it appears that vaporisation commences at the end of the pulse, for the longer pulses, and the widely used 2.5ms pulse, there is likely to be a significant time at the end of the pulse where the laser plume consists of both melt and vapour.

8.7.4 Solidification of melt pool

Having assumed that these annular rings are frozen in waves, then it also safe to assume that solidification times must be close to the propagation time for the waves. As shown in section 5.7.3, Rykalin [120] appears to have been the first author to have recognised the phenomenon of frozen waves for steel targets although he does not mention under what conditions they occur and as to how the rings might be reproduced. He does however attempt to establish the mechanism of formation of these waves by analysing the variation of the solidification rate of a small volume of molten metal with time by again approximating to a one dimensional model. This is

possible because the depth / diameter ratio of the pool is very small in the case of his study, and also in the case of the current study. Other assumptions are again that the superheating of the pool is not high and the temperature distribution is uniform due to convection currents. He calculates the solidification time to be in the order of 10 μs for steel. This calculated figure agrees very approximately with other workers such as Steen [53] who uses a similar semi quantitative analysis of solidification to estimate a solidification speed of 10 ms^{-1}. Using a similar technique, solidification times of 30 μs were identified for shallow melt pools in pure nickel [96]. Similar quantitative estimates by von Allmen [31] arrived at through calculation a value of 8ms^{-1} for solidification of an aluminium melt pool, giving in this case a solidification time of 27 μs. Semi quantitative estimates combined with some experimental measurements from [30] also gave similar pool solidification times of 40 μs. Peercy has collected approximate data on measured solidification rates for shallow metallic melt pools, he quotes figures of 7-15 ms^{-1} as typical [127]. As the minimum sector length for a temporally shaped pulse in this work was is 0.5 ms, and the total pulse length for the preferred parameters is 2.5 ms, it can be assumed that solidification is taking place within a very short time of the end of the laser pulse freezing in the annular waves.

1 From 0 to 10⁻¹³ s

collimated beam

laser beam on

focus lens

energy equipartition and randomisation

6061 Al target surface

2 from 10⁻¹³ to 0.001s

laser beam on

melt spot

temperature rises to vaporisation point

Melt depth $\propto 4\sqrt{kt}$

3 From 0.001-0.0025s

laser beam on

vaporisation starts

additional energy used to overcome L_v

waves generated by vapour recoil

blue laser plume 20nm particles

4 At 0.0025 s

solidification starts at end of 2.5ms pulse and takes ~30µs (3x10⁻⁶ s) - annular rings frozen in

wave propagation direction

Figure 8.1 Phenomenological model of laser spot melting

8.8 Solidification cracking

It has been shown, particularly in [128], for pulsed laser welding of an aluminium alloy (6061, 0.95% Mg) which had a similar magnesium content to the alloy used in this work (6016, 0.55% Mg) that some loss of this important alloying constituent can occur during pulsed laser welding. This has been shown to cause a loss of hardness in solidified weld metal. However, as concluded in [128,129 & 130] it is most unlikely that this reduction in hardness is responsible for cracking of pulsed solid state laser welds. The causes are far more likely to be weld restraint and the rapid heating and rapid cooling produced by this spot weld configuration. It should also be noted that non of the temporal pulse shapes used in this work reduced the incidence of solidification cracking.

In Matsunawa's work, [130], he also attempted to used pulse shaping specifically to reduce cracking in a 5083 aluminium target material. He employed an unrealistically long complex pulse shape, well outside the usual operating envelope of conventional solid state lasers, up to 20 ms pulse duration, and he claimed to have reduced solidification cracking in some welds. The only way he was able to eliminate it entirely was to pre heat the material above 773 K, a singularly impractical suggestion.

If, as shown earlier in this discussion, freezing is taking place in a relatively short time after the end of the pulse, it seems unlikely that modification of the heat input rate by pulse shaping at the beginning of the pulse will affect solidification or weld defects, despite this having been attempted by a number of authors [128-130].

It is therefore concluded that temporal pulse shaping is not capable of eliminating the problem of weld cracking in this instance. Secondly, although some of the conclusions of Matsunawa's are disputed, he has shown that if any blockage of the beam by the plume does occur, it only occurs after several milliseconds of the pulse. The majority of the low power welding applications for which solid state lasers are employed use shorter laser pulses, of the order of 2 - 3 ms, and hence plume blockage during commercial pulsed solid state laser welding conditions is not a problem.

8.9 Industrial relevance

The possible relevance of these phenomena is briefly examined.

Firstly, the metallographic work showed that each individual melt spot is essentially a shallow low irradiance spot weld, similar to the type of weld required for certain laser welding applications. In particular the weld regime is similar to those required for solid state laser welded microwave packages (aluminium alloys of a similar composition are used for this application and an even crack free weld surface is important for strength and cosmetic reasons). In this low duty cycle, low average power regime at 20 Hz, 5J, 2.5 ms for example, a simple calculation shows that the period between each laser pulse is 50 ms, whereas the laser pulse is only 2.5 ms long. Hence, the target is not irradiated for 47.5 ms, far too long for any keyhole to be maintained open and the regime is simply one of individual but overlapping (in space) spot welds. It has been noted that in the case of almost all temporally shaped pulse, a slight increase in penetration has been identified. As we have seen, the occasional occurrence of annular rings seems to be closely related to a peak pulse power/pulse energy threshold effect, associated with approaching material ejection. The ability to switch these rings on and off by using temporal pulse shaping may be a technique for avoiding the occurrence of annular rings whilst avoiding any loss of melt efficiency.

This increase is not likely however, to be of real interest in an industrial situation where the increase in penetration would be achieved more effectively by using higher pulse energy and laser parameters closer to the upper keyholing threshold. Enhanced penetration beyond that of these shallow (< 0.5 mm weld depth) temporally shaped, so called "conduction limited" welds can therefore only be achieved by using the laser close to the upper limits of irradiance identified earlier.

It is clear now that increasing weld depth simply by increasing pulse duration and pulse energy is not capable of producing spot welds deeper that 1-5 – 2mm. Laser welds deeper than this in aluminium are only possible by using higher average power continuous wave lasers where there is at least some possibility of maintaining a high irradiance keyhole weld.

Fig. 7.35 also confirms that using these laser parameters in the range of those used industrially for laser spot welding, there is a threshold effect associated with increasing average pulse irradiance. It is in this relatively narrow range of high pulse

irradiance parameters that a pulsed laser welding process needs to be established in order to obtain maximum weld penetration and weld speed for a given laser power. This work also suggests shows that this pulsed quasi keyhole regime is on the lower limit of material ejection and this explains why the operating envelope of the laser for this type of high penetration pulsed laser welding is narrow.

As discussed in section 8.4.1.2, a number of authors have also attempted unsuccessfully to produce crack free solid state laser pulse welded Aluminium Magnesium (AlMg) alloys without filler metal, [128,129, 141]. This cracking would inevitably affect the fatigue strength of any welded components and hence would limit the application of this technique to using employing lower strength commercial purity aluminium alloys, or to using AlSi filler metals.

Secondly, other possible applications for this type of surface have been suggested, in particular, the use of this type of laser treatment as a precursor to an adhesive bonding treatment or a laser weldbonding (combined welding & adhesive bonding) treatment. These possible applications rely primarily on controlling the process and overcoming the lack of consistency. In earlier work supervised by the author [138], this technique was investigated as a possible method of pre treating aluminium substrates prior to adhesive bonding. This work was loosely connected with [87] where similar work was performed using a CO_2 laser. The work was aiming to produce a combined cleaning / surface roughening effect. It was thought that maximising the annular rings may lead to increases in surface area and increased bond strength. It soon became clear that in all cases, although an improvement in bond strength was noted, this was small compared to other pre treatment techniques. In the case of [138], it was concluded that this was due to the production of an unstable, mechanically weak oxide which is an undesirable side effect of the melting of the surface oxide layer. A further problem is demonstrated by this work - it is clear that in fig. 7.11 for example, melting of the metal surface always occurs well before the melting of the surface oxide, this is to be expected because of the difference in their relative melting points. Because of this transmittance of the laser beam through the oxide layer, there appears to be no possibility of modifying the oxide layer in any useful way without the undesirable melting of the aluminium.

Thirdly, there is a particular regime used for laser forming which relies on a degree of surface melting [108] to produce three dimensional shapes from sheet

materials. An identification of the relevant laser thresholds for avoidance of this phenomenon may be of use.

Although the ring structures identified are obviously important in the topography of the surfaces produced, these surface features might also play a significant role in the optical properties of the surface. A regularly spaced series of rings may well increase the specular reflectivity of these surfaces in a controllable manner.

Finally, although there is some published information [128,129] on the use of temporal pulse shaping in laser spot welding, very little serious experimentally based work has been carried out (with the notable exception of [10]) to investigate and to understand the possible uses of this technique in industrial laser welding processes. It is hoped that this work might add to an improved understanding of the advantages and practical limitations of this feature of solid state lasers.

9. Conclusions & recommendations for further work

9.1 Conclusions

1. A threshold pulse irradiance value, $\sim$ 0.9 MWcm^{-2} was obtained experimentally by a straightforward laboratory technique, for the onset of enhanced coupling and melt ejection under the particular set of conditions used. This is within a range of values identified for other metals from the published literature.

2. For the range of irradiance studied, the instantaneous power of the pulse, and hence also the pulse irradiance, is the deciding factor in the melting efficiency of the beam.

3. For particular sets of laser conditions, a range of pulse irradiance values have been identified over which there is no increase in melting efficiency. This plateau appears not to be associated with a plume blocking effect and it occurs immediately prior to the onset of enhanced coupling of the laser beam to the surface. This previously unreported feature is an inevitable consequence of these constant pulse energy trials.

4. There is experimental evidence to suggest that as pulse irradiance approaches the melt ejection threshold, recoil vapour pressure produces increasingly prominent waves in the melt pool to the point at which the molten metal is ejected centrally from the melt pool in relatively large globules. This process therefore appears to be an important part of the initial stage of the molten metal removal process initiated by increasing irradiance of the incident beam.

5. The conditions under which the phenomenon of frozen in annular waves can be produced on solidified aluminium melt spots have been demonstrated and there is a previously unidentified threshold pulse irradiance for laser spot melting of aluminium associated with the production of frozen in annular rings. This has led to reliable and repeatable production, or avoidance of this phenomenon during laser spot welding of aluminium.

6. Temporal pulse shaping can be employed to avoid the formation of these annular waves, but for a constant pulse energy this reduces the peak pulse power and hence pulse irradiance.

7. There is evidence in the literature, supported by experimental evidence from this work, that for a constant pulse energy, altering the rising slope of the temporal laser pulse reduces reflection at the start of the laser pulse. This may be connected with increases in melting efficiency in the low irradiance conduction welding regime.

8. Using a typical welding pulse at a fixed pulse energy, no temporal pulse shapes were found which reduced the incidence of weld cracking on this target material in this highly restrained joint configuration.

9. Enhancing the anodised layer on the surface of the aluminium increases the absorption of the beam by the surface and increases the melting efficiency of the beam, even for a relatively low intensity, non-keyhole spot melting process.

10. Reducing the thickness of the oxide layer reduces the coupling of the beam into the surface of the aluminium, hence reducing the melting efficiency for all conditions studied.

11. The damping effect of an enhanced oxide layer appears to suppress or delay the occurrence of frozen in reactive vapour pressure produced waves.

9.2 Recommendations for further work

1. The determination of the pulse irradiance threshold for other relevant aluminium alloys and alloy systems would widen the scope of this work.

2. Similar trials on a range of different ferrous and non ferrous materials would allow thresholds to be identified in each case, thus improving understanding of the laser spot melting process.

3. Similar trials on other more weldable aluminium alloys might be investigated to avoid the problem of solidification cracking.

4. It should be possible using laser equipment with a higher peak power capability, and a similar technique to the current work to identify experimentally the upper intensity threshold for enhanced coupling for other aluminium alloys with alternative surface coatings. If these thresholds were identified for a particular laser, a series of rules suitable for a comprehensive database might be produced.

5. Based on the assumption that these rings are an inevitable part of the melt expulsion process, further theoretical analysis of the forces involved in the production of the annular rings may improve understanding of the material removal processes.

6. Using an oscilloscope with better time resolution and an up to date beam analyser would help in identifying more clearly the effective peak pulse powers necessary.

References;

1.   Einstein A., Phys. Z, **18** 121, 1917.

2.   Schawlow A, *Laser Light,* Scientific American, Vol. 219, No.3, September 1968, pp120-138.

3.   Maiman TH, *Stimulated Optical Radiation in Ruby*, Nature, August 1960.

4.   Patel CKN, 1964 Phys Rev 136 A1187.

5.   Anderson SG, *Review and forecast of laser markets.* Laser Focus World, January 1997.

6.   Belforte D & Levitt M, editors. *Economic Review & technology trends,* from Industrial Laser Handbook 1992-93. Springer Verlag, ISBN 0-387-97751-1.

7.   Wittrock U, *High-Power Nd:YAG Lasers* Adv. Mat. **4** (1992) pp 295-297

8.   Tonshoff HK, Meyer C, Beske E, *New Possibilities in Materials Processing with kW-Solid State Lasers.* SPIE Vol. 1277 High Power Solid State Lasers and Applications (1990), pp 199-208.

9.   Gitin M & Reingrube J., *Diode pumped solid state lasers show bright future.* Application Report, Industrial Laser Review, Dec. 1995.

10.   Bransch HN, Weckman D.C & Kerr HW, *Effects of pulse shaping on Nd:YAG spot welds in austenitic stainless steel.* Welding Journal, 73, issue 6 (1994) Welding Research Supplement, pp 141s - 151s.

11.   Tuersley IP, Hoult AP, Pashby IR, *The processing of a magnesium-alumino-silicate matrix, SiC fibre glass-ceramic matrix composite using a pulsed Nd-YAG laser,* J Mat. Sci. **31** (1996) pp 4111-4119

12.   Hoult AP, *Welding, cutting & drilling with the 1 kw solid state oscillator amplifier laser,* Proc. 6th Int. Conf. on Lasers in Manufacturing, LIM6, Birmingham, UK, Sept. 1989.

13.   Peters C, *Processing with multi-kilowatt solid state lasers,* Welding & Metal Fabrication, June 1996.

References

14. Croxford N, *Development of high average power solid state lasers for the engineering industry*. Proc. 6th int. conf. Lasers in Manufacturing, LIM 6, Birmingham, Oct. 1989.

15. Quantum Laser Engineering, Product Data sheet.

16. Fieret J, Terry MJ, Brooke-Ward A., *Aerodynamic Interactions during Laser Cutting*, SPIE Vol.668 (1986), pp 53-62.

17. *CADCAM for laser raises its profile*. Lasers and Power Beam Processing, March 1997.

18. Schuocker D, *The physical mechanism and theory of laser cutting*. Article in Industrial Laser Handbook, Penwell, 1987.

19. Van Dijk M, *Pulsed Nd: YAG Laser Cutting*, Industrial Laser Handbook, Penwell, 1989.

20. Herziger G et al. *Photon-Matter Interaction: Energy Coupling in Laser Processing*. Proc. LAMP '87, Osaka, Japan, May 1987.

21. Hachfeld KD., *Laser beam quality and brightness in industrial applications*. Industrial Laser Handbook, 1992-3, ed. Belforte D, Springer-Verlag. ISBN 0-387-97751-1.

22. Lumonics JK 700 series handbook, Lumonics Ltd, Cosford Lane, Rugby.

23. Matsunawa A, Yoshida H, Katayama S. *Beam Plume interaction in Pulsed Yag Laser Processing*. Proc. ICALEO '84.Vol.44-Materials Processing, Laser Inst America, Nov. 12-15, 1984, Boston, USA.

24. Zavecz TE, Saifi MA., Notis M., *Metal reflectivity under high intensity optical radiation*. App. Phys. Lett. **26**, (1975), pp 165-168.

25. Yilbas BS, Danisman K, Yilbas Z, *Measurement of temperature dependant reflectivity of Cu & Al in the range 30-1000°C*, Meas. Sci. Technol. **2**, (1991), pp .68-674.

26. Blidegn K & Olsen OF, *Investigation into the absorptivity change in metals with increased laser power,* in XI Int. Sym. on Gas Flow & Chem. Lasers & High-Power Laser Conf, Howard J. Baker, ed, Proc. SPIE 3092, (1997), pp 615-618. ISBN 0-8194-2507-9.

27. Ujihara K, *Reflectivity of metals at high temperatures,* J. App. Phys. **43**, (1972), pp2376-2383.

28.   Lewis GK & Dixon RD, *Plasma monitoring of laser beam welds.* Welding Research Supplement, 49-s, Feb. 1995.

29.   Arata Y, Miyamoto I, *Some fundamental properties of high power laser beam as a heat source, Report 2, CO_2 laser absorption characteristics of metal,* Trans. Jap. Welding Soc. **3**, no. 1, April 1972, pp 152-162.

30.   Matsunawa A et al. *Characteristics of plume induced by pulsed Nd:YAG Laser irradiation and their effects on Material Processing.* 3rd Int. Coll. on Welding and Melting by Electrons and Laser beams, Lyons, France, Sept. 1983.

31.   Von Allmen M., *Laser-Beam Interactions with Materials, Physical Principles & Applications* Springer-Verlag, Berlin, 2nd ed. 1995. ISBN 3-59401-9, ch. 2.

32.   Ursu I, Mihaelescu IN et al. *On the behaviour of aluminium under microsecond pulsed TEA CO2 laser radiation in vacuum.* J.Phys. D: Appl. Phys.,**17** (1984) pp 1315-1324.

33.   Walters CT & Clauer AH, *Transient reflectivity behaviour of pure aluminium at 10.6 μm.* Appl.Phys.Lett. **33** (8), (1978), pp 713-715.

34.   Perfect A, *The properties and performance of anodic films,* Proc. conf. on aluminium anodising, Nottingham, Sept.1961, published by The Aluminium Development Association, London.

35.   Peterson GP & Fletcher LS., *Measurement of the thermal contact conductance and thermal conductivity of anodised aluminium coatings.* J. Heat Transfer, Trans. ASME, vol.112, iss.3, Aug. 1990, pp. 579-585.

36.   Decker DL & Hodgkin VA, National Bureau of Standards Special Publication NBS-SP-620, 1981, p190.

37.   Prokhorov AM & Konov VI, *Laser Heating of Metals.* Adam Hilger Series on Optics & Optoelectronics, IOP, 1990. ISBN 0-7503-0040-X, ch. 6.

38.   Libenson MN, Romanov GS, Imas YA, *Temperature dependance of the optical properties of a metal in heating by laser radiation,* Soviet Physics - Technical Physics **13**, (1969), pp 925-927.

39.   Ready JF, *Change of reflectivity of metallic surfaces during irradiation by CO_2-TEA laser pulses.* IEEE J. Quantum Electronics, Vol. QE-12, no. 2, Feb. 1976.

40.   Hettche LR, Tucker TR et al. *Mechanical response and thermal coupling of metallic targets to high intensity 1.06 μm laser radiation.* J. App. Phys., **47**, no.4, (1976), pp 1415-1421.

41.   Kinsman G, Duley WW. *Excimer laser - induced oxidation and roughening of metal surfaces.* Proc. SPIE Vol 957 p105-110. Laser Beam Surface Treating and Coating, 1988.

42.   Dausinger F et al, *Welding of aluminium; a challenging opportunity for laser technology,* J. Laser Applications **8** (1996) pp 285-290

43.   Hoult AP, Shan MY, Bryden B, Pashby IR. *Semi quantitative approach to the effect of anodised layer thickness on laser cutting of aluminium alloy,* in XI Int. Sym. on Gas Flow & Chem. Lasers & High-Power Laser Conf, Howard J. Baker, ed, Proc. SPIE 3092, (1997), pp 776-780, ISBN 0-8194-2507-9

44.   Bankman A, *Colour and texture in anodic finishes.* Proc. conf. 'Anodising Aluminium', Nottingham, Sept. 1961. Pub; Aluminium Dev. Assoc., UK.

45.   Forsyth G, *Some further observations on the various features of aluminium alloy microstructures that are bodily transferred into the oxide coating formed by anodising.* Mat. Lett. **16** (1993), pp 113-122.

46.   Touloukian YS. (ed.), *Thermophysical properties of materials,* IFI/Plenum Press, 1970.

47.   Herziger G & Kreutz E W *Fundamentals of laser microprocessing of metals.* Physica Scripta. Vol. T13. (1986), pp 139-146.

48.   Russo AJ, Benson DA & Hadley GR. *Two dimensional modelling of conduction mode welding.*Proc. conf. ICALEO '84, vol. 44, (1984), pp 8-16.

49.   Vishnu RP, Li WB & Easterling KE, *Heat flow model for pulsed welding,* Mat. Sci. & Tech., **7**, (July 1997), pp 649-659.

50.   Ölçer NY, *On the theory of conductive heat transfer in finite regions,* Int. J. Heat Mass Transfer, **12** (1964) , pp 393-411.

51.   Metzbower EA, *Heat flow in laser beam welding,* Proc. 6th Int. Conf. on Applications of Lasers & Electro Optics, ICALEO'87, pp 37-45.

52.   Henry P, Chande T et al, *Modelling laser heating effects,* Proc. 6th Int. Conf. on Applications of Lasers & Electro Optics, ICALEO'82.

53. Steen WM, *Laser Materials Processing*. Springer Verlag, London, 1991, ISBN 3-540-19670-6, ch. 5.

54. Miller JE, Wineman JA, *Laser hardening at Saginaw steering gear*. Metal Prog. 111, no. 5, (May 1977), pp 38-43.

55. Von Allmen M, *Laser-Beam Interactions with Materials*, Springer-Verlag, Berlin, 1987. ISBN 3-540-17568-7, ch. 2.

56. Ion JC, *Modelling of laser processing*, in book: Industrial Laser Handbook 1992-3, ed. Belforte D, Springer Verlag. ISBN 0-540-97751-1

57. Ion JC, Shercliff HR & Ashby MF, *Diagrams for laser materials processing*, Acta Met. & Mat. **40**, no. 7, (1992), pp 1539-1551.

58. Hügel H, *Integration of laser materials processing in metal cutting machine tools*. Proc. LAMP '92, Nagaoka, Japan, June 1992, pp 565-570.

59. Kou S, Sun DK & Le YP. *A fundamental study of laser transformation hardening*,Met. Trans. A, **14A**, (April 1983), pp 643-653.

60. Amende W, *Transformation hardening of steel and cast iron with high power lasers*, in Industrial Applications of Lasers, ed. Koebner H, John Wiley, 1984, pp78-98.

61. Miyamoto I & Maruo H, *Novel laser beam shaping optics: LSV optics applications to transformation hardening and ceramic joining*, Proc. conf. ICALEO (1992), pp 88-102.

62. Mazumder J, *Mathematical modelling of laser surface treatments*, in 'Laser Surface Treatment of Metals' ed Draper CW, Martinus Nijhoff, NATO ASI series (1986), pp 185-199.

63. Ricciardi G, Cantello M. *Surface Treatments of automobile parts by RTM*. Proc SPIE 957 (1988) pp 66-74.

64. Brenner B & Reitzenstein W, *Laser hardening of turbine blades*, Ind. Laser Rev. April 1996, pp 1720.

65. Tamada K, Sato A, Nakagawa N. *Weight reduction technology by laser irradiation for body panels*. Proc. 19th IDDRG Cong. June 1996, pp 47-54.

66. Fairand BP & Clauer AH, J. Appl. Phys. **50** (3) March 1979, pp1497-1502.

67. Banas G et al, *Laser shock induced mechanical and microstructural modification of welded maraging steel*. J. Appl. Phys. **67** (5), March 1990.

68.   Sarady I, Magnusson CF, Wei L-Y, Meijer J, *Phase transformations by high intensity sub-microsecond laser pulses*, Proc. int. conf. ICALEO (1992)

69.   Fournier J, Fabbro R & Fabre E, *French study metal surface treatment by laser,* Ind. Laser Rev., October 1987, pp 40-47.

70.   Clauer AH, *New life for laser shock processing*, Industrial Laser Review, March 1996, pp 7-9.

71.   Iuchi T, et al, *Laser processing for reducing core loss of grain oriented silicon steel,* J. Appl. Phys. **53**, no.3 pt 2, (1982).

72.   Asmus JF, Munk WH & Murphy CG, *Studies on the interaction of laser radiation with art artefacts*, Proc. Soc. Photo-optical & Instr. Eng. **41**, (1973)

73.   Reitz W, *Laser ablation technology development*, Mats. & Manuf. Processes, **9**, no.3, (1994) pp 395-413.

74.   Srinavasan R, Mayne-Banton V, Appl. Phys. Letts. **41**, 576, (1982)

75.   Dyer PE, Oldershaw GA & Schudel D. *XeCl laser ablation of polyetheretherketone,* Appl. Phys. B **51**, (1990) pp 314-316

76.   Tavakoli SM, *Development of power beam techniques for surface modification of adherends and curing of adhesives.* TWI Project outline, GP/MAT/1034, TWI, Cambridge, England, April 1993.

77.   Arnold J, Stark U, Dausinger F, *Structuring of metals by ablation with excimer laser,* Proc. conf. ICALEO (1991), pp 414-423.

78.   Tönshoff HK, Gedrat O, *Removal process of ceramic materials with excimer radiation*, Proc. SPIE Vol. 1132 High Power Lasers & Laser Machining Technology (1989), pp 104-109.

79.   Thomas DW, Foulkes-Williams C, Rumsby PT & Gower MC. *Surface modification of polymers and ceramics induced by excimer laser radiation,* in Laser Ablation of Electronic Materials-Basic Mechanisms and Applications, ed. Fogarassy E, Elsevier (1992), pp 221-228.

80.   Peyre J-L, Riviere D, Vannier C, Villela G, *Excimer laser-induced etching of semiconductors and metals.* Electrical Communication, vol. 62, no. 3/4 (1988)

81.   Lu Y-F & Aoyagi Y, *Laser induced dry cleaning in air - a new surface cleaning technology in lieu of CFC solvents,* Jpn. J. Appl. Phys. **33**, (1994) pp L430-L433.

82.   Zapka W & Ziemlich W, *Efficient pulsed laser removal of 0.2 μm sized particles from a solid surface*. Appl. Phys. Lett. **58** (20), May 1991, pp2217-2219.

83.   Doyle DJ, *Excimer laser surface modification of high density polyethylene (HDPE) for enhanced bonding with adhesives*. Proc. conf. ICALEO (1992), pp 260-264.

84.   MacCormack M, *Cleaning up with lasers,* Industrial Laser Review, June 1996, pp7-8.

85.   Duley WW, Ogmen M, Steel T & Mihailov S, *Laser surfacing of High Density Polyethylene for reduction on fuel permeability,* J. Laser Applications, **4**, (1), 1992, pp22-28.

86.   Dyer PE, Oldershaw GA, Sidhu J, *CO_2 laser ablative etching of polyethylene terephthalate*, Appl. Phys. B **48,** (1989) pp 489-493.

87.   Critchlow GW, Brewis DM, Emmony DC & Cottam CA. *Initial investigation into the effectiveness of CO_2 laser treatment of aluminium for adhesive bonding,* Int. J. Adhesion & Adhesives **15** no. 4, (1995), pp 233-236..

88.   Groupe Quantel, *LASERBLAST, Cleaning, preparing and treating surfaces with a laser*. Product sheet from Lambda Photometrics Ltd, Herts, England.

89.   Pashby IR, Hoult AP & Nyiau C , *Precleaning and spot welding of an automotive body steel using a Nd:Yag laser.* SPIE 2993, (1997) pp 28-36.

90.   *Paint stripping using lasers*. Product sheet from Urenco Lasertechnik, Jülich, Germany.

91.   Foley JS, *Laser paint stripping: an automated solution,* Industrial Laser Review, August 1991, pp 4-9.

92.   Keranen DJ, *Laser based paint removal system,* Industrial Laser Review, April 1996, p6.

93.   Engel S, *Nd:YAG lasers strip paint effectively*, Laser Focus World, October 1992, pp 20-21.

94.   Ashidate S, Obara M, *Rust and paint stripping from power transmission towers with a pulsed Yag laser.* Proc. SPIE 3092, (1997) pp740-743.

95.   Matsunawa A, Katayama A, Ohmi Y, Kuroki T. *Formation of Amorphous Alloy Layer by Pulsed Laser*. Proc. LAMP '87, Osaka, May 1987, pp 441-446.

References

96.   Kear BH, Breinan EM, Greenwald LE, *Laser glazing - a new process for production and control of rapidly chilled metallurgical microstrutures*, Metals Technology, April 1979, pp 121-129.

97.   Luft U, Bergmann HW, Mordike BL, *Laser surface melting of aluminium alloys*, Optoelektronik Magazin, **3**, no.4, (1987) pp 435-440.

98.   Mordike BL, *Recent developments in the surface treatment of materials*, Proc. SPIE 1276, (1990), pp 332-342.

99.   Wehr M, Katayama S, Matsunawa A, *Ceramic coating of titanium by pulsed YAG laser*, Trans. JWRI. **16**, no. 1 (1987) pp 43-49.

100.   Koshy P, *Laser cladding techniques for application to wear and corrosion resistant coatings*, Proc. SPIE 527, (1985) pp 80-85.

101.   Volz R, *Production of load bearing and hardfacing layers on aluminium alloys with the CO_2 laser*. Proc. ICALEO (1992) pp 251-259.

102.   Eberl G. & Sutor U, *Laser machine tools for a new machining technology-Lasercaving*. MAHO Corporation promotional literature, Pfronten, Germany.

103.   Sturmer M, *Material removal processing with NdYag lasers*, SPIE 1864 (1993) pp 108-117.

104.   Ahlers R-J, Brandes A, *Lasercaving & Image processing: two technologoes combined*, SPIE 2246 (1994) pp 115-119.

105.   Minamide K, Suehiro J, Toshimitu T & Kawamoto T, *Laser system for dulling work roll by Q switched Nd:Yag laser*. Journal of Laser Applications, October 1989, pp 15-20.

106.   Scott DA, Brandt M, Dorien-Brown B. *Laser Dulling of Metal Surfaces*. ICALEO (1991) pp 23-31.

107.   Brown WL, *Laser processing of semiconductors*, in book; Laser Materials Processing, ed. Bass M, North-Holland, 1983, ch. 7, pp 339-401.

108.   Frackiewicz H, *High-technology metal forming*, Industrial Laser Review, October 1996, pp 15-17.

109.   Patel RS & Brewster MQ, *Effect of Oxidation and plume formation on high power Nd-Yag laser metal interaction*. Trans. ASME: J Heat Trans., **112**, Feb. 1990, pp170-177

110. Wang ZY, Liu JT, Hirak DM, Weckman DC & Kerr HW, *Measurement of pulsed laser beam dimensions using Kapton films,* Proc. ICALEO (1991) pp 74-83

111. Hirak DM, Weckman DC and Kerr HW, *Measurement of the spatial intensity distribution at the focal point of a converging/diverging laser beam.* Proc. ICALEO (1991) pp 64-73

112. Golubev VS, Banishev AF, Azharonok VV, Zabelin AM, *Non-stationary plasma-thermo-fluid dynamics and transition in processes of deep penetration laser beam-matter interaction.* SPIE 2207 (1994) pp248-255

113. Bass M, Nassar MA & Swimm RT, *Impulse coupling to aluminium resulting from Nd:glass laser irradiation induced material removal,* J.Appl.Phys. **61** (3), Feb. 1987, pp 1137-1144.

114. Lewis GK & Dixon RD, *Electron emission and Plasma formation during laser beam welding.* Welding Research Supplement, 71-s to 78-s, March 1995.

115. Prokhorov AM, Batanov VA, Bunkin FV & Fedorov VB, *Metal evaporation under powerful optical radiation,* IEEE J. Quant. Electronics. **QE-9** no.5 May 1973, pp503-510

116. Postacioglu N, Kapadia P, Davis M & Dowden J, *Upwelling in the liquid region surrounding the keyhole in penetration welding with a laser* J.Phys. D: Appl. Phys. **20** (1987) pp 340-345

117. Postacioglu N, Kapadia P & Dowden J, *Capillary waves on the melt pool in penetration welding with a laser,* J. Phys. D: Appl. Phys. **22** (1989) pp 1050-1061.

118. Gratzke U, Kapadia PD, Dowden J, Kroos J & Simon G, *Theoretical approach to the humping phenomenon in welding processes,* J. Phys. D: Appl. Phys. **25** (1992) pp 1640-1647.

119. Kreutz EW & Pirch N, *Melt dynamics in surface processing with laser radiation: calculations and applications,* SPIE 1276, (1990) pp 343-360.

120. Rykalin N., Uglov A. & Kokora A., *Laser Machining and Welding.* Pergamon Press, 1978 (English translation) ISBN 0-08-022724-4, ch. 6.

121. Maracas GN, Harris GL, Lee CA & McFarlane RA, *On the origin of periodic surface structures of laser annealed semiconductors,* Appl. Phys. Lett. **33** no. 5, (Sept. 1978) pp 453-455.

122. Wileman P, Coupland JM, Creasey CD, Rowley DM & Halliwell NA, *The laser strain gauge: micro-machining of diffraction gratings using an Excimer laser,* Strain **30** 1, (1994) pp 15-18

123. Bagratashvili VN et al, *Formation of periodic rings structures of relief and voids under laser vapor deposition of films,* Appl. Phys. A **52**, (1991) pp 438-444.

124. Kreutz EW, Krösche M, Herziger G, Wagner S, *Structure induced absorption during laser materials processing,* Proc. SPIE 650 (1986) pp 202-209

125. Rodwell M, *Surface tension effects in welding,* Welding Institute Research Bulletin, June 1985, pp 192-200.

126. Landau LD & Lifshitz EM, *Fluid Mechanics,* 2nd ed. Pergamon Press, 1987, ISBN 0-08-33933-6, ch. 7.

127. Peercy PS, *Solidification dynamics and microstructure of metals in pulsed laser irradiation,* in book "Laser surface treatment of metals", ed. Draper CW, Martinus Nijhoff, NATO ASI series (1986) pp 57-77.

128. Cieslak MJ, Fuerschbach PW, *On the weldability, composition and hardness of pulsed and continuous Nd:YAG laser welds in aluminium alloys 6061, 5456 and 5086.* Met. Trans. B, **19B,** April 1988, pp 319-329

129. Junai AA, van Dijk M, Hiensch M, Rindjers A, Notenboom G, Jelmorini G, *Pulsed Nd:YAG welding of crack sensitive aluminium-magnesium alloys,* Proc. SPIE 1277, (1990) pp 217-231

130. Matsunawa A, Katayama S, Ikeda H, Nishizawa K, *Effect of pulse shaping on defect reduction in pulsed laser welding,* Proc. ICALEO (1992) pp 547-556

131. Cohen MI & Epperson JP, *Application of Lasers to Microelectronic Fabrication,* in book "Electron Beam and Laser Beam Technology", ed. Marton L & El-Kareh AB, Academic Press, (1968) pp 139-186

132. Brienan EM & Kear BH, Rapid solidification laser processing at high power density, in book "Laser Materials Processing", ed. Bass. M, North Holland, (1983) Chapter 5, pp 235-295.

133. Mohanty PS, Kar A & Mazumder J, *A modeling study on the influence of pulse shaping on keyhole laser welding*, J. Laser Applns. **8** (1996) pp 291-297

134. Nonhof CJ, *Material Processing with Nd-Yag Lasers,* . Electrochemical Publications Ltd, Scotland, 1988, ISBN 0-901150231.

135. Treusch H - G, Herziger G, *Metal precision drilling with lasers,* SPIE 650 (1986) pp 220-225.

136. Powell J et al., CO_2 *laser cutting of aluminium alloys.* Proc. 6th Int. Conf. Lasers in Manufacturing, LIM-5, p15-24, Sept. 1988.

137. Davies RJ & Kinloch AJ, *The surface characterisation and adhesve bonding of aluminium,* in book; Adhesion 13, (1989) Elsevier Science Publications

138. Lu CH, *Laser surface treatment of aluminium for adhesive bonding* University of Warwick, Department of Engineering, MSc thesis, 1996.

139. *The properties of Aluminium and its alloys,* 8th ed. The Aluminium Federation, 1981.

140. Divergence of 701 laser, personal communication with W Goethals, Lumonics Ltd, Rugby

141. Wong CP, *An investigation into the Laser Surface texturing process,* University of Warwick, Dept. of Engineering, MSc thesis, 1995

142. Shan MY, *A study into the effect of anodized layer thickness on CO_2 laser cutting of an aluminium alloy,* University of Warwick, Dept. of Engineering, MSc thesis, 1994.

Bibliography;

- Arata Y & Miyamoto I. *Some Fundamental Properties of High Power Laser Beams as a Heat Source.* In; Plasma, Electron and Laser Beam Technology by Y.Arata, published by American Society for Metals, 1986.

- Bass M., *Material Processing - Theory and Practice; Vol. 3. Laser Material Processing.* North Holland Publishing Co., New York & Oxford, 1983. ISBN 0-444-86396-6, chapters 3 & 6.

- Bennett HE & Bennett JM, *Validity of the Drude Theory for silver, gold, and aluminium in the infrared,* in: Optical properties and electronic structure of metals & alloys, ed. Abeles F, North Holland, 1996.

- Born M. & Wolf E., *Principles of Optics,* 5th ed., Pergamon Press, 1981.

- Brace AW & Sheasby PG, *The Technology of Anodising Aluminium,* Technicopy Ltd, ISBN 0-905228-081

- Carslaw HS & Jaeger JC, *Conduction of Heat in Solids,* 2nd ed., Oxford University Press (Clarendon), London, 1979

- Charschan S S., ed. *Guide for Material Processing by Lasers,* prepared by Laser Institute of America, 2nd edition, 1977.

- Chryssolouris G., *Laser Machining. Theory and Practice,* Springer-Verlag. ISBN 3-540-97498-9.

- Crafer R. & Oakley P., *Laser Processing in Manufacturing,* Chapman & Hall, UK.

- Draper C. & Mazzoldi P., eds. *Laser Surface Treatment of Metals.* NATO ASI Series

- Duley W W., *Laser processing and analysis of Materials,* Plenum Press, New York, 1983, ISBN 0-306-41067-2.

- Holman JP, *Heat Transfer,* 7th ed., McGraw-Hill, 1990.

- Hummel RE, *Electronic properties of materials,* Springer Verlag, 1985.

- Kundu PK, *Fluid Mechanics,* Academic Press Inc., 1990, ISBN 0-12-428770-0

- Landau LD & Lifshitz EM, *Fuid Mechanics*, 2nd ed. Pergamon Press, 1987, ISBN 0-08-33933-6.

- Luxon J.T. & Parker D.E., *Industrial Lasers and their Applications*, 2nd ed. Prentice Hall Inc. 1992. ISBN 0-13-459538-6

- Mazumder J., *The State of the Art of Laser Materials Processing*. Industrial Laser Handbook, Annual Review of Laser Materials Processing, 1987.

- Nonhof C.J., *Material Processing with Nd-Yag Lasers*. Electrochemical Publications Ltd, ISBN 0-901150231.

- Ozisik MN, *Heat Conduction*, 2nd ed., John Wiley, 1993.

- Pedrotti F.L. & Pedrotti L.S., *Introduction to Optics*, Prentice Hall, 1987.

- Powell J., *CO_2 laser cutting*. 1st ed., Springer-Verlag, 1993.

- Prokhorov A.M. & Konov V.I., *Laser Heating of Metals*. Adam Hilger Series on Optics & Optoelectronics, IOP Publishing, 1990. ISBN 0-7503-0040-X. Chapter 6.

- Rykalin N., Uglov A. & Kokora A., *Laser Machining and Welding*. Pergamon Press. ISBN 0-08-022724-4

- Siegman A.E., *Lasers*, Oxford University Press, 1986.

- Smith D.Y., Shiles E. & Inokuti M., *The Optical Properties of Metallic Aluminium*.pp 369-403. From the Handbook of Optical Constants of Solids, ed Palik ED, Academic Press, 1985, ISBN 0-12-544420-6

- Steen W.M., *Laser Materials Processing*. Springer Verlag, Berlin. ISBN 3-540-19670-6.

- Svelto O., *Principles of Lasers*, 3rd ed. Plenum Press, New York ISBN 0-306-42967-5

- Vardy A., *Fluid Principles*, McGraw Hill, 1990. ISBN 0-07-707205-7

- Touloukian YS. (ed.), *Thermophysical properties of materials*, IFI/Plenum Press, 1970.

- Von Allmen M., *Laser-Beam Interactions with Materials*, Springer-Verlag, Berlin. ISBN 3-540-59401-9, 2nd ed. 1995

- Wilson J. & Hawkes J., *Lasers: principles & applications*, Prentice Hall International Series in Optoelectronics. ISBN 0-13-523705-X. Chapter 5.

- Young M, *Optics & Lasers*, 2nd ed., 1984, Springer-Verlag, ISBN 3-540-13014-4

Appendices;

**Alusuisse
Swiss Aluminium Ltd**

CH-3960 Sierre
Telephone : 41 27 575111
Fax: 41 27 562310

Technical Data Sheet

Anticorodal - 120®
(AA 6016)

September 1993 Edition

GENERAL INFORMATION

Anticorodal-120® is an AlMgSi alloy, and corresponds to the international designation AA 6016. The chemical composition of Anticorodal-120® has been optimised in order to achieve :

• high tensile strengths
• an excellent formability
• a good Weldability
• a high corrosion resistance
• stretcher strain free surfaces
• long term stability of tensile strength in T4 temper.

Therefore Anticorodal-120® is an ideal alloy for automotive body panel, with a high formability in T4 temper (stretcher strain free) and high strength after paint baking.

TEMPER

Anticorodal-120® is delivered in T4 temper , in order to achieve a high formability.

AUTOMOTIVE SPECIALITIES

Alusuisse is one of the leaders in surface treatment of aluminium, and can offer to customers surface textures (EDT, or similar) to improve formability of sheets, as well as various types of special surface treatments and coatings such as :

degreasing, etching, chromating, and coatings (Bonazinc 2000). The Bonazinc 2000 coating offers an efficient protection against corrosion, an enhancement of the formability and is an advantageous precoating for bonding and lacquering.

ALLOY DESCRIPTION

Chemical Composition (Weight %)

Si	Fe	Cu	Mn	Mg	Cr	Zn	Ti +Others
1.0 - 1.5	max 0.50	max 0.20	max 0.20	0.25 - 0.60	max 0.1	max 0.2	max 0.15

The alloy corresponds to AA 6016

Physical Properties (nominal values)

Density	2.70 g/cm^3
Modulus of Elasticity	70000 MPa
Coefficient of Thermal Expansion (20°-100°C)	23.4 10^{-6} K^{-1}
Thermal Conductivity	1.6 -1.9 W /cm K
Electrical Conductivity	26 - 30 m/Ωmm^2

PRODUCT AVAILABILITY

Anticorodal-120® in T4 temper is available in the following dimensions and special treatments (texture, coating) :

	Coil	Sheet
Thickness	0.7 - 4 mm	0.7 - 4 mm
Width	up to 2200 mm	up to 2200 mm
Length	-	up to 6000 mm
Texture	Mill-finish, EDT	Mill-finish, EDT
Coating	- yellow chromating - Bonazinc 2000	- yellow chromating - Bonazinc 2000

Other dimensions, textures and coatings on request

TYPICAL TENSILE STRENGTH
(Thickness range: 0.7 - 2.5 mm)

Temper	0.2%YS (MPa)	UTS (MPa)	A5 (%)	A80 (%)	Agl (%)
T4	105	205	28	25	20.5
T6*	210	260	16	13	

* Annealing condition : 200°C 1/2h

ANGE IN TENSILE STRENGTH

rmomechanical Treatments

icorodal-120® (Ac-120®) is an age hardening
y, which means that its tensile strength
eases after thermal treatments. Hardening
ves at three temperatures (160°C, 180°C and
0°C) are presented below .
e final properties of body panels in Anticorodal-
0® will depend mainly of the thermal treatment
curring during paint baking. To achieve
nificant strength levels the paint baking should
ts at least 1/2h at temperatures between 180°C
00°C.
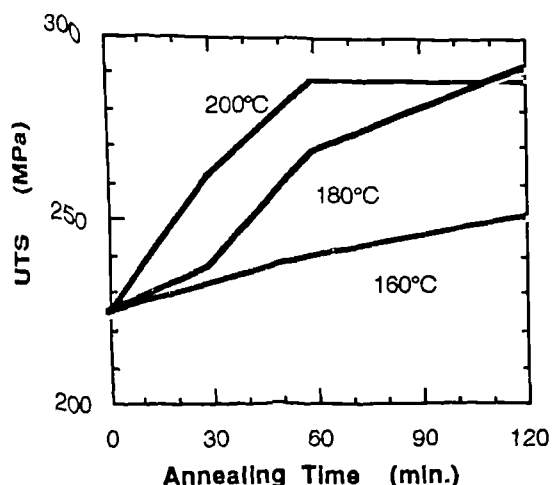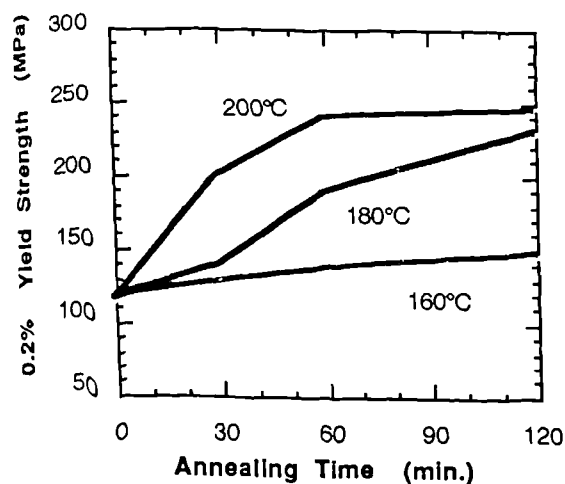
The hardening behaviour of Anticorodal-120® is
also influenced by cold deformation before
annealing. As an example : the effect of prior strain
(5%,10%) on artificial ageing at 180°C are shown
on the following graphics.
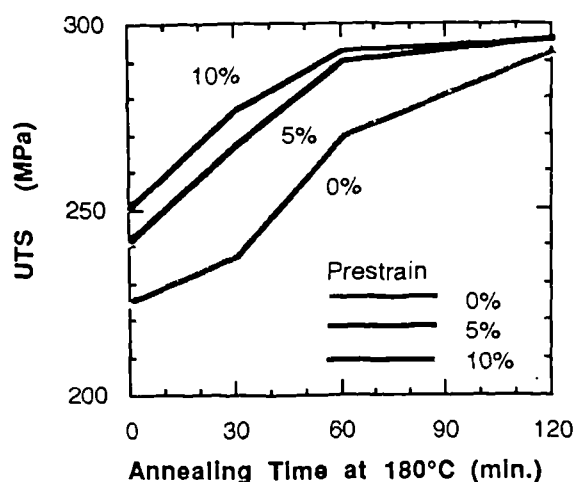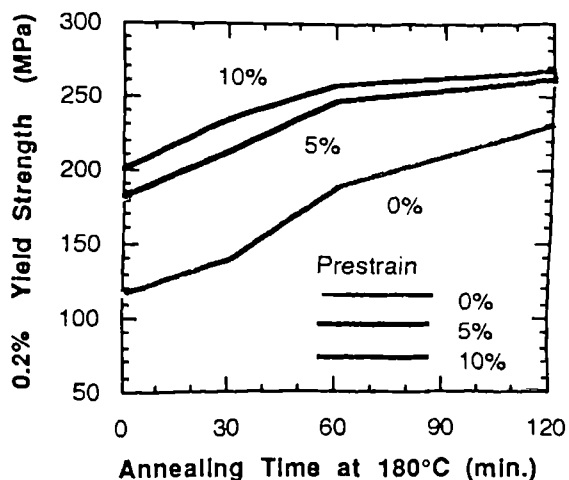
Strength Stability In T4 Temper

Anticorodal-120® in T4 temper ages very slowly at
room temperature and this induces a slight
increase of the mechanical values which is shown
on the drawing below .
This very poor hardening of Ac-120® doesn't alter
the formability of the alloy in T4 condition.

Alusuisse LQW
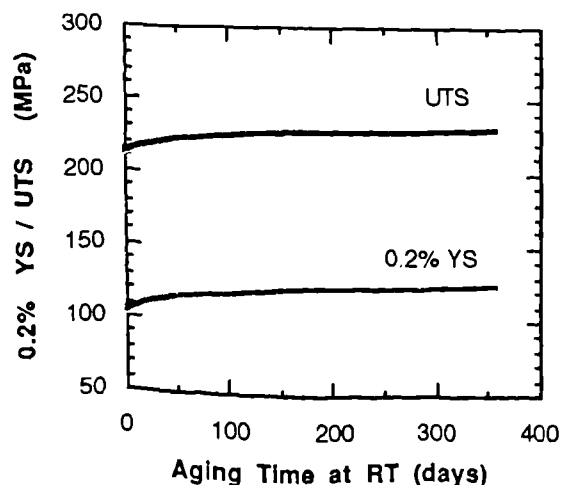
FATIGUE

The fatigue curve of Anticorodal-120® are presented on the following figure. 5% and 95% probability of rupture are plotted for the T4 and T6 (T6 = 180°C 1h) tempers and the curve for Ac-120® T4 with 18% prestrain is also shown.
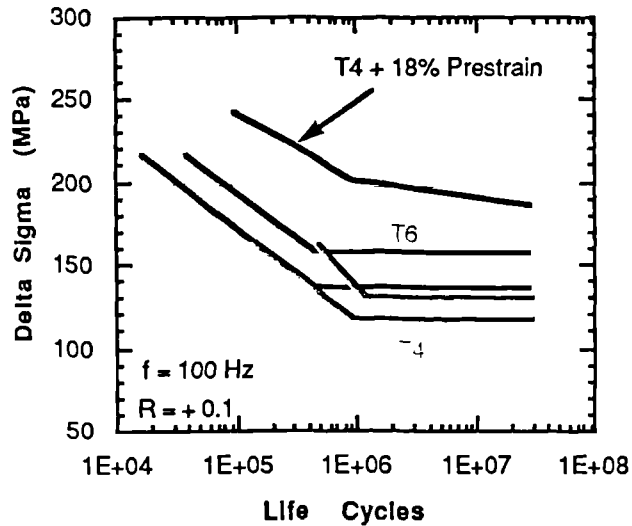
FORMABILITY

Anticorodal-120® shows an excellent formability and especially a good deep drawing behaviour, but its stretching aptitude is lower than that of steel. The main technological forming properties* of Anticorodal-120® are given in the Table below :

$n_{5\%}$	r_0	r_{45}	r_{90}	Δr	$\bar{r}$
0.26	0.64	0.53	0.66	0.15	0.58

* Medium Values

The curve of true stress versus true strain is presented in the next figure showing a magnification of the Yield Strength area.
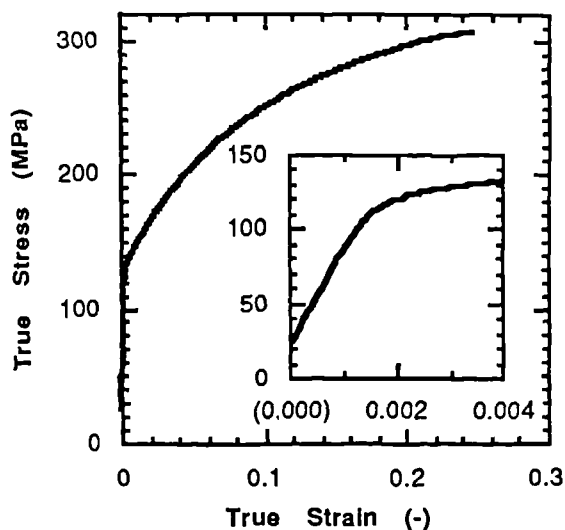
The forming limit curve of Ac-120 in T4 temper is shown in next figure.
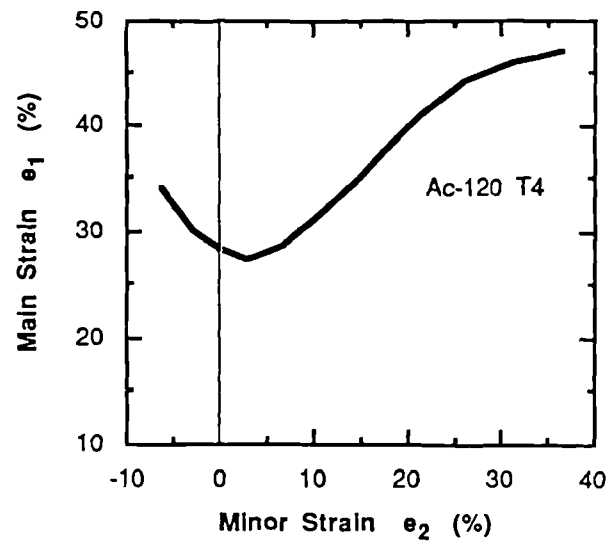
SURFACE TEXTURE

The usual surface texture of aluminium sheets is called **Mill-Finish**. This surface looks like a ridged surface in the rolling direction and is not ideal for forming due to its none isotropic form. A better surface texture for deep drawing is the **EDT** texture, which consists in a random pattern of small craters. These craters act as lubricant pockets and maintain a regular lubricant distribution during forming. The **EDT** texture brings the following advantages:

• a more regular distribution of deformation
• the possibility to form more difficult part without tearing of the sheet
• a lower scrap rate
• a reduction of rework
• for complicated parts an EDT sheet can avoid the use of expensive plastic foils (cost reduction)

the **EDT** texture is perfectly isotropic (Roughness identical in longitudinal and transverse directions) and offers the best solution to fulfil all requirements of outer body panels.

Table 1: Spot welding settings for Ac-120

Sheet Thickness (mm)	Electrode -ø (mm)	Electrode Radius (mm)	Current DC (KA)	Number of Cycles
0.8	16	75	24 - 30	3
1	16	75	25 - 32	3
1.25	16	100	26 - 34	4
1.5	16	100	27 - 35	5
2	20	100	30 - 38	6 - 8
2.5	20	150	34 - 42	7 - 9
3	20	150	38 - 45	8 - 10

Table 2 : Construction rules
(distance between spot welds , and overlap)

Sheet Thickness (mm)	Spot Weld - ø (mm)	Distance between Spot Welds (mm)	Overlap Distance (mm)
0.8	4.5	18	18
1	5	20	18
1.25	5.5	25	18
1.5	6	30	20
2	7	35	22
2.5	7.5	40	22
3	8	45	25

Table 3 : Typical strength of Spot Welds

Sheet Thickness (mm)	Spot Weld - ø (mm)	Shear Strength (kN)
0.8	4.5	2
1	5	2.8
1.25	5.5	3.5
1.5	6	4
2	7	5.5
2.5	7.5	6.3
3	8	7

Bonding

Bonding of aluminium is similar to bonding of steel. It has been shown that equivalent strength to the adhesive strength (with cohesive rupture) can be achieved. In general an alkaline pickling is a good surface preparation before bonding, and today adhesives (flexibilized epoxy) are available on the market that can bond on oily surfaces, like XW 1044-2 of CIBA GEIGY, and VP 480HC or High Tg of SIKA.

CORROSION

The resistance of Anticoroo kind of corrosion is good importance, because bod coated and lacquered, t consider the corrosion b lacquered product.
An excellent protectio lacquer/sheet surface is lacquered aluminium car bo time. The occurrence and p under the lacquer must be the aluminium with an anti like phosphating.
The ideal phosphate coatin one which produce dens containing controlled high of coating is also adequa panels.
The life time of phosphated is much better than that of is equivalent to that of zinc Table 4 shows the dept months of severe corr atmosphere (testing conc various alloys with differe shows that a dense pho bath gives the best corros

CHROMATING AN

Chromating

Chromating is an effic corrosion and can be us primers or lacquers.

Table 4 : Corrosi

Alloy
AlMg4.5 Mn (AA5182)
Ac-120® (AA6016)
Ac-120® (AA6016)
AlCu2.5Mg (AA2036)
AlMg4.5 Mn (AA5182)
Ac-120® (AA6016)
Ac-120® (AA6016)
Steel
Steel

Laquer : KTL + Primer
Test : Severe Corrosio
Data from K.Artl & T.B
"Entwicklung von Ober

CORROSION

The resistance of Anticorodal-120® to the various kind of corrosion is good but is not of great importance, because body panels are always coated and lacquered, therefore one should consider the corrosion behaviour of the final lacquered product.

An excellent protection of the interface lacquer/sheet surface is required in order that lacquered aluminium car bodies achieve a high life time. The occurrence and progression of corrosion under the lacquer must be avoided by protecting the aluminium with an anti-corrosion base coating like phosphating.

The ideal phosphate coatings for aluminium are the one which produce dense coating with a bath containing controlled high fluor amounts. This type of coating is also adequate to protect steel body panels.

The life time of phosphated aluminium body panels is much better than that of coated steel panels and is equivalent to that of zinc coated steel sheets.

Table 4 shows the depth of corrosion after 12 months of severe corrosion tests in a free atmosphere (testing condition: VDA 621-414) on various alloys with different protection. This table shows that a dense phosphating in a high fluor bath gives the best corrosion protection.

CHROMATING AND PRECOATING

Chromating

Chromating is an efficient protection against corrosion and can be used as a bonding coat for primers or lacquers.

Prelacquering

Alusuisse offers a prelacquering coating sold under the trade name **Bonazinc 2000** (from ICI). This product is based on an epoxy primer filled with zinc-phosphate powder, and is used to improve the corrosion resistance and the bonding of primer or lacquer. This product offers some interesting advantages :

• an enhancement of sheet formability
• an improvement of bonding strength of primer, lacquer or adhesives
• an improved corrosion resistance
• a better resistance to stone impact

LACQUER

Lacquering aluminium or steel is similar, and it is necessary to use a primer (1-2 μm) on which the lacquer bonds perfectly. Protection coating under the primer can be either chromating or phosphating.

TECHNICAL ASSISTANCE

An overview of the properties of Anticorodal-120®. have been given in this data sheet. The development division of the rolling-mill **Alusuisse Sierre** will answer more specific requests, and is ready to help in solving possible technical problems with users of this alloy :

Table 4 : Corrosion of various alloys and coatings.

Alloy	Phosphate	Rince	Corrosion Depth (mm)
AlMg4.5 Mn (AA5182)	dense coating (High F⁻)	H₂O or Cr VI	0
Ac-120® (AA6016)	dense coating (High F⁻)	H₂O	0
Ac-120® (AA6016)	dense coating (High F⁻)	Cr VI	0
AlCu2.5Mg (AA2036)	dense coating (High F⁻)	Cr VI	13
AlMg4.5 Mn (AA5182)	non dense coating (low F⁻)	H₂O or Cr VI	0
Ac-120® (AA6016)	non dense coating (low F⁻)	H₂O	15
Ac-120® (AA6016)	non dense coating (low F⁻)	Cr VI	0.5
Steel	dense coating (High F⁻)	H₂O or Cr VI	2.5 - 5.0
Steel	non dense coating (low F⁻)	H₂O or Cr VI	2.5 - 5.5

Laquer : KTL + Primer + Laquer
Test : Severe Corrosion in free atmosphere following VDA 621-414, Duration 12 monthes
Data from K.Artl & T.Brücken, " Die katodische Elektrotauchlackierung von Aluminium", DFO Conference: "Entwicklung von Oberflächenbehandlungen von Aluminium", 29.2-1.3.1988, Düsseldorf.

120 in T4 temper is

Ac-120 T4

20   30   40

aln e₂ (%)
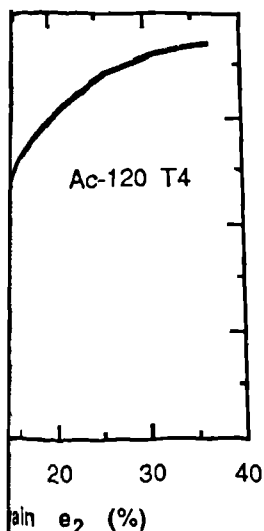
of aluminium sheets is
face looks like a ridged
ion and is not ideal for
sotropic form. A better
 drawing is the **EDT**
random pattern of small
as lubricant pockets and
ant distribution during
e brings the following

n of deformation
re difficult part without

EDT sheet can avoid the
foils (cost reduction)

tly isotropic (Roughness
nd transverse directions)
on to fulfil all requirements

JOINING

Spot welding

Two of the important factor to consider in using spot welding to join body panel are the strength achieved by spot welds and the life time of welding electrodes. The number of welds that an electrode can produce before being scraped is mainly controlled by the electrical resistance of the sheet surface, or in fact by the thickness of oxide layer on the sheet surface.

The electrical resistance on the surface of Anticorodal-120® sheets is relatively high, but it can be reduced either by a mechanical grinding, or by a chemical treatment of the surface (acid or alkaline pickling). The typical oxide layer after grinding is around 0.01 - 0.02 μm thick, and 0.001 - 0.002 μm thick after chemical pickling.

The life time of electrodes can be significantly improved if the treatments described above are applied directly in the production line.

Another way to improve the life time of electrodes is to use DC current welding machine and systems which continuously change the welding frequency.

The Tables 1 to 3 give reference values to spot weld sheets in Anticorodal-120® (without surface treatment).

MIG and TIG Welding

Anticorodal-120® can be welded by TIG or MIG and the filler metals to use are either S-AlSi5, or S-AlMg4.5Mn. Welding two different alloys is also possible without problems, for instance it is possible to weld AlMg3 or AlMg5Mn and Anticorodal®-120 .

Clinching

An interesting joining method is given by various clinching process like clinching and toxing. The advantages of these mechanical joining processes against spot welding lie in :

• lower equipment and toll costs
• lower production costs

The shear strength of clinch joints achieved is usually 50 - 80 % of the shear strength of equivalent spot welds. But the fatigue strength of clinch joints is usually equivalent or higher than that of spot welds.

Among the various producers of clinching equipment one can mention : BTM, Eckold, Homax, Kerb Konus and TOX.

Alusuisse LQW
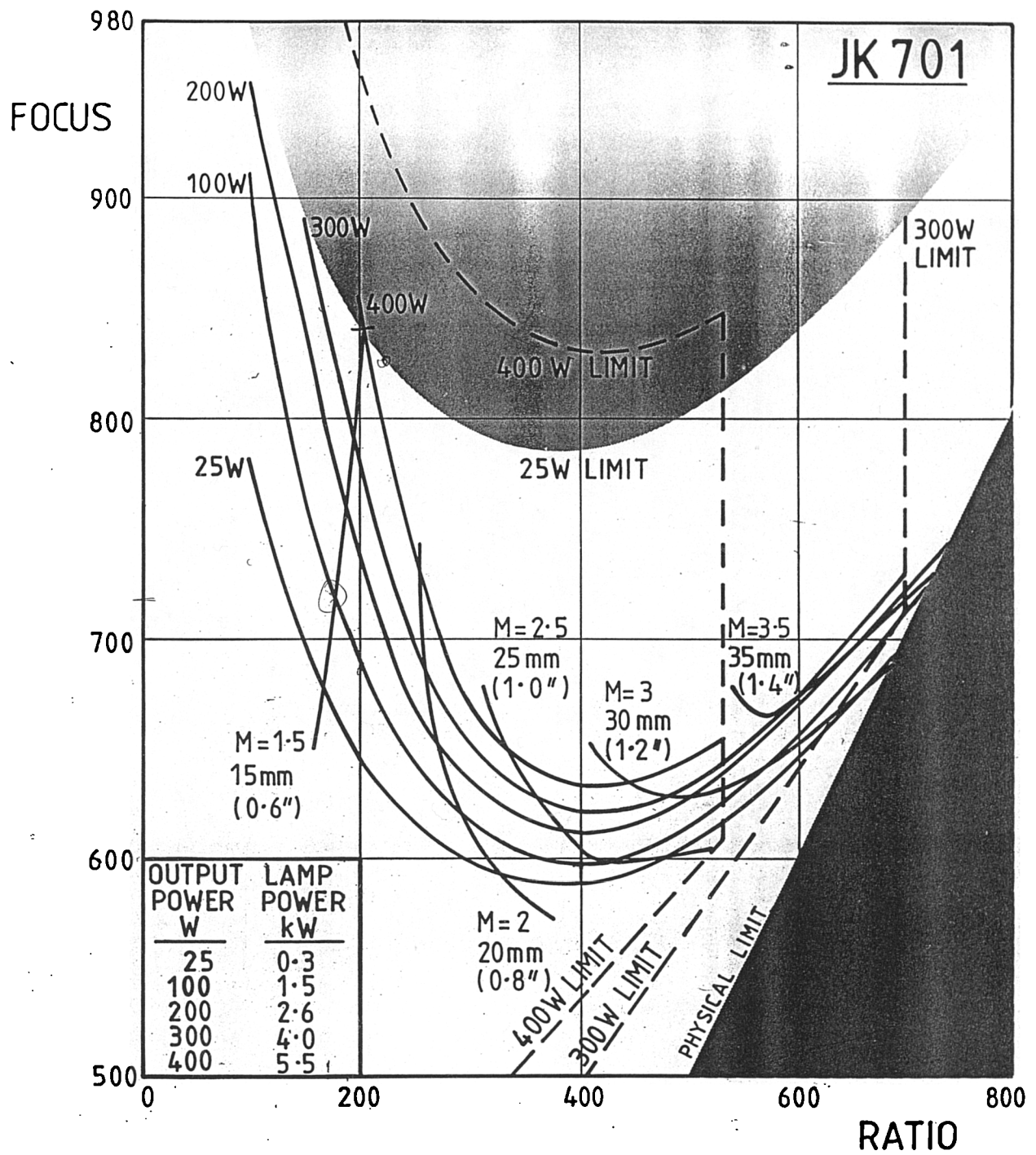
FIGURE 6.7A – JK 701 B.E.T. SETTINGS

Number:RY004790X   JK701-704 BEAM DELIVERY,CONV'L Lev:14 Rev:A   St: P
                                                                    P $

Component	Lv	Description	Ref	UoM	Qty	Rv	Kt	H	T	TXT
L25P9610X	25	M/C HD.FOR TV(NO FOC./V		EA	1.000		1			01
P44P4250D	50	MACHINING HEAD ASSY -BL		EA	1.000		1			02
L25C2910X	25	M/C HEAD + BINOCULAR		EA	1.000		1			03
L25H2570X	25	M/C HD FOR TV(NO VIEWER		EA	1.000		1			04
L25C2920X	25	M/C HEAD + TRINOCULAR F		EA	1.000		1			05
P4400150B	60	FOCUS LENS + ADAPTOR 80		EA	1.000		1			06
P4400160B	60	FOCUS LENS+ADAPTOR 120		EA	1.000		1			07
P4400210B	60	FOCUS LENS+ADAPT.45DIA1		EA	1.000		1			08
P4400200B	60	FOCUS LENS+ADAPT 45DIA2		EA	1.000		1			09
P4455330C	70	DRILL/CUT NOZZLE ASSY P		EA	1.000		1			10
P44K9140B	60	GAS NOZZLE ASSY JK704 8		EA	1.000		1			11
P44J2460B	60	GAS NOZZLE ASSY 120 MM		EA	1.000		1			12
P44J7010C	70	GAS NOZZLE +300 ADJUST		EA	1.000		1			13
P44W9410X	45	80mm DOUBLET+GAS NOZ AS		EA	1.000		1			14
M62F5960B	70	LENS ADAPTER ASSY 50DIA		EA	1.000		1			15
										16

0-MAY-1997 14:49:31.13

****

art Number:RY004940X   JK701-704 FOBD,GAS NOZZLES   Lev:16 Rev:A   St: P
                                                                      P S

tem Component	Lv	Description	Ref	UoM	Qty	Rv	Kt	H	T	TXT
010 P44H6510C	60	GAS NOZ COMPLETE,STD,50		EA	1.000		1			01
020 P44L0580C	60	GAS NOZ COMPL.50DI.F/O		EA	1.000		1			02
030 P59W6710X	70	KUGLER NOZZLE ASSY		EA	1.000		1			03

****

art Number:RY004760X   JK701-704 ACCESSORIES,SPECIFIC Lev:14 Rev:A   St: P
                                                                       P S

Item Component	Lv	Description	Ref	UoM	Qty	Rv	Kt	H	T	TXT
0010 P25C2820X	25	LOW DIVERGENCE KIT JK70	X	EA	1.000		1			01
0020 P25C2810X	25	LOW DIVERGENCE KIT JK70		EA	1.000		1			02
0030 P73D9890X	45	PUMP CHAMBER 6"X1/4" JK		EA	1.000		1			03
										04
12210110A		19 Dia Coated Window								05
										06
1222002940A		24 Dia Plan Slices								07
										08
123106074A		80 F/C Acro Lens 50ø								09
										10
12210180A		19 Dia X3 Shutter Window								11
										12
122200604A		M/C Mirror								13
										14
1234f2301		Slide 54 ø								15
										16

Buy / Build / Amend to be approved by the Design Authority / Project MGR

****

P55B6770B FLASHLAMPS FOR JK 701

Number:RY004770X   JK701-704 ACCESSORIES,BMC   Lev:14 Rev:A   St: P

Component	Lv	Description	Ref	UoM	Qty	Rv	Kt	P H	S T	TXT
E84X9450X	70	CTRL PANEL CONDUIT 1m T		EA	1.000	1				01
E84X9460X	70	CTRL PNL CONDUIT 2.5M T		EA	1.000	1				02
E84X9470X	70	CTRL PANEL CONDUIT 5m T		EA	1.000	1				03
E84X9480X	70	CTRL PANEL CONDUIT 10m		EA	1.000	1				04
E84X9490X	70	CTRL PANEL CONDUIT 15m		EA	1.000	1				05
E84X9500X	70	CTRL PANEL CONDUIT 30m		EA	1.000	1				06
B84Z0130K	70	CTRL PANEL KIT,GERMAN,7		EA	1.000	1				07
E84Z0140K	70	CTRL PANEL KIT,DUTCH,70		EA	1.000	1				08
E84Z0150K	70	CTRL PANEL KIT,FRENCH,7		EA	1.000	1				09
E84Z0160K	70	CTRL PANEL KIT,ITALIAN,		EA	1.000	1				10
B84Z0170K	70	CTRL PANEL KIT,SWEDISH,		EA	1.000	1				11
E84Z0180K	70	CTRL PANEL KIT,SPAINISH		EA	1.000	1				12

MAY-1997 14:06:42.59

****

E:F ACTION:L   JK-Lumonics Manufacturing System   VISIBILITY:INQ10
r: ORDER   ** S/L BOM Inquiry **   Date: 30 MAY 97
m: LTA4368:

Number:RY004750X   JK701-704 ACCESSORIES,COMMON   Lev:14 Rev:A   St: P

Component	Lv	Description	Ref	UoM	Qty	Rv	Kt	P H	S T	TXT
L25D8170C	25	POINTING HE-NE OPTION J		EA	1.000	1				01
L25D8970B	25	BET INT CONTROL PARTS J		EA	1.000	1				02
M80C2890C	25	SHUTTER+GAITERING+WINDO		EA	1.000	1				03
E84C5290X	70	POWER SUPPLY FEET KIT J		EA	1.000	1	Y			04
E84C5060C	70	HAND HELD SHUTTER BOX J		EA	1.000	1				05
E84C7020X	25	INSTALLATION KIT 5M JK7		EA	1.000	1				06
E85C3180D	25	CNC INTERFACE TYPE 1		EA	1.000	1	Y			07
M62F6330C	50	BOSS ASSEMBLY (M/C HEAD		EA	1.000	1				08
B83T0850X	60	TV CAMERA(FULNIX)+MON.+		EA	1.000	1				09
M62L1470B	50	LENS ADAPT+80 GAS BODY(		EA	1.000	1				10
1231060YA	90	LENS ACHR 80 F/L 50 DI		EA	1.000	1				11

****

E:F ACTION:L   JK-Lumonics Manufacturing System   VISIBILITY:INQ10
r: ORDER   ** S/L BOM Inquiry **   Date: 30 MAY 97
m: LTA4368:

Number:RY004630X   JK701-704 SPARES & REFURB   Lev:12 Rev:A   St: P

Component	Lv	Description	Ref	UoM	Qty	Rv	Kt	P H	S T	TXT
123301601	90	SAFETY WINDOW 100x200 T		EA	1.000	1				01
P55B6770B	70	F/TUBE 136/8 KR SUB INS		EA	1.000	1				02
123301301	90	GOGGLES YAG EN207		EA	1.000	1				03
M73J1740X	70	JK700 'O' RING SPARES K		EA	1.000	1				04
M73D2760X	30	ROUTINE MAINTENANCE KIT		EA	1.000	1				05
E73C5820X	45	SPARES FUSES KIT JK		EA	1.000	1	Y			06
550000101	90	FILTER CARBON		EA	1.000	1				07
										08
										09
										10
										11
										12
										13
										14
										15
										16

12200100A   14 Dm Sline

FIGURE 4.2B—LASER HEAD COMPONENT LOCATION
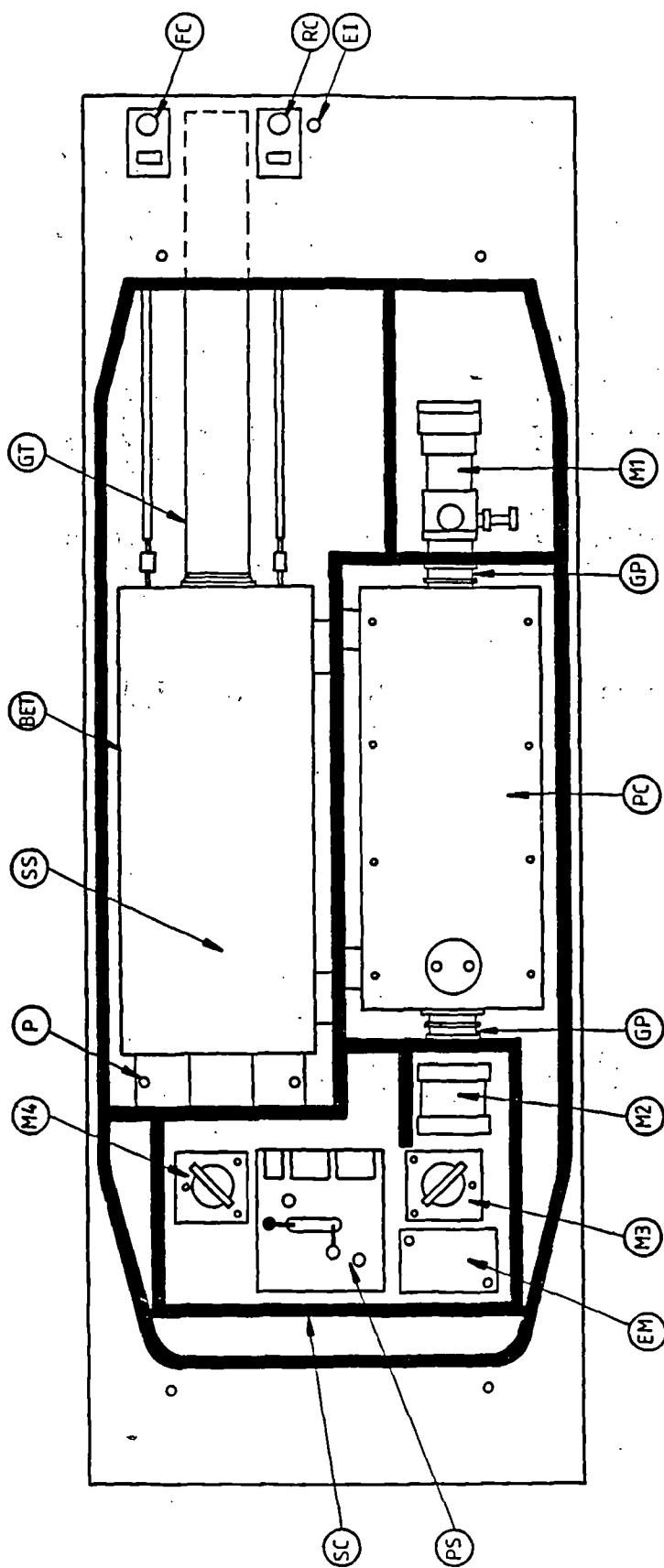
BET	—	BEAM EXPANDING TELESCOPE
EI	—	EMISSION INDICATOR
EM	—	ENERGY MONITOR
FC	—	BET FOCUS CONTROL
GP	—	BEAM TUBE (PTFE)
GT	—	BEAM TUBE (METAL)
M1	—	REAR MIRROR
P	—	PERISCOPE

M2	—	FRONT MIRROR
M3	—	FIRST STEERING MIRROR
M4	—	SECOND STEERING MIRROR
PS	—	PROCESS SHUTTER
RC	—	BET RATIO CONTROL
SC	—	SHUTTER COMPARTMENT
SS	—	SAFETY SHUTTER
PC	—	PUMPING CHAMBER
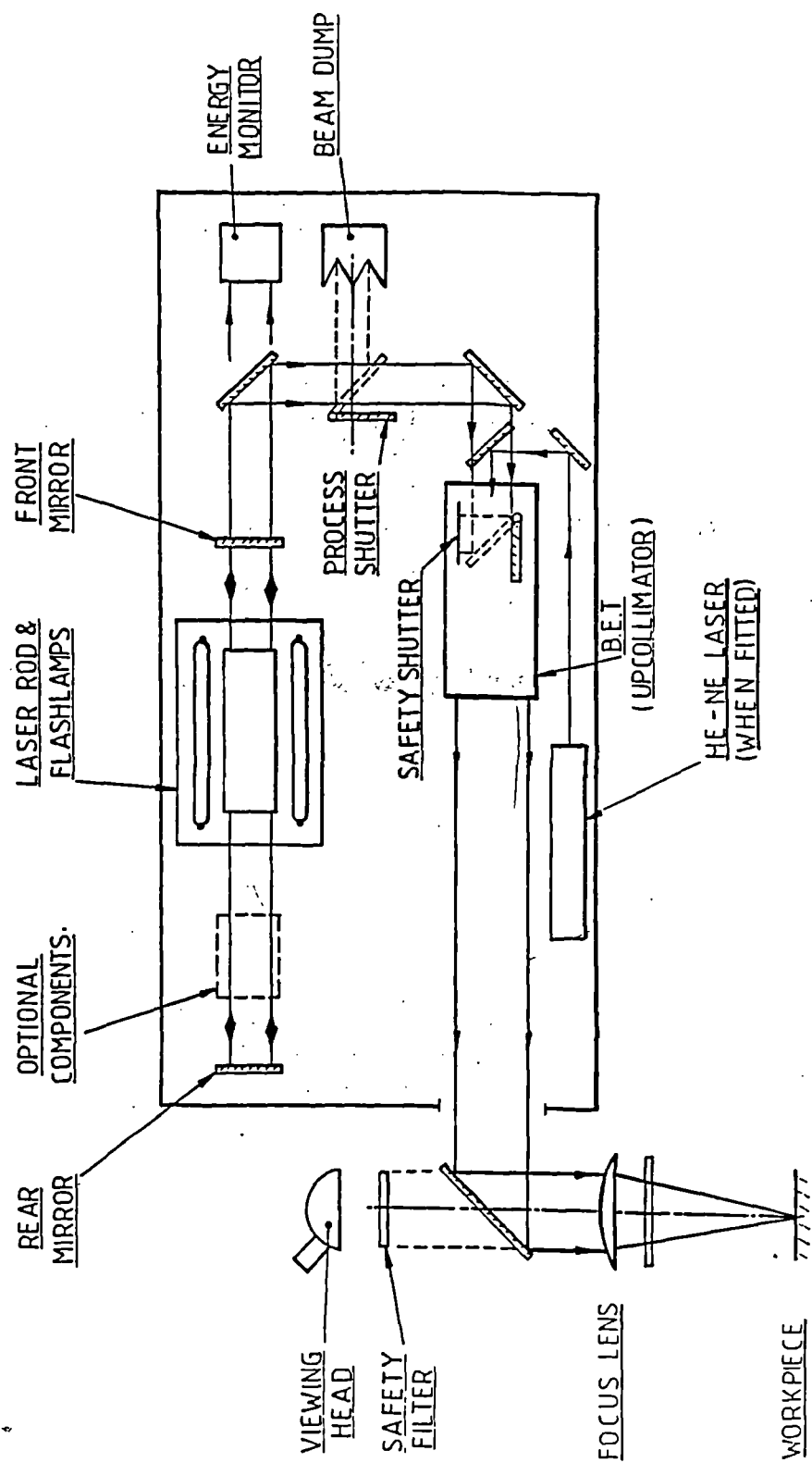
FIGURE 4.2 C   OPTICAL BEAMPATH

LUMONICS

JK PRODUCT DIVISION RUGBY ENGLAND

SERIAL No. 412340

MODEL JK701

220 380 415 VOLTS ~

50 Hz 3 PHASE 22 kVA 17 kW

MANUFACTURED APRIL 1987

FIGURE 4.3B SYSTEM DATA PLATE
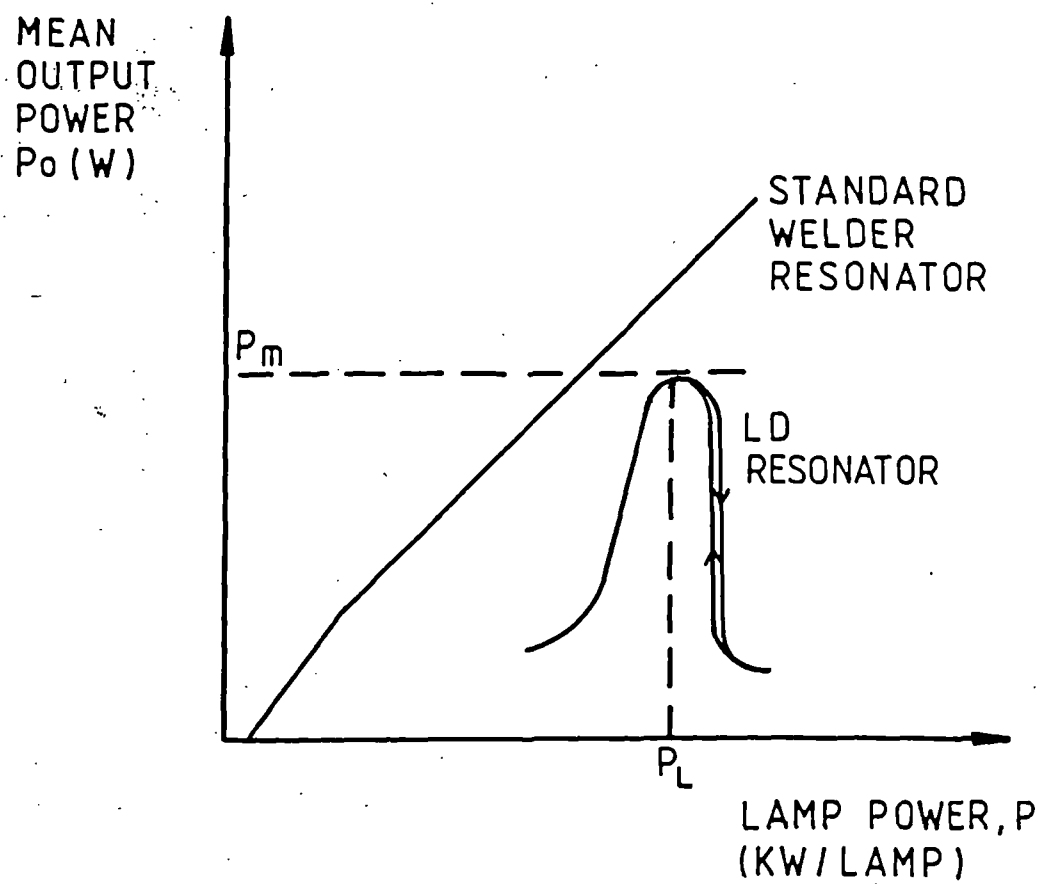
FIGURE 6.6A   INPUT-OUTPUT CHARACTERISTICS
OF LD RESONATOR

	S2 HEIGHT (%)	S1 WIDTH (mS)	S3 RATE (Hz)	ENERGY (J)	TOTAL INPUT POWER (kW)	SPECIFIED OUTPUT POWER (W)
JK701 OPTIMISE M1 AT	30	5	5	5-8	0·8-1·2	0-400
TYPICAL	65	6	20	20	11	
JK701 LD1 OPTIMISE M1 AT	50	2	35	1·7-2·1	5·8-6·2	135
OPTIMISE POWER AT	59	2	35	3·9-4·1	7·3-8·0	
JK701 LD2 OPTIMISE M1 AT	50	3	30	1·8-2·2	7·1-7·6	230
OPTIMISE POWER AT	86	2	30	8-9	9·8-11·0	

JK701 — SILVER — NO TUBE — R.MAX. M1 — M2

JK701 LD1 — BLACK — GOLD TUBE — SILVER TUBE — R.MAX. — T2 — GOLD L1 — T1 — M1 — M2

JK701 LD2 — BLACK — NO TUBE — BLACK TUBE — R.MAX. — T3 — BLACK L2 — T3 — M1 — M2

(handwritten annotation) SMALL SILVER EXTENSION

FIGURE 4.2D   JK701 RESONATOR DETAILS

Customer: University Of Warwick, Laser System Type: JK701

Customers Address: Dept Of Engineering, Serial No: 411660

Gibbet Hill Road,

Coventry.

Date:

1. Optical Inspection

COMPONENTS	TYPE	CONDITION	REPLACED/CLEANED	PART NO.	CHK.
Laser Rod	6 x 3/8	Good			✓
Flashlamps	KRIPTON	≠	C.		✓
Rear Mirror		Good.			✓
LD Optics (30% Mirror LD1 Telescope, CD2 Tele					N/A.
Front Mirror	60%	MARKED	C		✓
1st Turning Mirror	96%	Good			✓
Energy Monitor		Good			✓
Process Shutter Mirror		Good.			✓
Proc Shut Dump Window		Slight Mark			✓
2nd Turning Mirror	100%	Good.			✓
HeNe Beam Splitter		Good			✓
HeNe Turning Mirror		Good			✓
HeNe laser		HENE KEEPS TRIPPING OUT			✓
Safety Shutter		Good			✓
BET 2 Negative Lenses		1ST NEGATIVE LENS SLIGHTLY DAMAGED ~ C			✓
BET Positive Lens		Good			✓
Check BET Linear Travel		Good			✓
Machining Head		Good			✓
Check Pumping Chamber Gause (Filter)		Clear.			✓

COMPONENT/FUNCTION	CONDITION	REPAIR/REPLACE	CKD
Coolant System			
Drain Coolant System		Drained	✓
Flush Coolant System			N/A
Clean out Debris	NO DEBRIS FOUND		✓
Inspect Coolant Pipework & Connections			✓
Inspect Laserhead Coolant Pipework			✓
Replace De-ioniser & Filter	Pump Replaced – Noisy	Replaced.	✓
Refill with High Qual Distilled Water		Refilled.	✓
Check Chiller Operation	Chiller not coping because it vents into enclosed room		✓
Laser Head:			✓
Inspect Gaitering	NO FRONT MIRROR GAITER		✓
Inspect Electrical Connections			✓
Inspect Lamp Connections			✓
Check Process Shutter Condition			✓
Check Safety Shutter Condition			✓
Check Safety Labelling (JK700 Handbook)	OLD STYLE		✓
Electrical Cabinet			
Inspect Conduit and Wiring			✓
Inspect Internal Wiring			✓
Inspect Electrical Connections			✓
Check All Covers Fitted	NO SWITCHING MODULE COVERS – OLD LASER		✓
Safety Checks			
Check Process Shutter Operation			✓
Check Safety Shutter Operation			✓
Check Dump Components			✓
Check Dump Circuit Operation			✓
Check All Safety Covers			✓
Check Interlock Operation			✓
Check all Warning Labels Fitted			✓

3. CNC Checks

FUNCTION	CONDITION	REPAIR/REPLACE	CKD.
Check Alignment			✓
Check Performance	10mS 10Hz 31%	13.2J 131W	✓
Check BET Operation	Good.		✓
Check Machining Head Alignment	Aligned		✓

Lumonics Engineer: _____

Customer: _____

Date: _____

1

Appendix 4:
Laser characterisation at 1 kw peak pulse power

Pulse duration τ, ms	Pulse rate Hz	Lamp ht, %	Av. lamp power, kw	Pulse energy, J	Peak power, kw	Int. output power, w	Ext. output power, w	Loss %
0.5	5	40.1	0.10	0.5	1.00	2.5	NR	
1.0	5	40.1	0.15	1.0	1.00	5.0	NR	
4.0	5	35.0	0.45	4.0	1.00	20.0	NR	
5.0	5	34.1	0.50	5.0	1.00	25.0	22	12
10.0	5	32.2	0.95	10.0	1.00	50.0	43	14
13.0	5	31.3	1.20	13.0	1.00	65.0	NR	
15.0	5	31.0	1.35	15.0	1.00	75.0	NR	
20.0	5	31.0	1.80	20.0	1.00	100.0	82	18
0.5	10	32.5	0.10	0.5	1.00	5.0		
1.0	10	30.9	0.20	1.0	1.00	10.0		
2.0	10	31.0	0.40	2.0	1.00	20.0		
3.0	10	31.2	0.60	3.0	1.00	30.0		
5.0	10	30.2	1.05	5.0	1.00	50.0	44	12
10.0	10	29.8	1.80	10.0	1.00	100.0	84	16
15.0	10	30.1	2.60	15.0	1.00	150.0	125	17
20.0	10	30.4	3.60	20.0	1.00	200.0	164	18
0.5	20	30.3	0.25	0.5	1.00	10.0		
0.7	20	30.1	0.30	0.7	1.00	14.0		
1.0	20	29.8	0.45	1.0	1.00	20.0		
2.0	20	29.8	0.80	2.0	1.00	40.0	36	10
3.0	20	29.8	1.15	3.0	1.00	60.0		
4.0	20	29.8	1.50	4.0	1.00	80.0		
5.0	20	29.8	1.95	5.0	1.00	100.0		
8.0	20	29.9	2.95	8.0	1.00	160.0	137	14
12.0	20	30.9	4.30	12.0	1.00	240.0		
16.0	20	30.7	5.65	16.0	1.00	320.0	267	17
17.0	20	30.7	6.00	17.0	1.00	340.0		
0.5	50	26.3	0.70	0.5	1.00	25.0		
0.7	50	25.9	0.80	0.7	1.00	35.0	30	14
1.0	50	26.2	1.10	1.0	1.00	50.0	43	14
2.0	50	28.1	2.00	2.0	1.00	100.0	90	10
3.0	50	28.8	2.85	3.0	1.00	150.0	135	10
4.0	50	30.1	5.00	4.0	1.00	200.0	170	15
5.0	50	30.2	4.50	5.0	1.00	250.0	220	12
6.0	50	30.7	5.55	6.0	1.00	300.0	255	15
6.5	50	30.5	6.00	6.5	1.00	325.0		
0.5	75	27.7	1.10	0.5	1.00	37.5		
0.7	75	26.1	1.25	0.7	1.00	52.5		
1.0	75	27.5	1.70	1.0	1.00	75.0	65	13
1.5	75	28.4	2.40	1.5	1.00	112.5		
2.0	75	29.2	3.05	2.0	1.00	150.0		
2.5	75	29.5	3.70	2.5	1.00	187.5	163	13
3.0	75	29.7	4.30	3.0	1.00	225.0		
4.0	75	30.0	4.90	3.5	0.88	262.5		
4.2	75	30.3	5.60	4.0	0.95	300.0	255	15
0.5	100	27.0	1.40	0.5	1.00	50.0	44	12
0.7	100	26.8	1.70	0.7	1.00	70.0		
1.0	100	27.3	2.20	1.0	1.00	100.0		
1.3	100	28.1	2.80	1.3	1.00	130.0		
1.6	100	28.8	3.30	1.6	1.00	160.0		
1.8	100	29.3	3.70	1.8	1.00	180.0		
2.0	100	29.4	4.00	2.0	1.00	200.0	172	14
2.4	100	29.8	4.70	2.4	1.00	240.0		

Laser characterisation at 2 kw peak pulse power

Pulse duration τ, ms	Pulse rate Hz	Lamp ht, %	Av. lamp power, kw	Pulse energy, J	Peak power, kw	Int. output power, w	Ext. output power, w	Loss %
0.5	5	53.1	0.10	1.0	2.00	5		
1.0	5	53.2	0.20	2.0	2.00	10		
4.0	5	48.2	0.70	8.0	2.00	40	35	12.5
10.0	5	46.6	1.60	20.0	2.00	100		
15.0	5	46.3	2.50	30.0	2.00	150		
20.0	5	46.3	3.00	40.0	2.00	200	171	14.5
0.5	10	43.0	0.20	1.0	2.00	10	9	10.0
1.0	10	43.0	0.40	2.0	2.00	20		
1.5	10	44.0	0.50	3.0	2.00	30		
2.5	10	44.0	0.80	5.0	2.00	50	44	12.0
5.0	10	44.0	1.60	10.0	2.00	100		
10.0	10	44.0	3.00	20.0	2.00	200	167	16.5
20.0	10	45.0	6.00	39.0	1.95	390	328	15.9
0.5	20	41.0	0.35	1.0	2.00	20	19	5.0
1.0	20	42.5	0.70	2.0	2.00	40	37	7.5
1.5	20	42.3	1.00	3.0	2.00	60	54	10.0
1.6	20	42.9	1.10	3.2	2.00	64	55	14.1
1.7	20	43.1	1.10	3.4	2.00	68	58	14.7
1.8	20	43.0	1.20	3.6	2.00	72	63	12.5
1.9	20	43.2	1.30	3.8	2.00	76	66	13.2
2.0	20	42.4	1.30	4.0	2.00	80	70	12.5
2.1	20	43.2	1.40	4.2	2.00	84	73	13.1
2.2	20	43.4	1.50	4.4	2.00	88	76	13.6
2.3	20	43.7	1.55	4.6	2.00	92	81	12.0
2.4	20	43.7	1.60	4.8	2.00	96	84	12.5
2.5	20	42.1	1.60	5.0	2.00	100	88	12.0
2.6	20	43.3	1.70	5.2	2.00	104	89	14.4
2.7	20	43.2	1.80	5.4	2.00	108	91	15.7
2.8	20	43.2	1.80	5.6	2.00	112	95	15.2
2.9	20	43.3	1.90	5.8	2.00	116	98	15.5
3.0	20	41.9	1.90	6.0	2.00	120	105	12.5
5.0	20	43.2	3.10	10.0	2.00	200	174	13.0
7.5	20	44.3	4.50	15.0	2.00	300	258	14.0
8.0	20	45.0	5.00	16.0	2.00	320		
9.0	20	45.0	5.50	18.0	2.00	360		
9.8	20	45.0	6.00	19.6	2.00	392	328	16.3
0.5	50	38.6	1.15	1.0	2.00	50	44	12.0
0.7	50	40.2	1.40	1.5	2.14	75	62	17.3
1.0	50	40.2	1.80	2.0	2.00	100	87	13.0
1.5	50	40.8	2.55	3.0	2.00	150	134	10.7
2.0	50	42.2	0.34	4.0	2.00	200	164	18.0
2.5	50	43.2	4.10	5.0	2.00	250	227	9.2
3.0	50	44.0	4.90	6.0	2.00	300	266	11.3
3.5	50	44.5	5.75	7.0	2.00	350	303	13.4
3.7	50	44.5	6.00	7.5	2.03	375	313	16.5
						0		
0.5	75	39.0	1.65	1.0	2.00	75	64	14.7
0.7	75	38.9	2.05	1.4	2.00	105		
1.0	75	40.9	2.85	2.0	2.00	150		
1.3	75	41.5	3.55	2.6	2.00	195		
1.6	75	42.5	4.20	3.2	2.00	240	207	13.8
1.8	75	42.8	4.60	3.6	2.00	270		
2.0	75	42.8	5.00	4.0	2.00	300		
2.2	75	43.5	5.50	4.4	2.00	330		
2.4	75	43.5	5.95	4.8	2.00	360	308	14.4

Laser characterisation at 3 kw peak pulse power

Pulse duration τ, ms	Pulse rate Hz	Lamp ht, %	Av. lamp power, kw	Pulse energy, J	Peak power, kw	Int. output power, w	Ext. output power, w	Loss %
0.5	5	65.4	0.15	0.5	1.00	2.5		
1.0	5	65.4	0.30	3.0	3.00	15	12	20.0
2.0	5	64.2	0.50	6.0	3.00	30		
5.0	5	60.5	1.20	15.0	3.00	75	66	12.0
10.0	5	60.1	2.40	30.0	3.00	150	124	17.3
13.0	5	59.1	2.95	39.0	3.00	195	158	19.0
0.5	10	57.2	0.30	1.5	3.00	15		
0.7	10	57.4	0.45	2.1	3.00	21		
1.0	10	58.2	0.55	3.0	3.00	30	26	13.3
1.7	10	57.7	0.80	5.0	2.94	50		
2.0	10	57.3	0.95	6.0	3.00	60		
3.3	10	57.5	1.50	10.0	3.03	100		
5.0	10	57.0	2.20	15.0	3.00	150	125	16.7
7.0	10	57.8	3.10	21.0	3.00	210		
10.0	10	59.4	4.60	30.0	3.00	300		
12.0	10	59.0	5.40	36.0	3.00	360		
13.0	10	59.0	5.90	39.0	3.00	390	299	23.3
0.5	20	53.8	0.55	1.5	3.00	30	26	13.3
0.6	20	53.9	0.75	1.8	3.00	36		
0.7	20	53.9	0.80	2.1	3.00	42		
0.8	20	53.8	0.85	2.4	3.00	48		
1.0	20	54.6	1.00	3.0	3.00	60		
1.5	20	56.2	1.50	4.5	3.00	90		
1.7	20	56.0	1.70	5.0	2.94	100		
2.0	20	56.2	1.90	6.0	3.00	120	100	16.7
2.5	20	56.4	2.30	7.5	3.00	150		
3.0	20	57.5	2.80	9.0	3.00	180		
3.5	20	57.5	3.30	10.5	3.00	210		
4.0	20	58.8	3.60	12.0	3.00	240		
4.5	20	58.0	4.10	13.5	3.00	270		
5.0	20	58.0	4.50	15.0	3.00	300		
6.0	20	58.2	5.40	18.0	3.00	360		
6.5	20	58.5	5.85	19.5	3.00	390	320	17.9
6.6	20	58.5	5.00	20.0	3.03	400		
0.5	50	51.5	1.50	1.5	3.00	75	64	14.7
0.7	50	51.7	1.90	2.1	3.00	105	92	12.4
0.9	50	52.7	2.30	2.7	3.00	135	119	11.9
1.1	50	55.7	2.90	3.3	3.00	165	150	9.1
1.3	50	56.0	3.30	3.9	3.00	195	173	11.3
1.5	50	56.9	3.90	4.5	3.00	225	197	12.4
1.7	50	57.0	4.20	5.1	3.00	255	232	9.0
1.9	50	57.1	4.50	5.7	3.00	285	253	11.2
2.1	50	56.8	5.00	6.3	3.00	315	278	11.7
2.3	50	57.1	5.55	6.9	3.00	345	300	13.0
2.5	50	56.7	5.85	7.5	3.00	375	322	14.1
2.6	50	56.8	6.00	7.8	3.00	390		
0.5	75	50.9	2.35	1.5	3.00	113	95	15.6
0.7	75	52.8	2.90	2.1	3.00	158		
1.0	75	54.7	3.95	3.0	3.00	225	185	17.8
1.2	75	55.9	4.55	3.6	3.00	270		
1.5	75	56.2	5.50	4.5	3.00	338	300	11.1
1.6	75	56.4	5.90	4.8	3.00	360		
0.5	100	52.6	3.00	1.5	3.00	150	128	14.7

Laser characterisation at 4 kw peak pulse power

Pulse duration τ, ms	Pulse rate Hz	Lamp ht, %	Av. lamp power, kw	Pulse energy, J	Peak power, kw	Int. output power, w	Ext. output power, w	Loss %
0.5	5	78.4	0.20	2.0	4.00	10		
1.0	5	78.6	0.40	4.0	4.00	20		
2.0	5	75.7	0.70	8.0	4.00	40	34	15.0
5.0	5	72.7	1.60	20.0	4.00	100	85	15.0
10.0	5	72.7	3.10	40.0	4.00	200	165	17.5
0.5	10	67.7	0.35	2.0	4.00	20		
0.8	10	68.8	0.55	3.2	4.00	32	30	6.3
1.0	10	68.8	0.70	4.0	4.00	40		
1.2	10	68.8	0.85	5.0	4.17	50		
1.5	10	68.8	1.00	6.0	4.00	60		
2.0	10	69.8	1.30	8.0	4.00	80	69	13.8
2.5	10	70.8	1.60	10.0	4.00	100	85	15.0
3.0	10	70.2	1.90	12.0	4.00	120	100	16.7
3.5	10	69.3	2.10	14.0	4.00	140	115	17.9
4.0	10	69.3	2.40	16.0	4.00	160	131	18.1
5.0	10	70.1	3.00	20.0	4.00	200	165	17.5
5.5	10	70.3	3.25	22.0	4.00	220	177	19.5
6.0	10	71.5	3.65	24.0	4.00	240	195	18.8
7.0	10	71.5	4.30	28.0	4.00	280	225	19.6
8.0	10	70.8	4.80	32.0	4.00	320	251	21.6
9.0	10	71.8	5.50	36.0	4.00	360	279	22.5
10.0	10	71.7	6.00	40.0	4.00	400	304	24.0
0.5	20	60.8	0.75	2.0	4.00	40	35	12.5
0.7	20	62.7	2.00	2.8	4.00	56		
0.9	20	64.7	1.20	3.6	4.00	72		
1.1	20	67.0	1.50	4.4	4.00	88		
1.3	20	67.0	1.70	5.2	4.00	104		
1.5	20	66.0	1.90	6.0	4.00	120		
2.0	20	68.0	2.50	8.0	4.00	160	136	15.0
2.5	20	69.0	3.10	10.0	4.00	200		
3.0	20	69.2	3.65	12.0	4.00	240		
3.5	20	69.5	4.20	14.0	4.00	280		
4.0	20	69.5	4.80	16.0	4.00	320	276	13.8
4.5	20	69.5	5.00	18.0	4.00	360		
5.0	20	69.8	5.95	20.0	4.00	400	340	15.0
0.5	50	58.3	1.80	2.0	4.00	100	87	13.0
0.7	50	60.3	2.45	2.8	4.00	140	116	17.1
0.9	50	63.5	3.05	3.6	4.00	180	155	13.9
1.1	50	66.5	3.75	4.4	4.00	220	183	16.8
1.3	50	67.3	4.15	5.2	4.00	260	222	14.6
1.5	50	67.7	4.75	6.0	4.00	300	255	15.0
1.7	50	67.9	5.30	6.8	4.00	340	297	12.6
1.9	50	69.0	5.95	7.6	4.00	380	330	13.2
0.5	75	59.7	2.95	2.0	4.00	150	132	12.0
0.7	75	62.5	3.80	2.8	4.00	210	184	12.4
1.0	75	64.9	4.90	4.0	4.00	300	262	12.7
1.1	75	66.6	5.45	4.4	4.00	330		
1.2	75	67.0	5.90	4.8	4.00	360	310	13.9
0.5	100	65.0	3.90	2.0	4.00	200	181	9.5
0.6	100	63.0	4.50	2.4	4.00	240		
0.7	100	63.4	4.80	2.8	4.00	280	250	10.7
0.8	100	63.7	5.40	3.2	4.00	320		
0.9	100	63.7	5.95	3.6	3.94	355	311	12.4

Laser characterisation at 5 kw peak pulse power

Pulse duration τ, ms	Pulse rate Hz	Lamp ht, %	Av. lamp power, kw	Pulse energy, J	Peak power, kw	Int. output power, w	Ext. output power, w	Loss %
0.5	5	76.6	0.20	2.5	5.00	12.5		
1.0	5	90.7	0.50	5.0	5.00	25	22	12.0
1.2	5	90.8	0.50	6.0	5.00	30	27	10.0
1.5	5	89.3	0.65	7.5	5.00	37.5	34	9.3
2.0	5	87.3	0.85	10.0	5.00	50	43	14.0
5.0	5	84.3	1.95	25.0	5.00	125	104	16.8
0.5	10	81.9	0.50	2.5	5.00	25	22	12.0
1.0	10	81.5	0.85	5.0	5.00	50		
2.0	10	83.0	1.60	10.0	5.00	100		
3.0	10	81.0	2.30	15.0	5.00	150	126	16.0
4.0	10	82.0	3.00	20.0	5.00	200		
5.0	10	83.5	3.85	25.0	5.00	250	210	16.0
6.0	10	83.6	4.60	30.0	5.00	300		
7.0	10	83.3	5.30	35.0	5.00	350		
8.0	10	83.3	6.00	40.0	5.00	400	336	16.0
0.5	20	71.3	0.90	2.5	5.00	50	44	12.0
0.7	20	76.3	1.20	3.5	5.00	70		
0.9	20	79.3	1.50	4.5	5.00	90		
1.0	20	79.3	1.70	5.0	5.00	100		
1.1	20	78.3	1.80	5.5	5.00	110		
1.2	20	78.4	1.95	6.0	5.00	120		
1.4	20	78.4	2.20	7.0	5.00	140	120	14.3
1.6	20	80.4	2.60	8.0	5.00	160		
2.0	20	80.4	3.10	10.0	5.00	200		
2.5	20	81.6	3.80	12.5	5.00	250		
3.0	20	81.8	4.50	15.0	5.00	300		
3.5	20	81.5	5.30	17.5	5.00	350		
4.0	20	81.6	6.00	20.0	5.00	400	337	15.8
0.5	50	73.6	2.30	2.5	5.00	125	108	13.6
0.6	50	76.1	2.60	3.0	5.00	150	132	12.0
0.7	50	77.5	3.05	3.5	5.00	175	159	9.1
0.8	50	78.4	5.00	4.0	5.00	200	173	13.5
0.9	50	85.5	3.85	4.5	5.00	225	201	10.7
1.0	50	81.6	4.20	5.0	5.00	250	220	12.0
1.1	50	81.5	4.40	5.5	5.00	275	247	10.2
1.2	50	81.4	4.85	6.0	5.00	300	265	11.7
1.3	50	81.6	5.20	6.5	5.00	325	286	12.0
1.4	50	81.4	5.60	7.0	5.00	350	310	11.4
1.5	50	81.5	5.90	7.5	5.00	375	324	13.6
0.5	75	76.3	3.50	2.5	5.00	188	165	12.0
0.6	75	81.8	4.15	3.0	5.00	225		
0.7	75	79.3	4.55	3.5	5.00	263	236	10.1
0.8	75	78.8	4.95	4.0	5.00	300		
0.9	75	79.0	5.55	4.5	5.00	338		
1.0	75	79.1	6.00	5.0	5.00	375	322	14.1
0.5	100	78.6	4.65	2.5	5.00	250	234	6.4

Appendix 5;
Ranging trials, focus position, 50Hz, 2J

Pulse length, ms	Lamp ht, %	Av. lamp power, kw	Peak power, kw		Focus position	Spot diameter, mm						average dia. in mm
						1	2	3	4	5	6	
2	27.6	1.9	1.00	h	0	0.464	0.512	0.506	0.472	0.484	0.468	0.484
				v	0	0.478	0.496	0.518	0.476	0.554	0.542	0.511
												0.498
				h	0.4	0.458	0.440	0.454	0.456	0.416	0.454	0.446
				v	0.4	0.470	0.434	0.468	0.502	0.452	0.442	0.461
												0.454
					0.8 - no mark							
1	39.8	1.8	2.00	h	0	0.570	0.594	0.634	0.576	0.568	0.580	0.587
				v	0	0.574	0.614	0.614	0.588	0.584	0.588	0.594
												0.590
				h	0.4	0.566	0.558	0.568	0.600	0.546	0.594	0.572
				v	0.4	0.640	0.604	0.612	0.622	0.566	0.578	0.604
												0.588
				h	0.8	0.558	0.580	0.584	0.582	0.582	0.536	0.570
				v	0.8	0.570	0.646	0.568	0.614	0.600	0.608	0.601
												0.586
					1.2- no mark							
0.7	48.8	1.8	2.86	h	0	0.638	0.640	0.650	0.642	0.620	0.658	0.641
				v	0	0.708	0.668	0.632	0.640	0.610	0.644	0.650
												0.646
				h	0.4	0.648	0.630	0.654	0.684	0.690	0.678	0.664
				v	0.4	0.638	0.664	0.658	0.660	0.678	0.676	0.662
												0.663
				h	0.8	0.686	0.710	0.710	0.694	0.706	0.712	0.703
				v	0.8	0.666	0.734	0.708	0.660	0.664	0.728	0.693
												0.698
				h	1.2	0.668	0.662	0.658	0.648	0.698	0.636	0.662
				v	1.2	0.738	0.736	0.710	0.782	0.716	0.694	0.729
												0.696
				h	1.6	0.672	0.660	0.684	0.682	0.650	0.722	0.678
				v	1.6	0.734	0.726	0.724	0.706	0.706	0.720	0.719
												0.699
0.5	58.3	1.8	4.00	h	0	0.610	0.642	0.598	0.598	0.594	0.576	0.603
				v	0	0.598	0.646	0.594	0.632	0.582	0.586	0.606
												0.605
				h	0.4	0.618	0.632	0.636	0.638	0.678	0.630	0.639
				v	0.4	0.646	0.644	0.660	0.650	0.662	0.640	0.650
												0.645
				h	0.8	0.656	0.714	0.662	0.689	0.712	0.656	0.682
				v	0.8	0.69	0.696	0.684	0.682	0.7	0.676	0.688
												0.685
				h	1.2	0.698	0.708	0.706	0.724	0.72	0.74	0.716
				v	1.2	0.706	0.718	0.708	0.71	0.728	0.758	0.721
												0.719
				h	1.6	0.7	0.702	0.714	0.71	0.748	0.706	0.713
				v	1.6	0.766	0.736	0.722	0.718	0.768	0.742	0.742
												0.728

Ranging trials, focus position, 20Hz, 5J

Pulse length, ms	Lamp ht, %	Av. lamp power, kw	Peak power, kw		Focus position	Spot, mm 1	2	3	4	5	6	average dia. in mm
5	49.8	1.75	1.00	h	no mark							
2.5	43.2	1.65	2.00	h	0	0.776	0.712	0.702	0.688	0.718	0.742	0.723
				v	0	0.746	0.752	0.690	0.702	0.738	0.780	0.735
												0.729
				h	0.4	0.806	0.776	0.744	0.724	0.722	0.764	0.756
				v	0.4	0.829	0.804	0.778	0.780	0.772	0.780	0.791
												0.773
					0.8 - no mark							
1.7	55.1	1.6	2.94	h	0	0.750	0.796	0.778	0.766	0.772	0.808	0.778
				v	0	0.750	0.808	0.784	0.758	0.720	0.744	0.761
												0.770
				h	0.4	0.782	0.816	0.848	0.802	0.794	0.808	0.808
				v	0.4	0.772	0.752	0.744	0.796	0.782	0.818	0.777
												0.793
				h	0.8	0.866	0.850	0.874	0.850	0.858	0.836	0.856
				v	0.8	0.838	0.872	0.888	0.878	0.878	0.824	0.863
												0.859
				h	1.2	0.870	0.908	0.918	0.862	0.868	0.858	0.881
				v	1.2	0.886	0.902	0.928	0.928	0.892	0.906	0.907
												0.894
				h	1.6	0.868	0.854	0.868	0.932	0.840	0.846	0.868
				v	1.6	0.938	0.892	0.914	0.910	0.930	0.924	0.918
												0.893
1.3	63.8	1.6	3.85	h	0	0.680	0.692	0.766	0.764	0.784	0.776	0.744
				v	0	0.726	0.700	0.746	0.712	0.686	0.696	0.711
												0.727
				h	0.4	0.778	0.778	0.792	0.790	0.804	0.786	0.788
				v	0.4	0.730	0.764	0.794	0.792	0.732	0.738	0.758
												0.773
				h	0.8	0.840	0.860	0.856	0.878	0.876	0.848	0.860
				v	0.8	0.884	0.862	0.802	0.846	0.846	0.856	0.849
												0.855
				h	1.2	0.856	0.878	0.864	0.860	0.864	0.880	0.867
				v	1.2	0.858	0.890	0.868	0.868	0.822	0.846	0.859
												0.863
				h	1.6	0.898	0.944	0.874	0.920	0.960	0.904	0.917
				v	1.6	0.912	0.932	0.924	0.944	0.908	0.906	0.921
												0.919
				h	2	0.950	0.970	0.954	0.948	0.980	0.988	0.965
				v	2	1.030	0.984	0.870	0.944	1.022	0.974	0.971
												0.968
				h	2.4	0.978	0.976	0.930	1.010	1.078	0.914	0.981
				v	2.4	1.064	1.094	1.010	1.008	1.108	1.002	1.048
												1.014
1	77.9	1.65	5.00	h	0	0.748	0.742	0.826	0.720	0.792	0.742	0.762
				v	0	0.720	0.696	0.802	0.720	0.750	0.740	0.738
												0.750
				h	0.4	0.770	0.792	0.720	0.774	0.784	0.776	0.769
				v	0.4	0.828	0.796	0.708	0.856	0.810	0.812	0.802
												0.786
				h	0.8	0.782	0.778	0.77	0.852	0.812	0.806	0.800
				v	0.8	0.81	0.856	0.868	0.88	0.82	0.81	0.841
												0.820
				h	1.2	0.858	0.858	0.864	0.864	0.858	0.84	0.857
				v	1.2	0.884	0.878	0.866	0.908	0.846	0.94	0.887
												0.872
				h	1.6	0.884	0.908	0.902	0.904	0.916	0.92	0.906

Appendices: Experimental data

Ranging trials, focus position, 10Hz, 10J

Pulse length, ms	Lamp ht, %	Av. lamp power, kw	Peak power, kw		Focus position	Spot, mm 1	2	3	4	5	6	average dia. in mm
10	29.5	1.75	1.00	h	0	no significant surface melting						
5	44.2	1.6	2.00	h	0	0.758	0.744	0.748	0.754	0.728	0.732	0.744
				v	0	0.730	0.720	0.764	0.782	0.744	0.760	0.750
												0.747
				h	0.4	0.808	0.798	0.814	0.816	0.812	0.776	0.804
				v	0.4	0.800	0.836	0.842	0.860	0.848	0.872	0.843
												0.824
				h	0.8	0.824	0.896	0.852	0.850	0.856	0.806	0.847
				v	0.8	0.844	0.906	0.898	0.878	0.876	0.081	0.747
												0.797
				h	1.2	0.872	0.870	0.864	0.912	0.918	0.864	0.883
				v	1.2	0.914	0.940	0.908	0.944	0.910	0.902	0.920
												0.902
				h	1.6	0.950	0.984	0.878	0.928	0.938	0.884	0.927
				v	1.6	0.948	0.978	0.900	0.988	0.986	0.934	0.956
												0.941
				h	2	0.982	0.972	0.920	0.942	0.992	0.950	0.960
				v	2	1.018	1.048	0.982	1.010	1.024	0.992	1.012
												0.986
				h	2.4	0.960	0.972	0.970	0.886	0.934	0.918	0.940
				v	2.4	0.988	1.036	0.980	1.028	1.008	1.012	1.009
					no oxide disruption								0.974
3.3	57.7	1.5	3.03	h	0	0.808	0.834	0.844	0.850	0.836	0.836	0.835
				v	0	0.812	0.854	0.798	0.844	0.796	0.832	0.823
					lots of rings								0.829
				h	0.4	0.846	0.860	0.864	0.864	0.874	0.848	0.859
				v	0.4	0.848	0.832	0.828	0.816	0.844	0.846	0.836
												0.848
				h	0.8	0.902	0.898	0.894	0.896	0.900	0.894	0.897
				v	0.8	0.914	0.900	0.882	0.872	0.886	0.864	0.886
												0.892
				h	1.2	0.894	0.926	0.920	0.908	0.904	0.894	0.908
				v	1.2	0.896	0.904	0.894	0.908	0.903	0.852	0.893
												0.900
				h	1.6	0.898	0.920	0.926	0.922	0.920	0.918	0.917
				v	1.6	0.886	0.910	0.928	0.906	0.898	0.916	0.907
												0.912
				h	2.0	0.954	0.944	0.942	0.936	0.952	0.944	0.945
				v	2.0	0.942	0.976	0.960	0.920	0.948	0.942	0.948
												0.947
				h	2.4	0.978	0.992	0.980	0.986	0.986	0.976	0.983
				v	2.4	0.952	0.984	0.994	1.008	0.982	1.018	0.990
												0.986
				h	2.8	1.044	1.024	1.034	1.050	1.028	1.026	1.034
				v	2.8	1.034	1.044	1.036	1.048	1.056	1.080	1.050
												1.042
				h	3.2	1.040	1.010	1.042	1.008	1.028	1.042	1.028
				v	3.2	1.080	1.080	1.074	1.006	1.082	1.066	1.065
												1.047
				h	3.6	0.996	1.056	1.034	1.042	1.082	1.066	1.046
				v	3.6	1.054	1.052	1.066	1.040	1.076	1.064	1.059
					no surface disruption of oxide								1.052
2.5	68.5	1.55	4.00	h	0	0.858	0.888	0.898	0.914	0.932	0.856	0.891
				v	0	0.838	0.816	0.840	0.818	0.846	0.792	0.825
												0.858
				h	0.4	0.902	0.828	0.950	0.938	0.928	0.992	0.923
				v	0.4	0.840	0.900	0.870	0.838	0.844	0.832	0.854
												0.889

Appendix 6
Peak pulse power v spot dimensions, cross section

P pulse power, kW	Pulse duration,ms	spot depth mm	average depth, mm	spot dia. mm	av. dia. mm
6.25	0.8	0.36		0.95	
		0.36		0.92	
		0.40	0.373	0.92	0.930
5.56	0.9	0.23		0.88	
		0.23		0.87	
		0.33	0.263	0.91	0.887
5.00	1	0.23		0.87	
		0.23		0.85	
		0.25	0.237	0.85	0.857
4.55	1.1	0.22		0.86	
		0.22		0.84	
		0.22	0.220	0.85	0.850
4.17	1.2	0.19		0.77	
		0.20		0.82	
		0.20	0.197	0.80	0.797
3.85	1.3	0.20		0.78	
		0.20		0.81	
		0.22	0.207	0.85	0.813
3.57	1.4	0.23		0.88	
		0.22		0.88	
		0.22	0.223	0.85	0.870
3.33	1.5	0.20		0.81	
		0.22		0.86	
		0.21	0.210	0.83	0.833
3.13	1.6	0.22		0.86	
		0.21		0.84	
		0.21	0.213	0.84	0.847
2.94	1.7	0.20		0.82	
		0.20		0.81	
		0.20	0.200	0.81	0.813
2.63	1.9	0.20		0.85	
		0.20		0.85	
		0.21	0.202	0.87	0.857
2.50	2	0.21		0.89	
		0.20		0.83	
		0.20	0.203	0.86	0.860

Appendix 7:
Peak pulse power v spot diameter, standard mill finish

Pulse duration t, ms	P pulse power, kw	Line number	spot diameter in mm						Average	Std devn
0.8	6.25	1 h	0.968	0.930	0.932	0.962	1.080	0.930	0.967	0.038
		1v	0.850	0.794	0.924	0.796	1.004	0.862	0.872	0.062
		2h	0.968	0.962	0.942	0.946	0.948	0.952	0.953	0.008
		2v	0.876	0.970	0.896	0.876	0.878	0.896	0.899	0.024
		3h	0.976	0.964	0.968	0.964	1.018	0.892	0.964	0.024
		3v	0.890	0.942	0.930	0.884	0.900	0.804	0.892	0.032
		4h	0.934	0.976	0.976	0.998	0.972	0.988	0.974	0.014
		4v	0.910	0.880	0.892	0.882	0.910	0.980	0.909	0.024
									0.929	
0.9	5.56	1h	0.824	0.828	0.854	0.890	0.932	0.896	0.871	0.035
		1v	0.782	0.820	0.826	0.816	0.855	0.836	0.823	0.017
		2h	0.866	0.894	0.838	0.896	0.830	0.874	0.866	0.022
		2v	0.832	0.824	0.834	0.850	0.836	0.862	0.840	0.011
		3h	0.880	0.930	0.862	0.846	0.878	0.862	0.876	0.020
		3v	0.852	0.848	0.864	0.810	0.820	0.790	0.831	0.024
		4h	0.834	0.852	0.870	0.898	0.864	0.874	0.865	0.015
		4v	0.840	0.826	0.846	0.892	0.846	0.862	0.852	0.017
									0.853	
1.0	5.00	1h	0.832	0.866	0.844	0.892	0.832	0.854	0.853	0.017
		1v	0.804	0.812	0.856	0.818	0.812	0.802	0.817	0.013
		2h	0.956	0.870	0.858	0.824	0.842	0.840	0.865	0.032
		2v	0.952	0.814	0.818	0.804	0.818	0.774	0.830	0.041
		3h	0.800	0.874	0.858	0.850	0.864	0.850	0.849	0.016
		3v	0.848	0.818	0.808	0.802	0.846	0.794	0.819	0.018
		4h	0.844	0.846	0.844	0.848	0.886	0.860	0.855	0.012
		4v	0.816	0.84	0.85	0.812	0.908	0.826	0.842	0.025
									0.841	
1.1	4.55	1h	0.864	0.856	0.864	0.840	0.822	0.826	0.845	0.016
		1v	0.780	0.850	0.848	0.850	0.842	0.844	0.836	0.019
		2h	0.858	0.844	0.856	0.872	0.896	0.844	0.862	0.015
		2v	0.808	0.826	0.844	0.840	0.838	0.844	0.833	0.011
		3h	0.832	0.796	0.834	0.868	0.834	0.816	0.830	0.016
		3v	0.800	0.802	0.800	0.814	0.806	0.808	0.805	0.004
		4h	0.860	0.848	0.858	0.836	0.820	0.868	0.848	0.014
		4v	0.816	0.824	0.834	0.838	0.790	0.806	0.818	0.014
									0.835	
1.2	4.17	1h	0.834	0.836	0.834	0.818	0.854	0.812	0.831	0.011
		1v	0.762	0.814	0.782	0.746	0.782	0.794	0.780	0.017
		h	0.842	0.848	0.794	0.866	0.852	0.890	0.849	0.021
		v	0.798	0.810	0.796	0.818	0.842	0.808	0.812	0.012
									0.818	
1.3	3.85	h	0.874	0.842	0.872	0.848	0.880	0.876	0.865	0.014
		v	0.820	0.792	0.808	0.822	0.800	0.864	0.818	0.018
									0.842	
1.4	3.57	h	0.884	0.860	0.860	0.822	0.874	0.892	0.865	0.018
		v	0.864	0.818	0.794	0.798	0.812	0.788	0.812	0.019
									0.839	
1.5	3.33	h	0.846	0.844	0.862	0.864	0.862	0.870	0.858	0.009
		v	0.786	0.794	0.812	0.790	0.812	0.800	0.799	0.009
									0.829	no rings
1.6	3.13	h	0.862	0.802	0.856	0.864	0.820	0.834	0.840	0.021
		v	0.824	0.812	0.812	0.800	0.846	0.838	0.822	0.014
									0.831	
1.7	2.94	h	0.838	0.854	0.848	0.870	0.878	0.864	0.859	0.012
		v	0.838	0.828	0.824	0.828	0.810	0.824	0.825	0.006
									0.842	

Peak pulse power v spot diameter, etched

Pulse duration t, ms	P pulse power, kw	Line number	spot diameter in mm						Average	Std devn
0.8	6.25	h	0.868	0.846	0.852	0.902	0.892	0.882	0.874	0.018
		v	0.822	0.820	0.850	0.798	0.820	0.834	0.824	0.012
									0.849	
0.9	5.56	h	0.822	0.848	0.828	0.856	0.83	0.844	0.838	0.011
		v	0.796	0.8	0.854	0.828	0.79	0.804	0.812	0.019
									0.825	
1.0	5.00	h	0.858	0.848	0.81	0.824	0.784	0.794	0.820	0.024
		v	0.844	0.784	0.76	0.774	0.81	0.772	0.791	0.024
									0.805	
1.1	4.55	h	0.804	0.81	0.76	0.824	0.808	0.836	0.807	0.017
		v	0.784	0.758	0.788	0.788	0.789	0.804	0.785	0.009
									0.796	
1.2	4.17	h	0.818	0.822	0.806	0.821	0.824	0.82	0.819	0.004
		v	0.818	0.806	0.718	0.826	0.832	0.81	0.802	0.028
									0.810	
1.3	3.85	h	0.832	0.8	0.798	0.796	0.8	0.802	0.805	0.009
		v	0.814	0.798	0.768	0.8	0.782	0.804	0.794	0.013
									0.800	
1.4	3.57	h	0.732	0.764	0.784	0.83	0.79	0.776	0.779	0.022
		v	0.74	0.74	0.782	0.804	0.776	0.766	0.768	0.019
									0.774	
1.5	3.33	h	0.78	0.814	0.748	0.802	0.89	0.882	0.819	0.044
		v	0.816	0.732	0.722	0.832	0.83	0.802	0.789	0.041
									0.804	no rings
1.6	3.13	h	0.742	0.72	0.764	0.692	0.722	0.73	0.728	0.017
		v	0.74	0.73	0.738	0.672	0.698	0.694	0.712	0.024
									0.720	
1.7	2.94	h	0.698	0.74	0.71	0.758	0.748	0.744	0.733	0.019
		v	0.696	0.692	0.728	0.718	0.694	0.7	0.705	0.012
									0.719	
1.8	2.78	h	0.752	0.682	0.702	0.726	0.754	0.72	0.723	0.021
		v	0.678	0.654	0.686	0.684	0.696	0.692	0.682	0.010
									0.702	
1.9	2.63	h	0.722	0.712	0.7	0.722	0.702	0.72	0.713	0.008
		v	0.712	0.698	0.678	0.73	0.788	0.702	0.718	0.027
									0.716	
2.0	2.50	h	0.692	0.674	0.744	0.746	0.746	0.724	0.721	0.025
		v	0.714	0.666	0.746	0.768	0.738	0.714	0.724	0.026
									0.723	
2.5	2.00	h	0.542	0.552	0.55	0.544	0.54	0.56	0.548	0.006
		v	0.562	0.548	0.554	0.534	0.528	0.558	0.547	0.011
									0.548	
3.0	1.67	h	0.482	0.468	0.462	0.5	0.483	0.498	0.482	0.012
		v	0.522	0.486	0.478	0.484	0.472	0.474	0.486	0.012
									0.484	
4.0	1.25	h	0.38	0.388	0.39	0.384	0.394	0.378	0.386	0.005
		v	0.398	0.368	0.366	0.386	0.41	0.406	0.389	0.016
									0.387	
5.0	1.00	h	0.286	0.364	0.31	0.336	0.35	0.342	0.331	0.022
		v	0.268	0.37	0.342	0.292	0.32	0.282	0.312	0.032
									0.322	

Peak pulse power v spot diameter, anodised

Pulse duration	P pulse	Line	spot diameter in mm						Average	Std
t, ms	power, kw	number								devn
0.8	6.25	h	0.76	0.754	0.758	0.698	0.752	0.764	0.748	0.017
		v	0.78	0.73	0.748	0.69	0.716	0.714	0.730	0.023
									0.739	
0.9	5.56	h	0.762	0.76	0.748	0.782	0.768	0.758	0.763	0.008
		v	0.738	0.724	0.708	0.736	0.712	0.708	0.721	0.012
									0.742	
1.0	5.00	h	0.734	0.730	0.748	0.732	0.764	0.762	0.745	0.013
		v	0.696	0.694	0.676	0.700	0.712	0.720	0.700	0.011
									0.722	
1.1	4.55	h	0.740	0.732	0.732	0.748	0.750	0.746	0.741	0.007
		v	0.690	0.692	0.678	0.690	0.698	0.702	0.692	0.006
									0.717	
1.2	4.17	h	0.776	0.758	0.744	0.768	0.748	0.724	0.753	0.014
		v	0.726	0.702	0.732	0.718	0.692	0.726	0.716	0.013
									0.735	no rings
1.3	3.85	h	0.722	0.722	0.766	0.766	0.750	0.748	0.746	0.016
		v	0.708	0.720	0.722	0.740	0.732	0.736	0.726	0.010
									0.736	
1.4	3.57	h	0.756	0.750	0.748	0.752	0.738	0.758	0.750	0.005
		v	0.750	0.726	0.726	0.700	0.736	0.732	0.728	0.011
									0.739	
1.5	3.33	h	0.748	0.744	0.742	0.756	0.750	0.740	0.747	0.005
		v	0.722	0.734	0.724	0.730	0.692	0.698	0.717	0.014
									0.732	
1.6	3.13	h	0.766	0.758	0.744	0.762	0.762	0.764	0.759	0.006
		v	0.702	0.704	0.712	0.700	0.698	0.754	0.712	0.014
									0.736	
1.7	2.94	h	0.732	0.728	0.702	0.710	0.698	0.710	0.713	0.011
		v	0.704	0.652	0.648	0.660	0.676	0.682	0.670	0.017
									0.692	
1.8	2.78	h	0.722	0.700	0.716	0.714	0.752	0.694	0.716	0.014
		v	0.692	0.682	0.668	0.676	0.704	0.672	0.682	0.010
									0.699	
1.9	2.63	h	0.691	0.700	0.702	0.702	0.688	0.712	0.699	0.006
		v	0.680	0.694	0.650	0.650	0.696	0.684	0.676	0.017
									0.687	
2.0	2.50	h	0.706	0.722	0.7	0.686	0.69	0.7	0.701	0.009
		v	0.69	0.668	0.688	0.676	0.692	0.694	0.685	0.008
									0.693	
2.1	2.38	h	0.718	0.71	0.69	0.714	0.664	0.722	0.703	0.017
		v	0.692	0.672	0.688	0.694	0.664	0.7	0.685	0.011
									0.694	
2.2	2.27	h	0.682	0.704	0.682	0.698	0.712	0.706	0.697	0.010
		v	0.674	0.658	0.674	0.684	0.724	0.71	0.687	0.020
									0.692	
2.3	2.17	h	0.704	0.702	0.67	0.718	0.726	0.742	0.710	0.018
		v	0.692	0.666	0.692	0.696	0.686	0.71	0.690	0.010
									0.700	
2.4	2.08	h	0.736	0.69	0.704	0.732	0.726	0.694	0.714	0.018
		v	0.688	0.702	0.698	0.742	0.698	0.71	0.706	0.013
									0.710	
2.5	2.00	h	0.702	0.68	0.692	0.698	0.708	0.718	0.700	0.010
		v	0.672	0.684	0.718	0.692	0.708	0.738	0.702	0.019
									0.701	
3.0	1.67	h	0.62	0.644	0.65	0.664	0.68	0.672	0.655	0.017
		v	0.69	0.628	0.642	0.634	0.678	0.68	0.659	0.024

Appendix 8
Pulse shape spot dimensions

Mill finish					Etched					Anodised				
Pulse shape	spot depth mm	average depth, mm	spot dia. mm	av. dia. mm	Pulse shape	spot depth mm	average depth, mm	spot dia. mm	av. dia. mm	Pulse shape	spot depth mm	average depth, mm	spot dia. mm	av. dia. mm
	0.170		0.80			0.14		0.660			0.17		0.80	
1	0.170	0.170	0.76	0.768	1	0.14	0.140	0.650	0.653	1	0.16	0.167	0.80	0.800
	0.170		0.75			0.14		0.650			0.17		0.80	
	0.230		0.86			0.18		0.770			0.22		0.88	
2	0.230	0.230	0.85	0.850	2	0.19	0.183	0.770	0.763	2	0.21	0.220	0.88	0.883
	0.230		0.84			0.18		0.750			0.23		0.89	
	0.230		0.78			0.15		0.750			0.20		0.82	
3	0.150	0.177	0.78	0.783	3	0.15	0.150	0.750	0.747	3	0.20	0.203	0.83	0.830
	0.150		0.79			0.15		0.740			0.21		0.83	
	0.200		0.85			0.20		0.780			0.22		0.90	
4	0.220	0.213	0.86	0.860	4	0.25	0.217	0.780	0.787	4	0.23	0.223	0.90	0.900
	0.220		0.87			0.20		0.800			0.22		0.90	
	0.200		0.80			0.16		0.670			0.19		0.81	
5	0.180	0.183	0.80	0.797	5	0.17	0.167	0.690	0.680	5	0.20	0.193	0.79	0.797
	0.170		0.80			0.17		0.680			0.19		0.79	
	0.200		0.83			0.20		0.760			0.24		0.88	
6	0.200	0.200	0.83	0.828	6	0.20	0.200	0.760	0.760	6	0.23	0.243	0.87	0.877
	0.200		0.82			0.20		0.760			0.26		0.88	
	0.180		0.82			0.17		0.740			0.17		0.83	
7	0.180	0.180	0.81	0.810	7	0.18	0.180	0.740	0.740	7	0.16	0.167	0.83	0.830
	0.180		0.80			0.17		0.740			0.17		0.83	
	0.180		0.81			0.19		0.740			0.22		0.85	
8	0.170	0.167	0.80	0.803	8	0.16	0.160	0.730	0.730	8	0.20	0.210	0.85	0.847
	0.150		0.81			0.16		0.730			0.21		0.84	
	0.200		0.80			0.15		0.730			0.24		0.83	
9	0.190	0.193	0.8	0.79	9	0.15	0.15	0.68	0.68	9	0.24	0.24	0.83	0.83
	0.190		0.79			0.15		0.68			0.24		0.85	

Appendix 9

Pulse shape trials, mill finish, spot diameters

Pulse shape	h v	spot dia., mm						average dia. in mm
		1	2	3	4	5	6	
1		0.656	0.656	0.658	0.642	0.630	0.632	0.646
		0.654	0.662	0.658	0.660	0.654	0.694	0.664
								0.655
2		0.808	0.728	0.788	0.786	0.794	0.79	0.782
		0.782	0.752	0.768	0.796	0.798	0.784	0.780
								0.781
3		0.758	0.644	0.698	0.636	0.728	0.71	0.696
		0.696	0.732	0.7	0.668	0.708	0.714	0.703
								0.699
4		0.802	0.816	0.806	0.822	0.786	0.798	0.805
		0.798	0.786	0.774	0.79	0.818	0.742	0.785
								0.795
5		0.712	0.744	0.708	0.696	0.688	0.694	0.707
		0.686	0.706	0.684	0.732	0.69	0.684	0.697
								0.702
6		0.782	0.77	0.766	0.774	0.77	0.76	0.770
		0.728	0.758	0.684	0.728	0.714	0.704	0.719
								0.745
7		0.752	0.75	0.776	0.774	0.756	0.772	0.763
		0.668	0.672	0.692	0.676	0.672	0.678	0.676
								0.720
8		0.752	0.74	0.744	0.716	0.732	0.748	0.739
		0.666	0.634	0.704	0.698	0.746	0.748	0.699
								0.719

Pulse shape trials, etched, spot diameters

Pulse shape	h v	spot dia., mm						average dia. in mm
		1	2	3	4	5	6	
1		0.618	0.608	0.638	0.620	0.624	0.648	0.626
		0.606	0.600	0.620	0.614	0.630	0.642	0.619
								0.622
2		0.708	0.742	0.732	0.742	0.756	0.75	0.738
		0.706	0.696	0.692	0.704	0.734	0.684	0.703
								0.721
3		0.698	0.69	0.658	0.664	0.696	0.572	0.663
		0.664	0.642	0.618	0.644	0.656	0.628	0.642
								0.653
4		0.774	0.726	0.78	0.826	0.78	0.806	0.782
		0.7	0.69	0.758	0.75	0.714	0.744	0.726
								0.754
5		0.614	0.622	0.65	0.648	0.624	0.624	0.630
		0.642	0.594	0.606	0.598	0.61	0.594	0.607
								0.619
6		0.81	0.618	0.692	0.69	0.716	0.698	0.704
		0.698	0.69	0.772	0.68	0.7	0.702	0.707
								0.706
7		0.664	0.668	0.638	0.706	0.718	0.706	0.683
		0.662	0.674	0.674	0.706	0.694	0.676	0.681
								0.682
8		0.718	0.646	0.656	0.646	0.644	0.638	0.658
		0.712	0.628	0.65	0.63	0.642	0.648	0.652
								0.655

Pulse shape trials, anodised, spot diameters

Pulse	h	spot dia., mm						average
shape	v	1	2	3	4	5	6	dia. in mm
1		0.700	0.670	0.662	0.694	0.664	0.678	0.678
		0.668	0.666	0.696	0.698	0.658	0.682	0.678
								0.678
2		0.666	0.68	0.69	0.674	0.668	0.698	0.679
		0.712	0.684	0.684	0.684	0.692	0.702	0.693
								0.686
3		0.67	0.67	0.672	0.658	0.664	0.66	0.666
		0.66	0.65	0.656	0.646	0.632	0.652	0.649
								0.658
4		0.704	0.718	0.696	0.714	0.704	0.69	0.704
		0.69	0.716	0.696	0.706	0.686	0.704	0.700
								0.702
5		0.648	0.644	0.638	0.624	0.634	0.644	0.639
		0.626	0.612	0.598	0.632	0.63	0.65	0.625
								0.632
6		0.654	0.702	0.698	0.68	0.672	0.686	0.682
		0.666	0.666	0.662	0.658	0.666	0.674	0.665
								0.674
7		0.688	0.662	0.664	0.7	0.666	0.704	0.681
		0.674	0.652	0.658	0.664	0.672	0.668	0.665
								0.673
8		0.684	0.682	0.672	0.676	0.664	0.672	0.675
		0.658	0.66	0.67	0.648	0.638	0.662	0.656
								0.666

Appendix 10
20 Hz, 2.5 ms, 5J data - location of irregular melt spots

Spot Position

	1	2	3	4	5	6	7	8	9	10	11	12	13	14	15	16	17	18	19	20	21	22	23	24	25	26	27	28	29	30	31	32	33	34	35
1	X																																		
2	.																																		
3																																			
4																												X							
5							X																												
6									X				X				X	.																	
7																																			
8																				X															
9																																			
10																																	X		
11						X						X																							
12														X																	X				
13																																			
14																																			
15																			X																X
16																												X	X						
17																																			
18																																			
19																																			
20						X																						X							
21																																			
22																																			
23																												X							
24																																			
25																																			
26																																			
27																									X				X						
28									X														X												
29					X	X	X							X						X						X									
30					X																														
31																			X	X											X				
32										X						X	X																		
33																																			
34																																			
35			X										X																						
36																															X				
37							X																												
38				X								X																							
39														X																					
40																												X							

Distribution of spot diameters at 20Hz, 2.5ms, 5J.

Spot diameter, mm	no. of spots
< 0.704	4
0.704 - 0.714	5
0.714 - 0.724	9
0.724 - 0.734	8
0.734 - 0.744	3
0.744 - 0.754	1
0.754 - 0.764	2
0.764 - 0.774	0
0.774 - 0.784	1
0.784 - 0.794	1
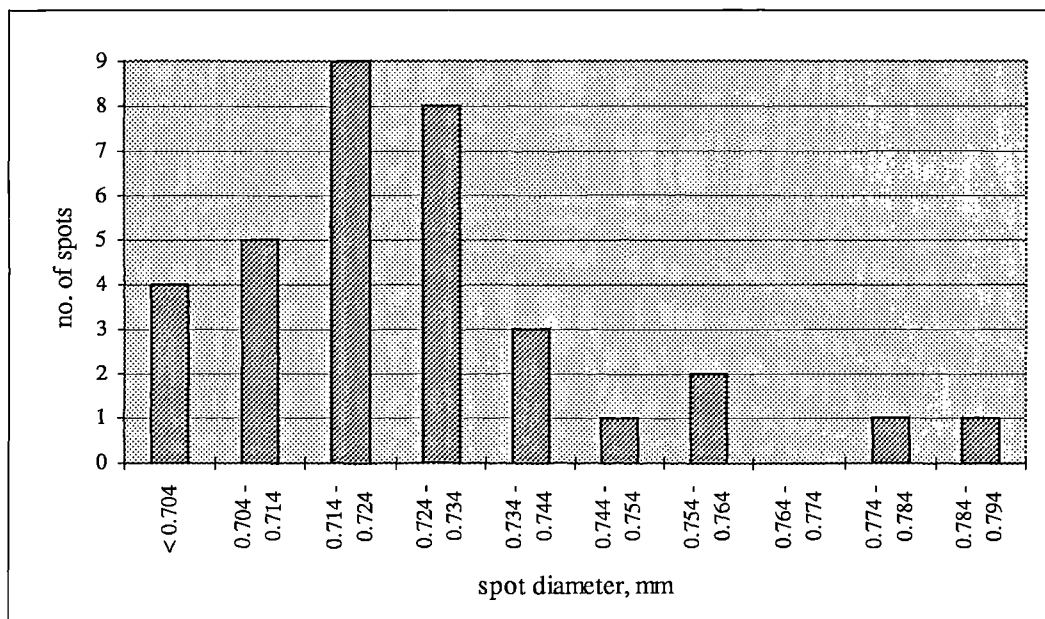
Bar chart of spot diameters at 20Hz, 2.5ms, 5J.